COLLECTED PAPERS

ON

COHERENT OPTO-ELECTRONICS

Volume 3

August 1987—June 1988

Associate Professor

Motoichi OHTSU

TOKYO INSTITUTE OF TECHNOLOGY

THE GRADUATE SCHOOL AT NAGATSUTA

4259 Nagatsuta, Midori-ku, Yokohama,

Kanagawa 227, JAPAN

PREFACE

This is a research review on coherent opto-electronics by Assoc. Prof. M. Ohtsu, Tokyo Institute of Technology. It contains copies of technical papers published in August 1987 - June 1988. M. Ohtsu thanks Assoc. Prof. Y. Teramachi of Institute of Vocational Training for his cooperation of research.

MEMBERS

Associate Professor

Motoichi OHTSU	(Dr. Eng.)

Graduate Students (Doctor Candidates)

Katsuhiko KUBOKI	(M. Eng.)
Minoru HASHIMOTO	(M. Eng.)
Hiroyuki FURUTA	(M. Eng.)
Kaoru YOKOTANI	(M. Eng.)
Chul Ho SING	(M. Eng.)

Graduate Students (Master Course)

Toru KATO	(B. Eng.)[a)]	(-1988.3)
Morihiro MURATA	(B. Eng.)	
Eiji IKEGAMI	(B. Eng.)	(1988.4-)
Motonobu KOUROGI	(B. Eng.)	(1988.4-)
Isao KOSHIISHI	(B. Eng.)	(1988.4-)

Undergraduate Students

Toshio NAKAHARA[b]	(-1988.3)
Yosuke NISHIJO[c]	(-1988.3)
Mitsuhiro TESHIMA	(1988.4-)
Hiromasa SUZUKI	(1988.4-)

Visiting Researchers

Toru IMAI[d]	

a) Presently with Sumitomo Shoji Ltd.

b) Presently with Itochu Ltd.

c) Presently with Nisho Iwai Ltd.

d) Permanent Address : Tokyo Aircraft Instrument Co. Ltd., Tokyo, Japan

LIST OF PAPERS

[I] IMPROVEMENTS IN COHERENCE OF LASERS

(a) Journal Papers

[1] M. Ohtsu and K.-Y. Liou, "Correlated spontaneous emission between two longitudinal modes in an extended-cavity semiconductor laser", Appl. Phys. Lett., Vol. 52, No.1, January 1988, pp. 10 - 12

[pp. 1 - 3]

[2] M. Ohtsu, "Realization of Ultrahigh Coherence in Semiconductor Laser by Negative Electrical Feedback", J. Lightwave Technol., Vol. 6, No.2, February 1988, pp. 245 - 256 (Invited paper)

[pp. 4 - 15]

[3] M. Ohtsu and M. Tabuchi, "Electrical Feedback and its Network Analysis for Linewidth Reduction of Semiconductor Laser", J. Lightwave Technol., Vol. 6, No.3, March 1988, pp. 357 - 369

[pp. 16 - 28]

[4] M. Ohtsu and T. Tako, "Coherence in Semiconductor Lasers", Progress in Optics XXV, Ed. by E. Wolf, Elsevier Science Publishers, Amsterdam, 1988, pp. 193 - 278 (Review paper)

[pp. 29 - 116]

[5] M. Ohtsu, "Precise Frequency Control of Semiconductor Lasers", Optical and Electro-Optical Engineering Contact, Vol. 26, No. 1, January 1988, pp. 35 - 42 (Review paper, in

Japanese)

[pp. 117 - 124]

[6] M. Ohtsu, "Frequency Control of Semiconductor Lasers", Jpn. J. of Optics, Vol. 17, No. 6, June 1988, pp. 272 - 278 (Review paper, in Japanese)

[pp. 125 - 131]

(b) International Conferences

[1] K. Kuboki, C.H. Shin, T. Kato and M. Ohtsu, "Performance and Its Evaluation of Optical Tracking Generator/Optical Frequency Synthesizer by Semiconductor Lasers", Conference on Precision Electromagnetic Measurements (CPEM'88), June 1988, Tsukuba, TUB1-5, pp. 24 - 25

[pp. 132 - 133]

[II] ANALYSES OF LASER DYNAMICS

(a) Journal Papers

[1] M. Ohtsu, K.-Y. Liou, E.C. Burrows, C.A. Burrus and G. Eisenstein, "Interferometric Method For Preventing Mode-Hopping In Tunable External-Cavity Semiconductor Lasers", Electron. Lett., Vol. 23, No. 21, October 1987, pp. 1111 - 1113

[pp. 134 - 136]

[2] M. Ohtsu and K.-Y. Liou, "Mode Stability of a Two-Wavelength

Hatakoshi, "Long-term measurement of earth strains and vibrations by a 50-m laser interferometer", Conference on Lasers and Electro-Optics (CLEO'88), April 1988, Anaheim, CA, TUQ5

[pp. 153 - 154]

[2] M. Hashimoto and M. Ohtsu, "Improvement of Frequency Accuracy In a Semiconductor Laser Pumped ^{87}Rb Atomic Clock", Conference on Precision Electromagnetic Measurements (CPEM'88), June 1988, Tsukuba, WEB2-4, pp. 82 - 83

[pp. 155 - 156]

Correlated spontaneous emission between two longitudinal modes in an extended-cavity semiconductor laser

M. Ohtsu[a] and K.-Y. Liou
AT&T Bell Laboratories, Crawford Hill Laboratory, Holmdel, New Jersey 07733

(Received 12 October 1987; accepted for publication 2 November 1987)

Recently, correlated spontaneous emission in a laser of three-level atoms has been analyzed theoretically and has been demonstrated experimentally using a three-level He-Ne Zeeman laser. We demonstrate that correlated spontaneous emission is also feasible in a semiconductor laser with a long extended cavity. As a result, the heterodyned spectral width between two lasing modes in a grating extended-cavity laser was reduced to below the spontaneous emission noise level. The laser can be used for high-precision optical-heterodyne sensing.

A technique commonly used for optical sensing is to measure the frequency shift of an optical heterodyned signal between two laser fields. These two fields may come from two highly coherent single-mode lasers or from two different longitudinal modes of a single laser. The quantum-noise-limited resolution of such a sensing system is mainly related to the intrinisic laser linewidths, which are combined in the linewidth of the heterodyned signal.

Scully[1] showed recently that it is possible to correlate the spontaneous emission into two different modes of the same laser so that the relative phase angle of the two modes remains constant in time. Although the two modes still have finite individual linewidths, their heterodyned linewidth can be nearly zero because their phase fluctuations due to the spontaneous emission noises are synchronized. This approach can be applied to a simple three-atomic-level laser, in which the transitions from the two upper levels to the lower level result in two lasing lines. The two upper levels can be correlated, for example, by applying an external microwave field at a frequency equal to their energy difference.[2] Using this method, the relative phase of the two lines is locked to the phase of the microwave field, and the spontaneous emission into the two lines is correlated. These ideas have been tested recently by Toschek and Hall[3] in an experiment using a He-Ne Zeeman laser. By applying a rf (radio frequency) magnetic field to the gain tube of the laser, they were able to reduce the linewidth of the Zeeman beat to a value lower than the Schawlow–Townes limit.

For semiconductor lasers, the idea of correlated spontaneous emission is not directly applicable, because the band structure of the semiconductor gain medium cannot be modeled as a three-level system. However, we report in this letter that it is possible to achieve correlated spontaneous emission in a semiconductor laser by coupling two cavity modes of the laser via optical sidebands, which are produced by modulating the injection current at a frequency equal to the frequency separation between the two modes. In our experiment, a passive extended cavity was added to a semiconductor laser chip to reduce the longitudinal mode separation to a few hundred MHz for current modulation, and correlated spontaneous emission between two neighboring cavity modes was demonstrated.

The experimental setup is shown in Fig. 1(a). A grating extended-cavity laser[4,5] was used. A fiber Mach–Zehnder interferometer and an avalanche photodiode were used for heterodyning. The signal was then amplified and analyzed using a spectrum analyzer. The gain medium in the extended cavity laser was a 1.3-μm wavelength InGaAsP semiconductor laser chip. One facet of this chip was antireflection coated. The light output from the coated facet was coupled to a diffraction grating using an objective lens with a 0.85 numerical aperture. The total length of this extended-cavity laser was 42 cm, which gave a longitudinal mode spacing of 360 MHz.

The laser oscillates with a single longitudinal mode stabilized by the frequency selective reflection from the grating. The grating can be rotated to tune the lasing frequency but a large tuning results in mode changes to successive longitudinal modes. A piezoelectric transducer (PZT) was used for fine tuning of the extended cavity length, which was con-

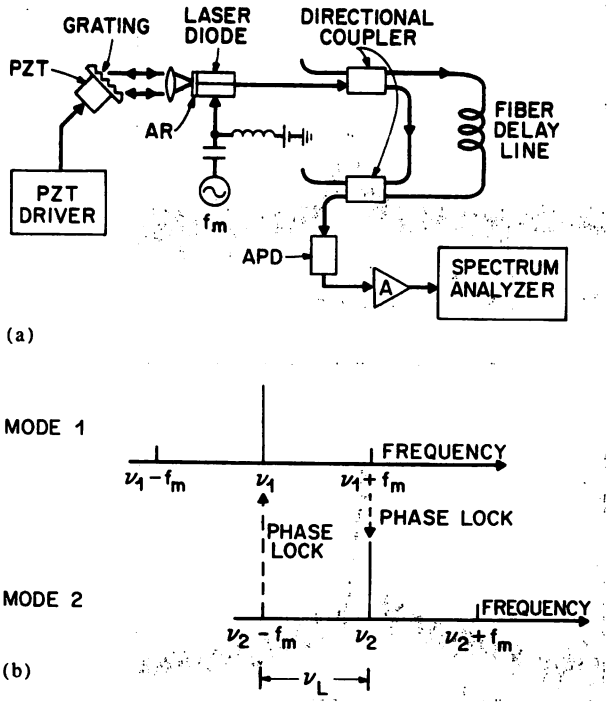

FIG. 1. (a) Experimental setup. PZT: piezoelectric transducer, AR: antireflection coating, f_m: modulation frequency of the injection current, APD: avalanche photodiode. (b) Schematic diagram showing the mode spectrum of the laser under current modulation at a frequency $\nu_L = \nu_2 - \nu_1$, where ν_1 and ν_2 are two lasing longitudinal modes.

[a] On leave from Tokyo Institute of Technology, Graduate School at Nagatsuta, Midori-ku, Yokuhama, Kanagawa 227, Japan.

 0003-6951/88/010010-03$01.00

trolled to operate the laser under the two-mode switching condition. A sinusoidal modulation current at 360 MHz was added to the injection current to generate AM (amplitude modulation) sidebands in the frequency domain.

Figure 1(b) shows schematically the two oscillating cavity modes at ν_1 and ν_2 and their AM sidebands. If the modulation frequency f_m is sufficiently close to the longitudinal mode separation $\nu_L = (\nu_2 - \nu_1)$, the AM sideband of one cavity mode is aligned with the other cavity mode, as shown in Fig. 1(b). The phase of the cavity mode is locked to the AM sideband aligned to it, similar to the case of injection locking, due to the nonlinear property of the laser. The relative phase between the ν_1 and ν_2 modes is therefore locked through their sidebands. Mathematically this is the same as the theory of Scully,[1,2] which shows that the relative phase angle of the two resonances is locked to the phase of the applied microwave modulation and the fluctuations of spontaneous emission into the two resonances are correlated.

The longitudinal mode spectrum of the laser was monitored using a scanning Fabry–Perot interferometer. Although the time-averaged spectrum was maintained to have two modes with equal intensities, the output light power switched randomly in time between the two modes. Because the two mode powers under this mode-hopping condition are anticorrelated in time, a Mach–Zehnder interferometer with a long fiber delay line, 2.8 km, was used in the experiment to increase the heterodyned signal.

Figure 2(a) shows a heterodyned spectrum of the laser under free-running condition, i.e., without current modulation. The full width at half-maximum (FWHM) was about 500 kHz. This linewidth is mainly governed by the sum of the independent phase fluctuations of the two modes due to the fluctuations of the spontaneous emission. When the modulation current at $f_m = 360\ \text{MHz} = (\nu_2 - \nu_1)$ was applied, the FWHM of the heterodyned spectrum, shown in Fig. 2(b), was reduced to about 25 kHz. The laser output with and without current modulation was monitored with a scanning Fabry–Perot interferometer, and two-mode operation with equal time-averaged intensities was maintained in both cases.

The difference ΔI between the peak heights of the heterodyned signals with and without the 360 MHz current modulation is plotted in Fig. 3 as a function of the modulation current amplitude i_m. The threshold current of the laser was 35 mA and the dc bias was 65 mA. Figure 4 shows the measured FWHM of the heterodyned spectrum as a function of i_m. A drastic decrease in FWHM with i_m was observed which saturated at a value approximately equal to the resolution limit of the Mach–Zehnder interferometer with a finite length of delay line (24 kHz resolution for a 2.8-km fiber used). These measurements confirm that the FWHM of the heterodyned spectrum between the two modes is reduced significantly by the current modulation, and indicate correlated spontaneous emission due to phase locking through the AM sidebands. The required modulation amplitude i_m is about 5 mA, which is small compared to the threshold current or the dc bias.

The phase locking between the two modes that results in correlated spontaneous emission can be discussed by analogy with injection locking through the AM sidebands. That is, one longitudinal mode is injection locked to the AM sideband of the other longitudinal mode. The locked longitudinal mode can be considered as the slave laser mode and the AM sideband is the master laser. The locking range, i.e., the maximum value of $|f_m - (\nu_2 - \nu_1)|$ for which injection locking can be maintained, is proportional to $\sqrt{p_m/p_s}$, where p_m and p_s are the optical power of the master and the slave laser mode, respectively. For an injection laser with a threshold current I_{th}, $\sqrt{p_s}$ is proportional to $\sqrt{(I/I_{\text{th}}) - 1}$ and

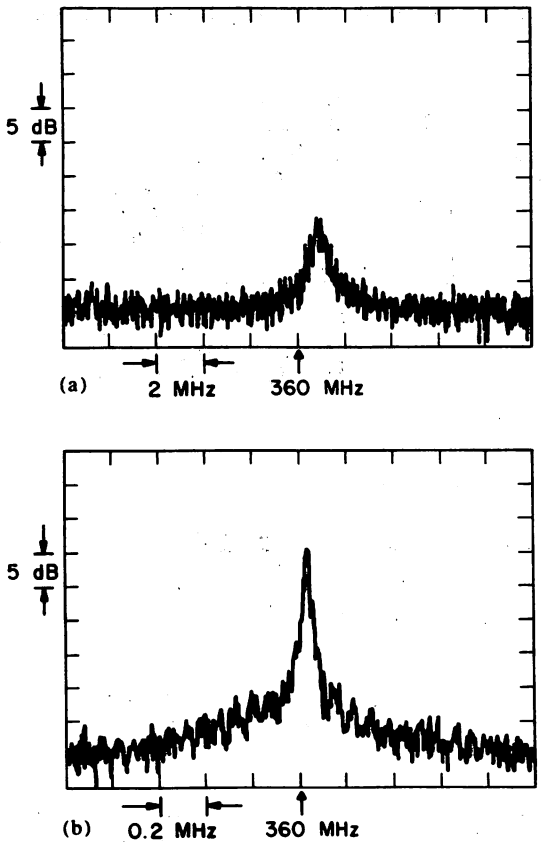

FIG. 2. Heterodyned spectra between the two longitudinal modes. (a) Without current modulation; (b) with current modulation, where the modulation amplitude $i_m = 8$ mA, $f_m = 360$ MHz, and the dc bias is 65 mA.

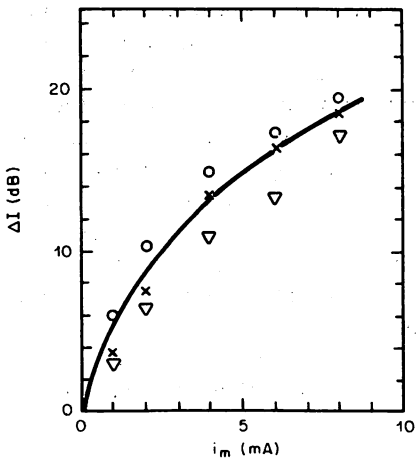

FIG. 3. Difference ΔI between the peak heights of the heterodyned signal with and without current modulation. The dc biases are 60.1 mA (○), 70.1 mA (×), and 80.0 mA (▽).

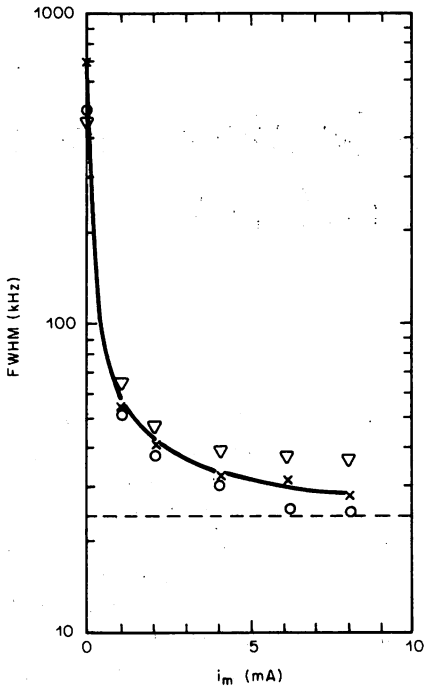

FIG. 4. Full width at half-maximum (FWHM) of the heterodyned spectrum with current modulation. The broken line represents the resolution of the measurement (24 kHz) governed by the finite length of the fiber delay line. The dc biases are the same as in Fig. 3.

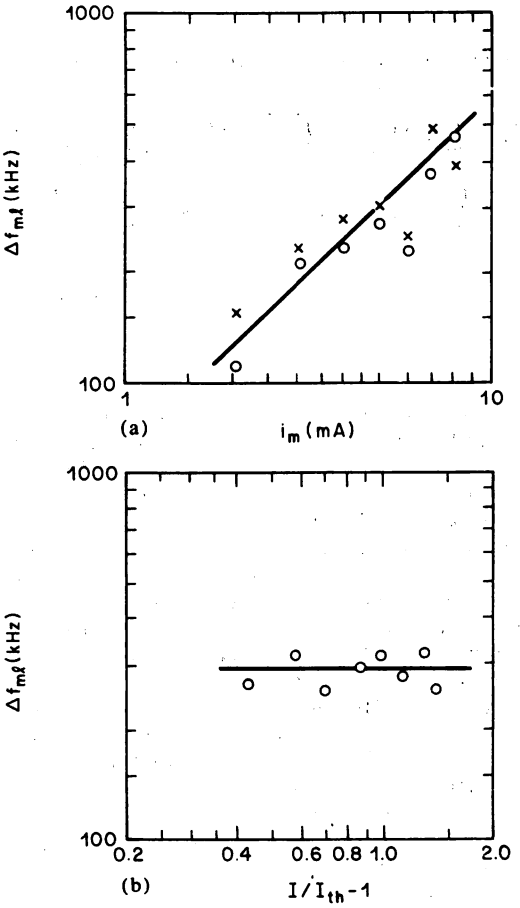

FIG. 5. (a) Relation between i_m and the lock range Δf_{ml}. The dc biases are 85.0 mA (O) and 65.0 mA (×). (b) The relation between the normalized dc bias $(I/I_{th}-1)$ and the locking range Δf_{ml}, for $i_m = 6$ mA.

$\sqrt{p_m}$ is proportional to $M\sqrt{(I/I_{\rm th})-1}$, where I is the dc bias and M is the modulation index of the amplitude of the optical electric field. Since the locking range is independent of $[(I/I_{\rm th})-1]$, and M is proportional to i_m the locking range can be expressed as

$$|f_m-(\nu_2-\nu_1)|_{\rm lock}\propto i_m. \tag{1}$$

To verify the above relationship experimentally, we define an easily measurable locking range, Δf_{ml}, as the value of $|f_m-(\nu_2-\nu_1)|$ at which the peak height of the heterodyned signal is reduced to one-half the heterodyned peak height when $|f_m-(\nu_2-\nu_1)|=0$. To a first-order approximation, Δf_{ml} defined here is proportional to the exact locking range $|f_m-(\nu_2-\nu_1)|_{\rm lock}$ in Eq. (1). The measured Δf_{ml} as a function of i_m is shown in Fig. 5(a), and the measured Δf_{ml} as a function of $[(I/I_{\rm th})-1]$ is plotted in Fig. 5(b). It is seen clearly that the locking range is proportional to i_m and is independent of $[(I/I_{\rm th})-1]$. These results clearly show that the mechanism of phase locking employed in this experiment to achieve correlated spontaneous emission can be interpreted by analogy with injection locking through the AM sidebands.

In summary, we have demonstrated that the linewidth of the heterodyned signal between two neighboring longitudinal modes of an extended-cavity semiconductor laser can be reduced by modulation of the injection current at a frequency equal to the frequency separation between the two modes. Limited by the resolution of the measurement setup, the two-mode heterodyned linewidth was reduced by a factor of 1/20 to 25 kHz, while the individual linewidths of the two modes remained unchanged. These observations demonstrate that it is feasible to lock the relative phase of two lasing modes in a semiconductor laser, or in other words, to correlate the fluctuations of spontaneous emission into the two modes. This correlated spontaneous emission semiconductor laser may be of interest for applications in optical heterodyne sensing with a precision better than that limited by the intrinsic spontaneous emission noise.

The authors would like to thank C. A. Burrus for the 1.3 μm laser chip and G. Eisenstein for facet antireflection coating, and also acknowledge E. C. Burrows for technical assistance.

[1]M. O. Scully, Phys. Rev. Lett. **55**, 2802 (1985).
[2]L. M. Pedrotti and M. O. Scully, in *Coherence, Cooperation, and Fluctuations*, edited by F. Haake, L. M. Narducci, and D. Walls (Cambridge University, London, 1986), p. 279.
[3]P. E. Toschek and J. L. Hall, paper WDD2 in Technical Digest of 15th International Quantum Electronics Conference, Baltimore, April 1987, p. 102.
[4]R. Wyatt and W. J. Devlin, Electron. Lett. **19**, 110 (1983).
[5]N. A. Olsson and J. P. van der Ziel, J. Lightwave Technol. **LT-5**, 510 (1987).

Realization of Ultrahigh Coherence in Semiconductor Lasers by Negative Electrical Feedback

MOTOICHI OHTSU

Abstract—**To be useful, an ultrahigh coherence semiconductor laser source requires high frequency stability, narrow linewidth, the capability of frequency tracking to a master laser, and stable frequency tuning. Negative electrical feedback is proposed to meet these four requirements simultaneously. Although the degree of frequency fluctuation which can be reduced by negative electrical feedback is limited by the noise contained in the feedback signal, theoretical calculations show that the fluctuations can be lower than the quantum noise limit. Experimental results obtained by the author are reviewed: 1) the stability of the center frequency of the laser field spectrum is improved to 1.4 $\times 10^{-12}$ for an integration time of 100 s; 2) the linewidth of the field spectrum is reduced to 200 kHz, which is narrower than the Schawlow–Townes linewidth due to spontaneous emission noise; 3) frequency tracking of a slave laser to a master laser is demonstrated with a capture range of 1.22 GHz, and the frequency stability of the slave laser is as high as that of the master laser given in 1); 4) stable frequency tuning of the slave laser is carried out under the condition of 3). A 47.4-GHz locking range is achieved in which a frequency stability as high as that of 3) is maintained for the slave laser.**

I. Introduction

HIGH TEMPORAL coherence is one of the advantageous properties of lasers. Because the degree of coherency is still influenced by several external noise sources (see, for example, [1]), numerous attempts at optimizing the temporal coherence have been made since the invention of the laser. These attempts have attracted the attention of many researchers because they represent the pursuit of an ideal light source, i.e., a perfectly sinusoidal electromagnetic wave in the optical frequency region.

Among several kinds of lasers, semiconductor injection lasers have been used as light sources for lightwave communication systems. However, the spectral properties and temporal coherence of semiconductor lasers still need to be improved if these lasers are to be used for coherent optical communications (see, for example, [2]), coherent optical measurements, and so on. Although these semiconductor laser devices have been designed and fabricated carefully, the temporal coherence of solitary semiconductor lasers is not yet high enough for these applications. Further improvement requires the addition of external electronic circuits or optical components to the laser. For example, an external mirror or grating has been used to provide optical feedback into the laser cavity to reduce the spectral linewidth [3], [4] or to tune the wavelength [3], [5]. Alternatively, electronic circuits have been developed to control the injection current to stabilize the center frequency of the field spectrum to about 1×10^{-12} [6]. A stable Fabry–Perot interferometer or gaseous absorption spectral lines have been employed as frequency references for this negative electrical feedback. Furthermore, injection locking phenomena have been utilized for frequency tracking or synchronization between two lasers [7].

These techniques have been employed separately to improve only one of several spectral properties to meet the requirement for a particular application. To realize ultrahigh coherence, however, a synthesized technique should be developed to improve all the spectral properties simultaneously. In this paper, a promising negative electrical feedback technique is proposed, and our recent results are reviewed.

II. Negative Electrical Feedback

Highly coherent oscillators in the microwave frequency region, e.g., cesium (Cs) and rubidium (Rb) atomic clocks, and the hydrogen (H) maser, are well developed for applications in communications, in primary standards of time, and so on (see, for example, [8]). For gas lasers, several techniques have also been developed to achieve a frequency stability of 1×10^{-14} [1], [9], and a subhertz linewidth has been realized for a dye laser [10].

It would be instructive to investigate the possibility of applying these established techniques to semiconductor lasers. From this investigation, it can be deduced that at least the following four requirements should be met simultaneously to improve the coherence of semiconductor lasers: 1) stabilization of the center frequency of the field spectrum, to obtain a light source with low frequency drift; 2) linewidth reduction of the field spectrum, to obtain a light source with low frequency- or phase-jitter; 3) frequency tracking to a highly coherent maser laser, to make a synchronized frequency chain by transferring the high coherence of a master laser to several slave lasers (this is required for applications to coherent/heterodyne optical communications, heterodyne optical measurements, and so on); 4) stable and wide-band frequency tuning, to realize a wide-band tunable coherent light source

Manuscript received May 6, 1986; revised June 15, 1987. This work was partially supported by the Ministry of Education, Science, and Culture of Japan under a Grant-in-Aid for Scientific Research, and by KDD Engineering and Consulting Foundation under Funds for International Communications Research.

The author is with the Graduate School at Nagatsuta, Tokyo Institute of Technology, Yokohama, Kanagawa 227, Japan.

IEEE Log Number 8717519.

0733-8724/88/0200-0245$01.00 © 1988 IEEE

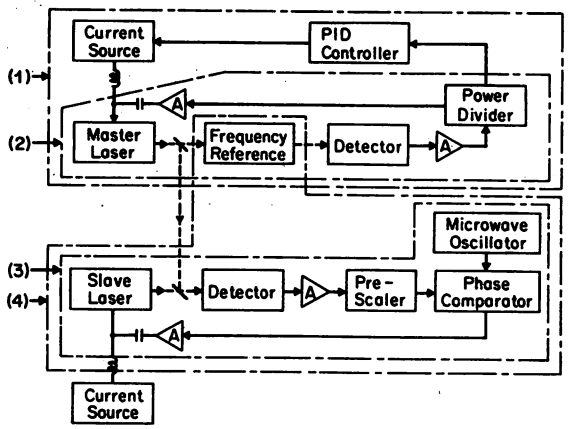

Fig. 1. Proposed experimental setup for meeting the four requirements simultaneously. A PID controller in block (1) is composed of a proportional amplifier, an integrator, and a differentiator.

for frequency multiplexing in coherent optical communications, high resolution laser spectroscopy, precise optical measurements, and so on.

Separate techniques have been developed for meeting only one of these requirements, as was described in Section I. For example, optical feedback has been employed for (2). However, this technique presents several problems, including chaotic instabilities which are dependent on the phase of the reflected light [11], [12], stochastic instabilities induced by random fluctuations of this phase [13], drastic increases in cavity volume, and decreases in direct frequency modulation index. For (3) or (4), injection locking has been employed. However, the dependence of the locking range (i.e., the frequency range in which locking can be maintained) on the powers of the two lasers may limit the reliability of this technique.

Each of the problems for these techniques should be solved. Furthermore, it is important that the above mentioned four requirements be met simultaneously to realize a highly coherent and reliable light source. A technique using negative electrical feedback to control the injection current, which was proposed previously by the author [6], [14], can be a promising one for this purpose.

Fig. 1 shows a schematic diagram of an experimental setup by which the four requirements can be simultaneously met. Each block (1)–(4) in this figure represents a feedback loop for treating requirements (1)–(4). The designs of blocks (1), (2), and (4) in this figure were based on the techniques used for gas and dye lasers [1], [10], and blocks (1) and (3) were based on the techniques for microwave oscillators [8], [10], [15]. This system would be bulky if it were constructed for gas or dye lasers. For semiconductor lasers, however, it can be very compact. The size can be reduced by integrating several electronic or optical components together with the laser devices in the future, and an ultrahigh-coherence miniature light source can be realized. Although simultaneous operation of the four blocks in Fig. 1 has not yet been demonstrated, the performance of each of these blocks have been evaluated. The details will be described in Section III.

The theoretical limit of the reduction of the frequency fluctuations will be discussed prior to reviewing the experimental results. In this discussion, it is assumed that quantum mechanically induced frequency fluctuations can be accurately measured by classical electrooptical techniques such as interferometric measurements or heterodyning, and that these frequency fluctuations can be compensated by applying the modulation of a macroscopic quantity to the laser [16]. These assumptions are valid for semiconductor lasers because the magnitude of the quantum noise is rather large and the frequency can be directly modulated by the injection current. Frequency fluctuations $\delta\nu(t)$ under this negative electrical feedback were estimated by a quantum mechanical Langevin's equation of motion, which is expressed as [16]

$$\delta\nu(t) \equiv \frac{1}{2\pi} \cdot \frac{d(\delta\phi(t))}{dt} = \Gamma_s(t) + \Gamma_c(t) - \int_0^\infty h_f(t') \cdot \left\{ \frac{1}{2\pi} \cdot \frac{d(\delta\phi(t-t'))}{dt} + \Gamma_n(t') \right\} dt' \quad (1)$$

where $\delta\phi(t)$ represents phase fluctuations, and $\Gamma_s(t)$ and $\Gamma_c(t)$ are the Langevin's forces for representing the contributions of spontaneous emission and carrier density fluctuations, respectively [17]. The impulse response of the feedback loop, the measured value of frequency fluctuations, and the noises contained in the feedback signal, are represented by $h_f(t')$, $d(\delta\phi(t-t'))/dt/2\pi$, and $\Gamma_n(t')$, respectively. A list of symbols used in this paper is given in Appendix I for the readers' convenience. The value of $\Gamma_n(t)$ is dependent on the noise magnitude and the sensitivity of the frequency discriminator. The first and second terms of this equation represent the quantum noise sources for the free-running laser. The third term, i.e., the integral, represents the effect of negative feedback. The magnitude of the frequency fluctuations can be derived from the Fourier transform of this equation, which is

$$F(f) = \frac{\Pi_s(f)}{1 + H(f)} + \frac{\Pi_c(f)}{1 + H(f)} - \frac{H(f)}{1 + H(f)} \cdot \Pi_n(f) \quad (2)$$

where f is the Fourier frequency, and F, H, Π_s, Π_c, and Π_n represent the Fourier transforms of frequency fluctuations $\delta\nu(t)(\equiv d(\delta\phi)/dt/2\pi)$, h_f, Γ_s, Γ_c, and Γ_n, respectively. The magnitudes of the first and second terms of this equation approach zero in the limit of an infinite negative feedback gain ($|H| \to \infty$). This means that the contributions of the quantum noise sources ($\Gamma_s(t)$, $\Gamma_c(t)$) can be completely removed by negative feedback. The magnitude of the third term approaches $|\Pi_n|$, which means that the frequency fluctuations can be ultimately

reduced to the value limited by the magnitude of the noise contained in the feedback signal. As will be shown in Section III, the value of this limit is much lower than that of the frequency fluctuations due to the quantum noise sources, from which it is expected that ultrahigh coherence can be realized in semiconductor lasers by negative electrical feedback.

The above discussion can also be applied to other types of feedback schemes and for other types of lasers, as long as the assumptions made for (1) are satisfied. In the case of a gas laser, however, it is known that $\Gamma_c(t) = 0$ and the fluctuations represented by $\Gamma_s(t)$ are much lower than those in semiconductor lasers because of the large Q-factor of the cavity. From these facts, it has been pointed out for gas lasers that the magnitude of the noise-limited fluctuations attained by negative feedback is still larger than that caused by the quantum noise sources if conventional frequency references, e.g., saturated absorption spectral lines of atoms or molecules, are employed [6]. However, the magnitude of the noise-limited fluctuations in gas lasers can be reduced to a value lower than that limited by quantum noise if an ultrahigh sensitivity frequency reference, e.g., a two-photon Ramsey spectral line in freely falling atoms [18], is employed in the future.

III. Experimental Approaches

A. Stabilization of the Center Frequency of the Field Spectrum

Stabilization of the center frequency and reduction of the linewidth of the field spectrum will be discussed in this and the next subsections, because the frequency stability[1] and linewidth have been conventionally used as measures of coherence for several applications. However, it should be pointed out that a primary measure of coherence should be the power spectral density of the frequency or phase fluctuations because the frequency stability and linewidth are governed by the power spectral density.

The stability of the center frequency of the field spectrum can be estimated by measuring the fluctuations of the beat frequency between two independent lasers. The Allan variance $\sigma_y^2(\tau)$ has been popularly used to evaluate the magnitude of fluctuations [21], by which not only stationary stochastic processes but also unstationary ones, e.g., random walk or flicker noise of frequency drifts, can be quantitatively represented. It corresponds to the second moment of the normalized fluctuating frequency $y(t)$ $(= \delta\nu(t)/\nu_0)$ measured within the integration time τ, where ν_0 is the nominal frequency of the laser.

The use of an analog integrator, i.e., a servo-amplifier with a higher gain at lower Fourier frequencies, is effective in reducing the drift. A Fabry–Perot interferometer has been conveniently employed as a frequency reference, and played the role of a frequency standard and a frequency discriminator in the feedback loop. Since the resonance frequency of this interferometer will drift with the ambient temperature, a more stable frequency reference is required to obtain a higher frequency stability. The spectral lines of stable atoms or molecules can be used as stable references. The absorption spectral lines of combination tones or the higher harmonics of vibration-rotation transitions in gaseous organic molecules, e.g., H_2O, CO_2, etc., are appropriate candidates for the frequency reference for 0.8-μm AlGaAs lasers [22], [23]. Since a large number of spectral lines are found near 0.8 μm, almost all the AlGaAs lasers can be tuned to at least one of them even though the wavelengths of the lasers can vary over a wide range. A problem is the low absorption coefficients of these lines, which may limit the sensitivity of frequency discrimination.

To overcome this difficulty, linear absorption or saturated absorption spectral lines of electronic transitions in alkali vapors, e.g., Cs [24], Rb [25], etc., can be used as references because of their large absorption coefficients. In contrast to the organic molecules, these vapors have only a few spectral lines near 0.8 μm, which may limit the number of lasers tunable to these references.

For 1.3–1.6 μm InGaAsP lasers, absorption spectral lines in organic molecules, e.g., NH_3, H_2O, etc., as given above, can be used [26].

Fig. 2 shows calculated results of fluctuations in the center frequency of the field spectrum of a single-mode AlGaAs laser, represented by the square root of the Allan variance $\sigma_y^2(\tau)$ [6]. Curve H represents the value given by the quantum noise sources, i.e., $\Gamma_s(t)$ and $\Gamma_c(t)$ in (1). Curve F represents the value when the contributions from external noise sources (fluctuations of ambient temperature and injection current) are also included. These two curves represent fluctuations of a free-running laser. Curve G represents the limit of residual frequency fluctuations under negative electrical feedback, obtained by letting $|H| \rightarrow \infty$ in (2). That is, it represents the limit given by the magnitude of the noises contained in the feedback signal. This estimation is obtained by assuming that the principal noise source in the feedback signal is from the photodetector, and that a linear absorption spectral line in Rb vapor is used as a frequency reference. On this curve, the square root of the Allan variance of residual frequency fluctuations is $\sigma_y = 1.7 \times 10^{-15}$ for an integration time τ of 100 s, which is as low as that of a hydrogen maser [8], [15]. This means that an extremely stable center frequency can be attained by negative electrical feedback.

Fig. 3 shows the experimental results for AlGaAs lasers [6]. The curves $FR_1 \sim FR_4$ represent the results for free-running lasers, while the curves $ST_1 \sim ST_3$ are for the lasers under negative electrical feedback. The curves F and H are copies of the curves F and H in Fig. 2, respectively. By comparing curves ST_2 and ST_3 with curve H, it can be seen that the frequency fluctuations were reduced

[1]Strict definitions of frequency stability as well as frequency reproducibility and accuracy of quantum oscillators (lasers, masers, and microwave atomic clocks) have not yet been clearly documented. However, a reasonable example of the definition is found in [19], [20], which are summarized in Appendix II. In the present paper, this definition is employed.

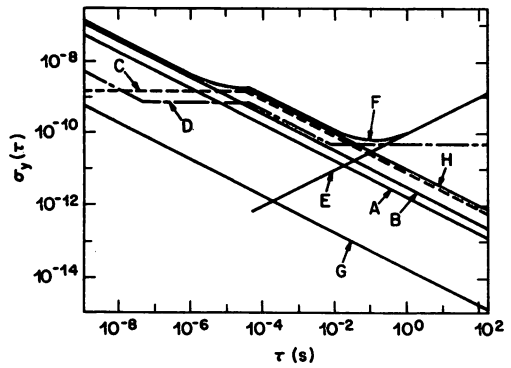

Fig. 2. Calculated results of the square root of the Allan variance $\sigma_y^2(\tau)$ of frequency fluctuations in 0.8-μm AlGaAs lasers [6]. *A*: Fluctuations due to spontaneous emission ($\Gamma_s(t)$ in (1)). *B*: Fluctuations due to carrier density fluctuations (Γ_c (t) in (1)). *C*: Fluctuations by current fluctuations induced by the carrier density fluctuations of the curve *B*. *D*: Fluctuations induced by fluctuations in injection current. *E*: Fluctuations induced by fluctuations in ambient temperature. *F*: Total fluctuations in a free-running laser (superposition of the curves *A*–*E*). *G*: Residual fluctuations in a laser under negative electrical feedback, which are limited by the noise from a detector. *H*: Contributions of quantum noise sources to a free-running laser (superposition of the curves *A*–*C*).

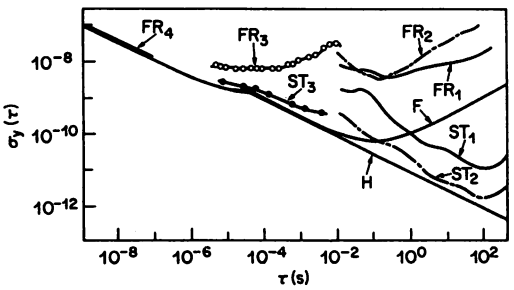

Fig. 3. Experimental results of the square root of the Allan variance of frequency fluctuations in 0.8-μm AlGaAs lasers [6]. FR_1–FR_4: Free-running lasers. ST_1–ST_3: Lasers under negative electrical feedback, for which an absorption spectral line in H_2O vapor, that of Rb vapor, and a Fabry-Perot interferometer were used as frequency references, respectively.

to a value limited by the quantum noise source, i.e., $\sigma_y = 1.4 \times 10^{-12}$ for $\tau = 100$ s. With further improvements in the performance of the servo-control circuit, approach to curve *G* in Fig. 2 can be expected. For 1.5-μm InGaAsP lasers, on the other hand, frequency fluctuations have been reduced to values as low as that of curve ST_1 in Fig. 3 [16], and further reductions can be expected.

It is known empirically that frequency drift cannot be reduced sufficiently for an integration time τ longer than about 1×10^4 s because of the intrinsic noise sources that cause the frequency drift of semiconductor lasers, the finite gain of the integrator in the feedback loop, and the frequency drift generated by the feedback loop itself. An insufficient reduction of the frequency drift would limit the frequency stability which has also been observed for other types of lasers and microwave oscillators [1], [8], [15]. As an example, a blue shift of 26-MHz/h in free-running 0.8-μm AlGaAs lasers has been observed within a period of more than six months even though they were operated under very stable conditions (fluctuations of the heat sink temperature and injection current were reduced to 1×10^{-5} K and 0.6 nA/$\sqrt{\text{Hz}}$ (at the Fourier frequency of 1 kHz), respectively) [27]. This frequency drift has not yet saturated after a continuous operation of more than six months, and cannot be reduced sufficiently due to the finite gain of the present feedback loop. Furthermore, variations in mode-hopping properties have also been observed in the six-month period [17]. The observed long-term variations in spectral properties are attributed to slow temporal decreases of thermal resistance due to the oxidation of the Indium bonding layer or the thermal effects induced by nonradiative recombination of carriers near the facets [27], [28].

These uncontrollable variations would limit the frequency reproducibility of the laser, and the reliability of coherent optical systems. To improve these properties, reduction and stabilizaton of the thermal resistance, and screening of laser devices, are required at the stage of laser fabrication. Detection and compensation of the long-term variations of spectral properties using a microcomputer, which have been employed for microwave oscillators, may be an effective technique applicable to semiconductor lasers [29].

B. Linewidth Reduction of the Field Spectrum

Since the field spectrum is given by the Fourier transform of the autocorrelation function of the amplitude of the laser electric field, its spectral lineshape depends on the magnitude of the phase fluctuation with a slowly varying amplitude. Therefore, the spectral linewidth depends on the magnitude of the phase fluctuation or that of the frequency fluctuation as long as $|y(t)| = |\delta\nu(t)/\nu_0| \ll 1$.

The linewidth can be measured from the beat spectrum between two independent lasers, by a delayed self-heterodyning technique [30], or by using a high-resolution scanning Fabry–Perot interferometer [31]. For accurate measurements, the integration time of the measurements should be long enough to maintain high resolution, which is a consequence of the uncertainty principle between frequency and time. At the same time, this integration time should be short enough to avoid the effect of frequency drift, because the frequency of the free-running laser exhibits a random walk process due to the fluctuation of the ambient temperature or the injection current. Because of these requirements on the integration time, the spectral linewidth is not necessarily an accurate measure of coherence. The power spectral density or the Allan variance of the frequency fluctuation should be used as a primary measure. Since spectral linewidth is used for several applications, however, discussions will be focused on spectral linewidth in this subsection. In this discussion, it is assumed that a suitable integration time has been used for accurate measurements.

The frequency fluctuation induced by spontaneous emission ($\Gamma_s(t)$ of (1)) is a white noise, which gives a Lorentzian lineshape. Its linewidth $\Delta\nu_{ST}$ is given by the Shawlow–Townes formula [32], and is inversely proportional to the laser power and *Q*-factor of the cavity. This formula is applicable to general lasers. In addition to this

linewidth, anomalous dispersion due to carrier density fluctuations ($\Gamma_c(t)$ of (1)) induces an extra broadening of the lineshape, which is a specific broadening mechanism in semiconductor lasers.

The linewidth governed by these two quantum noise sources is given by the modified Schawlow–Townes formula [33]:

$$\Delta\nu_{FR} = \Delta\nu_{ST} \cdot (1 + \alpha^2), \qquad (3)$$

where α is a parameter which represents the magnitude of the contribution from the carrier density fluctuation, and has been called the linewidth enhancement factor. Its value has been reported as 2–6 [6], [33]–[36]. The linewidth given by this formula is larger than those in other kinds of lasers because the cavity Q-factor of the semiconductor laser is smaller and the contribution from the carrier density fluctuation is larger than in other lasers. The measured linewidths are in the range of several megahertz to several hundreds of megahertz. Furthermore, relaxation oscillations due to carrier density fluctuations can induce FM sidebands spaced about 1 GHz from the optical carrier frequency ν_0.

In addition to such a large linewidth, a power-independent linewidth has also been observed, which is about 0.6–0.9 MHz for AlGaAs lasers at room temperature [33], [37]. The origin of this width has been reported to be power-independent carrier density fluctuations [38], thermal fluctuations of electronic state occupancy [39], power independent flicker noise of the electron mobility [40], and so on.

To reduce such a large linewidth by negative electrical feedback, frequency fluctuations for $f \leq \Delta\nu_{FR}$ should be reduced, where f is the Fourier frequency [14]. If the bandwidth of the feedback loop is larger than $\Delta\nu_{FR}$, and if (1) and (2) are valid, the linewidth can be reduced to a value limited by noise contained in the feedback signal. Fig. 4 shows the noise-limited linewidth as a function of the reflectance R_{FP} of the Fabry–Perot interferometer used as a frequency discriminator [14], where it has been assumed again that the principal noise source contained in the feedback signal was from the photodetector, and that a Fabry–Perot interferometer 1 cm long was used as the frequency discriminator. The difference between curves A and B is caused by the difference in the values of excess noise factors (M^x) of a Ge–APD (A) and a Ge–p-i-n (B) photodiode [14]. This figure indicates that a narrow linewidth of about 1 kHz can be obtained. It should be noted that the calculations and experiments discussed in this subsection are for a 1.5-μm InGaAsP laser, while the discussions in other subsections are for a 0.8-μm AlGaAs laser. However, the discussions in this subsection are also applicable to 0.8-μm AlGaAs lasers.

By negative electrical feedback, we have obtained a 330-kHz linewidth for a 1.5-μm InGaAsP laser which has a 5-MHz linewidth under free-running conditions [14]. More recently the linewidth was reduced to 200 kHz, which is 1/25 times that of the free-running laser [41]. It should be pointed out that the field spectrum under electrical feedback was very stable because this feedback is inherently negative, which is not necessarily the case for optical feedback. Fig. 5 shows the progress of our experimental results. This figure shows that recently obtained linewidths are already narrower than $\Delta\nu_{ST}$ of (3) because the value of the linewidth enhancement factor for InGaAsP lasers is about 2.2 [42], i.e., $1 + \alpha^2 = 5.84$. This result indicates that linewidths narrower than that limited by quantum noise sources can be achieved and proves the validity of the argument in Section II.

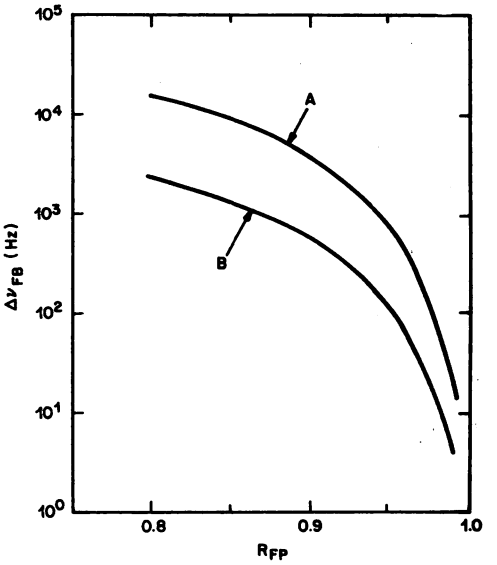

Fig. 4. Calculated results of the relation between the detector-noise-limited linewidth of a 1.5-μm InGaAsP laser and the reflectance R_{FP} of the Fabry–Perot interferometer used as a frequency discriminator [14]. Curves A and B represent the results when a Ge–APD and a Ge–p-i-n photodiode were used in the feedback loop, respectively.

However, the linewidths shown by Fig. 5 are still larger than those of Fig. 4. One of the reasons is the upper limit of the gain of the servoamplifier in the feedback loop, which was imposed to avoid oscillation at a higher Fourier frequency. This oscillation is induced by the phase delays of the direct frequency modulation of the laser, by the response characteristics of the electronic circuits in the feedback loop, and by the finite length of the feedback loop. Fig. 6 shows an example of simulated power spectral density of frequency fluctuations for a laser under negative electrical feedback. For this simulation, the transfer functions of all the components in the feedback loop were estimated by measuring their response characteristics and the phase delay [43] mentioned above. An oscillation can be seen at a Fourier frequency near 30 MHz, at which the phase delay reaches 180°. Using a laser with a small phase delay, reducing the length of the feedback loop, and optimizing the design of the phase compensation circuit in the servoamplifier are required to suppress this oscillation and to increase the feedback gain.

Curve A of Fig. 7 shows the power spectral density of frequency fluctuations for a free-running 1.5-μm InGaAsP laser measured with the present experimental setup [43]. It can be approximated as a white noise for Fourier frequencies lower than 100 MHz. Curve B represents the

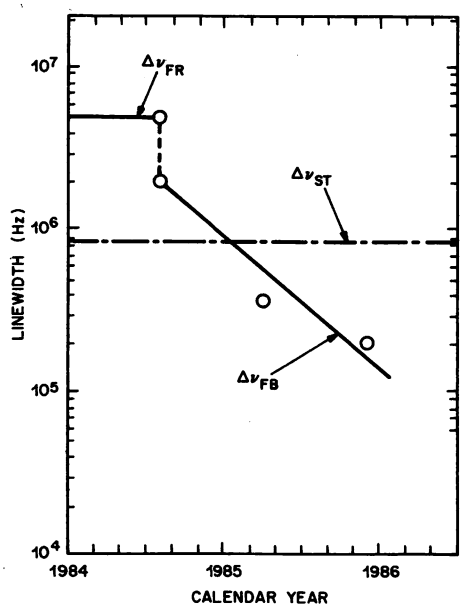

Fig. 5. Progress in linewidth reduction for 1.5-μm InGaAsP lasers by negative electrical feedback [14], [41]. $\Delta\nu_{FB}$: Linewidth under negative electrical feedback. $\Delta\nu_{FR}$: Linewidth of a free-running laser given by (3). $\Delta\nu_{ST}$: Linewidth due to spontaneous emission, which is given by the Schawlow-Townes formula. All the values of linewidth given here were measured at $I/I_{th} = 2.4$, where I and I_{th} represent the dc injection current and its threshold value, respectively.

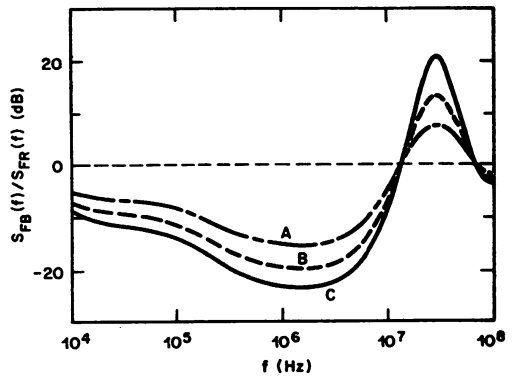

Fig. 6. An example of simulated results of the power spectral densities $S_{FB}(f)$ of frequency fluctuations under negative electrical feedback [43]. This value is normalized to that of the free-running laser $S_{FR}(f)$. The feedback gain was increased in going from curve A to B to C.

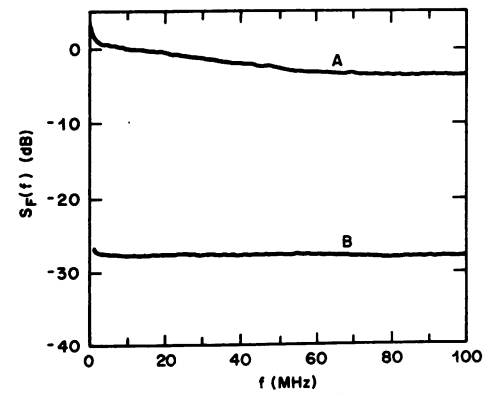

Fig. 7. The power spectral density of frequency fluctuations in a free-running 1.5-μm InGaAsP laser [43]. A: Measured value of frequency fluctuations. B: The noise induced by laser power fluctuations.

noise component contained in the curve A which was induced by laser power fluctuations. This curve was obtained by measuring the laser power fluctuation with the Fabry–Perot interferometer removed from the setup in Fig. 1. An optical attenuator was installed alternatively in front of the detector to adjust precisely the dc laser power. Comparison of curves A and B shows that the signal-to-noise ratio in the frequency fluctuation measurements was about 28 dB (= 600). Assuming that the feedback loop is constructed according to the optimum design mentioned above to maximize its gain, the frequency fluctuation can be reduced until the signal-to-noise ratio is decreased to unity. Therefore, Fig. 7 shows that the linewidth can be reduced to about 1/600 times that of a free-running laser using the present experimental setup, because the linewidth is proportional to the magnitude of the power spectral density, as long as it can be approximated as white noise.

Increases in laser power fluctuation should be taken into account for this estimation because the InGaAsP laser (DFB type) used for Figs. 5 and 7 is a conventional one which has only one electrode. For such a conventional laser, the laser power fluctuations usually increase when the injection current is controlled to reduce the frequency fluctuations [44]. Calculations were carried out using Fig. 7 to estimate these increases. The result confirmed that the increases were less than 10 percent of the fluctuation in a free-running laser, which does not sacrifice much of the accuracy of the estimated limit for linewidth reduction using electrical feedback. It can then be concluded that the optimal feedback loop in the present experimental setup can reduce the linewidth to about 1/600 times that of the free-running laser, i.e., to about 8 kHz.

A novel type of semiconductor laser has been developed recently whose cavity is divided into two parts with segmented electrode [45]–[48]. One segment was used as an active region for laser oscillation, and the other was used as a phase modulator. If the injection currents for both parts are simultaneously controlled in a mutually correlated manner, frequency fluctuations can be reduced while maintaining low enough power fluctuations to improve the coherence. For example, direct frequency modulation characteristics have been improved by controlling the currents applied to the segmented electrode for applications in coherent optical communications [49].

Further increases in the total gain of the feedback loop can be expected if the sensitivity of frequency discrimination is increased. In the case of Figs. 5 and 7, it can be realized by using a Fabry–Perot interferometer with a higher resolution. Fig. 8 shows the relation between the width of the resonance curve of the Fabry–Perot interferometer $\Delta\nu_{FP}$ and the detector-noise-limited linewidth of the laser under electrical feedback [43]. For this estimation, it was assumed that the required phase compensation discussed above was made by the optimum design of the servoamplifier. Since $\Delta\nu_{FP}$ is inversely proportional to the sensitivity of frequency discrimination, the noise-limited linewidth decreases with decreasing $\Delta\nu_{FP}$, which is rep-

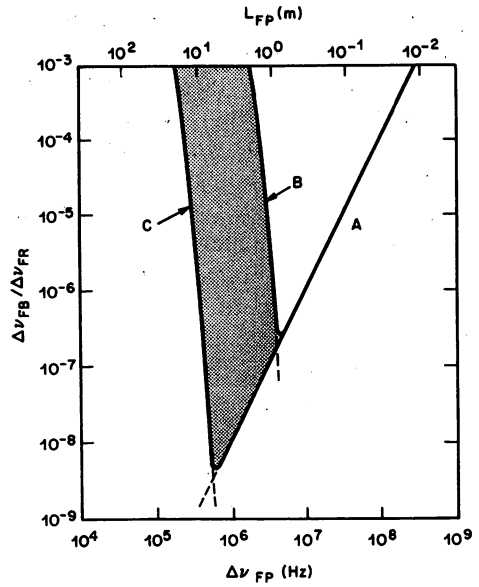

Fig. 8. Relation between the detector-noise-limited linewidth $\Delta\nu_{FB}$ of a 1.5-μm InGaAsP laser under feedback and the width of the resonance curve of a Fabry–Perot interferometer $\Delta\nu_{FP}$ used as a frequency discriminator [43]. The linewidth $\Delta\nu_{FB}$ is normalized to that of the free-running laser $\Delta\nu_{FR}$. L_{FP}: the length of the interferometer, where the reflectances of its mirrors were assumed as 90 percent. The linewidth $\Delta\nu_{FB}$ is decreased with decreasing $\Delta\nu_{FP}$, i.e., increasing the feedback gain, which is represented by the curve A. Further decreases in $\Delta\nu_{FP}$ would induce a rebroadening of $\Delta\nu_{FB}$, which is represented by the meshed area between the curves B and C.

resented by curve A. This increase in sensitivity is equivalent to the technique of employing the ultranarrow spectral line of two-photon optical Ramsey spectroscopy described in Section II. In the present case, however, a decrease in $\Delta\nu_{FP}$ would also reduce the bandwidth of the feedback loop and induce a rebroadening of the laser linewidth, because $\Delta\nu_{FP}$ gives the response bandwidth of the interferometer. This effect is represented by the meshed area between curves B and C in this figure. This figure shows that a linewidth about 10^{-8}–10^{-7} times that of a free-running laser, i.e., a subhertz linewidth, can be obtained if $\Delta\nu_{FP}$ is about 1–10 MHz. This subhertz linewidth is predicted by neglecting the effect of the increase in power fluctuations of a conventional laser, which was estimated earlier to be less than 10 percent of that of a free-running laser [43].

A long Fabry–Perot interferometer has been fabricated recently using low-loss optical fiber [50]–[51]. It can be used as a sensitive frequency discriminator if the value of $\Delta\nu_{FP}$ is adjusted to about 1 MHz–10 MHz. The length of such an interferometer is given on the abscissa of Fig. 8, where the reflectances of the end mirrors of the interferometer are assumed to be 90 percent. It is seen that the minimum laser linewidth is obtained when the length of the fiber is about 1–10 m. Such a fiber interferometer can be wound around a small cylinder to reduce the volume of the system.

Even though the FM noise at the tail of field spectrum is not reduced because of the finite bandwidth of the electrical feedback loop, it has been confirmed that the profile around the peak of the field spectrum can be well approximated as a very narrow Lorentzian [41], [43]. Therefore, electrical feedback can be an effective technique to improve temporal coherence of light sources especially for low-to-medium bit rate coherent optical communication and narrow bandwidth sensing systems such as the fiber gyroscope.

C. Frequency Tracking to a Highly Coherent Master Laser

The technique of frequency tracking of a slave laser to a highly coherent master laser can be very useful for applications to coherent/heterodyne optical communications, heterodyne optical measurements, and so on. A frequency offset locking method proposed by the author as a stable and accurate technique for frequency tracking [52], [53] is described in this subsection.

The experimental setup is shown in block (3) of Fig. 1. The injection current of the slave laser is controlled to lock the divided beat frequency between the slave and master lasers to the frequency of a microwave local oscillator. By this negative electrical feedback, the frequency of the slave laser ν_S is given by

$$\nu_S = \nu_M \pm \nu_B = \nu_M \pm M \cdot \nu_L \qquad (4)$$

where ν_M, ν_B, and ν_L are frequencies of the master laser, beat signal, and the microwave oscillator, respectively. The integer M represents a division rate of the beat frequency provided by a prescaler. This formula shows that the locked frequency of the slave laser is offset by $\pm M \cdot \nu_L$ with respect to the frequency of the master laser. This technique is called frequency offset locking. It has been employed for gas lasers [9], [54]. For semiconductor lasers, it has been used in experimental coherent/heterodyne optical communication systems [55], [56]. Since accurate performance evaluations have not yet been fully documented for semiconductor lasers, improved experiments were carried out in the present study.

Instead of controlling the frequency of the beat signal, its phase, i.e., the time integral of frequency, was controlled in the present experiments to reduce the frequency drift and to improve the accuracy of frequency tracking. For this purpose, the phase of the beat signal was compared with that of the microwave oscillator using a digital phase comparator which consisted of binary up-counters, down-counters, full adders, and a D/A converter. This scheme is partly equivalent to a phase locked loop for a conventional electronic circuit (see, for example, [57]). To detect a large phase fluctuation, however, the dynamic range of the present phase comparator was designed to be $2\pi \times 2^{11}$ rad, which was much larger than that of a conventional phase locked loop for electronic circuits.

Experiments were carried out for 0.8-μm AlGaAs lasers. Figs. 9(a) and (b) show waveforms of output signals from the phase comparator under free-running and frequency offset locked conditions, respectively. Fig. 9(c) shows the fluctuation of the beat frequency. It is seen that the beat frequency was tightly locked by the present phase

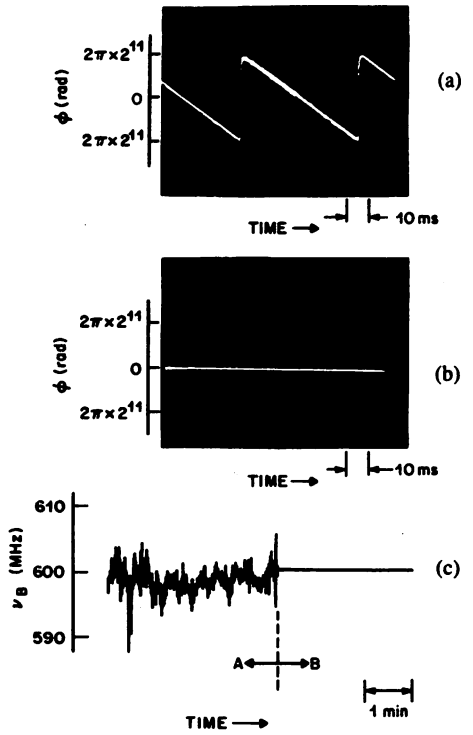

Fig. 9. Output signals from a phase comparator under (a) free-running, and (b) frequency offset locking conditions [53]. The ordinates of these figures represent a phase difference between the signal from the microwave oscillator and the beat signal whose frequency has been divided by M. (c) Fluctuations in the beat frequency ν_B. Parts A and B represent the waveforms under free-running and frequency offset locked conditions, respectively [53], where M was fixed at 500 and the locked value of ν_B was 0.6 GHz.

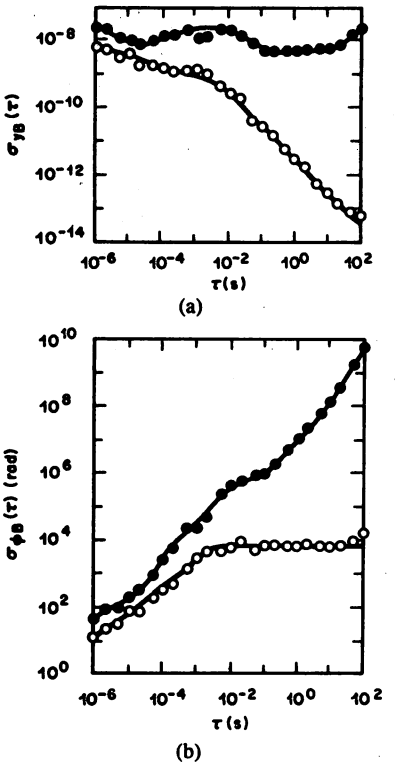

Fig. 10. The square roots (a) of the Allan variance $\sigma^2_{yB}(\tau)$ of the normalized frequency fluctuations, and (b) that of $\sigma^2_{\phi B}(\tau)$ of the phase fluctuations in the beat signal [53]. The black and white circles represent the values under free-running and frequency offset locked conditions, respectively.

control scheme. The bandwidth of the feedback loop was 1 MHz. As will be shown in Section III-D the locking range of the beat frequency was 1.58 GHz. On the other hand, it was determined empirically that the capture range of the beat frequency was 1.22 GHz, i.e., the free-running beat frequency ν_B can be fixed at $M \cdot \nu_L$ if ν_B stayed within this range. Such a large capture range was due to the large dynamic range of the phase comparator mentioned above. The capture range was limited mainly by the response speed of the photodiode (a Si-APD used in the present experiments) and the prescaler.

Fig. 10(a) shows the square root of the Allan variance $\sigma^2_{yB}(\tau)$ of the beat frequency fluctuation, which is normalized to the nominal laser frequency ($y_B(t) = \delta\nu_B(t)/\nu_0$) [53]. A computerized Allan-variance real-time processing system was developed and used for these measurements [53], [58]. Since the directly controlled quantity was not the frequency of the beat signal but its phase, the Allan variance $\sigma^2_{\phi B}(\tau)$ of the phase fluctuations was also estimated from Fig. 10(a) and is given by Fig. 10(b), where the relation $\sigma^2_{\phi B}(\tau) = (2\pi\nu_0\tau)^2 \cdot \sigma^2_{yB}(\tau)$ was used. Reductions in frequency and phase fluctuations by the frequency offset locking technique are clearly seen in these figures. It is also seen that the effects of frequency offset locking increases with the integration time, which means that frequency drift was sufficiently reduced. For example, Fig. 10(a) shows that $\sigma_{yB}(\tau) = 3 \times 10^{-14}$ for $\tau =$ 100 s, i.e., the residual frequency fluctuation was as low as 11 Hz.

In the present experiments, the beat frequency fluctuation was reduced to a value limited by the noise due to round-off error in pulse number counting, which was generated at the D/A converter in the phase comparator. The magnitude of this error was multiplied by M to give the magnitude of the noise. The magnitudes of other noise, e.g., the detector noise, were estimated to be lower than this noise. Further reduction in the beat frequency fluctuation can be expected with a lower division rate M obtained by using a faster phase comparator and a higher frequency microwave oscillator.

Since frequencies of the master laser and the beat signal were locked by different and independent feedback loops, their residual fluctuations were uncorrelated. Therefore, the Allan variance of the frequency fluctuation of the slave laser can be expressed as

$$\sigma^2_{yS} = \sigma^2_{yM} + \sigma^2_{yB}. \tag{5}$$

Since it can be approximated that $\sigma^2_{yM} >> \sigma^2_{yB}$ for $\tau \geq 1$ μs by comparing Fig. 10(a) with the curves $ST_1 - ST_3$ in Fig. 3, (5) means that $\sigma^2_{yS} \cong \sigma^2_{yM}$, i.e., the residual frequency fluctuation of the slave laser was as low as that of the master laser. From this estimation, it is confirmed that accurate frequency tracking of the slave laser to the master laser was realized. In other words, the high coherence of the master laser was transferred to the slave laser.

D. Stable and Wide-Band Frequency Tuning

A highly stable, reproducible, and accurate technique for wide-band frequency tuning is required for several applications. Frequency offset locking can also be considered as a candidate for such a technique. In this technique, the slave laser frequency can be swept in a stable manner by sweeping the microwave frequency with a sweep speed which falls within the bandwidth of the feedback loop. Fig. 11 shows the beat frequency ν_B which was varied by stepwise sweep of the microwave frequency at a 20-MHz interval. Here, the division rate M of the prescaler was fixed at 500 for $\nu_B < 0.7$ GHz, and at 2000 for $\nu_B \geq 0.7$ GHz, respectively, which was required because of the limited bandwidth of the prescalar used. As shown in this figure, a stable sweep was carried out for 24 MHz $\leq \nu_B \leq$ 1.6 GHz. This means that the locking range of the beat frequency was 1.58 GHz and the frequency tuning range of the slave laser was 3.16 GHz. The locking range was limited by the following factors: the sensitivity of phase comparison was not high enough for $\nu_B < 24$ MHz because of the low phase fluctuation which was proportional to the beat frequency; for $\nu_B > 1.6$ GHz, on the other hand, the sensitivity was also reduced because of the limited response speed of the Si–APD and of the prescaler.

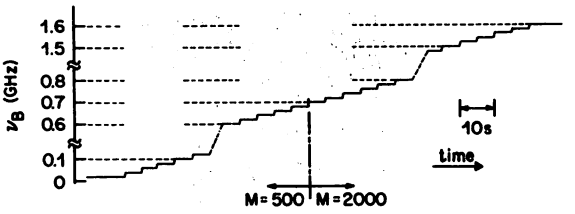

Fig. 11. The beat frequency ν_B which was varied by a stepwise sweep of the microwave frequency of a 20-MHz interval [53]. The division rate M of the prescaler was fixed at 500 for $\nu_B < 0.7$ GHz, and 2000 for $\nu_B \geq 0.7$ GHz.

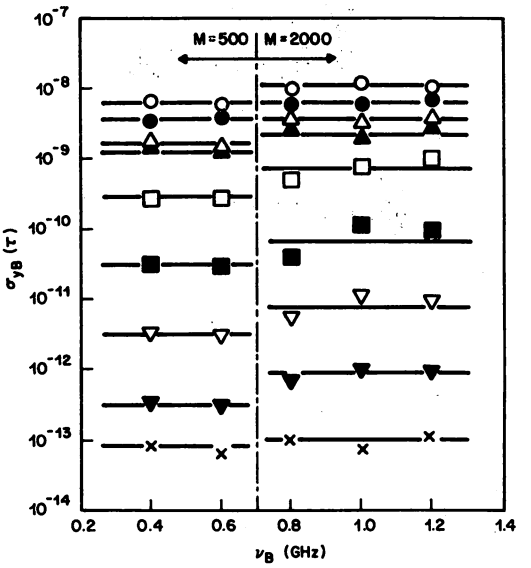

Fig. 12. The relation between the square roots of the Allan variance $\sigma^2_{y_B}(\tau)$ and the beat frequency ν_B within its locking range [53]. The integration time τ of the fluctuation measurements were 1 μs (○), 10 μs (●), 100 μs (△), 1 ms (▲), 10 ms (□), 100 ms (■), 1 s (▽), 10 s (▼), and 100 s (×).

As shown in Fig. 12, it was confirmed that within the locking range the magnitude of frequency fluctuation is independent of the beat frequency. In this figure, fluctuations for $\nu_B \geq 0.7$ GHz are slightly larger than those for $\nu_B < 0.7$ GHz due to the contribution of a round-off error from the phase comparator, which is proportional to the division rate M of the prescaler, as was explained in Section III-C.

There are two promising ways to further increase the range of stable frequency tuning of the slave laser. They are schematically explained by Fig. 13(a) and (b). As shown by Fig. 13(a), one of the methods is to achieve discrete tuning of the master laser frequency by locking it to successive frequencies of a frequency reference grid which are nearly equally spaced. For each locked frequency of the master laser, the frequency offset locking technique is applied to the slave laser. By this control scheme, a stable and accurate sweep of the slave laser frequency can be realized. Absorption spectral lines of combination tones or higher harmonics of vibration-rotation transitions in organic molecules can be used as a frequency reference grid. This is because a large number of lines are distributed within a several gigahertz or several tens of gigahertz interval in the near infrared wavelength region and some of their absolute frequencies have already been calibrated with an accuracy of about 1×10^{-6} to 7×10^{-8} [23], [26]. Spectral lines of electronic transitions in I_2 vapor can be a very promising frequency reference grid for shorter wavelength, visible semiconductor lasers in the future [59], [60].

In the present experiment, equally spaced resonance frequencies of a Fabry–Perot interferometer were used as a simple frequency reference grid. The master laser frequency was locked to fifteen successive resonance frequencies. For each locked frequency of the master laser, frequency offset locking was applied to the slave laser to reduce the fluctuations in the beat frequency to values as low as those shown in Figs. 10 and 12. By this locking method, the stable frequency tuning range of the slave laser was extended to 47.4 GHz.

The number of lines of a frequency reference grid to which the master laser can be locked was limited by mode-hopping phenomena in the master laser. A laser without mode-hopping can improve the frequency tuning range. A recently developed 1.5-μm InGaAsP DFB laser may be used for this purpose because its wavelength can be continuously varied over 15 nm without mode-hopping by temperature change under free-running condition. This corresponds to a frequency range of 2 THz [61]. A stable wide-band frequency tuning of more than 1 THz can be expected if these kinds of lasers are employed with frequency offset locking.

The second method is to prepare a number of slave lasers and to apply frequency offset locking to adjacent lasers using a common microwave oscillator. This is schematically illustrated in Fig. 13(b). Since the frequency of

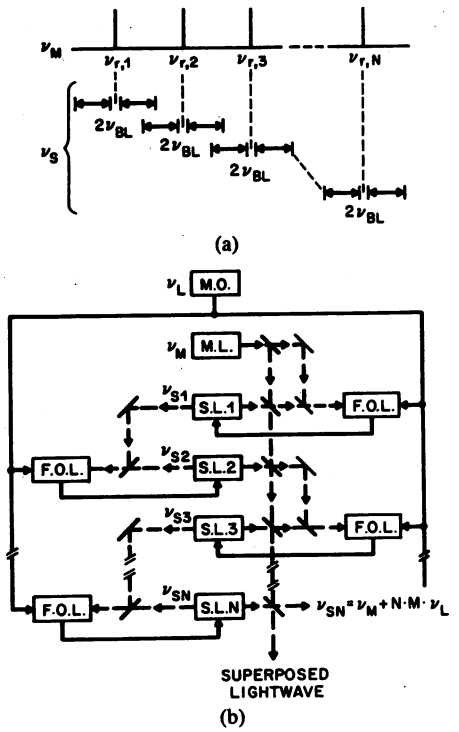

Fig. 13. Two possible ways of extending the range of stable frequency sweep of the slave laser. (a) The master laser frequency ν_M is successively locked to one of the reference grid frequencies ($\nu_{r,1} < \nu_{r,2} < \cdots < \nu_{r,N}$). For each locked frequency of the master laser, frequency offset locking is applied to the slave laser. ν_{BL}: The locking range of the beat frequency. (b) A number of slave lasers are prepared and frequency offset locking is applied between each of the adjacent lasers by using a common microwave oscillator. Since the frequency of the Nth slave laser ν_{SN} can be fixed at $\nu_M + N \cdot M \cdot \nu_L$, it can be swept over a wide range by sweeping ν_L. M.O.: microwave oscillator. M.L.: master laser. S.L.i: ith slave laser ($i = 1, 2, \cdots, N$). F.O.L.: servocontrol circuit for frequency offset locking.

the Nth slave laser can be fixed at $\nu_M + N \cdot M \cdot \nu_L$, the range of stable frequency tuning for this laser becomes N times wider than that of the first slave laser. Such a frequency offset locked laser array is of interest for ultrashort light pulse generation because the lightwave superposed by all the laser beams from the array is mode locked. This is because the frequency difference between neighboring slave lasers is fixed at $M \cdot \nu_L$, and all lasers have the common high-coherence property of the master laser. Generation of an ultrashort light pulse train can be expected if the lightwaves from all the lasers are superposed under appropriate conditions and the value of $N \cdot M \cdot \nu_L$ is large enough. The absolute frequency of the mode locked laser system is stable because the master laser frequency is tightly locked to a stable reference frequency.

In principle, the techniques shown in Fig. 13 can be applied to conventional semiconductor lasers. However, it would be more advantageous to use longitudinal-mode stabilized lasers (e.g., DFB, DBR, C^3 lasers, and so on) to avoid mode-hopping, which limits the range of continuous frequency tuning.

IV. Summary

Negative electrical feedback is proposed as a promising technique for simultaneously meeting four requirements for ultrahigh coherence in semiconductor lasers. Theoretical estimations show that the frequency fluctuation can be reduced to a value limited by noise contained in the feedback signal, which is lower than the value limited by quantum noise sources of the laser. Recent experimental results, by the author, are reviewed. They are summarized as follows.

1) Stability of the center frequency of field spectrum: $\sigma_y(\tau) = 1.4 \times 10^{-12}$ for $\tau = 100$ s (for a 0.8-μm AlGaAs laser).
2) Linewidth of the field spectrum: 200 kHz, which is 1/25 times that of the free-running laser (for a 1.5-μm InGaAsP laser). It is estimated to be narrower than the value given by the Schawlow–Townes formula.
3) Frequency tracking: the capture range of the beat frequency is about 1.22 GHz, and the stability of the beat frequency is $\sigma_{yB}(\tau) = 3 \times 10^{-14}$ for $\tau = 100$ s (for a 0.8-μm AlGaAs laser).
4) Stable frequency tuning: the locking range of the beat frequency using the frequency offset method is 1.58 GHz, and the total frequency tuning range of the slave laser is 47.4 GHz. Stability of the beat frequency as high as that of 3) is maintained (for a 0.8-μm AlGaAs laser).

An improved experimental setup is now under preparation to achieve higher coherence. Further improvements in the performance of this system can be expected when a novel integrated laser device with lower drift and improved FM response characteristics are used in the future.

Appendix I
List of Symbols

F	Fourier transform of $\delta\nu(t)$.
f	Fourier frequency.
H	Fourier transform of $h_f(t)$.
$h_f(t)$	Impulse response of the feedback loop.
L_{FP}	Length of a Fabry–Perot interferometer.
M	Division rate of the beat frequency provided by a prescalar.
N	Number of lines of frequency reference grid, or number of slave lasers.
R_{FP}	Reflectance of mirrors of a Fabry–Perot interferometer.
$S_F(f)$	Power spectral density of frequency fluctuations.
$S_{FB}(f)$	Power spectral density of frequency fluctuations of a laser under negative electrical feedback.
$S_{FR}(f)$	Power spectral density of frequency fluctuations of a free-running laser.
t	Time.
t'	Time.
y	Normalized frequency fluctuations.
$y_B(t)$	Normalized beat frequency fluctuations.
α	Linewidth enhancement factor.

$\Gamma_c(t)$ Langevin's force of carrier density fluctuations.
$\Gamma_n(t)$ Langevin's force of the noise contained in the feedback signal.
$\Gamma_s(t)$ Langevin's force of spontaneous emission.
$\Delta\nu_{FB}$ Laser linewidth under negative electrical feedback.
$\Delta\nu_{FP}$ Width of a resonance curve of a Fabry–Perot interferometer.
$\Delta\nu_{FR}$ Linewidth of a free-running laser.
$\Delta\nu_{ST}$ Linewidth given by the Schawlow–Townes formula.
$\delta\nu(t)$ Frequency fluctuations.
$\delta\nu_B(t)$ Beat frequency fluctuations.
$\delta\phi(t)$ Phase fluctuations.
ν_B Beat frequency.
ν_{BL} Locking range of the beat frequency.
ν_L Signal frequency from a microwave local oscillator.
ν_M Frequency of a master laser.
ν_0 Nominal frequency of the laser, i.e., optical carrier frequency.
$\nu_{r,i}$ The ith reference frequency provided by a frequency reference grid ($i = 1 \sim N$).
ν_S Frequency of a slave laser.
$\nu_{S,i}$ Frequency of the ith slave laser ($i = 1 \sim N$).
Π_c Fourier transform of Γ_c.
Π_n Fourier transform of Γ_n.
Π_s Fourier transform of Γ_s.
$\sigma_y^2(\tau)$ Allan variance of normalized frequency fluctuations.
$\sigma_{yB}^2(\tau)$ Allan variance of the normalized beat frequency fluctuations.
$\sigma_{yM}^2(\tau)$ Allan variance of the normalized frequency fluctuations of a master laser.
$\sigma_{yS}^2(\tau)$ Allan variance of the normalized frequency fluctuations of a slave laser.
$\sigma_{\phi B}^2(\tau)$ Allan variance of the phase fluctuations of the beat signal.
τ Integration time.
ϕ Phase.

Appendix II

In the present paper, definitions of frequency stability, reproducibility, and accuracy of quantum oscillators follow those of [19] and [20], and are summarized as follows:

Stability: A sequence of N readings of a particular oscillator frequency in a particular adjustment, against a comparison oscillator assumed temporally constant, will show fluctuations. The standard deviation of these observations is often called the stability [19].

Reproducibility: A sequence of comparisons for independent adjustments of a particular oscillator frequency, against a reference oscillator frequency available and temporally constant, will yield a standard deviation. The standard deviation of such observations may be called the reproducibility. In this sense, reproducibility indicates the degree of resettability of the frequency [19].

Accuracy: Accuracy means fractional uncertainty in determining an atomic transition frequency of the free atom and is expressed by 3σ limits for statistically determined frequencies [20].

Acknowledgment

The author would like to express his thanks to Dr. K. Nakagawa of NTT Trunk Transmission Division for providing the opportunity for this publication, and to Dr. T. Yamamoto and Dr. S. Akiba of KDD Research and Development Laboratories for valuable discussions. He is also much indebted to his graduate students, S. Kotajima, K. Kuboki, N. Tabuchi, and T. Ouchi, for their intensive support to this work.

References

[1] A. Brillet and P. Cerez, "Laser frequency stabilization by saturated absorption," *J. Physique*, vol. 42, pp. 73–82, 1981.
[2] T. Okoshi, "Recent progress in heterodyne/coherent optical-fiber communications," *J. Lightwave Technol.*, vol. LT-2, pp. 341–346, 1984.
[3] M. Fleming and A. Mooradian, "Spectral characteristics of external-cavity controlled semiconductor lasers," *IEEE J. Quantum Electron.*, vol. QE-17, pp. 44–59, 1981.
[4] F. Favre, D. Le Guen, and J. C. Simon, "Optical feedback effects upon laser diode oscillation field spectrum," *IEEE J. Quantum Electron.*, vol. QE-18, pp. 1712–1717, 1982.
[5] K. H. Cameron, M. R. Matthews, T. G. Hodgikinson, and W. J. Devlin, "Frequency-stable packaged 20-kHz linewidth 1.5-μm InGaAsP external cavity laser used in an experimental heterodyne optical fiber system," in *Tech. Dig. Conf. Lasers and Electrooptics* (Baltimore, MD), May 21–24, 1985, pap. TUC5.
[6] M. Ohtsu, H. Fukada, T. Tako, and H. Tsuchida, "Estimation of the ultimate frequency stability of semiconductor lasers," *Japan J. Appl. Phys.*, vol. 22, pp. 1157–1166, 1983.
[7] S. Kobayashi and T. Kimura, "Injection locking in AlGaAs semiconductor laser," *IEEE J. Quantum Electron.*, vol. QE-17, pp. 681–689, 1981.
[8] P. Kartaschoff, *Frequency and Time*. London, U.K.: Academic, 1978.
[9] M. Ohtsu, S. Katsuragi, and T. Tako, "Performance of a frequency-offset locked He-Xe laser system at 3.51 μm," *IEEE J. Quantum Electron.*, vol. QE-17, pp. 1100–1106, 1981.
[10] J. L. Hall, D. Hills, C. Salomon, and M. Rayman, "Stable lasers: Progress and applications," in *Tech. Dig. Conf. Lasers and Electrooptics* (Baltimore, MD), May 21–24, 1985, pap. FM3.
[11] K. Ikeda, "Multiple-valued stationary state and its instability of the transmitted light by a ring cavity system," *Opt. Commun.*, vol. 30, pp. 257–261, 1979.
[12] H. Kawaguchi and K. Otsuka, "A new class of instabilities in a diode laser with an external cavity," *Appl. Phys. Lett.*, vol. 45, pp. 934–936, 1984.
[13] R. Lang and K. Kobayashi, "External optical feedback effects on semiconductor injection laser properties," *IEEE J. Quantum Electron.*, vol. QE-16, pp. 347–355, 1980.
[14] M. Ohtsu and S. Kotajima, "Linewidth reduction of a semiconductor laser by electrical feedback," *IEEE J. Quantum Electron.*, vol. QE-21, pp. 1905–1912, 1985.
[15] *Proc. IEEE* (Special Issue on Frequency Stability), vol. 54, no. 2, Feb. 1966; also *J. Physique*, tome 42, Colloque C-8, supplement au no. 12, Dec. 1981.
[16] Y. Yamamoto, O. Nilsson, and S. Saito, "Theory of negative frequency feedback semiconductor laser," *IEEE J. Quantum Electron.*, vol. QE-21, pp. 1919–1928, 1985.
[17] H. Haug, "Quantum-mechanical rate equation for semiconductor lasers," *Phys. Rev.*, vol. 184, pp. 338–347, 1969.
[18] R. G. Beausoleil and T. W. Hansch, "Two-photon optical Ramsey spectroscopy of freely falling atoms," *Opt. Lett.*, vol. 10, pp. 547–549, 1985.

[19] R. E. Beehler, R. C. Mockler, and J. M. Richardson, "Cesium beam atomic time and frequency standards," *Metrologia*, vol. 1, pp. 114–131, 1965.
[20] R. E. Beehler and D. J. Glaze, "The performance and capability of cesium beam frequency standards at the National Bureau of Standards," *IEEE Trans. Instrum. Meas.*, vol. IM-15, pp. 48–55, 1966.
[21] D. W. Allan, "Statistics of atomic frequency standards," *Proc. IEEE*, vol. 54, pp. 221–230, 1966.
[22] H. Tsuchida, M. Ohtsu, and T. Tako, "Frequency stabilization of AlGaAs semiconductor laser to the absorption line of water vapor," *Japan J. Appl. Phys.*, vol. 21, pp. L1–L3, 1982.
[23] K. Fukuoka, M. Ohtsu, and T. Tako, "Accurate wavelength measurements of the absorption lines in H_2O vapor by a 0.8-μm AlGaAs laser," *Japan J. Appl. Phys.*, vol. 23, pp. L117–L120, 1984.
[24] T. Yabuzaki, A. Ibaragi, H. Hori, M. Kitano, and T. Ogawa, "Frequency-locking of a GaAlAs laser to a Doppler-free spectrum of the Cs-D_2 line," *Japan J. Appl. Phys.*, vol. 20, pp. L451–L454, 1981.
[25] H. Tsuchida, M. Ohtsu, T. Tako, N. Kuramochi, and N. Oura, "Frequency stabilization of AlGaAs semiconductor laser based on the ^{85}Rb-D_2 line," *Japan J. Appl. Phys.*, vol. 21, pp. L561–L563, 1982.
[26] M. Ohtsu, H. Kotani, and H. Tagawa, "Spectral measurements of NH_3 and H_2O for pollutant gas monitoring by 1.5-μm InGaAsP/InP lasers," *Japan J. Appl. Phys.*, vol. 22, pp. 1553–1557, 1983.
[27] M. Ohtsu, M. Hashimoto, and H. Ozawa, "A highly stabilized semiconductor laser and its application to optically pumped Rb atomic clock," *Proc. 39th Ann. Symp. Frequency Control* (Philadelphia, PA), May 29–31, 1985, pp. 43–53.
[28] F. Favre and D. Le Guen, "Emission frequency stability in single-mode-fiber optical feedback controlled semiconductor lasers," *Electron. Lett.*, vol. 19, pp. 663–665, 1983.
[29] H. Okazaki, M. Ohtsu, and T. Tako, "Frequency control of semiconductor lasers using a microcomputer," *Trans. IECE Japan*, vol. J67-C, pp. 651–655, 1984 (in Japanese).
[30] T. Okoshi, K. Kikuchi, and A. Nakayama, "Novel method for high resolution measurement of laser output spectrum," *Electron. Lett.*, vol. 16, pp. 630–631, 1980.
[31] T. Takakura, K. Iga, and T. Tako, "Linewidth measurements of a single longitudinal mode AlGaAs laser with a Fabry-Perot interferometer," *Japan J. Appl. Phys.*, vol. 19, pp. 725–727, 1980.
[32] A. Blaquiere, "Spectre d'un oscillateur maser; relation avec la theorie des autooscillateurs nonlineares classiques," *Compt. rend.*, vol. 26, pp. 2929–2931, 1962.
[33] D. Welford and A. Mooradian, "Output power and temperature dependence of the linewidth of single-frequency CW (GaAl)As diode lasers," *Appl. Phys. Lett.*, vol. 40, pp. 865–867, 1982.
[34] C. Henry, "Theory of the linewidth of semiconductor lasers," *IEEE J. Quantum Electron.*, vol. QE-18, pp. 259–264, 1982.
[35] I. D. Henning and J. V. Collins, "Measurements of the semiconductor laser linewidth broadening factor," *Electron. Lett.*, vol. 19, pp. 927–929, 1983.
[36] K. Kikuchi and T. Okoshi, "Estimation of linewidth enhancement factor of AlGaAs lasers by correlation measurement between FM and AM noises," *IEEE J. Quantum Electron.*, vol. QE-21, pp. 669–673, 1985.
[37] W. Elsasser, E. O. Gobel, and J. Kuhl, "Coherence properties of gain- and index guided semiconductor lasers," *IEEE J. Quantum Electron.*, vol. QE-19, pp. 981–985, 1983.
[38] D. Welford and A. Mooradian, "Observation of linewidth broadening in (GaAl)As diode lasers due to electron number fluctuations," *Appl. Phys. Lett.*, vol. 40, pp. 560–562, 1982.
[39] K. Vahala and A. Yariv, "Occupation fluctuation noise: A fundamental source of linewidth broadening in semiconductor lasers," *Appl. Phys. Lett.*, vol. 43, pp. 760–764, 1984.
[40] M. Ohtsu and S. Kotajima, "Derivation of the spectral width of a 0.8-μm AlGaAs laser considering $1/f$ noise," *Japan J. Appl. Phys.*, vol. 23, pp. 760–764, 1984.
[41] M. Ohtsu, "Attempts at realizing ultrahigh coherence in semiconductor lasers," in *Pap. Tech. Group IECE Japan*, Dec. 23, 1985, no. OQE-123 (in Japanese).
[42] K. Kikuchi and T. Okoshi, "Measurement of field spectra of 1.3-μm InGaAsP DFB lasers," *Electron. Lett.*, vol. 21, pp. 217–218, 1985.
[43] N. Tabuchi, T. Ouchi, and M. Ohtsu, "Linewidth reduction of a semiconductor laser by electrical feedback," in *Pap. Tech. Group IECE Japan*, June 1986 (in Japanese).
[44] H. Tsuchida and T. Tako, "Relation between frequency and intensity stabilities in AlGaAs semiconductor laser," *Japan J. Appl. Phys.*, vol. 22, pp. 1152–1156, 1983.
[45] Y. Tohmori, Y. Suematsu, H. Tsushima, and S. Arai, "Wavelength tuning of GaInAsP/InP integrated laser with butt-jointed built-in distributed Bragg reflector," *Electron. Lett.*, vol. 19, pp. 656–657, 1983.
[46] L. D. Westbrook, A. W. Nelson, P. J. Fiddyment, and J. V. Collins, "Monolithic 1.5-μm hybrid DFB/DBR lasers with 5-nm tuning range," *Electron. Lett.*, vol. 20, pp. 957–959, 1984.
[47] M. Yamaguchi, M. Kitamura, S. Murata, I. Mito, and K. Kobayashi, "Wide range wavelength tuning in 1.3-μm DBR-DC-PBH-LD's by current injection into the DBR region," *Electron. Lett.*, vol. 21, pp. 653–656, 1985.
[48] Y. Tohmori, K. Komori, S. Arai, Y. Suematsu, and H. Oohashi, "Wavelength tunable 1.5-μm GaInAsP/InP bundle-integrated-guide distributed Bragg reflector (BIG = DBR) lasers," *Trans. IECE Japan*, vol. E68, pp. 788–790, 1985.
[49] S. Yamazaki, K. Emura, M. Shikada, M. Yamaguchi, and I. Mito, "Realization of flat FM response by directly modulating a phase tunable DFB laser diode," *Electron. Lett.*, vol. 2, pp. 283–285, 1985.
[50] L. F. Stokes, M. Chodorow, and H. J. Shaw, "All-single-mode fiber resonator," *Opt. Lett.*, vol. 7, pp. 288–290, 1982.
[51] S. Araki and M. Ohtsu, "A ring Fabry-Perot type fiber gyroscope for earthquake detection and prediction," in *Pap. Tech. Group IECE Japan*, Mar. 17, 1986, no. OQE85-170 (in Japanese).
[52] K. Kuboki and M. Ohtsu, "Frequency offset locking of semiconductor lasers," in *Pap. Tech. Group IECE Japan*, June 17, 1985, no. OQE85-29 (in Japanese).
[53] M. Ohtsu, "Demonstration and application of frequency stabilization and linewidth reduction in semiconductor lasers," in *Tech. Dig. Conf. Lasers and Electrooptics* (San Francisco, CA), June 9–13, 1986, pap. WB4.
[54] J. L. Hall and C. J. Borde, "Measurement of methane hyperfine structure using laser saturated absorption," *Phys. Rev. Lett.*, vol. 30, pp. 1101–1104, 1973.
[55] F. Favre and D. Le Guen, "Spectral narrowing by optical feedback," in *Proc. Int. Conf. Lasers '83* (San Francisco, CA), Dec. 12–16, 1983, R. C. Powell, Ed. McLean, VA: STS Press, 1984, pp. 79–84.
[56] K. Emura, M. Shikada, S. Fujita, I. Mito, H. Honmou, and K. Minemura, "Novel optical FSK heterodyne single filter detection system using a directly modulated DFB-laser diode," *Electron. Lett.*, vol. 20, pp. 1022–1023, 1984.
[57] A. Blanchard, *Phase-Locked Loops*. New York: Wiley, 1976.
[58] I. Siio, M. Ohtsu, and T. Tako, "Real-time processing system of the measurement of laser frequency stability," *Trans. IECE Japan*, vol. J64-C, pp. 204–208, 1981.
[59] K. Kobayashi, I. Mito, and T. Suzuki, "626.2-nm pulsed operation (300K) of an MOCVD grown AlGaInP double heterostructure laser," in *Proc. 5th Conf. Solid-State Devices and Materials* (Kobe, Japan), Aug. 30–Sept. 1, 1984, pap. LD 6-1.
[60] S. Gerstenkorn and P. Luc, "Atlas du spectre d'absorption de la molecule d'iode," Laboratoire Aime-Cotton CNRS II, Orsay, France, 1978.
[61] Y. Tohmori, "Dynamic single-mode (DSM) lasers and wavelength tuning," Ph.D. thesis, Tokyo Institute of Technology, Tokyo, Japan, Mar. 1986.

*

Motoichi Ohtsu was born in Kanagawa, Japan, on October 5, 1950. He received the B.S., M.S., and Ph.D. degrees in electronics engineering from the Tokyo Institute of Technology, Tokyo, Japan, in 1973, 1975, and 1978, respectively.

In 1978, he was appointed a Research Associate, and in 1982, became an Associate Professor at the Tokyo Institute of Technology. From September 1986 to July 1987, on leave of absence from Tokyo Institute of Technology, he joined AT&T Bell Laboratories, Crawford Hill Laboratory, Holmdel, NJ. His main fields of interest are frequency control of lasers, analysis of dynamic behavior of lasers and its applications to coherent optical measurements, optical communications, and microwave atomic clocks. He has written seven books.

Dr. Ohtsu is a member of the Institute of Electronics and Communication Engineers of Japan, the Institute of Electrical Engineers of Japan, the Japan Society of Applied Physics, and the Optical Society of America. In 1982 he was awarded a prize from the Japan Society of Applied Physics. He was also awarded the Issac Koga Gold Medal from the International Union of Radio Science (URSI) in 1984.

Electrical Feedback and its Network Analysis for Linewidth Reduction of a Semiconductor Laser

MOTOICHI OHTSU AND NOBORU TABUCHI

Abstract—**The center frequency of the field spectrum of a 1.5-μm InGaAsP DFB laser was stabilized by negative electrical feedback. The resultant residual frequency fluctuation was $\sigma = 3.6 \times 10^{-11}$ for an integration time of 10 s. The linewidth of the field spectrum was simultaneously reduced by using another electrical feedback loop. Its minimum value was 360 kHz, which as 1/27 times that of the free-running condition. It was confirmed that this linewidth was narrower than the one determined by the magnitude of the spontaneous emission of the free-running laser. The field spectrum was very stable, and the value of the linewidth was kept constant in time for more than 40 h. Network analysis was carried out to realize further reductions of the linewidth. It was found from this analysis that an IM noise-limited linewidth, i.e., 1/630 times that of the free-running condition for the present laser, can be expected by decreasing the delay time of the feedback loop to 0.6 ns, and by increasing a low frequency cutoff to 16 kHz. It was pointed out that a linewidth of between 58 mHz and 2.9 Hz, limited by the IM noise of the laser and the bandwidth of the FM noise discriminator, can be expected by optimizing the sensitivity of the FM noise discriminator.**

I. Introduction

THE performance of semiconductor lasers has recently been improved to the extent that they can be used for a variety of applications such as sensing and communications. If they are to be used for passive ring cavity-type fiber gyroscopes [1], optically pumped Rubidium and Cesium atomic clocks [2], and coherent optical communication systems [3], improvement of their temporal coherence is required. It can be deduced from well-developed techniques for coherent microwave oscillators [4] and gas lasers [5] that at least four requirements should be simultaneously considered to effect this improvement. They are 1) stabilization of the center frequency of the field spectrum, 2) linewidth reduction of the field spectrum, 3) frequency tracking to another highly coherent laser, and 4) stable and accurate frequency sweeping. One of the authors has proposed that electrical feedback is a promising technique to meet these criteria simultaneously [6], [7]. Some of these techniques were demonstrated also by Saito *et al.* [8], [9]. The first criterion 1) has been demonstrated to obtain stability as high as 10^{-12} [10], and the technique of frequency offset locking [11] has fulfilled requirements 3) and 4).

Manuscript received April 24, 1987; revised July 7, 1987. This work was partially supported by a Grant for Scientific Research from the Ministry of Education, Science and Culture of Japan.

The authors are with the Tokyo Institute of Technology, Yokohama 227, Japan.

IEEE Log Number 8718502.

For the second requirement 2), it has been proposed that the linewidth can be reduced with FM noise reduction by electrical feedback within the Fourier frequency range f, lower than the linewidth of the free-running laser $\Delta\nu_{FR}$ (i.e., $f \leq \Delta\nu_{FR}$) [12], [13]. It has been pointed out in [7] and [13] that this technique has several advantages. For example, the laser cavity structure does not have to be modified, is more stable than with an optical feedback technique which employs an external mirror or fiber to form an extended cavity [14], and so on. Even though the FM noise at the tail of field spectrum is not reduced because of the finite bandwidth of the electrical feedback loop, it has been confirmed that the profile around the peak of the field spectrum can be well approximated as a very narrow Lorentzian [6], [7], [12]. Therefore, even though electrical feedback cannot provide system performance for high bit rate coherent optical communications better than the optical feedback scheme, it can be an effective technique to improve temporal coherence of light sources, especially for low-to-medium bit rate coherent optical communications and narrow bandwidth sensing systems, such as the above mentioned fiber gyroscope [1] and optically pumped atomic clocks [2].

In the present work, electrical feedback was utilized to reduce the linewidth and stabilize the center frequency simultaneously, demonstrating the technique proposed above. Furthermore, the electrical feedback network was analyzed for further reductions of linewidth, because the details of the network analysis had not yet been given in the previous work [12], [13].

II. Experimental Apparatus

Four kinds of 1.5-μm InGaAsP distributed feedback (DFB) lasers were prepared for the present work. The lasers A, B, and C were buffer-layer loaded planoconvex-waveguide (BL-PCW)-type [15]. Laser D was a double channel planar-buried-heterostructure (DC-PBH)-type [16]. The threshold currents of these lasers were 30, 56, 58, and 16 mA, respectively, at 20°C.

Fig. 1 shows an experimental apparatus for linewidth reduction and center frequency stabilization. The laser was fixed on a heat sink composed of a copper block and a Peltier element. The temperature fluctuations of the heat sink were detected by a sensitive thermistor bridge and reduced to 0.1 mK at 20°C by using a temperature control circuit. An optical isolator consisting of a Faraday rotator

0733-8724/88/0300-0357$01.00 © 1988 IEEE

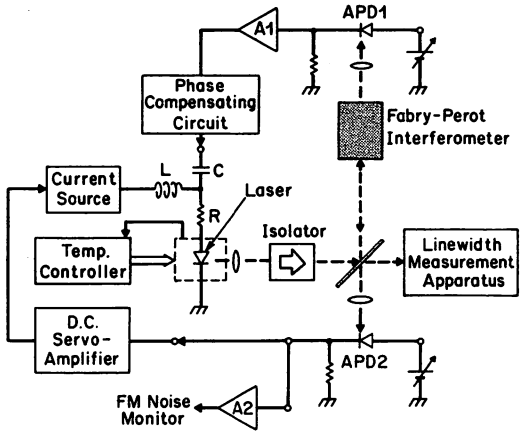

Fig. 1. Experimental apparatus.

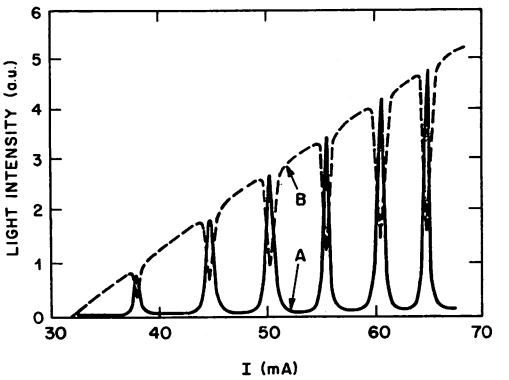

Fig. 2. Resonance curves of a Fabry-Perot interferometer obtained by sweeping the dc injection current I. Curve A: Transmitted light. Curve B: Reflected light.

and two polarizers was used to prevent injection of the reflected light from external optical components into the laser.

A 3-cm-long Fabry-Perot interferometer made of a cylindrical rod of fused silica was used for frequency reference and as an FM noise discriminator. Dielectric multilayers were coated on both ends of the rod to obtain a reflectivity of 80 percent. For linewidth reduction, the slope of the resonance curve of the light transmitted through the Fabry-Perot interferometer was used as an FM noise discriminator. This resonance curve is shown as curve A in Fig. 2. Its full-width at half maximum (FWHM) was 400 MHz. The FM response characteristics of this Fabry-Perot interferometer are described in Appendix A. Lengths of electrical cables and optical path in the feedback loop were 10 and 23 cm, respectively. Both of these paths delay signal propagation through the feedback loop, with a total delay time of 1.1 ns. For the servo-amplifier A1 in Fig. 1, a wide-band operational amplifier (Signetics NE5539) was used. Its gain was fixed at 35 dB, and the delay time of signal propagation through this amplifier was measured as being 3.5 ns. The total gain of the feedback loop was varied by varying the bias voltage of a Ge-avalanche photodiode (APD1). A phase compensating circuit was employed for fine adjustment of the bandwidth and gain of the feedback loop, whose characteristics will be presented in Section VI.

In addition to the feedback loop for linewidth reduction, another feedback loop was employed for simultaneous stabilization of the center frequency of the field spectrum. The slope of the resonance curve of light reflected from the Fabry-Perot interferometer (curve B in Fig. 2) was also used as an FM noise discriminator for this feedback loop, and the photocurrent of a Ge-APD (APD2) was fed back to the laser after it was amplified by a dc servo-amplifier with a high frequency cutoff of 130 Hz.

Furthermore, the slope of the resonance curve of the reflected light was also used to monitor the FM noise characteristics under feedback for linewidth reduction, i.e., the output signal from wide-band amplifier A2 in Fig. 1 was used for monitoring. This same signal was also used to measure the stability of the center frequency of the field spectrum.

The field spectrum was observed by the delayed self-homodyne technique [17] using a single mode optical fiber with a cutoff wavelength of 1.2 μm. The fiber length was 1.5 km, which corresponded to a resolution of 45 kHz for the linewidth measurement [17].

III. FM Noise and FM Response Characteristics of the Lasers

Laser A was used for the experiments of linewidth reduction in Section V. The power spectral density of its FM noise is shown in Fig. 3 for various power levels. It is seen that the FM noise is governed by $1/f$ noise for $f < 50$ kHz. However, it can be approximated as a white noise for $f \geq 50$ kHz, i.e., for the Fourier frequency range which gives the main contribution to the linewidth of field spectrum. The magnitude of this white noise was proportional to $(I/I_{th} - 1)^{-1}$, where I and I_{th} are the dc injection current and its threshold value, respectively. This means that the white noise is quantum FM noise due to spontaneous emission and carrier density fluctuations [10].

Fig. 4(a) and (b) shows the FM response characteristics of the four lasers by injection current modulation, measured by using a microwave network analyzer (Anritsu MS560J). The Fabry-Perot interferometer was used as a frequency discriminator. For these measurements, the AM response characteristics of the lasers were simultaneously measured, and their contribution to the measured FM response was corrected by the method of [18]. The contribution from the FM response characteristic of the Fabry-Perot interferometer was also corrected by using the result of Appendix A.

Fig. 4(a) shows the frequency deviation for each of the four lasers. Each of the curves in this figure exhibits a minimum, and there is a large difference in the position of this minimum for each of the lasers. These values are distributed in the range of between 2 kHz and 2 MHz. The frequency deviation at the lower and higher modulation frequency sides of this minimum can be attributed to thermal and carrier effects, respectively [19]. Fig. 4(b) illustrates that the laser frequency has 180° phase delay

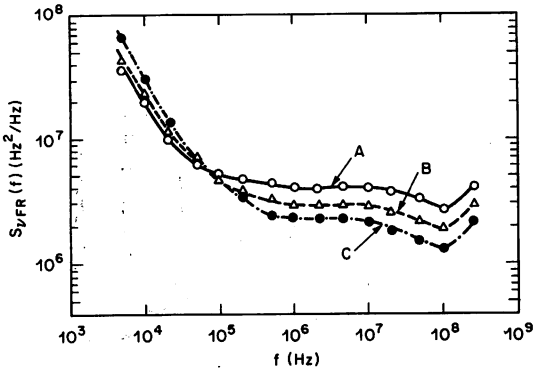

Fig. 3. Power spectral density of FM noise of laser A under free-running condition. Curves *A*, *B*, and *C* are for $(I/I_{th} - 1)^{-1} = 1.25$, 0.75, and 0.57, respectively.

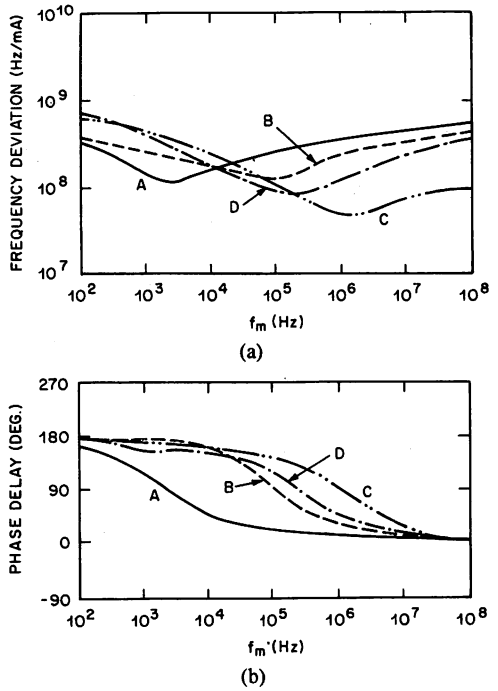

Fig. 4. FM response characteristics of lasers *A*, *B*, *C*, and *D*. f_m represents modulation frequency of the injection current. (a) Frequency deviation. (b) Phase delay.

at low modulation frequency, and approached 0° delay asymptotically at high modulation frequencies. In this figure, there is also a large difference in the profile of this asymptotic variation for each of the lasers. The phase delays of lasers B, C, and D did not have constant values in the modulation frequency range from 10 kHz to 10 MHz, which is an important frequency range for the linewidth reduction feedback loop. This complicated the design of the feedback loop. On the other hand, as laser A had a nearly constant phase delay in this modulation frequency range, this laser alone was suitable for the present experiments of linewidth reduction. That is, design of the feedback loop assumed that laser A had nearly 0° phase delay in the modulation frequency range higher than about 10 kHz. However, since laser A did not exhibit a constant phase delay in the frequency range below 10 kHz, the low frequency cutoff of the feedback loop was restricted, as will be discussed in Section VI.

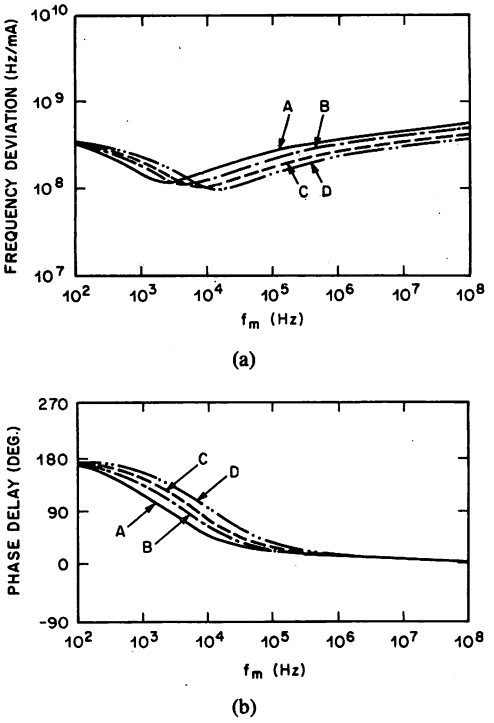

Fig. 5. Dependence of FM response characteristics of laser A on the dc injection current *I*. (a) Frequency deviation. (b) Phase delay. Curves *A*, *B*, *C*, and *D* are for $(I/I_{th} - 1)^{-1} = 2.78$, 1.00, 0.81, and 0.47, respectively.

Fig. 5(a) and (b) shows the dependence of the FM response characteristic of laser A on the dc injection current. It is seen from Fig. 5(b) that the lower limit of the modulation frequency range in which the phase delay was maintained at 0° was increased by an increase of the dc injection current. This means that the feedback loop should be designed so that its low frequency cutoff increases for large dc injection current to maintain stable linewidth reduction. In other words, the bandwidth of the feedback loop should be reduced for larger injection current, which affects the values of linewidth under feedback, as will be shown in Fig. 8.

IV. Limit of Linewidth Reduction

As presented in Fig. 3, it is shown that the quantum FM noise of the semiconductor laser can be detected by classical opto-electronic techniques such as interferometry. Furthermore, as depicted in Fig. 4, the laser frequency can be directly modulated by macroscopic quantities such as injection current. Therefore, the laser frequency can be countermodulated by the injection current to cancel such detected quantum FM noise. This effect of negative electrical feedback can be expressed by the following quantum mechanical Langevin equation of motion if the bandwidth of the feedback loop is assumed to be infinite [20]:

$$\delta\nu(t) = \Gamma_s(t) + \Gamma_c(t) - \int_0^\infty h(\tau) \cdot \{\delta\nu(t-\tau) + \Gamma_n(\tau)\}\, d\tau \qquad (1)$$

where $\delta\nu(t)$ is the frequency fluctuation at time t. Langevin forces Γ_s and Γ_c represent the two quantum FM noise sources for the free-running laser due to spontaneous emission and carrier density fluctuations, respectively. The convolution integral on the right-hand side of this equation represents the effect of negative electrical feedback, where $\delta\nu(t-\tau)$ is the detected FM noise, Γ_n is the noise magnitude generated from the feedback loop, and $h(\tau)$ is the impulse response of the feedback loop. The Fourier transform of (1) gives

$$F(f) = \frac{\Pi_s(f)}{1+H(f)} + \frac{\Pi_c(f)}{1+H(f)} - \frac{H(f)}{1+H(f)} \cdot \Pi_n(f) \quad (2)$$

where F, Π_s, Π_c, Π_n, and H represent the Fourier transforms of $\delta\nu$, Γ_s, Γ_c, Γ_n, and h, respectively. In this equation, the values of the first and second terms of the right-hand side approach zero for infinite gain of the feedback loop ($|H| \to \infty$), while that of the third term approaches $|\Pi_n|$. This means that the contributions from the two quantum FM noise sources can be suppressed by high feedback gain, and that the magnitude of the FM noise can be ultimately reduced to a value limited by the noise generated from the feedback loop. In other words, if a high gain, low noise feedback loop is employed, a very high temporal coherence can be artificially realized, resulting in a lower FM noise than the quantum FM noise level of the free-running laser. For this reason, it can be claimed that electrical feedback is a promising technique for improving the temporal coherence of semiconductor lasers.

In the remainder of this section, the narrowest linewidth to be expected is estimated by evaluating the noise magnitude generated from the present feedback loop (Π_n in (2)). It was found in preliminary measurements that the principal noise source of the FM noise detection was the IM noise of the laser. The FM noise was detected by APD1 after FM/IM conversion by the Fabry–Perot interferometer. Therefore, the magnitude of this IM noise contributes to Π_n in (2). Curve A of Fig. 6 shows the power spectral density of this IM noise of laser A under free-running conditions, where the dc injection current was fixed at 60 mA (i.e., $(I/I_{th}-1)^{-1} = 1.0$). The curve B in this figure is that for the FM noise which was detected after FM/IM conversion. Both curves show that these noises can be approximated as white noises, with a ratio between these of a magnitude of 28 dB, which corresponds to the signal-to-noise ratio (S/N) of the present FM noise detection. Therefore, with an infinite gain and bandwidth of the feedback loop, the power spectral density of the FM noise can be reduced until S/N is reduced to 0 dB (i.e., $|F| = |\Pi_n|$ in (2)), which means that the FM noise can be reduced to -28 dB ($= 1/630$) times that of the free-running condition. For this estimation, it was assumed that the increases in IM noise under feedback can be neglected, as is confirmed in Appendix B. It can be concluded from this estimation that the linewidth can be also reduced to $1/630$ times that of the free-running condition because the white FM noise gives a Lorentzian field spectrum whose linewidth is proportional to the magnitude of the FM noise [10], [13].

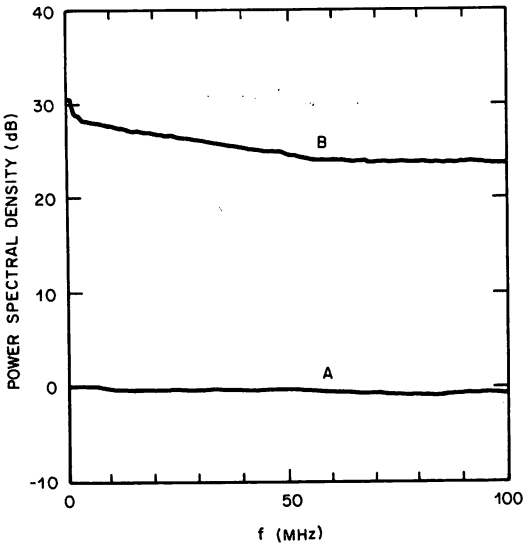

Fig. 6. Power spectral densities of the IM noise (curve A), and FM noise (curve B). The latter was measured after FM/IM conversion. These results are for laser A under free-running condition at $(I/I_{th}-1)^{-1} = 1.0$.

V. Experimental Results

Fig. 7 shows the result of center frequency stabilization of the field spectrum of laser A. For this experiment, the steepest point on the resonance curve of the reflected light from the Fabry–Perot interferometer was used as a frequency reference. Therefore, this result represents the frequency traceability of the laser to the Fabry–Perot interferometer, and is expressed by the square root of the Allan variance σ^2 [21] of the residual frequency fluctuations. Curve A in this figure shows that long-term frequency fluctuations were reduced by the feedback, with the value of σ at the integration time $\tau = 10$ s being 3.6×10^{-11}, which is about -22 dB times lower than that of the free-running condition (curve B).

When the feedback loop for center frequency stabilization was closed, the feedback loop for linewidth reduction was also closed. Curve A in Fig. 8 shows a relation between $(I/I_{th}-1)^{-1}$ and the linewidth (FWHM) of the field spectrum of laser A under feedback. This result was obtained by using optimum values of the feedback parameters, which were found from the network analysis described in Section VI. Curve A in this figure has its minimum at $(I/I_{th}-1)^{-1} = 1.0$, which is 360 kHz, and $1/27$ times that of the free-running condition. Fig. 9(a) shows a profile of the field spectrum having this minimum linewidth, while Fig. 9(b) is that of the free-running condition for comparison.

The linewidth under the free-running condition has been given by the modified Schawlow–Townes formula [22], which is expressed as

$$\Delta\nu_{FR} = \Delta\nu_{sp}(1+\alpha^2). \quad (3)$$

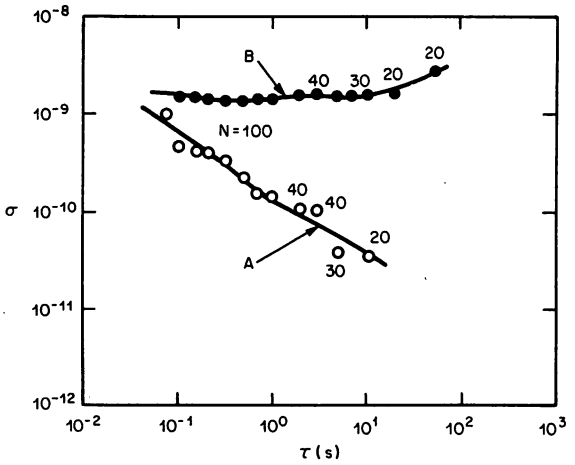

Fig. 7. Square root of the Allan variance σ^2 of residual center frequency fluctuations of laser A which was stabilized to the Fabry-Perot interferometer. N and τ are number of data and integration time of measurement, respectively. Curves A and B represent the values under feedback and free-running conditions, respectively.

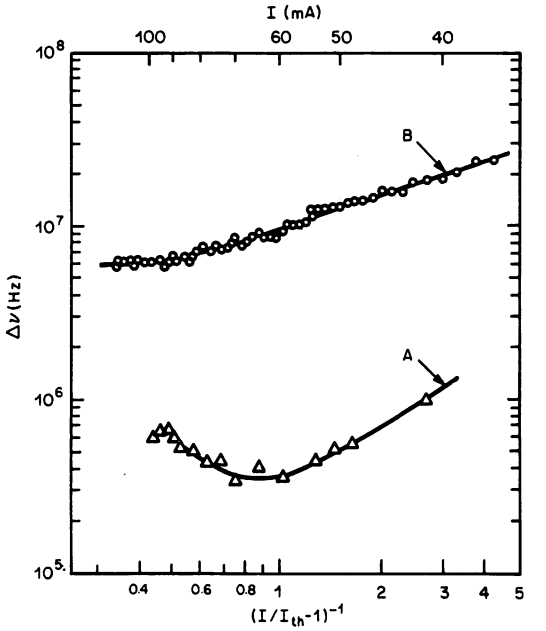

Fig. 8. Relation between $(I/I_{th} - 1)^{-1}$ and the linewidth of laser A. Curves A and B are for feedback and free-running conditions, respectively.

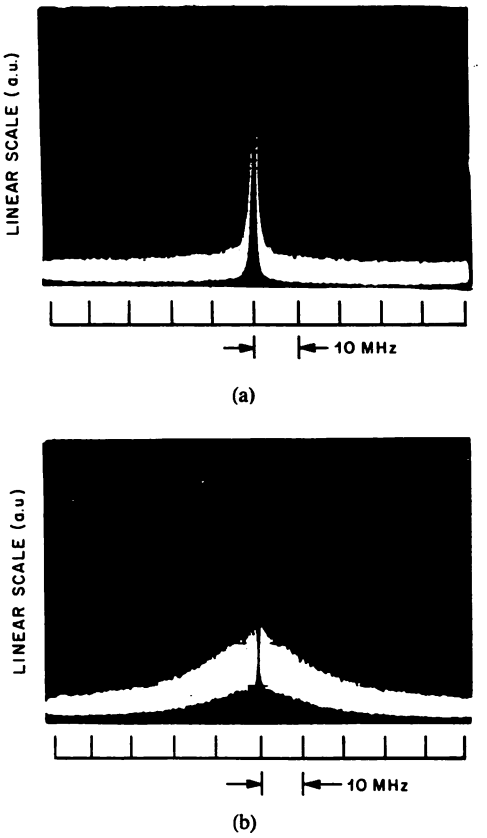

Fig. 9. Profile of field spectrum of laser A at $(I/I_{th} - 1)^{-1} = 1.0$. (a) Under feedback condition. (b) Under free-running condition.

In this equation, $\Delta\nu_{sp}$ represents the contribution from spontaneous emission, which corresponds to Π_s in (2). The quantity α is a linewidth enhancement factor due to carrier density fluctuations [22], and $\Delta\nu_{sp} \cdot \alpha^2$ corresponds to Π_c in (2). Reported values of the linewidth enhancement factor at 1.52-μm wavelength are $3.7 \leq \alpha \leq 5.0$ if the bandgap is assumed to be constant (see [23, fig. 1(a)]) or $1.5 \leq \alpha \leq 2.2$ if the bandgap is assumed to be dependent on the carrier density (see [23, fig. 1(b)]). This leads to $1/26.0 \leq 1/(1 + \alpha^2) \leq 1/14.7$ or $1/5.9 \leq 1/(1 + \alpha^2) \leq 1/3.3$. Therefore, the factor of $1/27$ obtained from Fig. 8 implies that the linewidth realized by the present feedback is narrower than the value of $\Delta\nu_{sp}$ determined from the magnitude of the spontaneous emission, which is consistent with the result of the theoretical discussion in Section IV.

Curve A in Fig. 8 shows that the value of the linewidth under feedback increased for $(I/I_{th} - 1)^{-1} > 1.0$. One of the reasons is a decrease in laser power at lower dc injection current, i.e., a decrease in the feedback gain. The other reason is that the feedback bandwidth was not wide enough to compensate for the broader linewidth $\Delta\nu_{FR}$ at lower dc injection current. Curve A also shows that the linewidth increased for $(I/I_{th} - 1)^{-1} < 1.0$. This is caused by a decrease in the feedback gain due to a decrease in the feedback bandwidth. This decrease in the bandwidth is due to the increase in the lower end of the feedback passband which was required to maintain a stable field spectrum, as will be described in Section VI. This increase was caused by the dependence of the phase delay characteristics in the FM response of laser A on the dc injection current, as was given by Fig. 5(b). That is, the lower limit of the modulation frequency range, in which phase delay was maintained at 0°, increased with an increase in the dc injection current.

The profile of the field spectrum given by Fig. 9(a) was very stable in spite of ambient temperature fluctuations, mechanical vibrations, and acoustic vibrations in the laboratory. That is, its linewidth was kept constant in time for more than 40 hours, as is shown in Fig. 10. Such high stability can be attributed to the simultaneous stabilization of the center frequency of the field spectrum, by which the feedback gain for linewidth reduction was also stabi-

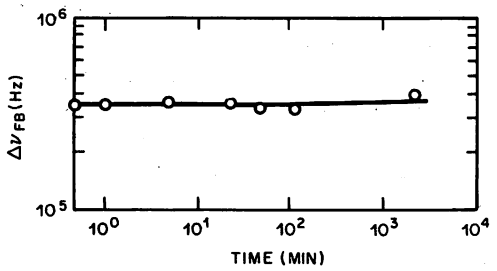

Fig. 10. Time dependence of the linewidth of laser A under feedback. $(I/I_{th} - 1)^{-1} = 1.0$.

lized. Furthermore, it can be also attributed to the fact that the electrical feedback employed here was inherently negative. It is not always possible to obtain such high stability by optical feedback, as this method sometimes induces chaotic instability [24] or coherence collapse [25].

VI. Network Analysis of the Feedback Loop

It was expected from Fig. 6 that the limit of linewidth reduction of laser A by the present experimental setup was −28 dB (= 1/630) that of the free-running condition. However, the minimum of the linewidth obtained in Section V was 360 kHz, which was 1/27 times that of the free-running condition. The difference between the expected limit and the experimental result was due to the limited gain of the feedback loop, which was caused by its limited bandwidth. In this section, the results of network analysis are described to discuss the gain and bandwidth of the feedback loop for the purpose of further linewidth reduction.

A transfer function of the feedback loop can be measured by using a network analyzer, connected between, e.g., the phase compensating circuit and the capacitor C in Fig. 1. In this case, the corresponding expression of the transfer function is given by

$$H = H_C \cdot H_L \cdot H_F \cdot H_A \cdot H_P \cdot H_D \tag{4}$$

where H_C is the transfer function of a circuit composed of a capacitor C, a resistor R, and the impedance of the laser diode in Fig. 1. This is expressed as

$$H_C = \frac{1/R}{1 + 2\pi f_l/s} \tag{5}$$

where s is the Laplace transform complex variable. In this equation, the impedance of the laser diode can be neglected because its actual value is much less than R. A low frequency cutoff f_l is given by $1/2\pi CR$, which was adjusted to about 5 kHz in the experiments. H_L is the transfer function of the FM response of the laser, for which the measured value of laser A in Fig. 4 was used. H_F is the transfer function of the Fabry-Perot interferometer and APD1 in Fig. 1. Since the laser frequency was locked to the steepest point of resonance curve of the Fabry-Perot interferometer, H_F can be expressed as

$$H_F = \frac{3\sqrt{3}}{4} \cdot \frac{R_A \cdot I_A}{\Delta\nu_{FP}} \cdot \frac{1}{1 + s/2\pi f_{FP}} \tag{6}$$

where R_A and I_A represent the load resistor and bias current for APD1, respectively. To derive this equation, it was approximated that the Fabry-Perot interferometer was a low-pass filter with the high frequency cutoff f_{FP} (see Appendix A), and that its resonance curve was Lorentzian. H_A is the transfer function of the amplifier A1. This is expressed as

$$H_A = \frac{G_0}{1 + s/2\pi f_h} \tag{7}$$

where G_0 is the gain and has a value of 35 dB. f_h is the high frequency cutoff, which has been limited by the manufacturer of the amplifier to ensure stable operation. This value was 10 MHz for the value of gain specified. H_P is the transfer function of the phase compensating circuit, which was composed of capacitors and resistors. Since phase lag-lead compensation [26] was employed in the present experiments, it is expressed as

$$H_P = \frac{(1 + s/2\pi f_1)(1 + s/2\pi f_2)}{(1 + sn/2\pi f_1)(1 + s/2\pi f_2 n)} \tag{8}$$

where $n = 3$, $f_1 = 25$ MHz, and $f_2 = 51$ MHz. H_D is the transfer function which represents the delay of signal propagation in the feedback loop. This is expressed as

$$H_D = \exp(-s\tau_D) \tag{9}$$

where τ_D represents the total delay time (4.6 ns in the present experiments), which was composed of contributions from the lengths of the electrical cable and optical path (1.1 ns) and that of amplifier A1 (3.5 ns). By replacing s by $i2\pi f$ in (4)-(9), the Bode plots, i.e., dependence of $|H|$ and arg (H) on the Fourier frequency f, are obtained. They are given by curves A in Figs. 11(a) and (b) for $(I/I_{th} - 1)^{-1} = 1.0$. Curves B in these figures represent the results measured for laser A by using a network analyzer. Curves C, D, E, and F in Fig. 11(b) are arg (H_L), arg $(H_C \cdot H_A \cdot H_P)$, arg (H_D), and arg (H_F), respectively. Curves A and B agree with each other, from which the validity of the analytical model can be confirmed. A slight disagreement between these curves for $f < 1$ kHz is due to the effect of the notch filter, composed of the junction capacitance of the laser and the inductance L in Fig. 1, which was not taken into account in (4).

The ratio between the power spectral density of the FM noise $S_{\nu FB}$ under feedback, and $S_{\nu FR}$ under the free-running condition, is estimated by using the transfer function H, which is expressed as

$$S_{\nu FB}/S_{\nu FR} = \left|\frac{1}{1 + H}\right|^2. \tag{10}$$

Curve A of Fig. 12 represents the result calculated by using (4)-(10). Curve B in this figure represents the experimental result for laser A at $(I/I_{th} - 1)^{-1} = 1.0$ for comparison, and was measured by using the reflection-mode of the Fabry-Perot interferometer, the detector APD2, and a wide-band amplifier A2 in Fig. 1. These two curves agree with each other, from which high accuracies of calculation and measurement are confirmed. The value

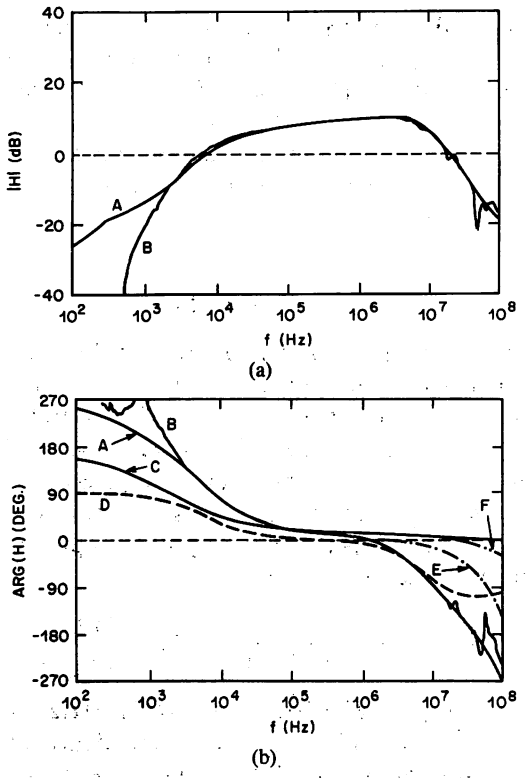

Fig. 11. (a)(b) Bode plots of the transfer function of the feedback loop for linewidth reduction of laser A. $(I/I_{th} - 1)^{-1} = 1.0$. Curves A and B are calculated and measured values, respectively. The curves C, D, E, and F in (b) are arg (H_L), arg $(H_C \cdot H_A \cdot H_P)$, arg (H_D), and arg (H_F), respectively.

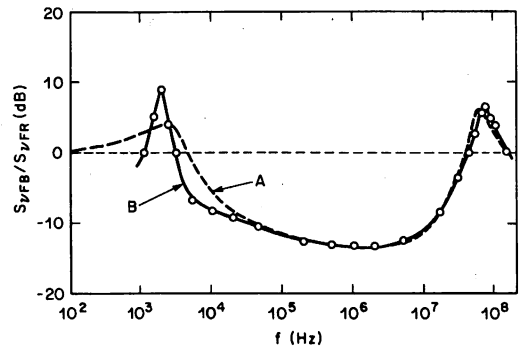

Fig. 12. Ratio between the power spectral densities of the FM noise under feedback $S_{\nu FB}$ and under free-running condition $S_{\nu FR}$. Curve A is a calculated result. Curve B and open circles are measured results for laser A at $(I/I_{th} - 1)^{-1} = 1.0$.

of the ratio $S_{\nu FB}/S_{\nu FR}$ for these curves was about -14 dB ($= 1/27$) within the feedback passband. This supports the fact that the linewidth of the laser A at $(I/I_{th} - 1)^{-1} = 1.0$ was reduced to $1/27$ times that of the free-running condition by the experiments in Section V.

As shown in Fig. 12, the FM noise is decreased only within the feedback passband. This indicates that the field spectrum, especially its tail, is no longer Lorentzian, and the linewidth cannot be defined in any general sense. In fact, spectral linewidth is not a relevant parameter for the S/N ratio of, for example, high bit-rate coherent optical communication systems. The magnitude of the FM noise power spectral density at a certain frequency should be a more relevant parameter than the linewidth for these systems. However, since the profile around the peak of the field spectrum can still be well approximated as a very narrow Lorentzian, which has been pointed out in Section I, the linewidth is still a relevant parameter for low-to-medium bit-rate coherent optical communication systems and narrow bandwidth sensing systems. Therefore, discussions in this paper are still focused on the linewidth for these systems.

Curve B in Fig. 12 has two resonant peaks, at $f = 65$ MHz and 2 kHz. These two peaks limited the higher and lower ends of the feedback passband obtained by the present experimental setup. The peak height at $f = 65$ MHz was $+6$ dB. It was caused by H_D in (4), i.e., the time delay of signal propagation in the feedback loop. This height was increased by further increases in the feedback gain, which induced FM sidebands on the field spectrum. These FM sidebands were found at ± 65 MHz away from the optical carrier component. An example of such a field spectrum is shown in Fig. 13. Once these FM sidebands appeared, further increases in the feedback gain enhanced the FM sidebands, which caused the optical carrier component to disappear without inducing further linewidth reduction. Therefore, generation of FM sidebands indicated the maximum employable feedback gain and the attainable narrowest linewidth. Since it was confirmed that no FM sidebands were observed if this peak was lower than $+6$ dB, it was deduced that the maximum feedback gain should be such to maintain the height of this peak below this value. It was found effective to use the phase compensating circuit of (8) to increase the feedback gain 3 dB more without inducing FM sidebands. The field spectrum of Fig. 9(a) was observed under such a feedback condition.

Since further increases in the feedback gain induced FM sidebands, a linewidth narrower than $1/27$ times that of the free-running condition was not obtained in the experiment. To enable further reduction of the linewidth by increasing the gain would require a decreased delay time of the feedback loop, i.e., thereby allowing an increase in the higher end of the feedback passband. Fig. 14 gives a relation between the delay time and the height of the peak, which was calculated by using (4)–(10). Curve B in this figure shows that the peak height is kept at $+6$ dB and the value of $S_{\nu FB}/S_{\nu FR}$ has almost a constant value of -28 dB ($= 1/630$) in the feedback passband if the delay time is 0.6 ns. Therefore, it can be expected that the feedback gain can be increased to realize the IM noise-limited linewidth of laser A, i.e., $1/630$ times that of the free-running condition, without inducing FM sidebands, if the delay time is decreased to as short as 0.6 ns. Since the main contribution to the delay time in the present experimental apparatus was from the amplifier A1, this contribution can be reduced to as short as 0.2 ns if it is replaced by a faster GaAs IC [27], [28]. In this case, the delay time due to the lengths of electrical cable and optical path may be as long as 0.4 ns to still maintain 0.6 ns total delay time. This corresponds to a 12-cm length, which can be

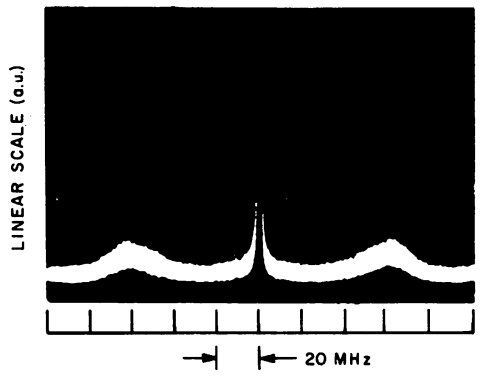

Fig. 13. Profile of the field spectrum on which FM sidebands appeared at ±65 MHz away from the optical carrier component. Operating parameters were the same as those of Fig. 9(a) except that the feedback gain was slightly increased.

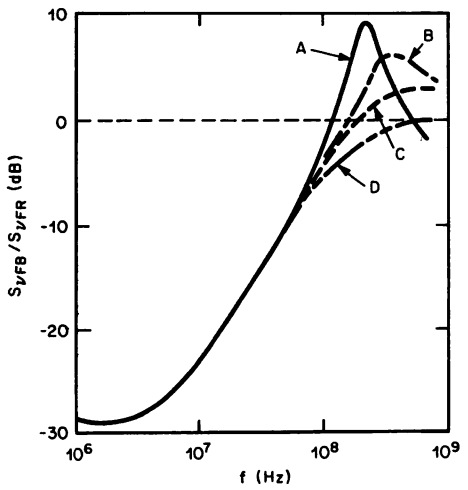

Fig. 14. Calculated result of the relation between $S_{\nu FB}/S_{\nu FR}$ and the delay time τ_D. Curves *A*, *B*, *C*, and *D* are for τ_D = 1 ns, 0.6, 0.3, and 0 ns, respectively.

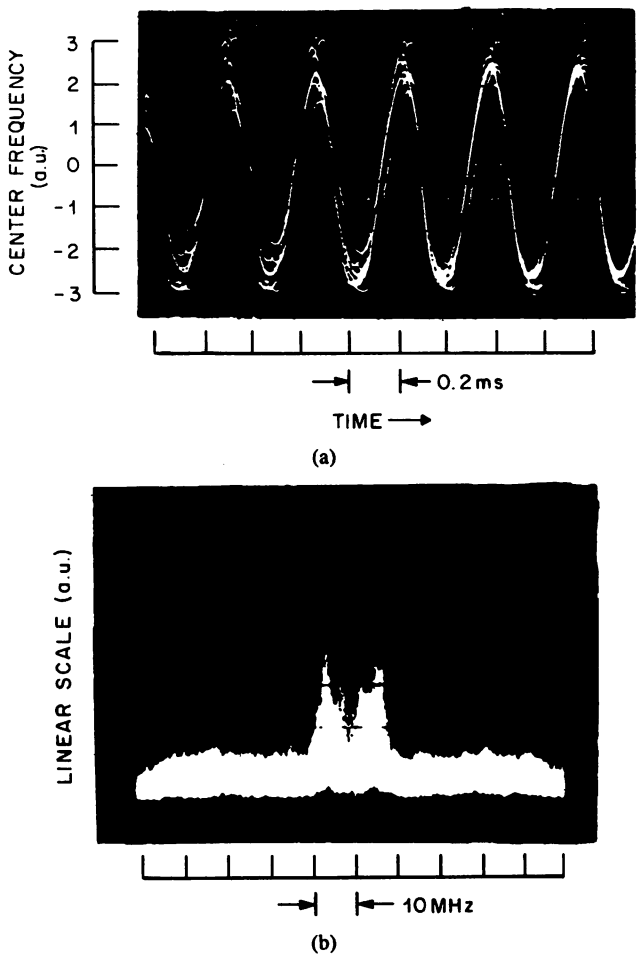

Fig. 15. (a) Observed instability of the center frequency of the field spectrum of laser A. Operating parameters were the same as those of Fig. 9 except that f_l was decreased to 3 kHz. (b) Profile of unstable field spectrum observed under the same condition of (a).

long enough to be realized by using conventional discrete electrical and optical components. In other words, the delay time of 0.6 ns can be realized without employing any novel optoelectronic integrated circuits if a faster amplifier, e.g., a GaAs IC, is employed. For this reason, further reductions of the linewidth and IM noise-limited value can still be expected for laser A. If an optoelectronic integrated circuit is realized for this feedback loop in the future, the bandwidth of the negative feedback will be ultimately limited by the delay time of the amplifier A1. Therefore, it can be estimated that the ultimate limit of the feedback bandwidth should be about 1 Ghz if the above mentioned GaAs IC is employed for amplifier A1.

For curve *B* of Fig. 12, the height of the peak at f = 2 kHz was +8 dB. This was induced by the phase delay of H_L in (4), i.e., this was caused by the fact that the phase delay of the FM response of the laser A was not constant but was increased for lower modulation frequency f_m, as was shown in Fig. 5(b). The phase delays in other transfer functions of (4) gave additional contributions to enhance this peak. A principal factor among these additional contributions was the low frequency cutoff f_l of (5), i.e., the height of this peak was increased if the value of low frequency cutoff f_l was decreased. This increase in the peak height induced an instability of the field spectrum. An example of this instability is shown by Fig. 15(a) and (b), where the value of f_l was intentionally decreased to 3 kHz. Fig. 15(a) shows that the center frequency of the field spectrum oscillated with the frequency f = 2 kHz. Due to this oscillation, an instability was induced in the field spectrum, as is shown in Fig. 15(b). However, when the peak height of curve *B* in Fig. 12 was as low as +8 dB, the stable field spectrum of Fig. 9(a) was obtained without incurring such instability. It was deduced from this fact that the value of low frequency cutoff f_l has to be kept high enough so that the height of this peak can be maintained lower than +8 dB.

For further increases in the feedback gain, the value of low frequency cutoff f_l has to be increased to maintain this peak height lower than +8 dB. Fig. 16 shows the relation between the peak height and the value of f_l calculated by using (4)–(10). Curve *B* in this figure shows that the peak height is kept at +8 dB and the value of $S_{\nu FB}/S_{\nu FR}$ takes almost a constant value of −28 dB (= 1/630) in the feedback passband if f_l is increased to 16 kHz. Therefore, it can be expected that the feedback gain can be increased

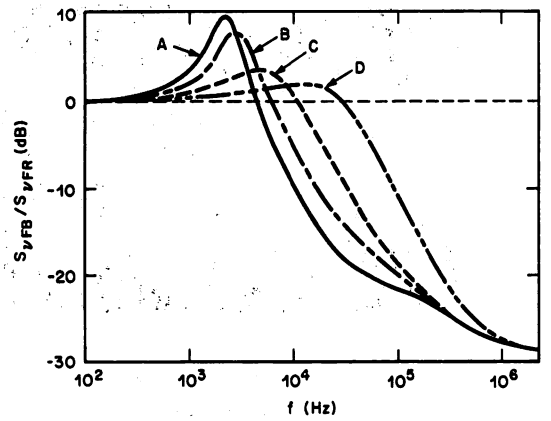

Fig. 16. Calculated result of the relation between $S_{\nu FB}/S_{\nu FR}$ and the low frequency cutoff f_l. Curves A, B, C, and D are for f_l = 10, 16, 30, and 100 kHz, respectively.

to realize the value of IM noise-limited linewidth for laser A if f_l is increased to 16 kHz. Though this increase in f_l slightly sacrifices the lower end of the feedback passband, the instability of the field spectrum can be suppressed. Since the peak at f = 2 kHz is due to the phase delay characteristics in FM response of laser A itself, it will disappear and f_l can be decreased to zero if a laser with a constant phase delay in FM response is used in the future.

From the discussion given in this section, it is confirmed that the calculated result of the network analysis agrees with the experimental results, which makes this analytical model useful for designing the feedback loop. The linewidths shown in Figs. 8 and 9(a) were obtained by using the optimum values of feedback parameters found using this analytical model. Furthermore, it was found that the IM noise-limited linewidth, i.e., 1/630 times that of the free-running condition, can be expected for laser A by decreasing the delay time of 0.6 ns and by increasing the low frequency cutoff to 16 kHz in the present experimental apparatus.

The FM noise was not reduced for f < 2 kHz by the present feedback loop because the lower end of the feedback passband was limited by f_l and phase delay in FM response of the laser. This means that slow frequency drift was not reduced by this feedback loop. However, since another feedback loop was provided in the present experimental apparatus to reduce the FM noise for f < 130 Hz, this frequency drift was actually reduced as shown in Fig. 7, and a stable field spectrum was obtained. The slow frequency drift will be also simultaneously reduced by the feedback loop for linewidth reduction if a laser with a constant phase delay in FM response is used in the future. This is because the lower end of the feedback passband can be decreased to zero for such a laser, which makes the experimental setup less elaborate.

VII. A Possibility of Reducing the IM Noise-Limited Linewidth

It was confirmed in Section VI that the linewidth can be reduced to the value limited by the IM noise of laser A if a sufficient bandwidth of the feedback loop was obtained by appropriately adjusting the values of τ_d and f_l. Under the assumption of sufficient bandwidth, a reduction of this IM noise-limited linewidth of laser A becomes possible by improving the sensitivity of the FM noise discriminator. Power fluctuations of the transmitted laser light through the Fabry-Perot interferometer are induced by the laser fequency fluctuations $\delta\nu$ as well as by the incident power fluctuations δP. The power fluctuations δP_ν induced by $\delta\nu$ are expressed as

$$\delta P_\nu = \frac{3\sqrt{3}}{4} \cdot \frac{P_0}{\Delta\nu_{FP}} \cdot \delta\nu \tag{11}$$

where P_0 represents the dc power incident on the Fabry-Perot interferometer. To derive this equation, the resonance curve of the Fabry-Perot interferometer was approximated as a Lorentzian with a linewidth of $\Delta\nu_{FP}$ (FWHM), and the laser frequency was assumed to be locked at the steepest point of the slope of the resonance curve of the interferometer. On the other hand, the power fluctuation δP_I induced by δP is given by

$$\delta P_I = \tfrac{3}{4} \cdot \delta P. \tag{12}$$

The ratio between δP_ν and δP_I gives the signal-to-noise ratio of the FM noise detection, which is expressed as

$$S/N = \frac{3P_0^2}{(\Delta\nu_{FP})^2} \cdot \frac{S_{\nu FR}}{S_{IFR}}. \tag{13}$$

In this equation, δP_ν and δP_I have been replaced by their power spectral densities $S_{\nu FR}$ and S_{IFR}, respectively. An example of the value of S/N for laser A has been given by the ratio of the values of curves A and B in Fig. 6. That is, curves A and B in this figure correspond to S_{IFR} and $(3P_0^2/(\Delta\nu_{FP})^2)S_{\nu FR}$ in (13), respectively. Since curve B was approximated as white noise, the field spectrum under free-running condition can be approximated as a Lorentzian and its linewidth given by $\Delta\nu_{FR} = \pi S_{\nu FR}$ [10], [13]. On the other hand, since the reduced power spectral density $S_{\nu FB}$ of the FM noise under feedback can be also approximated as white noise within the feedback passband (see Fig. 12), the field spectrum under feedback can be also approximated as a Lorentzian except for its tails. This means that its linewidth is also approximated as $\Delta\nu_{FB} = \pi S_{\nu FB}$. Furthermore, as is given in Appendix B, increases in the magnitude of IM noise are negligible under the feedback condition for linewidth reduction. Therefore, the IM noise-limited linewidth under feedback can be given by substituting S/N = 1 into (13), and is expressed as

$$\frac{\Delta\nu_{FB}}{\Delta\nu_{FR}} = \frac{(\Delta\nu_{FP})^2}{3P_0^2} \cdot \frac{S_{IFR}}{S_{\nu FR}}. \tag{14}$$

As an example of this result, it has been estimated in Section IV that the value of $\Delta\nu_{FB}/\Delta\nu_{FR}$ is 1/630 for the case of Fig. 6 at $(I/I_{th} - 1)^{-1} = 1.0$.

The value $\Delta\nu_{FB}/\Delta\nu_{FR}$ in (14) is decreased by decreasing $\Delta\nu_{FP}$, i.e., by using a more sensitive FM noise discrimi-

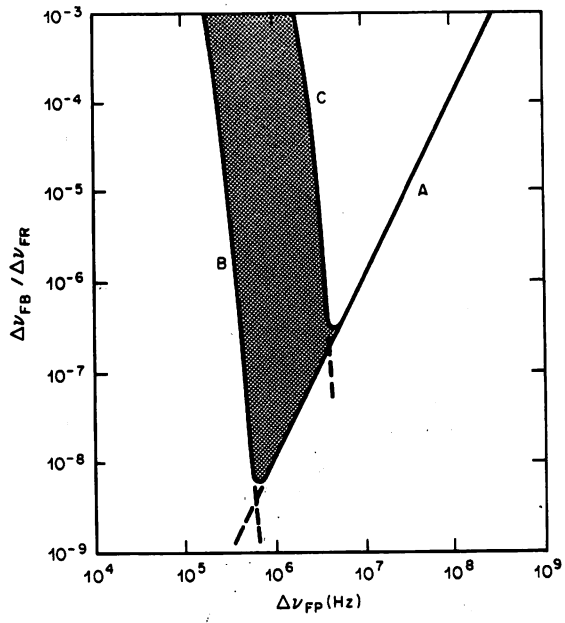

Fig. 17. Calculated result of the relation between $\Delta\nu_{FP}$ and $\Delta\nu_{FB}/\Delta\nu_{FR}$ for laser A at $(I/I_{th} - 1)^{-1} = 1.0$. The curve A represents the value limited by the IM noise of the laser. The curves B and C are the values limited by the bandwidth of the Fabry-Perot interferometer. These two curves are for $\kappa = 50$ and 5, respectively. The meshed area between these two curves corresponds to the result for $5 < \kappa < 50$.

nator. Curve A of Fig. 17 shows a relation between $\Delta\nu_{FP}$ and $\Delta\nu_{FB}/\Delta\nu_{FR}$ calculated by using (14). For this calculation, the numerical values of Fig. 6 were also employed, i.e., $\Delta\nu_{FB}/\Delta\nu_{FR} = 1/630$ at $\Delta\nu_{FP} = 400$ MHz for $(I/I_{th} - 1)^{-1} = 1.0$. It can be recognized from this curve that a very narrow linewidth $\Delta\nu_{FB}$ is to be expected by decreasing $\Delta\nu_{FP}$.

However, a decrease in $\Delta\nu_{FP}$ induces a decrease in bandwidth f_{FP} of the Fabry-Perot interferometer (6) because $\Delta\nu_{FP}$ is proportional to f_{FP}. This decrease can limit the bandwidth of the feedback loop if $\Delta\nu_{FP}$ is very narrow, which will violate the assumption for the discussion in this section, i.e., sufficient bandwidth of the feedback loop. In the case of insufficient bandwidth B of the feedback loop, i.e., if the bandwidth is not large enough as compared with the value of the linewidth $\Delta\nu_{FR}$, the value of $\Delta\nu_{FB}/\Delta\nu_{FR}$ of (14) has to be modified, as has already been given by [13, fig. 3]. Using the result given in this figure, a modified expression for insufficient feedback loop bandwidth can be written as

$$\frac{\Delta\nu_{FB}}{\Delta\nu_{FR}} = \frac{(\Delta\nu_{FP})^2}{3P_0^2} \cdot \frac{S_{IFR}}{S_{\nu FR}} + \left[1 - \frac{(\Delta\nu_{FP})^2}{3P_0^2} \frac{S_{IFR}}{S_{\nu FR}}\right] \cdot \exp\left(-\kappa B/\Delta\nu_{FR}\right). \quad (15)$$

The second term in the right-hand side of this equation represents the effect of insufficient bandwidth, where the parameter κ takes a value between 5 and 50. If the feedback bandwidth is limited by the bandwidth of the Fabry-Perot interferometer, B has to be replaced by f_{FP}, where f_{FP} is approximated as $\Delta\nu_{FP}/3.5$ (see Appendix A). Curves B and C of Fig. 17 represent the values of the second term of (15) obtained by this replacement. These are the results for $\kappa = 50$ and 5, respectively. The meshed area between these two curves corresponds to the result for $5 < \kappa < 50$.

It is concluded from this discussion that the relation between $\Delta\nu_{FP}$ and $\Delta\nu_{FB}/\Delta\nu_{FR}$ is given by the curve A and the meshed area of Fig. 17. The minimum of $\Delta\nu_{FB}/\Delta\nu_{FR}$ occurs either at the intersection of curves A and B and gives 6×10^{-9}, or at the intersection of curves A and C and gives 3×10^{-7}. Since $\Delta\nu_{FR}$ was 9.7 MHz at $(I/I_{th} - 1)^{-1} = 1.0$ (see curve A of Fig. 8), the above mentioned minima correspond to $\Delta\nu_{FB} = 58$ mHz and 2.9 Hz, respectively. The values of $\Delta\nu_{FP}$ for giving these minima are 820 kHz and 6.8 MHz, respectively, which correspond to the length of the Fabry-Perot interferometer of 9.3 m and 1.1 m for a mirror reflectivity of 80 percent. A fiber ring cavity [1] can be used to reduce a volume of such a long Fabry-Perot interferometer.

VIII. Summary

The center frequency of the field spectrum of a DFB-type 1.5-μm InGaAsP laser was stabilized by electrical negative feedback, where a Fabry-Perot interferometer was used as a frequency reference and FM noise discriminator. The resultant residual frequency fluctuation was $\sigma = 3.6 \times 10^{-11}$ at an integration time of 10 s. Linewidth reduction of the field spectrum was simultaneously carried out by using a second feedback loop. Its minimum value was 360 kHz, which was 1/27 times that of the free-running condition. It was confirmed that this linewidth was narrower than that determined by the magnitude of spontaneous emission fluctuations of the free-running laser. The profile of the field spectrum under feedback was stable, and its linewidth was kept constant in time for more than 40 h.

Network analysis was carried out, and its results agreed well with the experimental results. It was found by this analysis that any feedback gain was limited by the finite bandwidth of the feedback loop. The limited bandwidth was due to the delay time of signal propagation through the feedback loop, and modulation frequency dependence of the phase delay in the FM response of the present laser. It was also found that an IM noise-limited linewidth, i.e., 1/630 times that of the free-running condition, can be expected for the present laser by decreasing the delay time to 0.6 ns, and by increasing the low frequency cutoff to 16 kHz.

Furthermore, it was pointed out that a linewidth of between 58 mHz and 2.9 Hz, limited by the IM noise of the present laser and the bandwidth of the Fabry-Perot interferometer, is to be expected by optimizing the sensitivity of the Fabry-Perot interferometer.

Appendix A
Transfer Function of a Fabry-Perot Interferometer

A Fabry-Perot interferometer was used as an FM/IM converter for FM noise detection in the present experi-

ment. To derive its transfer function, the modulated optical frequency $\nu(t)$ of the incident light is expressed as

$$\nu(t) = \nu_0 + \nu_M \cdot \cos(2\pi f_m t) \quad \text{(A1)}$$

which corresponds to the input signal to this FM/IM converter. In this equation, ν_0 is the nominal optical frequency, ν_M is the maximum frequency deviation, and f_m is the modulation frequency. The electric field of the incident light under frequency modulation is given by

$$E(t) = E_0 \cdot \exp\left[i\left\{2\pi\nu_0 t + \frac{\nu_M}{f_m} \cdot \sin(2\pi f_m t)\right\}\right] \quad \text{(A2)}$$

where E_0 is an amplitude. The light power transmitted through the Fabry-Perot interferometer is given by superposing multiple reflected lightwaves, which is expressed as

$$I(t) = I_0(1-R)^2\left|\sum_{k=1}^{\infty} R^{k-1} \cdot \exp\left[i\left\{2\pi\nu_0 t_k + \frac{\nu_M}{f_m} \cdot \sin(2\pi f_m t_k)\right\}\right]\right|^2 \quad \text{(A3)}$$

where R is the power reflectivity of the mirrors, and

$$I_0 = E_0^2$$

$$t_k = t - (k-1) \cdot 2nL/c \quad (k = 1, 2, 3, \cdots) \quad \text{(A4)}$$

where c is the speed of light in vacuum, L is the length of the interferometer, and n is the refractive index of the medium inside the interferometer.

Equation (A3) corresponds to an output signal from the FM/IM converter, which can be expressed as

$$I(t) \equiv I_M \cos(2\pi f_m t + \phi). \quad \text{(A5)}$$

Relations between I_M, ϕ, and f_m were derived by computer simulation. A calculated result is shown by Figs. 18(a) and (b), which correspond to the transfer function of the Fabry-Perot interferometer. In this figure, a normalized magnitude of response (rather than I_M) is illustrated in Fig. 18(a), which is defined by

$$C \equiv \left(\frac{I_M}{I_0}\right)\Big/\left(\frac{\nu_M}{\Delta\nu_{FP}}\right). \quad \text{(A6)}$$

Here, $\Delta\nu_{FP}$ is the FWHM of the resonance curve of the Fabry-Perot interferometer, which is given by

$$\Delta\nu_{FP} = \frac{c}{2nL} \cdot \frac{1-R}{\pi\sqrt{R}}. \quad \text{(A7)}$$

The parameter α_{FP} used in the caption of this figure represents a detuning of the laser frequency ν_0 from the resonance frequency of the Fabry-Perot interferometer ν_{FP}, which is defined by

$$\alpha_{FP} \equiv \frac{\nu_0 - \nu_{FP}}{\Delta\nu_{FP}}. \quad \text{(A8)}$$

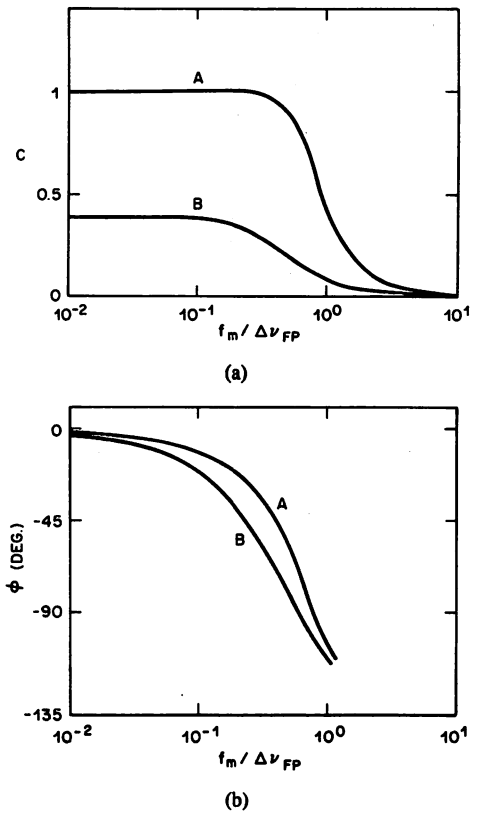

Fig. 18. Calculated result of the FM response characteristics of a Fabry-Perot interferometer. Curves A and B are for $\alpha_{FP} = 0.5$ and 0.05, respectively.

The result of Fig. 18(a) agrees well with the previously presented one [29], from which the accuracy of the present simulation can be confirmed. Fig. 18(b) shows the result for ϕ in (A5), which had not been given in [29].

From Fig. 18, it can be concluded that the Fabry-Perot interferometer is well approximated as a first-order low-pass filter whose transfer function is expressed by

$$H_{FP}(s) = \frac{C_0}{1 + s/2\pi f_{FP}} \quad \text{(A9)}$$

where C_0 is the value of C at $f_m = 0$. A high frequency cutoff f_{PF} can be approximated from Fig. 18 as

$$f_m = \Delta\nu_{FP}/3.5. \quad \text{(A10)}$$

The results given by (A9) and (A10) were used for the discussions in the text.

Appendix B
Estimation of Increases in IM Noise Under Feedback for Linewidth Reduction

The magnitude of the IM noise may be increased when the injection current is controlled to reduce the linewidth. This magnitude is estimated in this appendix. Fluctuations in frequency $\delta\nu_{FB}$ and power δP_{FB} under feedback condition are expressed as

$$\delta\nu_{FB} = A_I \cdot \delta I + \delta\nu_{FR} \quad \text{(B1a)}$$

$$\delta P_{FB} = B_I \cdot \delta I + \delta P_{FR} \quad \text{(B1b)}$$

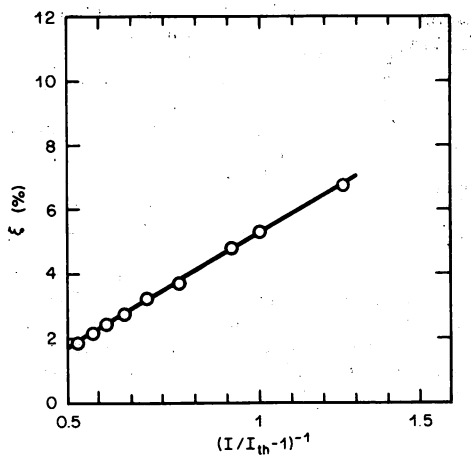

Fig. 19. A relation between $(I/I_{th} - 1)^{-1}$ and the rate of increase ξ in the magnitude of IM noise of laser A under the feedback condition for linewidth reduction.

where δI is the change in injection current required for feedback, and $\delta\nu_{FR}$ and δP_{FR} are fluctuations in frequency and power under free-running condition, respectively. A_I is the frequency modulation efficiency, which is given by curve A of Fig. 4(a) for laser A. Though the precise value along this curve depends on the modulation frequency, A_I can be approximated as 0.6 GHz/mA. B_I is the coefficient for power variation due to injection current variation, which is expressed as

$$B_I = \frac{P_0}{I - I_{th}} \tag{B2}$$

where P_0 is a laser power at the dc injection current I.

If the frequency fluctuations are eliminated by controlling the injection current ($\delta\nu_{FB} = 0$), the power fluctuation δP_{FB} is derived from (B1a) and (B1b), and is expressed as

$$\delta P_{FB} = -\frac{B_I}{A_I} \cdot \delta\nu_{FR} + \delta P_{FR}. \tag{B3}$$

By using (B2) and (B3), the power spectral density S_{IFB} of the IM noise under feedback is expressed by those of IM noise S_{IFR} and FM noise $S_{\nu FR}$ under the free-running condition. This is

$$S_{IFB} = \frac{P_0^2}{A_I^2 \cdot (I - I_{th})^2} \cdot S_{\nu FR} + S_{IFR} + 2\gamma \frac{P_0}{A_I(I - I_{th})} \sqrt{S_{\nu FR} \cdot S_{IFR}}, \tag{B4}$$

where γ is a degree of correlation between $\delta\nu_{FR}$ and δP_{FR}. The value of γ has been reported as being 0.9 for AlGaAs lasers [30]. This value was also employed here for the present InGaAsP laser, which would not underestimate the value of S_{IFB} very much because $|\gamma| \leq 1$. If the rate of increase ξ in the magnitude of IM noise under the feedback is defined by

$$\xi \equiv \frac{S_{IFB} - S_{IFR}}{S_{IFR}} \tag{B5}$$

this rate can be derived from (B4) as

$$\xi = \frac{P_0^2}{A_I^2 \cdot (I - I_{th})^2} \cdot \frac{S_{\nu FR}}{S_{IFR}} + 2\gamma \frac{P_0}{A_I(I - I_{th})} \sqrt{\frac{S_{\nu FR}}{S_{IFR}}}. \tag{B6}$$

Fig. 19 shows the value of ξ estimated by substituting the value of $S_{\nu FR}$ of Fig. 3 and the simultaneously measured value of S_{IFR} into (B6). Since the value of ξ in this figure is lower than 10 percent, it can be concluded that the increase in the magnitude of IM noise under feedback can be neglected, i.e., S_{IFB} is approximated as S_{IFR} for the discussion in the text.

References

[1] M. Ohtsu and S. Araki, "Using a 1.5 μm DFB InGaAsP laser in a passive ring cavity-type fiber gyroscope," *Appl. Opt.*, vol. 26, pp. 464-470, 1987.
[2] M. Hashimoto and M. Ohtsu, "Experiments on a semiconductor laser pumped Rubidium atomic clock," *IEEE J. Quantum Electron.*, vol. QE-23, pp. 446-451, 1987.
[3] T. Okoshi, "Recent progress in heterodyne/coherent optical-fiber communications," *J. Lightwave Technol.*, vol. LT-2, pp. 341-346, 1984.
[4] P. Kartashoff, *Frequency and Time*. London, England: Academic, 1978.
[5] A. Brillet and P. Cerez, "Laser frequency stabilization by saturated absorption," *J. de Phys.*, vol. 42, pp. 73-82, 1981.
[6] M. Ohtsu, "Demonstration and application of frequency stabilization and linewidth reduction in semiconductor lasers," in *Tech. Dig. CLEO '86*, (San Francisco, CA), June 1986, p. 154.
[7] M. Ohtsu, "Realization of ultrahigh coherence in semiconductor lasers by electrical negative feedback," *J. Lightwave Technol.*, vol. 6, no. 2, pp. 245-256, Feb. 1988.
[8] S. Saito, O. Nilsson, and Y. Yamamoto, "Coherent FSK transmitter using a negative feedback stabilized semiconductor laser," *Electron. Lett.*, vol. 20, pp. 703-704, 1984.
[9] S. Saito, O. Nilsson, and Y. Yamamoto, "Frequency modulation noise and linewidth reduction in a semiconductor laser by means of negative frequency feedback technique," *Appl. Phys. Lett.*, vol. 46, pp. 3-5, 1985.
[10] M. Ohtsu, H. Fukada, T. Tako, and H. Tsuchida, "Estimation of the ultimate frequency stability of semiconductor lasers," *Japan. J. Appl. Phys.*, vol. 22, pp. 1157-1166, 1983.
[11] K. Kuboki and M. Ohtsu, "Frequency offset locking of AlGaAs semiconductor lasers," *IEEE J. Quantum Electron.*, vol. QE-23, pp. 388-394, 1987.
[12] M. Ohtsu and S. Kotajima, "Linewidth reduction of a 1.5 μm InGaAsP laser by electrical feedback," *Japan J. Appl. Phys.*, vol. 24, pp. L256-258, 1985.
[13] M. Ohtsu and S. Kotajima, "Linewidth reduction of a semiconductor laser by electrical feedback," *IEEE J. Quantum Electron.*, vol. QE-21, pp. 1905-1912, 1985.
[14] F. Favre, D. LeGuen, and J. C. Simon, "Optical feedback effects upon laser diode oscillation field spectrum," *IEEE J. Quantum Electron.*, vol. QE-18, pp. 1712-1717, 1982.
[15] Y. Noda, K. Saki, and Y. Matsushima, "High temperature CW operation of 1.5 μm buffer-layer loaded planoconvex waveguide lasers," *Electron. Lett.*, vol. 17, pp. 226-227, 1981.
[16] M. Kitamura, M. Yamaguchi, S. Murata, I. Mito, and K. Kobayashi, "Low-threshold and high-temperature single-longitudinal-mode operation of 1.55 μm-band DFB-DC-PBH LDs," *Electron. Lett.*, vol. 20, pp. 595-596, 1984.
[17] T. Okoshi, K. Kikuchi, and A. Nakayama, "Novel method for high resolution measurement of laser output spectrum," *Electron. Lett.*, vol. 16, pp. 630-631, 1980.
[18] K. Kikuchi, T. Fukushima, and T. Okoshi, "Frequency-modulation characteristics of semiconductor lasers: deviation from theoretical prediction by rate equation analysis." *Electron. Lett.*, vol. 22, pp. 741-742, 1986.
[19] S. Kobayashi, Y. Yamamoto, M. Ito, and T. Kimura, "Direct fre-

quency modulation in AlGaAs semiconductor lasers," *IEEE J. Quantum Electron.*, vol. QE-18, pp. 582-595, 1982.
[20] Y. Yamamoto, O. Nilsson, and S. Saito, "Theory of negative frequency feedback semiconductor laser," *IEEE J. Quantum Electron.*, vol. QE-21, pp. 1919-1928, 1985.
[21] D. W. Allan, "Statistics of atomic frequency standards." *Proc. IEEE*, vol. 54, pp. 221-230, 1966.
[22] D. Welford and A. Mooradian, "Output power and temperature dependence of the linewidth of single-frequency CW (GaAl)As diode lasers," *Appl. Phys. Lett.*, vol. 40, pp. 865-867, 1962.
[23] M. Osinski and J. Buus, "Linewidth broadening factor in semiconductor lasers—An overview," *IEEE J. Quantum Electron.*, vol. QE-23, pp. 9-29, 1987.
[24] R. Lang and K. Kobayashi, "External optical feedback effects on semiconductor injection laser properties," *IEEE J. Quantum Electron.*, vol. QE-16, pp. 347-355, 1980.
[25] D. Lenstra, B. H. Verbeek, and A. J. den Boef, "Coherence collapse in single-mode semiconductor lasers due to optical feedback," *IEEE J. Quantum Electron.*, vol. QE-21, pp. 674-679, 1985.
[26] H. S. Baeck, *Practical Servomechanism Design*. New York, NY: McGraw Hill, 1968.
[27] Anadigics Product Data Sheet, "ADA25001, DC-2.5 GHz GaAs IC amplifier," Warren, NJ, 1987.
[28] D. Hornbuckle, "GaAs IC direct-coupled amplifiers," in *1980 IEEE MTT-S Int. Microwave Symp. Dig.*, pp. 387-389, 1980.
[29] J. Helmcke, S. A. Lee, and J. L. Hall, "Dye laser spectrometer for ultrahigh spectral resolution," *Appl. Opt.*, vol. 21, pp. 1686-1694, 1982.
[30] K. Kikuchi, T. Okoshi, and T. Kawai, "Estimation of linewidth enhancement factor of CSP-type AlGaAs lasers from measured correlation between AM and FM noises," *Electron. Lett.*, vol. 20, pp. 450-451, 1984.

*

Motoichi Ohtsu was born in Kanagawa, Japan, on October 5, 1950. He received the B.S., M.S., and Ph.D. degrees in electronics engineering from the Tokyo Institute of Technology, Tokyo, Japan, in 1973, 1975, 1978, respectively.

In 1978, he was appointed a Research Associate, and in 1982, became an Associate Professor at the Tokyo Institute of Technology. From September 1986 to July 1987, on leave of absence from Tokyo Institute of Technology, he joined AT&T Bell Laboratories, Crawford Hill Laboratory, Holmdel, NJ. His main fields on interest are the frequency control of lasers, analysis of dynamic behavior of lasers, and its applications to coherent optical measurements, optical communications, and microwave atomic clocks. He has written seven books.

Dr. Ohtsu is a member of the Institute of Electronics, Information, and Communication Engineers of Japan, the Institute of Electrical Engineers of Japan, the Japan Society of Applied Physics, and the Optical Society of America. In 1982, he was awarded a prize from the Japan Society of Applied Physics. He was awarded the Issac Koga Gold Medal from the International Union of Radio Science (URSI) in 1984.

*

Noboru Tabuchi was born in Tokyo, Japan, in June 1961. He received the B.S. and M.S. degrees in electronics engineering from the Tokyo Institute of Technology, Tokyo, Japan, in 1985, and 1987, respectively. He is now at Nippon Telegraph and Telephone Company, Tokyo, Japan. He is interested in frequency control of semiconductor lasers for coherent optical sensing and communication.

Mr. Tabuchi is a member of the Japan Society of Applied Physics.

E. WOLF, PROGRESS IN OPTICS XXV

II

COHERENCE IN SEMICONDUCTOR LASERS

BY

MOTOICHI OHTSU

Graduate School at Nagatsuta
Tokyo Institute of Technology
4259 Nagatsuta, Midori-ku, Yokohama 227, Japan

TOSHIHARU TAKO

Department of Physics, Faculty of Science and Technology
Science University of Tokyo
4671 Yamazaki, Noda, Chiba 278, Japan

CONTENTS

§ 1. Introduction

Pulsed oscillations in semiconductor lasers were announced in 1962 by four groups (HALL, FENNER, KINGSLEY, SOLTYS and CARLSON [1962], NATHAN, DUMKE, BURNS, DILL and LASHER [1962], QUIST, REDIKER, KEYES, KRAG, LAX, MCWHORTER and ZEIGER [1962], HOLONYAK and BEVANCQUA [1962]). Following these pioneering works, continuous wave oscillations at room temperature were obtained by ALFEROV, ANDREEV, PORTNOI and TRUKAN [1969] and by HAYASHI, PANISH, FOY and SUMSKI [1970], where the idea of double-hetero structure was employed. Remarkable progress in semiconductor laser research has been subsequently carried out, and many kinds of lasers with sophisticated structures, for example, single-mode and integrated lasers, have been fabricated.

Semiconductor lasers have a number of favorable characteristics, such as their small size, low electrical power consumption, and fast response, which have enabled their application in communication and optical disk memory. In addition to industrial applications, they are potentially very useful as coherent light sources in the field of optics. Furthermore, the use of these lasers together with optical fibers, that is, new optical transmission media, makes other applications possible, such as precise optical measurements and the sensing of several physical and chemical quantities.

Semiconductor lasers have certain unique oscillation mechanisms and characteristics when they are compared with other types of lasers. For example, temporal coherence is lower; that is, frequency noise intensities are higher than those of gas lasers or dye lasers because of the presence of a smaller cavity Q, larger and faster fluctuations in carrier density which makes the adiabatic approximation invalid, and the existence of other specific noise sources.

Since the investigations of these noise generation mechanisms are connected with nonlinear oscillation theory, quantum-statistical mechanics, semiconductor physics, and stochastic process theory, they have attracted the attention of many researchers. Analyses of these mechanisms and reduction of noise are essential if these lasers are to be used as coherent light sources.

This review will examine structures, oscillation mechanisms, characteristics of noise and temporal coherence, techniques of noise reduction and improve-

ment in coherence, and applications of highly coherent lasers in the field of optics.

§ 2. Structures and Oscillation Mechanisms

2.1. STRUCTURES

Most of the recently available, popular semiconductor lasers are AlGaAs lasers, which function at the wavelength of 0.7–0.9 μm and are used for optical disk memories, optical measurements, optical sensors, and other applications. Progress in the development of shorter-wavelength lasers has recently occurred, resulting in the successful production of a laser with the shortest wavelength (626.2 nm) by KOBAYASHI, HINO and SUZUKI [1984], which shows pulsed oscillation at room temperature.

InGaAsP lasers, with a wavelength of 1–2 μm, have been used for optical communication because optical fibers show null dispersion at 1.3 μm, and also show the lowest available losses of 0.2 dB/km at 1.55 μm. This lowest loss value has been demonstrated by MIYA, TERUMURA, HOSAKA and MIYASHITA [1979].

Lead-chalcogenide lasers with wavelengths longer than several μm also have been used for spectroscopy of organic molecules. Although they oscillate only at low temperatures, oscillation at room temperature (290 K) has been demonstrated by FREED, BIELINSKI, LO and PARTIN [1984].

Figure 1 shows the typical structure of an AlGaAs laser. Its active layer of GaAs is sandwiched between p-AlGaAs and n-AlGaAs cladding layers, which is called a double-hetero structure. The active layer forms a waveguide that is 1–10 μm wide, 0.1–0.2 μm thick, and 200–500 μm long.

The profile of the refractive index along the x-axis of this figure has been adjusted in recently available practical lasers so that only the lowest transverse mode can oscillate. Lasers with such a profile of the refractive index are called index-guided or *transverse*-mode controlled lasers, and the profile design is called the transverse-mode control technique. Figure 2 shows cross-sections of typical index-guided lasers, examples of which are buried heterostructure (BH) lasers (TSUKADA [1974]), transverse junction stripe (TJS) lasers (NAMIZAKI, KAN, ISHII and ITO [1974]), and channelled substrate planar (CSP) lasers (DOI, CHINONE, AIKI and ITO [1979]). This review discusses those index-guided lasers in which only the lowest transverse mode can oscillate.

NAKAMURA, AIKI, CHINONE, ITO and UMEDA [1978] have proved experi-

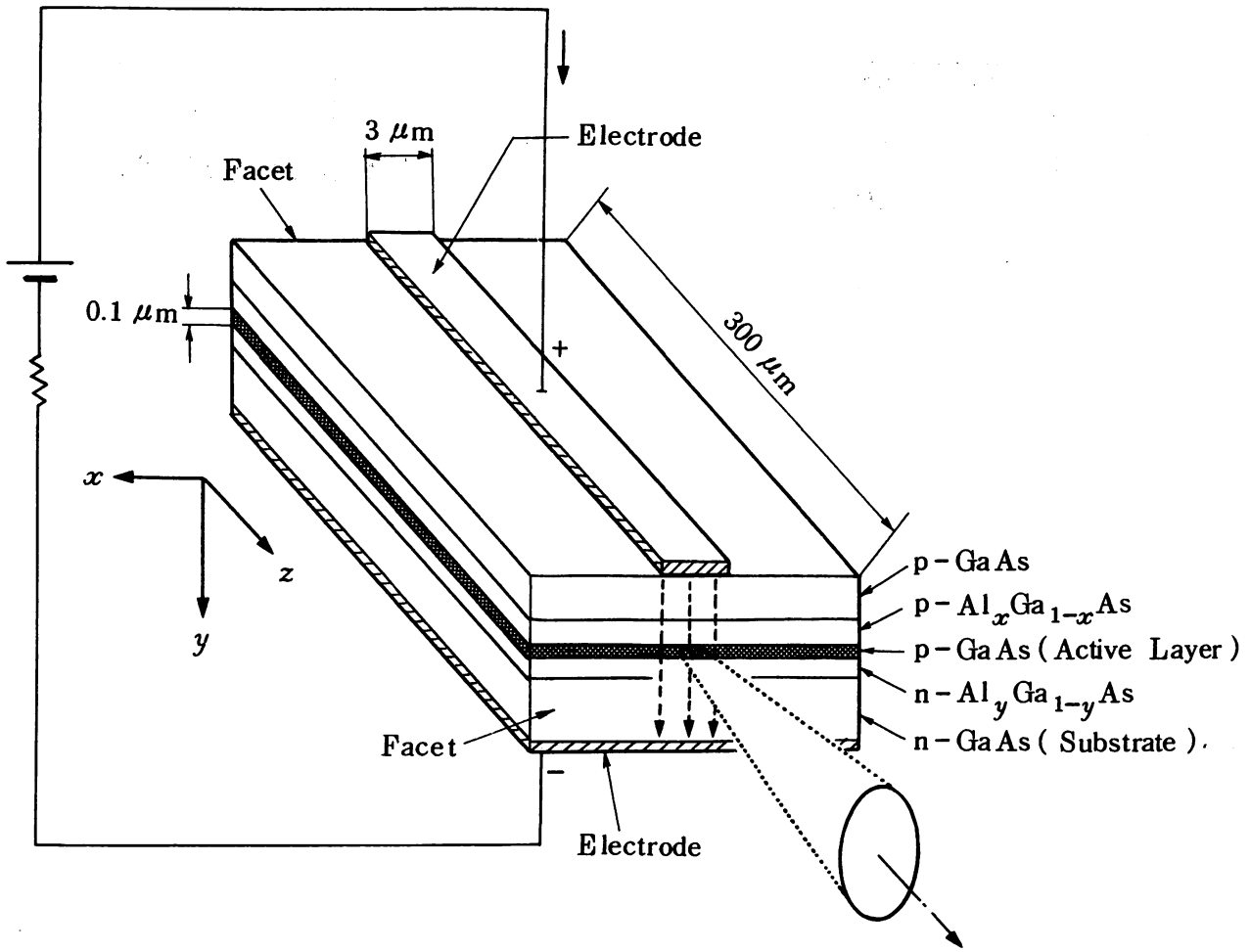

Fig. 1. Typical structure of an AlGaAs laser.

mentally that a transverse-mode controlled laser also has a tendency to oscillate only with a single longitudinal mode. COPELAND [1980] has pointed out that this tendency is due to the DX centers in the cladding layer, which work as saturable absorbers to suppress satellite longitudinal modes. However, sufficiently clear explanations about the longitudinal-mode selection mechanism have not yet been given.

Even though such lasers can oscillate with a single longitudinal mode under certain conditions of operation (e.g., injection current, ambient temperature, etc.), the oscillating longitudinal mode would suddenly change if a slow variation in these conditions should occur. This effect results because the gains for neighboring longitudinal modes are almost equal, and these modes are strongly coupled with each other. This mode alternation is called mode-hopping. Furthermore, multilongitudinal-mode oscillations will occur in these lasers when they are directly modulated by a large-amplitude AC injection current. However, for several applications lasers are desired that always show a single longitudinal oscillation, even under these dynamic conditions. The

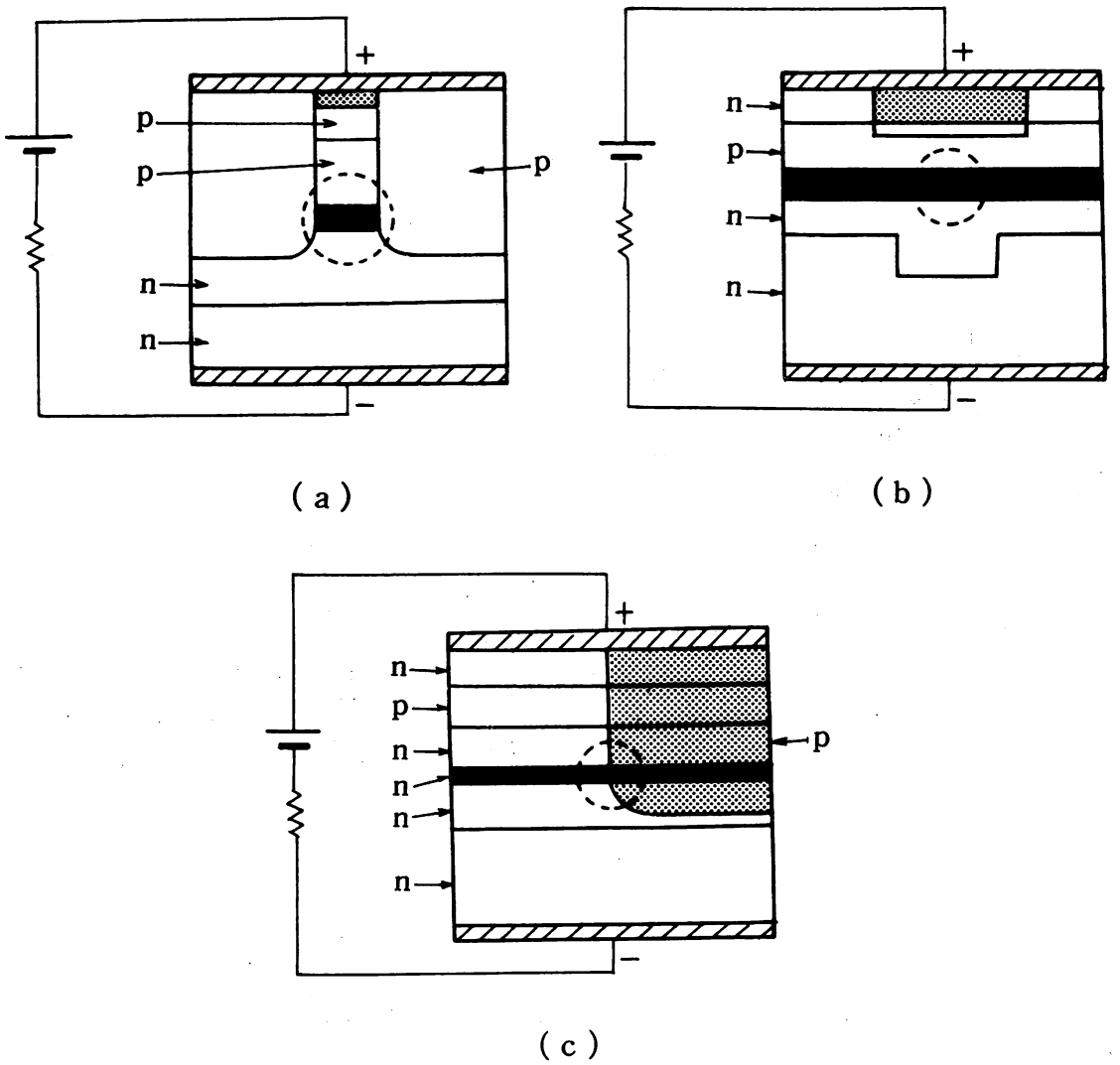

Fig. 2. Cross-sections of typical index-guided lasers: (a) Buried heterostructure (BH-type) laser. (After TSUKADA [1974].) (b) Channeled substrate planar (CSP-type) laser. (After DOI, CHINONE, AIKI and ITO [1979].) (c) Transverse junction stripe (TJS-type) laser. (After NAMIZAKI, KAN, ISHII and ITO [1974].)

design of this type of laser is sometimes called *longitudinal*-mode control technique.

For these designs, diffraction gratings are sometimes installed along or adjacent to the waveguide of the active layer. In this case only one longitudinal mode can oscillate: the mode whose wavelength coincides with the groove spacing of the diffraction grating. Typical lasers with this single longitudinal-mode oscillation are distributed feedback (DFB) lasers (KOGELNIK and SHANK [1971], AIKI, NAKAMURA, UMEDA, YARIV, KATZIR and YEN [1975], UTAKA, AKIBA, SAKAI and MATSUSHIMA [1981], MATSUOKA, NAGAI, ITAYA, NOGUCHI, SUZUKI and IKEGAMI [1982]) and distributed Bragg reflector (DBR) lasers (REINHART, LOGAN and SHANK [1975], TSANG and WANG [1976], KAWANISHI, SUEMATSU, UTAKA, ITAYA and ARAI [1979],

UTAKA, KOBAYASHI, KISHINO and SUEMATSU [1980], ABE, KISHINO, SUEMATSU and ARAI [1981]). Figure 3 shows the structures of these lasers. Another type of single longitudinal-mode lasers, called the cleaved coupled cavity laser (TSANG, OLSSON and LOGAN [1983]), has been developed; these are composed of two cleaved cavities.

Furthermore, quantum-well structures have been introduced into the lasers to reduce the threshold current and to improve the temperature dependence of oscillation characteristics (HOLONYAK, KOLBAS, DUPIUS and DAPKUS [1980]).

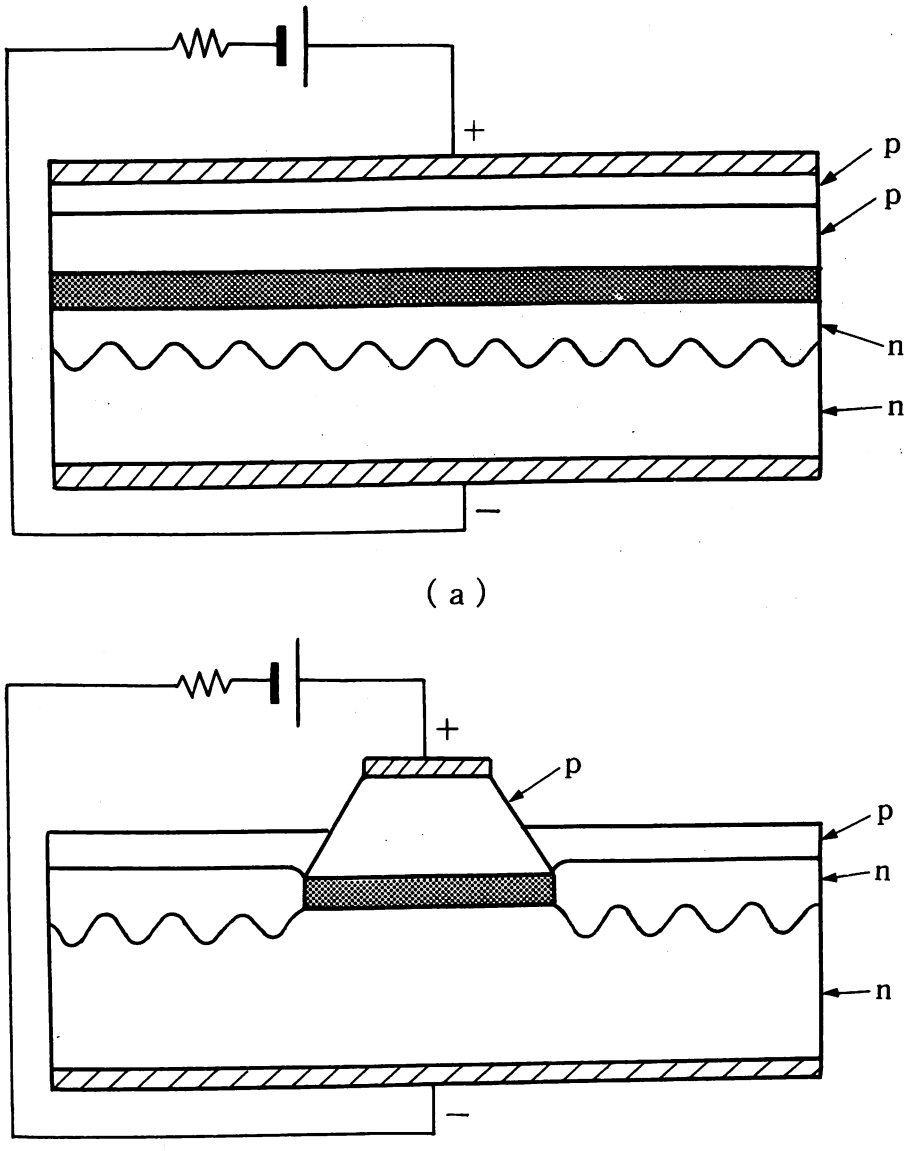

Fig. 3. Structures of longitudinal-mode stabilized lasers. (a) Distributed feedback (DFB-type) laser. (After KOGELNIK and SHANK [1971], AIKI, NAKAMURA, UMEDA, YARIV, KATZIR and YEN [1975], UTAKA, AKIBA, SAKAI and MATSUSHIMA [1981], and MATSUOKA, NAGAI, ITAYA, NOGUCHI, SUZUKI and IKEGAMI [1982].) (b) Distributed Bragg reflector (DBR-type) laser. (After REINHART, LOGAN and SHANK [1975], TSANG and WANG [1976], KAWANISHI, SUEMATSU, UTAKA, ITAYA and ARAI [1979], UTAKA, KOBAYASHI, KISHINO and SUEMATSU [1980], and ABE, KISHINO, SUEMATSU and ARAI [1981].)

2.2. OSCILLATION MECHANISMS AND THEIR FORMULATION

Current injected into a p–n junction can provide electrons and positive holes into the conduction and valence bands, respectively, which work as carriers. Laser oscillations are generated by stimulated emission from these carriers and optical positive feedback from a waveguide-type cavity.

STATZ, TANG and LAVINE [1964] and SUEMATSU, AKIBA and HONG [1977] have proposed rate equations for the photon densities S_i of the ith longitudinal mode and carrier density N_c. For single longitudinal mode oscillation in simple form, equations are expressed as

$$\frac{dS_i}{dt} = g(N_c - N_G)S_i + \frac{CN_c}{\tau_r} - \frac{S_i}{\tau_p}, \tag{2.1}$$

$$\frac{dN_c}{dt} = \frac{I}{eV_a} - g(N_c - N_G)S_i - \frac{N_c}{\tau_s}. \tag{2.2}$$

Here, g is a constant that is proportional to the stimulated emission rate, and N_G is the minimum carrier density required to keep a positive gain for oscillation. C is the spontaneous emission coefficient, representing the portion of the spontaneous emission energy which works as a trigger for the laser oscillation of the ith mode. SUEMATSU and FURUYA [1977] have estimated the value of C as being 10^{-6}–10^{-4}. τ_r is the lifetime of the carriers, which is due to radiative recombination, and τ_s is the total lifetime of the carriers, which is due to radiative and nonradiative recombination. τ_p is the photon lifetime, I is the injection current, e is the electron charge, and V_a is the volume of the active layer.

The use of these rate equations can lead to quantitative descriptions of the characteristics of laser power and several transient phenomena. By including spatial profiles of carriers and optical fields into these equations, relations between the structures of laser waveguides and several oscillation characteristics have been discussed. The results of these discussions have been commonly applied in designing reliable laser structures.

For more quantitative estimations of oscillation gain the density-matrix approach with third-order approximation developed for gas lasers by LAMB [1964] can be used. This approach has been applied to semiconductor lasers by YAMADA and SUEMATSU [1981], and the resultant rate equations for the square of the field amplitude E_i of the ith mode and the carrier density N_c are

$$\frac{d|E_i|^2}{dt} = \frac{c}{n}[\tilde{\alpha}_i^{(1)} - \alpha_{th} - \tilde{\alpha}_i^{(3)} \cdot |E_i|^2 - \tilde{\alpha}_{i(j)}^{(3)}|E_j|^2]|E_i|^2 + \frac{Ch\nu_i N_c}{2n\varepsilon_0\tau_r}, \tag{2.3}$$

$$\frac{dN_c}{dt} = n\sqrt{\frac{\varepsilon_0}{\mu_0}}\sum_i \frac{2}{h\nu_i}\tilde{\alpha}_i^{(1)} \cdot |E_i|^2 - \frac{N_c}{\tau_s} + \frac{I}{eV_a}. \tag{2.4}$$

In eq. (2.3) c is the speed of light, n is the refractive index of the active layer, $\tilde{\alpha}_i^{(1)}$ is the linear gain, and α_{th} is the cavity loss. In eq. (2.4) ε_0 is the permittivity constant of the vacuum, μ_0 is the permeability constant of the vacuum, h is Planck's constant, and ν_i is the oscillation frequency of the ith mode.

These rate equations can be applied in discussing phenomena such as mode competition, since eq. (2.3) contains the self-saturation coefficient $\tilde{\alpha}_i^{(3)}$ as well as the cross-saturation coefficient $\tilde{\alpha}_{i(j)}^{(3)}$, which represent the gain saturation.

The temporal variation of N_c given by eq. (2.4) is fast because the carrier lifetime τ_s is as short as 3 ns. This means that the adiabatic approximation cannot be applied for N_c, which also means that the coefficients $\tilde{\alpha}_i^{(1)}$, $\tilde{\alpha}_i^{(3)}$, and $\tilde{\alpha}_{i(j)}^{(3)}$ in eq. (2.3) are not constants but depend on N_c. The formulation for describing the dynamics of semiconductor lasers is different from that for conventional lasers because of the dependence on N_c.

These rate equations also can be obtained by applying fully quantum-mechanical treatments. HAUG [1969] has derived the equations by combining the quantum-mechanical theory for gas and solid-state lasers with the theory for interband transitions of carriers in semiconductors. In this treatment, first equations for the photon creation and annihilation operators (b^+ and b), and for the operator for the dipole moment induced by interband transitions are derived; then the adiabatic approximation is applied for the dipole moment; this leads to the quantum-mechanical rate equations for photon density S ($= b^+ b$) and carrier density N_c. They can be expressed as

$$\frac{dS}{dt} = -\frac{S}{\tau_p} + E_{sp} + GS + F(t), \tag{2.5}$$

$$\frac{dN_c}{dt} = P - R_{sp} - GS - E_{sp} + F_c(t). \tag{2.6}$$

In eq. (2.5), E_{sp} is the rate of spontaneous emission that is proportional to C of eq. (2.1), G is a coefficient representing the rate of stimulated emission, and $F(t)$ is the Langevin force for photon density fluctuations. In eq. (2.6) P is the pumping rate, R_{sp} is the total rate of spontaneous emission, and $F_c(t)$ is the Langevin force for carrier density fluctuations. Detailed explanations on each quantity of these equations can be found in HAUG's paper [1969]. Equations (2.5) and (2.6) contain quantum-mechanical fluctuation terms, which means that they correspond to the quantum-mechanical descriptions of eqs. (2.1) and (2.2).

Rate equations (2.5 and 2.6) describe only the power of the laser, which means that they cannot be used to describe the topics treated by the present review, that is, the temporal coherence characteristics of the laser. In general, rate equations cannot be used to discuss topics such as oscillation frequency, quantum frequency noise, spectral linewidth, synchronization phenomena, and others. For these discussions, it is necessary to use equations for the phase of the lightwave, as derived by HAUG and HAKEN [1967]. The equation for the photon creation operator b^+ is derived by means of an adiabatic approximation for the dipole moment, as was the case for eqs. (2.5) and (2.6); this leads to the equation for the amplitude $B^+(t)$ of the lightwave as follows:

$$\frac{dB^+}{dt} = \beta(d - B^+B)B^+ + \tilde{F}e^{-i\Omega t}, \tag{2.7}$$

where

$$B^+(t) = b^+(t)\exp(-i\Omega t). \tag{2.8}$$

In eq. (2.7) Ω is the angular frequency of laser oscillation. The d in the first term of the right-hand side of this equation is a complex linear gain, the second term represents the gain saturation that corresponds to $\tilde{\alpha}_i^{(3)}$ of eq. (2.3), and the third term is the Langevin force representing quantum noise. If the Langevin force is removed from this equation, it is reduced to the well-known Van der Pol equation.

The equation for carrier density fluctuations δN_c can be derived from eq. (2.6), and the equations for amplitude fluctuations δB and phase fluctuations $\delta\phi$ of the lightwave can be derived from eq. (2.7). These equations, which have been formulated by YAMAMOTO [1983], are expressed as

$$\frac{d(\delta N_c)}{dt} = -\left[\frac{1}{\tau_s} + \frac{v_s}{\mu^2}\frac{d\chi_r}{dN_c}B_0^2\right]\delta N_c - 2\frac{v_s}{\mu^2}\chi_r B_0\delta B + F_c(t), \tag{2.9}$$

$$\frac{d(\delta B)}{dt} = \frac{1}{2}\frac{v_s}{\mu^2}\frac{d\chi_r}{dN_c}B_0\delta N_c + F_B(t), \tag{2.10}$$

$$\frac{d(\delta\phi)}{dt} = -\frac{1}{2}\frac{v_c}{\mu^2}\frac{d\chi_i}{dN_c}\delta N_c + F_\phi(t). \tag{2.11}$$

In these equations χ_r and χ_i are the real and imaginary parts of the nonlinear complex susceptibility, respectively, and B_0 is the stationary value of the field

amplitude of the lightwave. F_c, F_B, and F_ϕ are Langevin forces. For details on other coefficients in these equations we refer the reader to the original paper.

The characteristics of frequency noise, spectral linewidth and temporal coherence can be discussed by using these equations.

§ 3. Noise and Temporal Coherence

Intensity and frequency noise in single longitudinal-mode semiconductor lasers will be examined in this section. Spectral linewidth, which is related to frequency noise and is one of the measures representing temporal coherence, will also be discussed.

3.1. INTENSITY NOISE

Intensity noise can be derived from the quantum mechanical rate equations (2.5 and 2.6). Small-signal analyses of fluctuations in photon number and carrier density around their stationary values give the magnitudes of these fluctuations; for example, the power spectral density of the photon number density can be derived from these equations, expressed as

$$S_s(f) = \frac{A_s^2 + B_s^2 f^2}{(a_s^2 - f^2)^2 - b_s^2 f^2}. \tag{3.1}$$

Here, A_s, B_s, a_s, and b_s are constants that depend on the values of the second-order moments of the Langevin forces in eqs. (2.5) and (2.6). It is well known that the values of these moments may be compared with each coefficient of eqs. (2.5) and (2.6) by using the fluctuation–dissipation theorem, which has been discussed by SARGENT, SCULLY and LAMB [1974].

The profile of the power spectral density represented in eq. (3.1) exhibits a resonant peak at the Fourier frequency of about a_s. A detailed expression for the resonant frequency has been obtained by IKEGAMI and SUEMATSU [1967], in the equation

$$f_r = \frac{1}{2\pi}\sqrt{\frac{I/I_{th} - 1}{\tau_s \tau_p}}. \tag{3.2}$$

This is called the relaxation oscillation frequency, which depends on the carrier lifetime τ_s, photon lifetime τ_p, and the injection current normalized to its threshold value, I/I_{th}. This resonance phenomenon occurs because of the

dynamic behavior of the photon in the cavity, which is governed by the second-order lag system. That is, the carriers injected into the active layer exhibit a time lag τ_s until they emit photons by carrier recombination, and the emitted photons also exhibit a time lag τ_p until they disappear from the cavity. Such a second-order lag system generally exhibits resonance, which has been called relaxation oscillation in the case of semiconductor lasers. The frequency of this oscillation, shown in eq. (3.2), takes a value of several GHz because τ_s and τ_p are approximately 3 ns and 1 ps, respectively. Figure 4 shows the power spectral density of eq. (3.1) and its measured value, as obtained by YAMAMOTO, SAITO and MUKAI [1983]. Although the noise characteristics of the Fourier frequency lower than 1 MHz are not shown in this figure, it is empirically known that noise caused by temperature variation and $1/f$ noise are usually observed in this range.

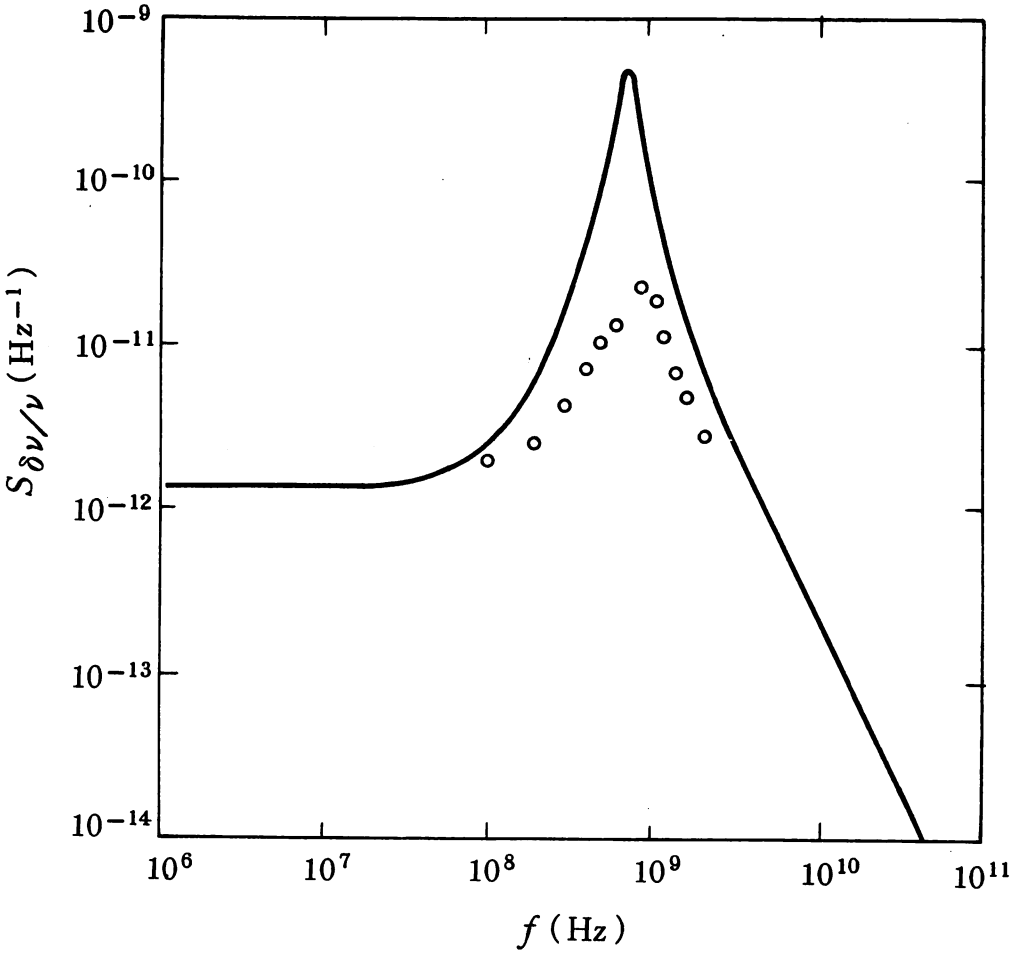

Fig. 4. The power spectral density of intensity noise in a CSP-type AlGaAs laser. The solid curve and the open circles represent theoretical and experimental results, respectively. (After YAMAMOTO, SAITO and MUKAI [1983].)

3.2. FREQUENCY NOISE

Frequency noise from several sources can be derived from eq. (2.11). Figure 5 illustrates the power spectral density of frequency noise (YAMAMOTO, SAITO and MUKAI [1983]). The first fundamental noise source is quantum fluctuations, that is, fluctuations resulting from spontaneous emission [second term of eq. (2.11)], which induces white noise. The power spectral density of frequency noise from this source can be expressed as (OHTSU, FUKADA, TAKO and TSUCHIDA [1983])

$$S_y(f) = \frac{h}{8\pi^2 \nu_0 P_0}\left(\frac{c}{nL}\right)^2\left(\alpha_i L + \ln\frac{1}{R}\right)\left(\ln\frac{1}{R}\right) n_{sp}\,. \tag{3.3}$$

In this equation the quantity y represents the normalized frequency fluctuations $\delta\nu(t)/\nu_0$, with $\delta\nu(t)$ the frequency fluctuations and ν_0 the nominal frequency of the laser, P_0 is the output power from the cavity, c is the speed of light, n is the refractive index of the active layer, L is the cavity length, R is the reflectivity of the cavity end-facet, and α_i is the intracavity loss. The quantity

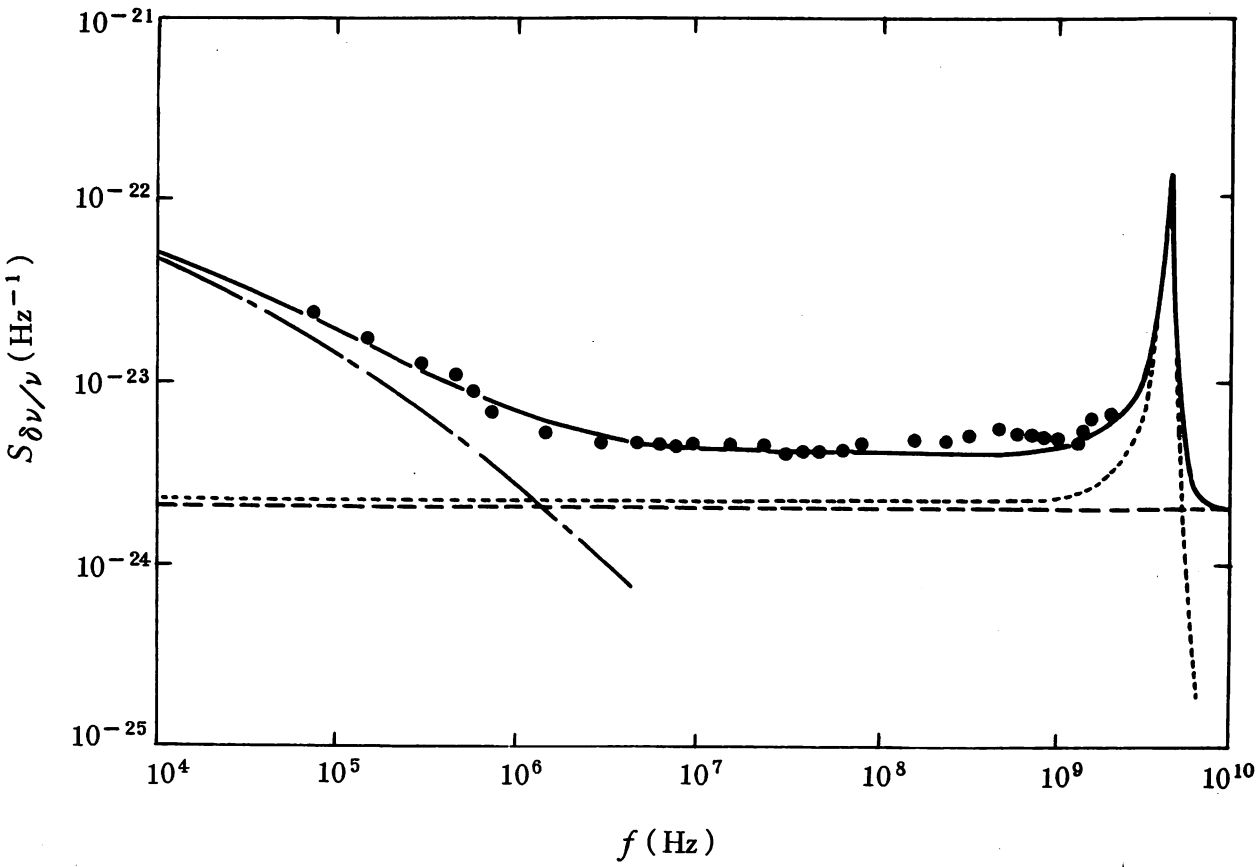

Fig. 5. The power spectral density of frequency noise in a CSP-type AlGaAs laser. (After YAMAMOTO, SAITO and MUKAI [1983].) Dashed line, noise induced by fluctuations of spontaneous emission; dotted curve, noise induced by carrier density fluctuations; dash–dotted curve, noise induced by current fluctuations; solid curve, total noise; solid dots, experimental results.

n_{sp} is the spontaneous emission factor, which is proportional to the spontaneous emission factor C of eq. (2.1) and is expressed as (WELFORD and MOORADIAN [1982a])

$$n_{sp} = \frac{1}{1 - \exp\left(\dfrac{h\nu_0 + E_{Fv} - E_{Fc}}{kT}\right)}, \tag{3.4}$$

where E_{Fv} and E_{Fc} are quasi-Fermi levels of the valence and conduction bands, respectively, k is Boltzmann's constant, and T is the temperature.

The second intrinsic noise source is the carrier density fluctuations induced by fluctuations of spontaneous emission [the first term of eq. (2.11)]. The power spectral density of the noise induced by this source exhibits a resonant peak at the relaxation oscillation frequency of eq. (3.2), as is the case for the intensity noise.

Furthermore, the injection current and temperature vary depending on carrier density fluctuations. All of these factors contribute as intrinsic noise sources. When lasers are used for optical measurements, it is common to apply a measure for frequency noise in the time domain instead of the power spectral density (which is a measure in the frequency domain). The most precise such measure is the Allan variance proposed by ALLAN [1966] and defined as

$$\sigma_y^2(\tau) = \lim_{N\to\infty} \frac{1}{N-1} \sum_{k=1}^{N-1} \frac{(\bar{y}_{k+1} - \bar{y}_k)^2}{2}. \tag{3.5}$$

In this definition $\bar{y}_k$ is the averaged value of a fluctuating quantity $y(t)$ over a time period τ. The time period τ is called the integration time, and N is the number of data. Using the definition given by ALLAN [1966], the values $\bar{y}_k$ and $\bar{y}_{k+1}$ must be successively measured by a frequency counter, for which the gate-closed time of the counter must be zero between the succeeding time periods for measurement. This procedure enables quantitative evaluation not only of stationary processes but also of nonstationary fluctuation processes such as random walk and flicker noise.

The Allan variance can also be derived from the power spectral density $S_y(f)$ by

$$\sigma_y^2(\tau) = 2\int_0^\infty S_y(f) \frac{\sin^4(\pi f\tau)}{(\pi f\tau)^2}\, df. \tag{3.6}$$

Examples of this conversion for several fluctuation processes have been summarized by BARNES, CHI, CUTLER, HEALELY, LEESON, MCGUNIGAL,

MULLEN, SMITH, SYDNOR, VESSOT and WINKLER [1971], and are shown in Table 1.

Frequency noise of semiconductor lasers has been evaluated by using the square root of the Allan variance (OHTSU, FUKADA, TAKO and TSUCHIDA [1983]); the results are shown in fig. 6. In this figure, the contribution of external noise sources, such as noise of current sources and fluctuations of ambient temperature, is also identified along with the intrinsic noise sources shown in fig. 5. A theoretical estimation of fig. 6 shows that the magnitude of frequency noise of a free-running laser is $\sigma_y(\tau) > 6 \times 10^{-12}$. Experimental results are given later in this review by fig. 14 in § 4.3.2, where measured values of frequency noise are $\sigma_y(\tau) > 3 \times 10^{-9}$ for a free-running laser.

3.3. SPECTRAL LINEWIDTH

The spectral profile of laser oscillation is given by the power spectral density of the amplitude of the electric field of the light, that is, the Fourier transform of the autocorrelation function of the amplitude. The autocorrelation function is expressed as

$$\begin{aligned} R_E(\tau) &= \langle E(t+\tau)\cdot E^*(t)\rangle \\ &= E_0^2 \langle \exp[\mathrm{i}\{2\pi\nu_0\tau + \phi(t+\tau) - \phi(t)\}]\rangle \\ &= E_0^2 \langle \exp[\mathrm{i}\{2\pi\nu_0\tau + \delta\phi(\tau)\}]\rangle \\ &\approx E_0^2 \exp[\mathrm{i}2\pi\nu_0\tau - \tfrac{1}{2}\langle \delta\phi^2\rangle], \end{aligned} \tag{3.7}$$

TABLE 1.
Relation between the power spectral density and the Allan variance (After BARNES, CHI, CUTLER, HEALELY, LEESON, MCGUNIGAL, MULLEN, SMITH, SYDNOR, VESSOT and WINKLER [1971].)

$S_y(f)$		$\sigma_y^2(\tau)$
$h_2 f^2$ $(2\pi f_h \tau \gg 1)$	[a]	$h_2 \frac{3f_h}{(2\pi)^2}\tau^{-2}$
$h_1 f^1$ $(2\pi f_h \tau \gg 1)$	[a]	$h_1 \frac{1}{(2\pi)^2}[\frac{9}{2} + 3\ln(2\pi f_h\tau) - \ln 2]\,\tau^{-2}$
$h_0 f^0$		$\frac{1}{2}h_0\,\tau^{-1}$
$h_{-1} f^{-1}$		$(2\ln 2)h_{-1}\tau^0$
$h_{-2} f^{-2}$		$\frac{1}{6}(2\pi)^2 h_{-2}\tau^1$

[a] A low-pass filter with a cutoff frequency f_h was used.

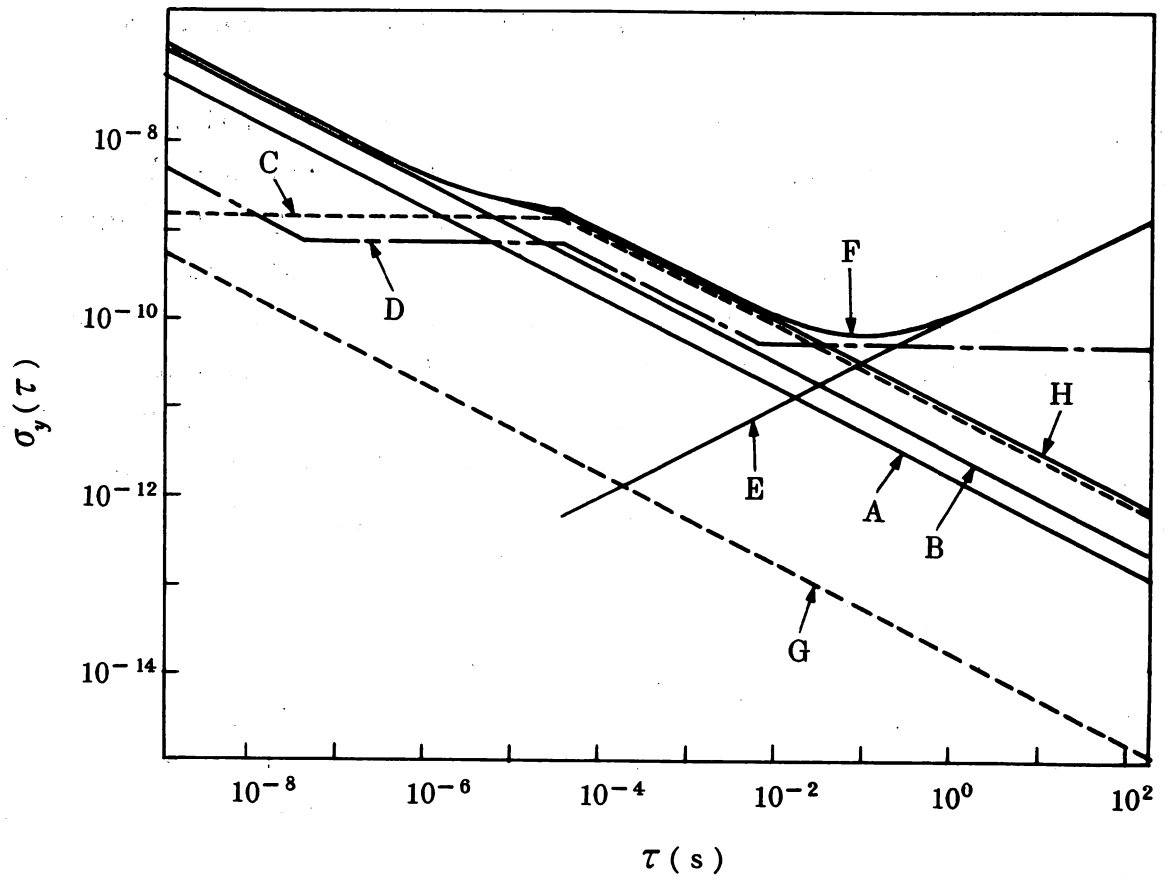

Fig. 6. Square root of the Allan variance of frequency noise in an AlGaAs laser. (A) Noise induced by fluctuations of spontaneous emission; (B) noise induced by carrier density fluctuations; (C) noise induced by current fluctuations; (D) noise induced by current source noise; (E) noise induced by fluctuations of ambient temperature; (F) noise in a free-running laser, sum of noise contributions from all the sources (A)–(E); (G) ultimate noise limit of a frequency-stabilized laser; (H) noise given by intrinsic noise sources of (A), (B) and (C). (After OHTSU, FUKADA, TAKO and TSUCHIDA [1983].)

where the asterisk represents the complex conjugate, E_0 is the amplitude of the electric field, and $\langle \delta\phi^2 \rangle$ is the second-order moment of phase fluctuations. This moment is proportional to the second-order moment of frequency fluctuations, that is, the Allan variance, which is expressed as

$$\langle \delta\phi^2 \rangle = (2\pi\nu_0\tau)^2 \cdot \sigma_y^2(\tau) . \tag{3.8}$$

Among the intrinsic noise sources the contribution of spontaneous emission to eq. (3.8) should be considered as the first step, which appears as the second term of the right-hand side of eq. (2.11). Since eq. (3.3) gives the magnitude of the frequency noise induced by this source, the use of eq. (3.3) and table 1 shows the Allan variance of frequency noise induced by spontaneous emission. This is expressed as

$$\sigma_y^2(\tau) = \frac{h}{16\pi^2\nu_0 P_0}\left(\frac{c}{nL}\right)^2\left(\alpha_i L + \ln\frac{1}{R}\right)\left(\ln\frac{1}{R}\right) n_{sp} \cdot \tau^{-1} . \tag{3.9}$$

Straightforward calculations can easily show that the spectrum of laser oscillation has a Lorentzian profile by Fourier transform of $R_E(\tau)$ if eqs. (3.8) and (3.9) are substituted into eq. (3.7). The contribution of spontaneous emission to the linewidth (full width at half-maximum [FWHM]) is therefore expressed as

$$\Delta\nu = \frac{h\nu_0}{8\pi P_0}\left(\frac{c}{nL}\right)^2\left(\alpha_i L + \ln\frac{1}{R}\right)\left(\ln\frac{1}{R}\right)n_{sp}\,. \tag{3.10}$$

This expression, derived by BLAQUIERE [1962], is called the Schawlow–Townes formula.

As the second step, the contribution of carrier density fluctuations in the first term of eq. (2.11) is taken into account. Since the linewidth would be increased by this contribution, eq. (3.10) must be modified, and the resultant expression is given by

$$\Delta\nu = \frac{h\nu_0}{8\pi P_0}\left(\frac{c}{nL}\right)^2\left(\alpha_i L + \ln\frac{1}{R}\right)\left(\ln\frac{1}{R}\right)n_{sp}(1+\alpha^2)\,. \tag{3.11}$$

This formula has been proposed by WELFORD and MOORADIAN [1982a] and is called the modified Schawlow–Townes formula. In this equation α is called the linewidth enhancement factor, which represents the contribution of carrier density fluctuations. HENRY [1982] has pointed out that α is given by the ratio between the real ($\delta n'$) and imaginary ($\delta n''$) parts of the changes in complex refractive index of the active layer induced by carrier density fluctuations ($\alpha = \delta n'/\delta n''$).

The absolute values of α for AlGaAs lasers have been measured as being 3.8–6 by WELFORD and MOORADIAN [1982a] and by HENRY [1982]. For InGaAsP lasers the absolute values have been estimated as being 2.2–2.8 by KIKUCHI and OKOSHI [1985].

Figure 7 shows an example of measured values of spectral linewidth of an AlGaAs laser (WELFORD and MOORADIAN [1982b]). As shown by this figure, the linewidth usually measures between several MHz and several hundreds of MHz. Actual values of the linewidth often vary, depending on device and operating conditions.

Equation (3.11) shows that the linewidth should approach zero with increasing laser power P_0. However, this is not the case in fig. 7, where the linewidth takes a non-zero value at $P_0^{-1} = 0$; this has been called a power-independent linewidth. WELFORD and MOORADIAN [1982b] and ELSÄSSER, GÖBEL and KUHL [1983] have reported the values of this linewidth as being between

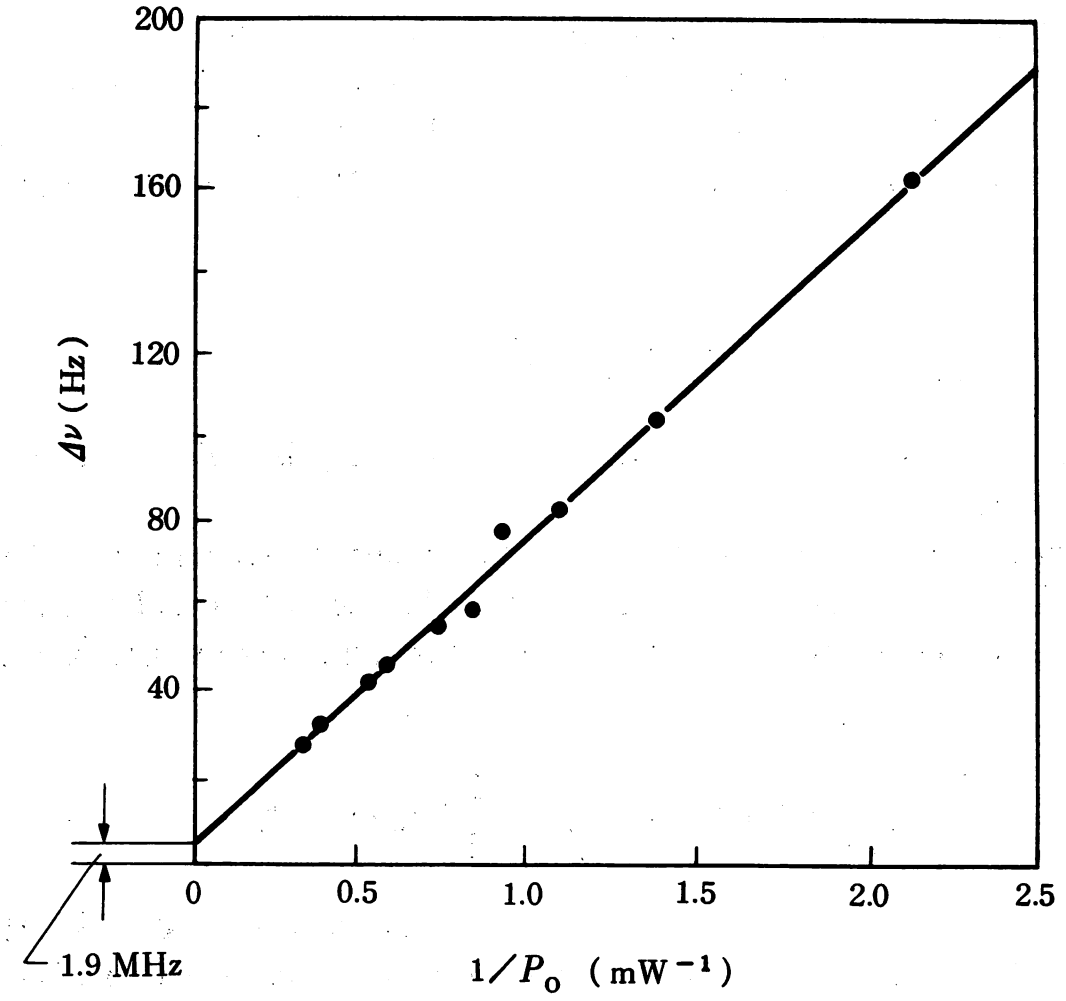

Fig. 7. An example of measured values of the spectral linewidth of an AlGaAs laser. (After WELFORD and MOORADIAN [1982b].)

0.6–1.9 MHz. The origins of this linewidth have been attributed to the power-independent carrier density fluctuations (WELFORD and MOORADIAN [1982b]), to fast thermal fluctuations of electronic state occupancy (VAHALA and YARIV [1983]), to flicker noise in frequency induced by carrier mobility fluctuations (OHTSU and KOTAJIMA [1984]), and to other factors.

§ 4. Improvement of Temporal Coherence

Estimations made in § 3.2 show that the magnitude of frequency noise in semiconductor lasers is as high as 10^{-8}, and that the spectral linewidths exceed several MHz. Since these values do not yet satisfy the requirements for application in coherent optical measurements, coherent optical communications, and other procedures, demands on improving temporal coherence have been growing recently.

The following five subjects are relevant areas for study to meet the demands of this expanding field:

(1) Linewidth reduction of the field spectrum;
(2) Stabilization of center frequency of the field spectrum;
(3) Improvements of frequency reproducibility;
(4) Frequency tracking to another, highly coherent laser;
(5) Stable and wideband frequency sweep.

These subjects will be reviewed in this section. Definitions of frequency stability, reproducibility, and accuracy are given in the Appendix.

4.1. COMPARISONS WITH MICROWAVE OSCILLATORS AND OTHER TYPES OF LASERS

Prior to reviewing techniques for improving temporal coherence of semiconductor lasers, we will examine and compare other types of highly coherent oscillators.

Cesium (Cs) atomic clocks (9.2 GHz) and rubidium (Rb) atomic clocks (6.8 GHz) have been used as primary and secondary standards of time, respectively. A review by KARTASCHOFF [1978] describes the use of resonance frequencies of electronic transitions in Cs or Rb atoms as frequency references to control the frequencies of voltage-controlled crystal oscillators. They are called passive-type frequency standards, and demonstrate a high performance level; for example, a frequency stability of 10^{-14} and frequency accuracy of 10^{-13} have been achieved in Cs atomic clocks.

Furthermore, by employing a frequency synchronization technique, the frequency of a Cs atomic clock can be accurately tracked by Rb atomic clocks. The frequency of the Rb atomic clock also can be tracked by conventional, lower-stability quartz crystal oscillators. Using this technique, a hierarchy from higher to lower frequency stability has been established for microwave oscillators. They have been used to provide synchronized clock pulses for microwave communication networks, remote sensing, astronomy, ranging, and other applications.

A hydrogen maser (1.4 GHz) is another type of highly coherent microwave oscillator; it utilizes stimulated emission resulting from the electronic transitions in hydrogen atoms. This oscillator is called an active-type frequency standard. It has been used in very long baseline interferometry (VLBI) because of its high short-term frequency stability, measuring as high as 10^{-15}.

As mentioned earlier, microwave oscillators have demonstrated high levels of temporal coherence because of the following reasons:

(1) The spectroscopic properties of atomic resonance lines have been thoroughly investigated in order to use them as frequency references.

(2) Electronic circuits for frequency control have been fully provided.

(3) Direct frequency measurements are possible.

(4) The lowest mode of microwave cavities has been used for microwave oscillation.

(5) In the case of active-type frequency standards such as hydrogen masers, a pulling effect fixes the oscillation frequency close to the resonance frequency of the maser medium because the Q-value of the maser medium is larger than that of the cavity in the microwave frequency region.

In contrast to microwave oscillators, general lasers possess the following characteristics, which can sometimes cause deterioration of temporal coherence:

(i) Direct frequency measurements are impossible because of their ultrahigh frequencies of about 1–100 THz, which would decrease accuracy and reproducibility of frequency measurements.

(ii) Higher-order cavity modes have been used for oscillation; this can induce multilongitudinal mode oscillations, mode-hopping, and other characteristics.

(iii) A pulling effect fixes the oscillation frequency close to one of the resonance frequencies of the *cavity* because the Q-value of the cavity is larger than that of the laser medium. This induces fluctuations and drifts in oscillation frequency by means of mechanical vibration or thermal expansion of the cavity.

In general, the temporal coherence of lasers is not necessarily superior to that of microwave oscillators. Despite these characteristics, lasers do possess the potential for exhibiting higher temporal coherence in the future because of a higher Q-value of the cavity and higher frequency than those demonstrated by microwave oscillators. Furthermore, lasers can be used as versatile light sources for optical measurements because of their widely distributed wavelengths, between the far infrared and ultraviolet regions.

For gas and dye lasers, frequency stabilization techniques have been developed satisfactorily by using resonance lines of stable atoms or molecules, or stable Fabry–Perot interferometers as frequency references. BRILLET and CEREZ [1981] have described the attainment of a frequency stability of 10^{-13} for gas and dye lasers and as high as 10^{-14} for a specially designed helium–xenon laser at 3.51 μm (OHTSU, KATSURAGI and TAKO [1981]) and for dye lasers (HALL, SALAMON and HILS [1986]). A spectral linewidth in the subhertz region has been already attained for a dye laser (HALL, SALAMON and HILS [1986]).

If semiconductor lasers are compared with these lasers, they demonstrate the following specific features:

(a) The cavity Q-value is smaller because of the smaller cavity volume.

(b) The carrier density fluctuates rapidly, and the cutoff frequency of its power spectral density is as high as the relaxation oscillation frequency.

(c) Carriers are optically pumped by injected light.

(d) Variations in the values of mole fraction of compound semiconductor materials and cavity sizes can reduce the reproducibility of oscillation characteristics, which also reduces the frequency reproducibility.

These features can enhance the oscillation instabilities and deterioration in temporal coherence due to spontaneous emission or external signals injected into the cavity.

Despite these drawbacks, semiconductor lasers are still useful for practical applications in several optical systems because of their small volume and low power consumption. For these practical uses efforts have recently been made to improve their temporal coherence.

4.2. THEORETICAL BACKGROUND OF NEGATIVE FEEDBACK FOR IMPROVING TEMPORAL COHERENCE

Control of the laser frequency can be achieved by controlling the resonance frequency of the laser cavity. In the case of semiconductor lasers this can be done by varying the refractive index or the length of the cavity through changes in the injection current or ambient temperature. The resultant frequency shift $\delta\nu$ can be expressed as

$$\delta\nu = -\nu_0\left[A\frac{1}{n}\delta N_c(I) + (\alpha_T + \beta_T)\cdot\delta T_1(I) + (\alpha_T + \beta_T)\cdot\delta T_2\right]. \qquad (4.1)$$

The first term on the right-hand side of eq. (4.1) represents the effect of variation in the refractive index resulting from carrier density variation $\delta N_c(I)$ by means of the injection current I, with A a proportionality constant. The second term represents the effects of variations in the refractive index and the cavity length resulting from temperature variation $\delta T_1(I)$ by means of the injection current. The coefficients α_T and β_T are proportionality constants for these variations, respectively. The third term represents the same effects caused by variations in ambient temperature δT_2. Numerical values of the proportional constants in this equation are summarized in table 2.

For frequency control, injection current control is more effective than controlling the ambient temperature because temperature response is slower.

TABLE 2
Typical values of the constants in eq. (4.1) for AlGaAs and InGaAsP lasers.

	AlGaAs	InGaAsP
A	$-4.0 \times 10^{-27}\,m^3$	$-7.0 \times 10^{-27}\,m^3$
n	3.5	3.5
α_T	$5 \times 10^{-6}\,K^{-1}$	$5.4 \times 10^{-6}\,K^{-1}$
β_T	$1 \times 10^{-4}\,K^{-1}$	$1.0 \times 10^{-4}\,K^{-1}$

Figures 8 and 9 show response characteristics of frequency modulation by means of the injection current. Figure 8 shows experimental results of frequency deviation $|\partial\nu/\partial I|$ measured by KOBAYASHI, YAMAMOTO, ITO and KIMURA [1982]. In this figure it can be seen that the primary contribution comes from the thermal effect of the second term of eq. (4.1) for the modulation of frequency ranges lower than several MHz, whereas the carrier effect dominates in the higher frequency ranges. In addition, the carrier effect attains the relaxation oscillation frequency of eq. (3.2), which limits the response bandwidth of frequency control by the injection current.

Figure 9 shows the experimental results of phase delay $\arg(\partial\nu/\partial I)$ measured by JACOBSEN, OLESEN and BIRKEDAHL [1982]. This phase delay is also governed by thermal and carrier effects, as it was for $|\partial\nu/\partial I|$. This figure shows

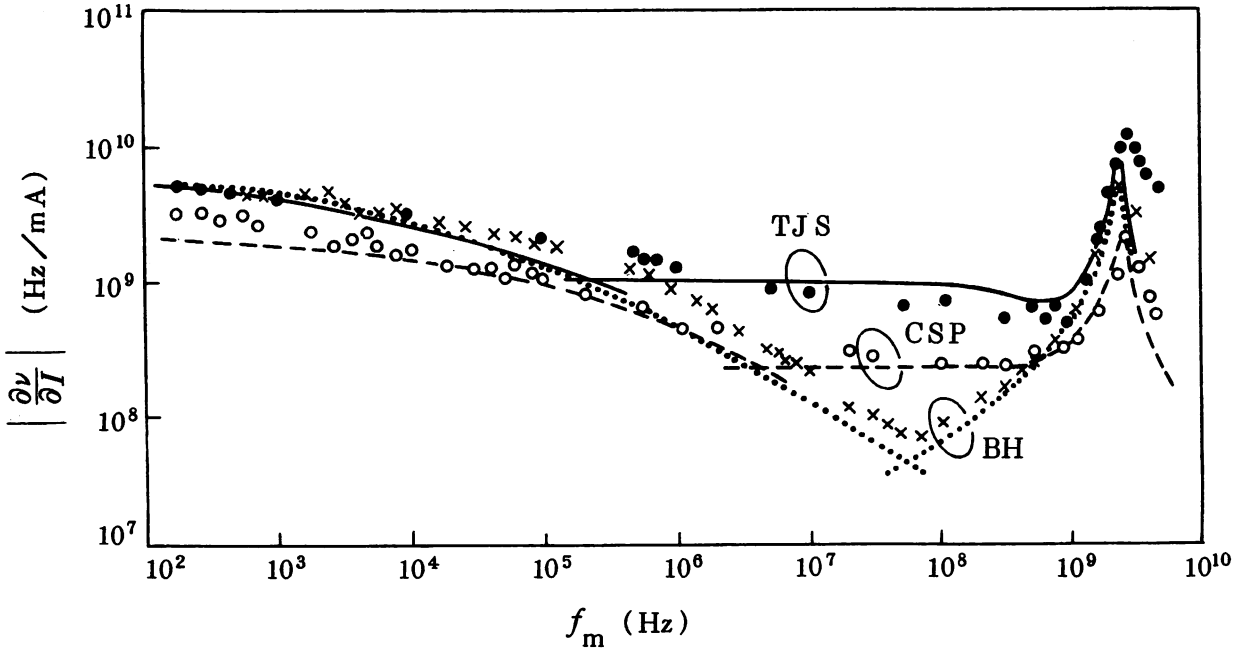

Fig. 8. Characteristics of frequency deviation of TJS-, CSP-, and BH-type AlGaAs lasers obtained by modulating the injection current. Curves and symbols represent theoretical and experimental results, respectively. (After KOBAYASHI, YAMAMOTO, ITO and KIMURA [1982].)

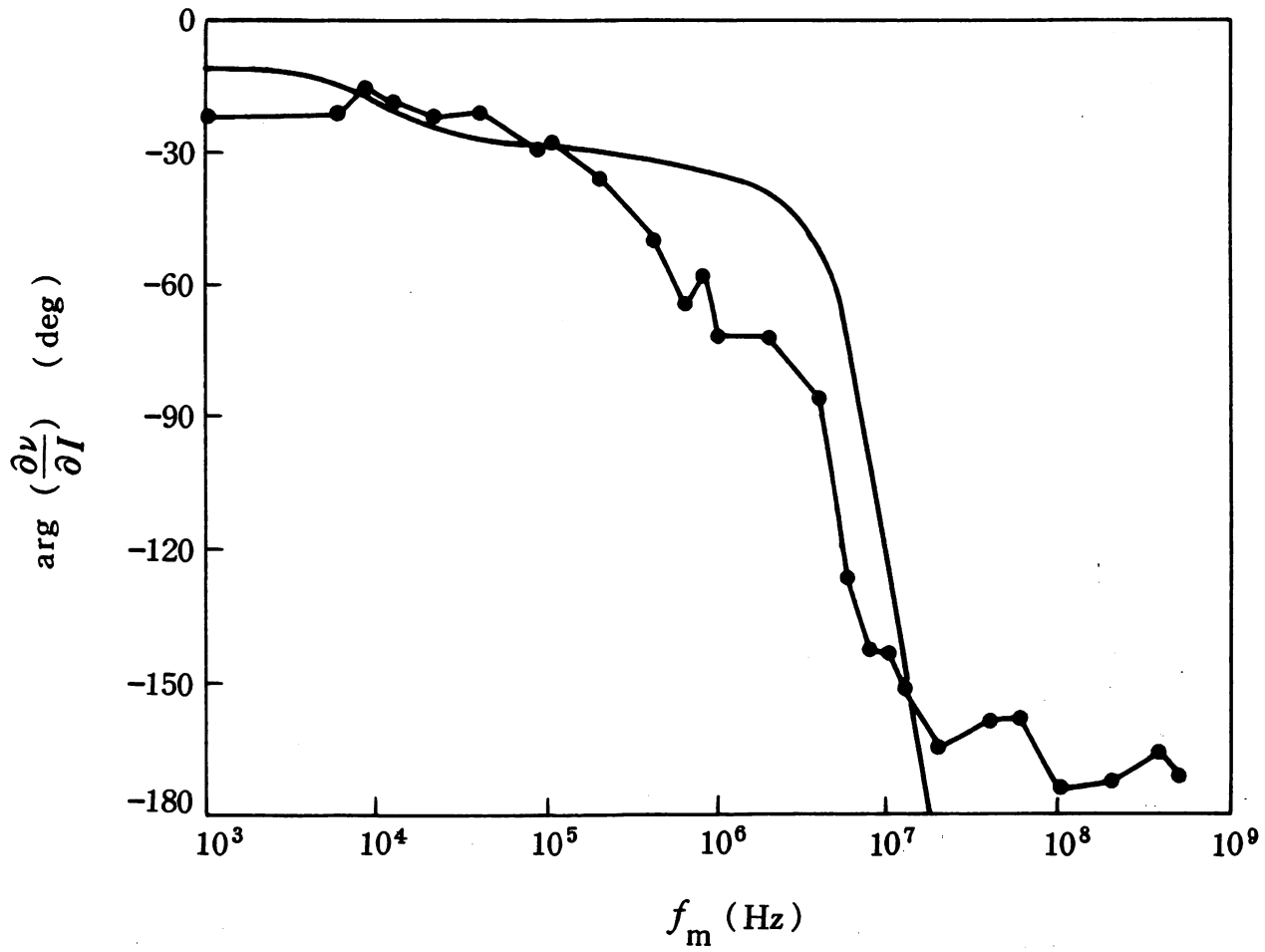

Fig. 9. Characteristics of the phase delay of frequency modulation of a CSP-type AlGaAs laser by injection current. Curve and dots represent theoretical and experimental results, respectively. (After JACOBSEN, OLESEN and BIRKEDAHL [1982].)

that the phase delay increases with increasing modulation frequency, which means that phase-lead compensation, that is, an analog differentiator, is required in a servocontrol loop for negative feedback.

Insufficient stabilization of the ambient temperature can induce frequency drift, which takes a larger value of the Allan variance in the range of longer integration time τ. Therefore, the use of an amplifier with higher gain at a lower Fourier frequency range, that is, an analog integrator, effectively reduces the drift.

In addition to these electronic components, a frequency reference is required to fix the frequency at a constant value. Absorption spectra in atoms or molecules and a Fabry–Perot interferometer can be employed for this reference. A block diagram of electrical feedback is shown in fig. 10.

In the following calculations minimum attainable frequency fluctuations are estimated in cases where frequency deviations from this reference can be accurately measured and where sufficient bandwidth of negative feedback is ensured. This estimation was carried out by YAMAMOTO, NILSSON and SAITO

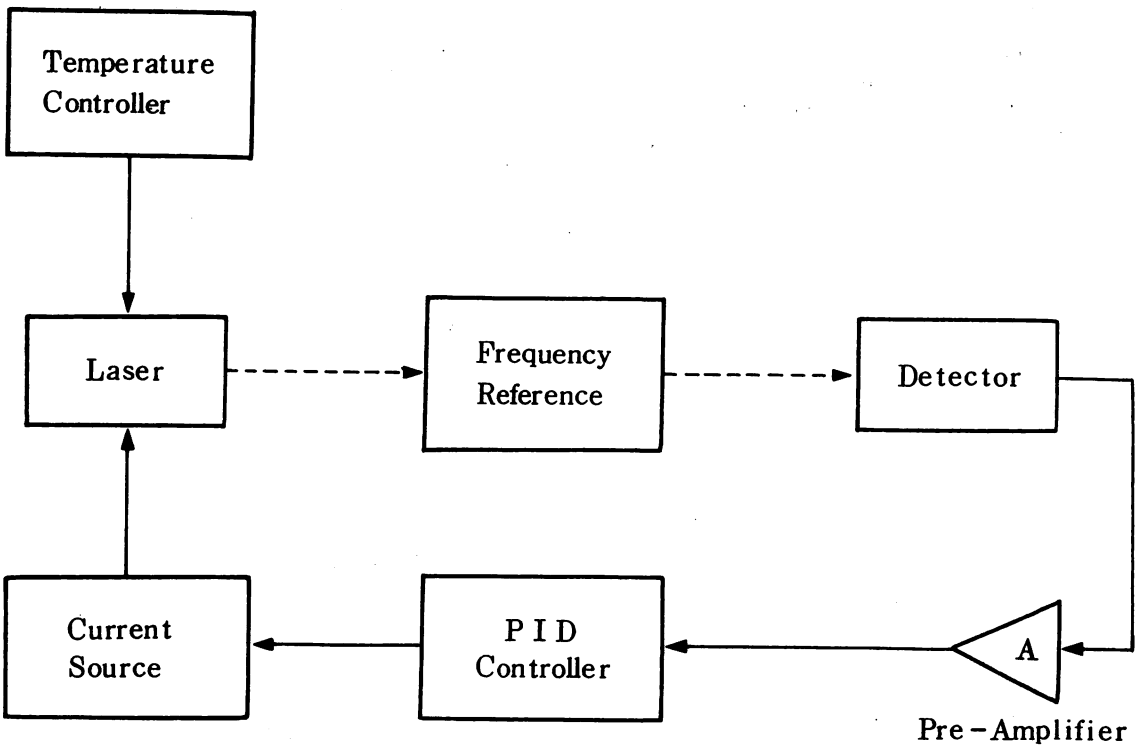

Fig. 10. Block diagram of electrical feedback. PID controller: Proportional amplifier, analog Integrator, and Differentiator for feedback.

[1985], who added a term representing a negative feedback effect to the equation for phase fluctuations of eq. (2.11). This is expressed as

$$\frac{\mathrm{d}(\delta\phi)}{\mathrm{d}t} = -\frac{1}{2}\frac{v_s}{\mu^2}\frac{\mathrm{d}\chi_i}{\mathrm{d}N_c}\delta N_c + F_\phi(t) - \int_0^\infty h_f(\tau')\left[\frac{\mathrm{d}(\delta\phi(t-\tau'))}{\mathrm{d}t} + \Gamma(t-\tau')\right]\mathrm{d}\tau' , \tag{4.2}$$

where h_f is the impulse response of the feedback loop, and $\Gamma(t-\tau')$ is the magnitude of the noise generated in the feedback loop. Fourier transform of this equation gives

$$\Phi = \frac{1}{\mathrm{i}\omega}\frac{\Phi_c + \Phi_F}{1+H} - \frac{1}{\mathrm{i}\omega}\frac{H}{1+H}\Xi , \tag{4.3}$$

where, Φ, H, and Ξ are the Fourier transforms of $\delta\phi$, h_f, and Γ, respectively. Φ_C and Φ_F represent the Fourier transforms of the first and second terms of the right-hand side of eq. (4.2), respectively. i is the imaginary unit and ω the Fourier angular frequency. The first term vanishes for infinite gain ($H \to \infty$); that is, the quantum noise contributions of carrier density fluctuations and spontaneous emission, which are the intrinsic noise sources for free-running lasers, can be suppressed by infinitely increasing the feedback gain. Since the

second term approaches a finite value Ξ with increasing H, it can be estimated that phase fluctuations can be reduced to a value limited by the noise of the feedback loop in the case of infinite feedback gain. This means, for example, that the spectral linewidth can be reduced to a value narrower than that given by the Schawlow–Townes formula (3.10) if a low-noise, high-gain feedback loop is used.

A fundamental noise component of this feedback loop can be shot noise from the photodetector. For example, fig. 11 shows the minimum attainable linewidth of an InGaAsP laser of 1.5 μm wavelength, as derived by OHTSU and KOTAJIMA [1985a], which is limited by the shot noise. For this estimation it was assumed that a Fabry–Perot interferometer of 1 cm long was used as a frequency discriminator for fluctuation measurements. This figure shows that a linewidth as narrow as 1 kHz–100 Hz may be expected, depending on the finesse of the interferometer. The highest frequency stability as limited by the

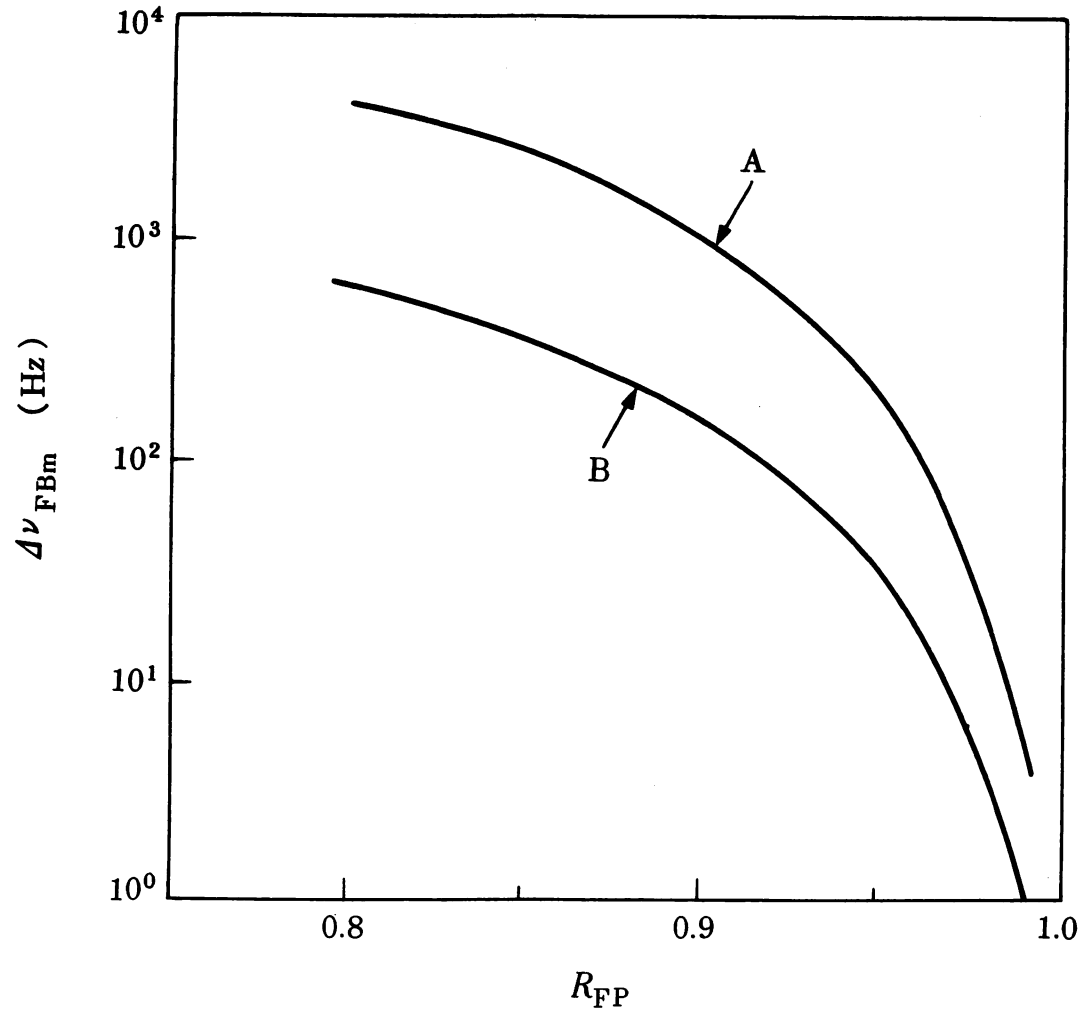

Fig. 11. Minimum attainable linewidth of an InGaAsP laser by means of electrical feedback. R_{FP}, reflectance of the mirrors of a 1-cm-long Fabry–Perot interferometer used as frequency discriminator; (A) result limited by noise from a germanium-avalanche photodiode; (B) result limited by noise from a germanium-PIN photodiode. (After OHTSU and KOTAJIMA [1985a].)

detector shot noise can also be estimated. For example, its value for an AlGaAs laser has been estimated by OHTSU, FUKADA, TAKO and TSUCHIDA [1983] as

$$\sigma_y(\tau) = 1.7 \times 10^{-14} \tau^{-1/2}, \tag{4.4}$$

assuming that an absorption line in ^{85}Rb vapor was used as a frequency reference. This result is portrayed by curve G in fig. 6. This stability is as high as that of a hydrogen maser, which implies that a semiconductor laser possesses the potential of becoming a high-coherence oscillator.

4.3. EXPERIMENTAL APPROACH FOR FREQUENCY NOISE REDUCTION

The experimental results of the five subjects described earlier are reviewed in this section.

4.3.1. *Linewidth reduction of the field spectrum*

It is effective to increase the cavity Q for linewidth reduction because the linewidth is inversely proportional to the cavity Q, as shown by eq. (3.11). With this idea in mind an external mirror was installed close to the laser, facing its cavity facet, thus forming a three-mirror cavity whose cavity Q is larger than that of the solitary laser. WYATT and DEVLIN [1983] narrowed the linewidth to 10 kHz by this configuration. FAVRE, LE GUEN and SIMON [1982] connected a fiber to the laser facet and used the other facet of the fiber as an external mirror to form a longer cavity, obtaining a linewidth as narrow as 30 kHz. In another technique this external waveguide mirror was integrated by FUJITA, OHYA, MATSUDA, ISHINO, SATO and SERIZAWA [1985].

This technique is called optical feedback, since the output laser beam from the solitary laser is injected into the laser again after being reflected from the external mirror surface. Although this technique has become popular because of its simple configuration, it presents the following problems:

(1) It sacrifices an advantageous property of the semiconductor laser cavity, namely, smallness.

(2) The linewidth can vary temporally as a result of phase fluctuations of the reflected light induced by mechanical vibration of the external mirror or thermal extension of the optical fiber. Even if these fluctuations are absent, a chaotic instability of laser oscillation can be induced, which depends on the absolute value of this phase. This phenomenon will be described in § 5.1.

(3) The index of direct frequency modulation by the injection current is decreased.

A electrical feedback technique has been proposed recently by OHTSU and KOTAJIMA [1985a,b] to overcome these difficulties; here the frequency noise is reduced within the Fourier frequency range of $f \leqq \Delta\nu_{FR}$, where $\Delta\nu_{FR}$ is the linewidth of the free-running laser. In principle the linewidth can be reduced to the value given by fig. 10 if the feedback loop has a bandwidth as wide as $\Delta\nu_{FR}$, and if frequency fluctuations are measured accurately and compensated by direct frequency control. In this technique the cavity size does not have to be increased, oscillation instabilities cannot be induced because the feedback is essentially negative, and the frequency modulation index does not decrease when the modulation frequency is higher than the cutoff frequency of the feedback. Furthermore, in the future the optical and electronic components in this feedback loop can be integrated with the laser diode in order to realize a miniature coherent light source. Thus the technique offers several advantages when compared with conventional techniques of optical feedback.

Figure 12 shows experimental results for the 1.5 μm InGaAsP laser (DFB type) that were obtained by OHTSU and KOTAJIMA [1985a]. A Fabry–Perot interferometer 1 cm long was used as a frequency discriminator. Another detection scheme for frequency fluctuations is heterodyning with another, highly coherent laser; this method was employed by SAITO, NILSSON and YAMAMOTO [1985]. As can be seen in fig. 12 the linewidth was reduced to 330 kHz, which is $\frac{1}{15}$ times that of the free-running laser. By improving the experimental setup, OHTSU [1985a] recently obtained a reduced linewidth of 200 kHz, which is $\frac{1}{25}$ times that of the free-running laser. With values of $\frac{1}{15}$ and $\frac{1}{25}$, the linewidth was narrowed to a value less than the value from the Schawlow–Townes formula, since $1 + \alpha^2$ of eq. (3.11) is less than 8.9, which is estimated by using the already reported value of the linewidth enhancement factor, that is, 2.2–2.8 for InGaAsP lasers (KIKUCHI and OKOSHI [1985]). These results validate the discussion in § 4.2, which was based on eq. (4.3).

TABUCHI, OUCHI and OHTSU [1986] estimated the narrowest linewidth obtainable by employing the present experimental setup. The result of the signal-to-noise ratio of the frequency fluctuation measurements used for this estimation showed that the linewidth can be narrowed to as little as 10 kHz by reducing the phase delay of the present feedback loop. This means that the experimental results may achieve the minimum attainable linewidth of fig. 11. It was estimated that a sufficiently low phase delay can be achieved if the electrical length of the feedback loop is as short as 10 cm. This length can be realized by slight modifications in the experimental setup presently used,

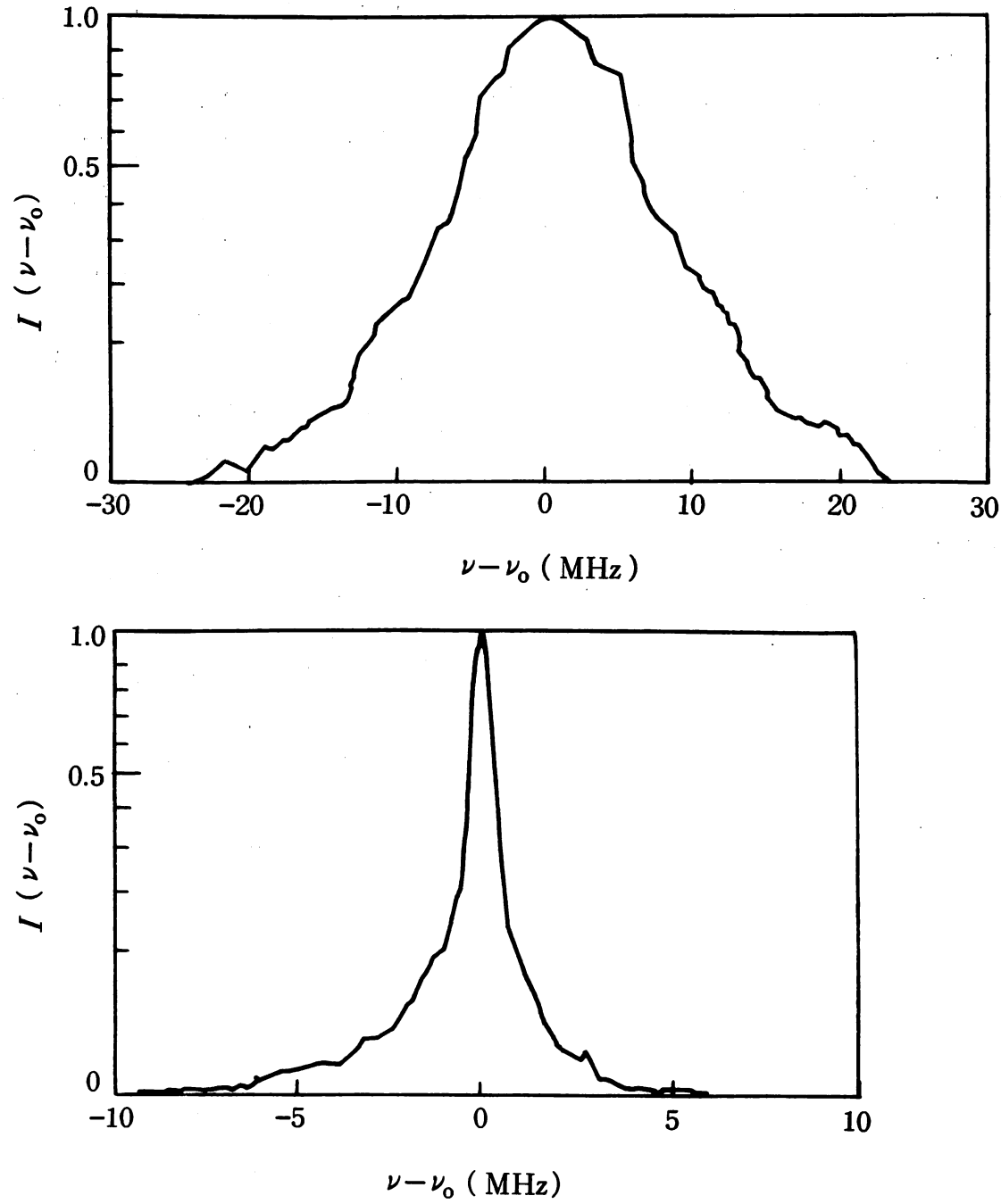

Fig. 12. Experimental results of linewidth reduction of an InGaAsP laser by electrical feedback. The upper and lower figures show field spectra for free-running and feedback conditions, respectively. (After OHTSU and KOTAJIMA [1985a].)

without the necessity for strict integration of the feedback loop, which also makes this feedback scheme practical and attractive.

Further linewidth reductions can be expected if a more sensitive frequency discriminator is used, since it will improve the signal-to-noise ratio of frequency fluctuation measurements and reduce the detector-noise-limited value. A long Fabry–Perot interferometer fabricated by using a low-loss optical fiber

(STOKES, CHODOROW and SHAW [1982]) is a promising candidate for such a discriminator. Figure 13 shows an estimated result of the relation between the detector-noise-limited value of the reduced linewidth $\Delta\nu_{FB}$, the resonance linewidth $\Delta\nu_{FP}$ of the Fabry–Perot interferometer with interferometer mirrors of 90% reflectivity, and the interferometer length L_{FP} (TABUCHI, OUCHI and OHTSU [1986]). It can be seen that the detector-noise-limited value decreases with increasing interferometer length, which is represented by curve A in fig. 13.

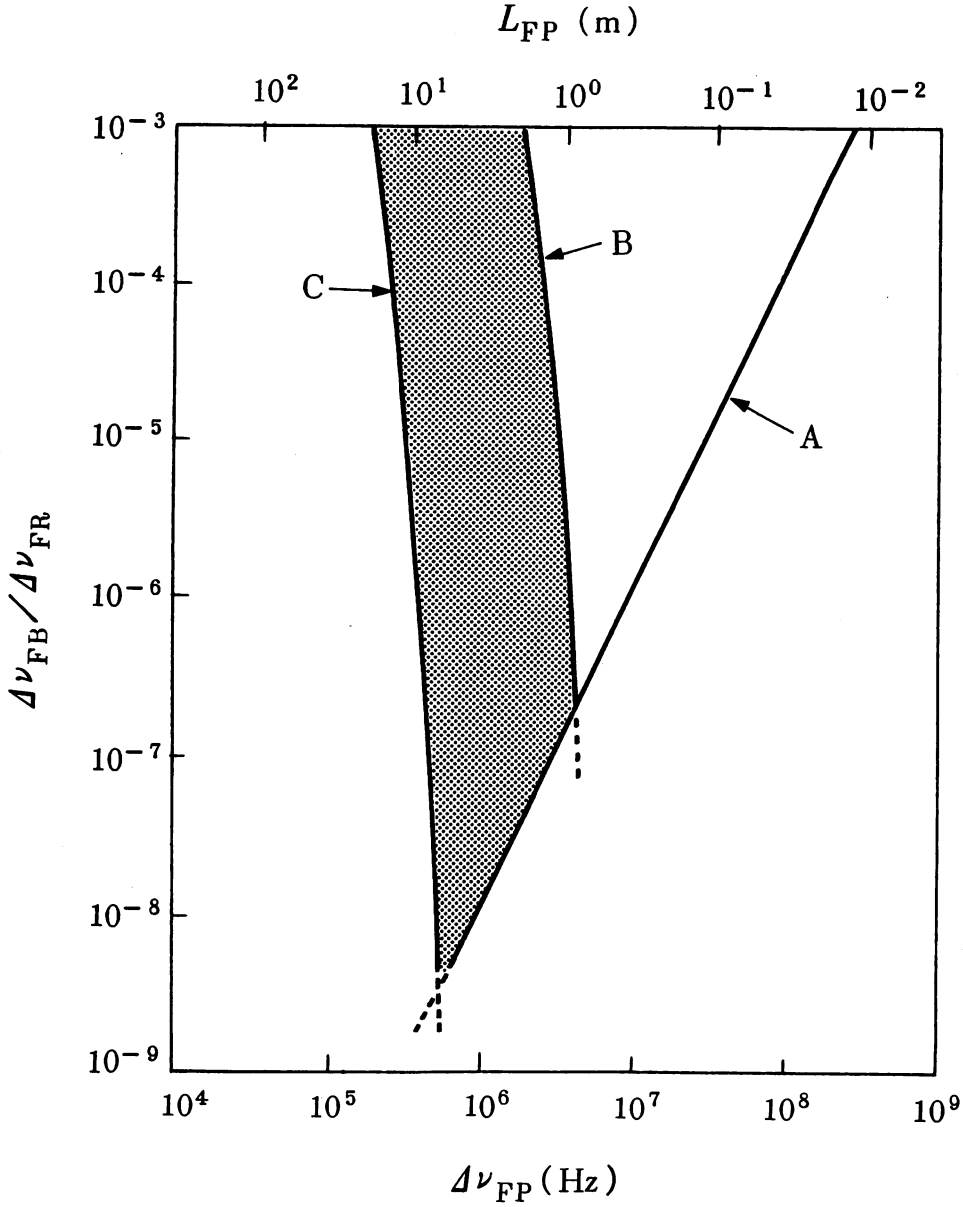

Fig. 13. Estimated result of the relation between the detector-noise-limited value of the reduced linewidth $\Delta\nu_{FB}$ of an InGaAsP laser and the resonance linewidth $\Delta\nu_{FP}$ of the Fabry–Perot interferometer. $\Delta\nu_{FR}$, linewidth of the free-running laser; L_{FP}, length of the Fabry–Perot interferometer with 90% mirror reflectivity. Curve (A) represents the effect of linewidth reduction with decreasing $\Delta\nu_{FP}$, which is due to increases in sensitivity of frequency discrimination. The meshed area between curves B and C represents the effect of linewidth rebroadening with decreasing $\Delta\nu_{FP}$, which is induced by the decrease of the bandwidth of the feedback loop. (After TABUCHI, OUCHI and OHTSU [1986].)

However, further increases in the length would induce rebroadening of the linewidth, since the bandwidth of the interferometer is decreased, which also limits the bandwidth of the feedback loop. This effect is represented by a meshed area between curves **B** and **C** in fig. 13. It can be seen in this figure that the minimum of the detector-noise-limited linewidth can be expected at an interferometer length of 1–10 m, which is a reasonable value for fabricating the fiber interferometer by using presently available fiberoptic technology. The minimum linewidth is about 1×10^{-7} times that of the free-running laser; that is, it is possible to obtain a linewidth as narrow as 1 Hz. Furthermore, induced increases in intensity noise are estimated as being less than 5% that of the free-running laser in the case of electrical feedback for frequency noise reduction (TABUCHI, OUCHI and OHTSU [1986]). From these estimations it is realistic to expect high coherence in semiconductor lasers in the future by using the electrical feedback technique.

4.3.2. *Stabilization of the center frequency of the field spectrum*

Since changes in ambient temperature cause drifts in the center frequency of the field spectrum, reduction of the low Fourier components of the frequency noise is required to improve the frequency stability. For this reason it is effective to control the injection current by using an analog differentiator and integrator, as was described in § 4.2. A proportional amplifier is sometimes used in parallel with these amplifiers, i.e., PID control is used. Since the gain of the actual integrator is finite, the Fourier frequency range in which the servocontrol is effective is higher than 0.1 mHz. Thus, it is difficult to reduce drift at integration times longer than about 1×10^4 s by means of the practical feedback loop, which limits the frequency reproducibility. This phenomenon will be discussed in § 4.3.3.

A Fabry–Perot interferometer can be used as the simplest frequency reference for frequency stabilization. However, the resonance frequency of the interferometer can drift as a result of the ambient temperature fluctuations. Stabilization of such a resonance frequency itself has been carried out by using a 633 nm helium–neon laser with a higher frequency stability to compensate for this drift (TSUCHIDA, OHTSU and TAKO [1981]). For stabilization at integration times less than 10 ms, a simple Fabry–Perot interferometer, such as one made by a rigid quartz block, can be used because the effects of ambient temperature fluctuations are less at these short integration times. Curve C_2 of fig. 14 represents the result obtained from using such a simple interferometer.

For higher frequency stability more stable frequency references are required

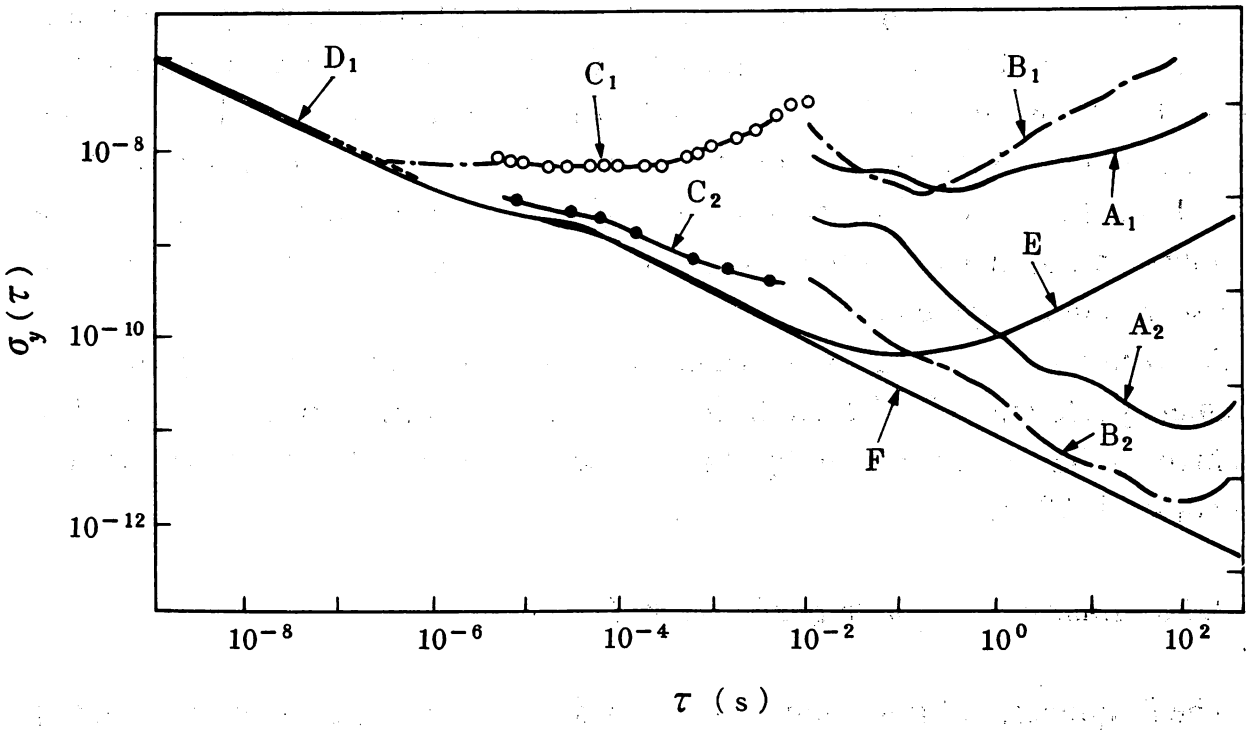

Fig. 14. Experimental results of stability measurements of the center frequency of the field spectrum of AlGaAs lasers. A_1, B_1, C_1, D_1, free-running lasers. Curves A_2, B_2 and C_2 represent results stabilized by using absorption lines in H_2O vapor, ^{85}Rb–D_2 vapor, and a resonance line of a rigid Fabry–Perot interferometer, respectively. Curves E and F are copies of curves F and H in fig. 6. (After OHTSU, FUKADA, TAKO and TSUCHIDA [1983].)

that are almost independent of ambient circumstances. The center frequency of a spectral line of a stable atom or molecule can be used as such a reference. For example, absorption lines of combination tones or higher harmonics of the vibration–rotation transitions in organic molecules (water, ammonia, etc.) can be used for near-infrared semiconductor lasers with wavelengths of 0.7–1.6 μm (OHTSU, KOTANI and TAGAWA [1983] and FUKUOKA, OHTSU and TAKO [1984]). Since a great number of these lines are found in the near-infrared region, the frequency of each semiconductor laser can be tuned at least to one of them, which makes these lines popular and stable frequency references. However, the sensitivity of the frequency discrimination of these references is rather low because of their low absorption coefficients.

In contrast, the resonance lines of the electronic transitions in alkali vapors (e.g., cesium, rubidium, etc.) can be used as highly sensitive frequency references because they exhibit large absorption coefficients in the wavelength region of 0.8 μm (YABUZAKI, IBARAGI, HORI, KITANO and OGAWA [1981] and TSUCHIDA, OHTSU, TAKO, KURAMOCHI and OURA [1982]). In this case further increases in the sensitivities can be expected because a narrower spectral line can be obtained by using the technique of saturated absorption spectroscopy. Characteristics of this spectral profile will be described in § 6.2.

Curves A_2 and B_2 of fig. 14 represent the results obtained by using absorption lines in H_2O and ^{85}Rb as the frequency references, respectively. It is seen that curve B_2 almost approaches the curve **F**; that is, a stability as high as the one limited by the spontaneous emission was realized. The value of curve B_2 is $\sigma_y = 1.4 \times 10^{-12}$ at an integration time τ of 100 s. Further improvements of the stability and approach to the curve **G** of fig. 6 can be expected by improving the servocontrol system.

Absorption spectral lines in water and ammonia have been employed as frequency references for 1.5 μm InGaAsP lasers, for which a frequency stability as high as that of curve A_2 in fig. 14 has been obtained (OHTSU, KOTANI and TAGAWA [1983]).

4.3.3. *Improvement of frequency reproducibility*

The frequencies of free-running semiconductor lasers are widely distributed because of their higher frequency and the lower accuracy in device fabrication in comparison with microwave oscillators. Furthermore, it is difficult to reduce frequency drift at integration times longer than about 1×10^4 s because of the finite gain of the analog integrator for servocontrol, as was described in § 4.3.2. These facts limit the frequency reproducibility of semiconductor lasers. Although frequency reproducibility as high as 1×10^{-7} has been obtained from frequency stabilization by using absorption lines in water and ammonia as frequency references (OHTSU, KOTANI and TAGAWA [1983] and FUKUOKA, OHTSU and TAKO [1984]), this has not been high enough for applications such as coherent optical measurements. Despite this fact, few approaches have been carried out to improve the frequency reproducibility.

As the first step in improving the frequency reproducibility, it is essential to investigate the characteristics of the frequency reproducibility of free-running lasers. Figure 15 shows the result of continuous measurements for this purpose of frequency drift in free-running AlGaAs lasers (OHTSU, HASHIMOTO and OZAWA [1985]). One of the spectral lines in rubidium ($F = 1$ component in ^{87}Rb–D_2) was used as a frequency reference for frequency measurements. The effects of fluctuations in ambient temperature and injection current were neglected because these were kept as low as 1×10^{-5} K and 0.6 nA/$\sqrt{\text{Hz}}$, respectively. It can be seen from this figure that the laser exhibits a blue shift of 26 MHz/h for 600 h just after the start of measurements, and a blue shift of 8.6 MHz/h can still be observed after six months. Furthermore, variations in mode-hopping properties can also be observed. FAVRE and LE GUEN [1983a] have attributed these long-term variations in spectral properties to slow

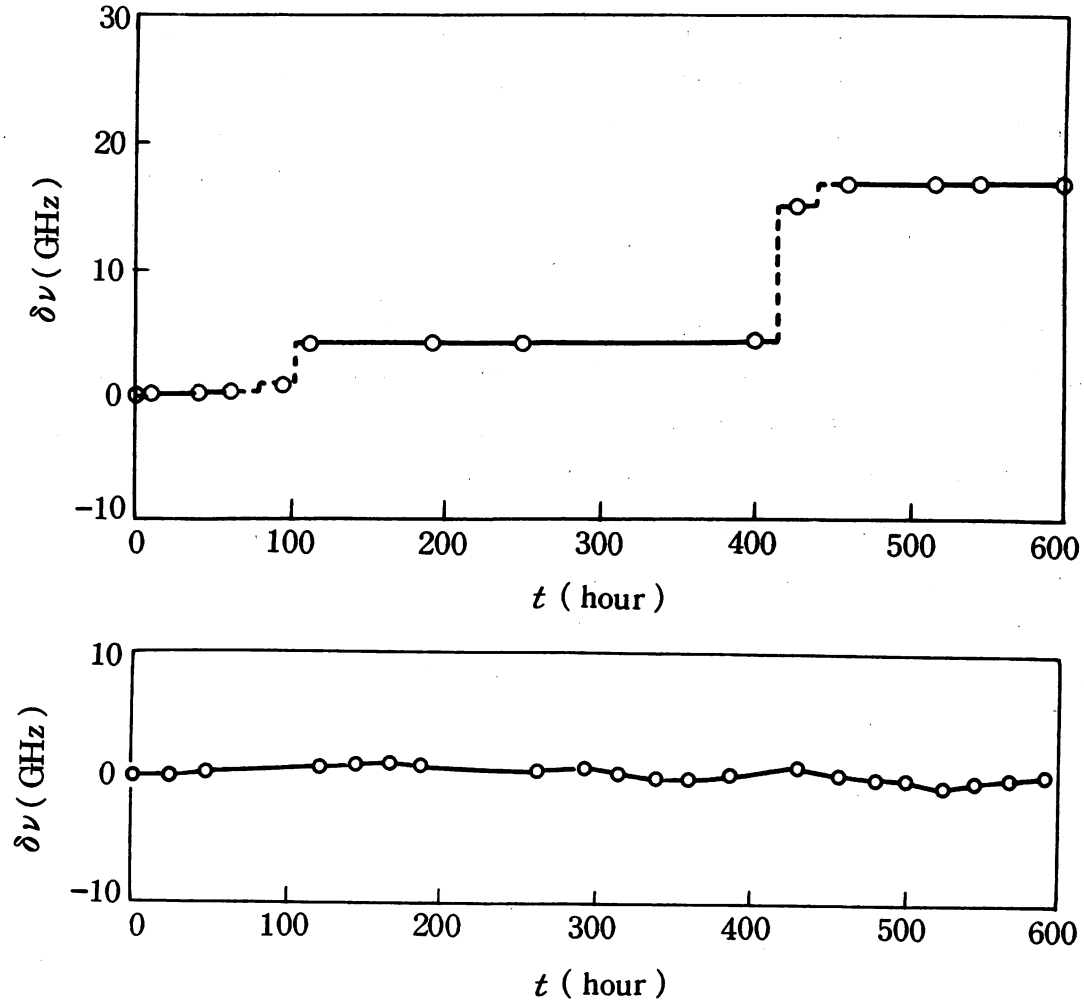

Fig. 15. The results of continuous measurements of frequency drift in free-running AlGaAs lasers. The lower curve was obtained six months later than the upper curve. (After OHTSU, HASHIMOTO and OZAWA [1985].)

temporal decreases of thermal resistance resulting from oxidation of the indium bonding layer or from thermal effects induced by nonradiative carrier recombination near the facets.

Decrease and stabilization of thermal resistance and screening of laser devices are required at the device fabrication stage in order to reduce these uncontrollable variations. OKAZAKI, OHTSU and TAKO [1984] demonstrated that detection and compensation of such long-term variations of spectral properties by using a microcomputer are also effective ways of improving the frequency reproducibility. These techniques have already been employed for microwave oscillators.

4.3.4. *Frequency tracking to another, highly coherent laser*

If the coherence in a laser is improved by using the techniques described in §§ 4.3.1–4.3.3, it can be used as a master laser in coherent optical measurement

systems. In these systems it is useful if the high coherence of the master laser can be transferred to other lasers, or, in other words, if the frequencies of slave lasers can be accurately tracked to the master laser frequency. By using these procedures a series of highly coherent lasers can be constructed, which allows the realization of a hierarchy similar to that for microwave oscillators described in §.4.1.

A popular technique for frequency tracking utilizes the phenomenon of injection locking. As shown in fig. 16, the frequency of a slave laser can be locked to the master laser frequency when light from the master laser is injected into the slave laser cavity. This phenomenon has been observed not only in lasers but also in general nonlinear self-sustained oscillators, and it is called injection locking (VAN DER POL [1927]).

The locking range, that is the frequency range in which the slave laser frequency is locked to the master laser frequency, has been derived by LANG [1982] and is expressed as

$$-\frac{1}{2\tau_p}\sqrt{(P_m/P_s)(1+\alpha^2)} \leqslant \omega_m - \omega_s \leqslant \frac{1}{2\tau_p}\sqrt{P_m/P_s}, \tag{4.5}$$

where P_m, P_s, ω_m and ω_s are the laser powers and angular frequencies of the master and slave lasers, respectively, τ_p is the photon lifetime of the slave laser, and α is the line enhancement factor given in § 3.3. This factor appears in eq. (4.5) to represent the effect of the simultaneously induced modulations in frequency and amplitude of the slave laser, which is due to the carrier density modulation by the injected light of the master laser. Since the locking range is inversely proportional to τ_p, that is, the cavity Q, injection locking easily occurs in semiconductor lasers because of their lower cavity Q.

As shown in fig. 17, the slave laser frequency precisely tracks that of the master laser under injection locking. Furthermore, the phase and power of the slave laser can also be varied by sweeping the master laser frequency. These effects have been applied in several studies in which the injection-locked slave laser is used as an optical amplifier for coherent optical communications (KOBAYASHI and KIMURA [1982]). The measured gain–bandwidth value of

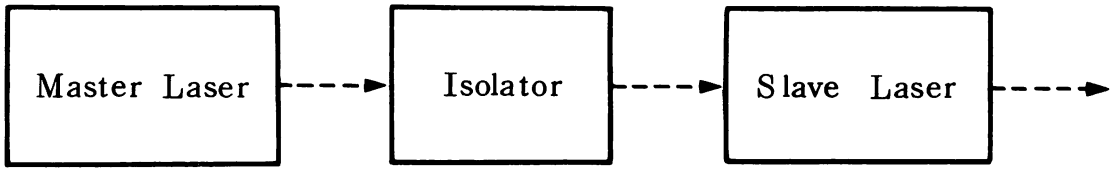

Fig. 16. Block diagram for observing injection locking.

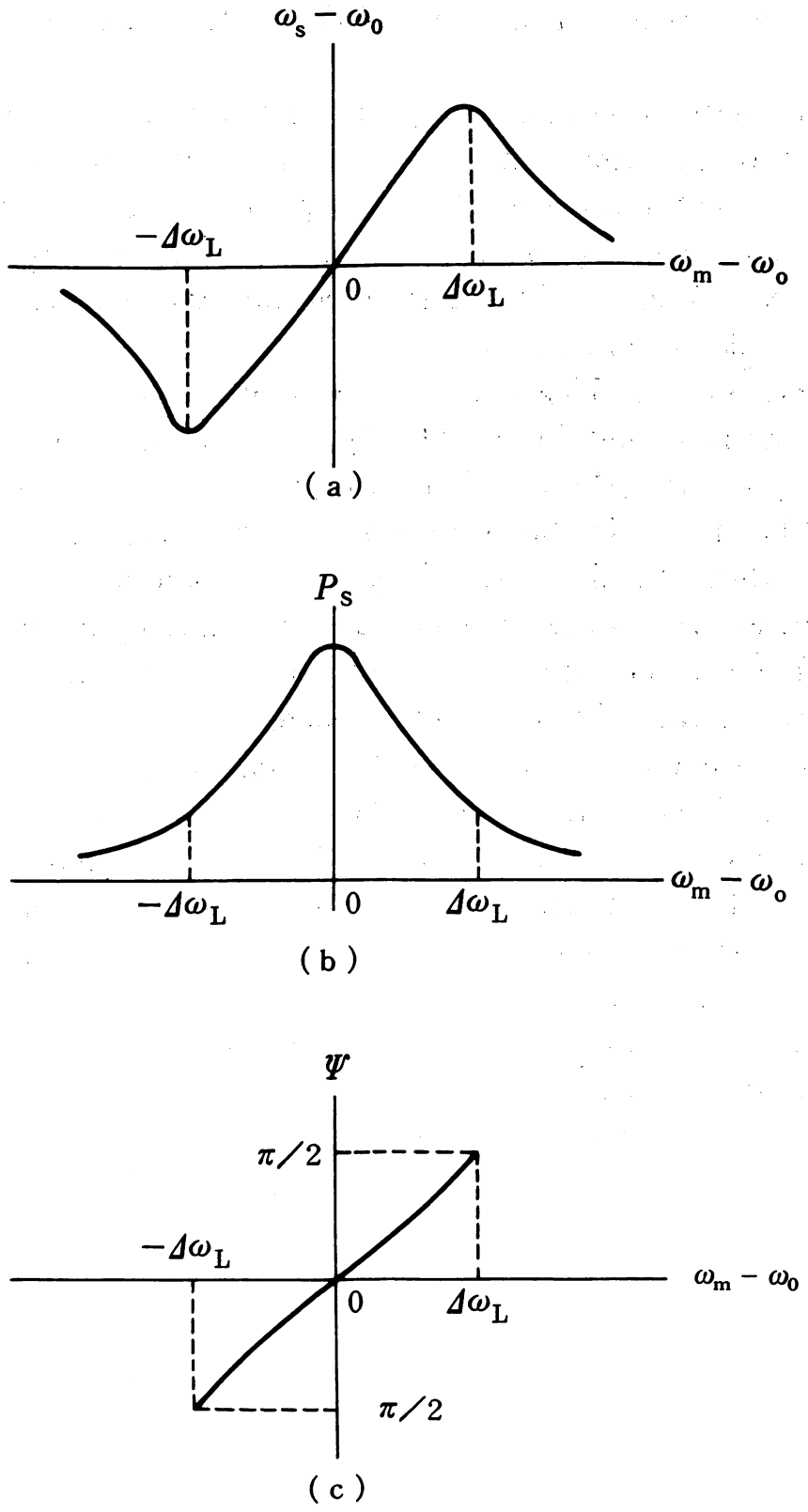

Fig. 17.(a,b) Relations between (a) the angular frequencies of the master laser, ω_m, and the slave laser, ω_s, and (b) the angular frequency of the master laser and the power of the slave laser P_s. (c) Phase difference between the master and slave laser Ψ. The locking range is represented by $2 \cdot \Delta\omega_L$, which corresponds to eq. (4.5).

these AlGaAs laser amplifiers is 35 GHz (KOBAYASHI and KIMURA [1981]).

Although injection locking is physically interesting as a phenomenon, it presents several problems if it is used as a practical technique for accurate transfer of high coherence, since this locking range depends on the powers of both lasers, thus requiring high master laser power and low power fluctuations of both lasers. Because of these requirements, the practical experimental apparatus would be complicated.

A frequency offset locking technique has been proposed to overcome these difficulties (KUBOKI and OHTSU [1987]). This technique had already been applied to gas lasers (HALL and BORDE [1973], OHTSU, KATSURAGI and TAKO [1981]). Figure 18 shows a schematic explanation of frequency offset locking, in which the slave laser frequency is controlled so that the beat frequency between the two lasers is locked to the frequency of a local microwave oscillator. In the actual experimental setup the phase instead of the frequency of the beat signal was locked to that of the microwave signal in order to improve the accuracy of frequency tracking and to obtain a wider bandwidth for the feedback loop (KUBOKI and OHTSU [1987]). For this phase-locking technique a digital phase comparator was developed. The bandwidth of the feedback loop was 1.5 MHz. From this explanation it can be deduced that this technique is similar to the phase-locked loop used for conventional electronic circuits. A different feature of the present feedback loop is the design of the dynamic range of the phase comparator, which is $2\pi \times 2^{11}$ rad. This enables the detection of much larger phase fluctuations in the lightwave than is possible with the conventional phase-locked loop. Figure 19 shows a result obtained for AlGaAs lasers (KUBOKI and OHTSU [1987]), in which the frequency stability of the locked beat signal is given by curve **B** and is expressed as

$$\sigma_{y\,\mathrm{b}}(\tau) = 1.3 \times 10^{-12} \cdot \tau^{-1}, \qquad 1\ \mu\mathrm{s} \leqslant \tau \leqslant 100\ \mathrm{s}\,. \tag{4.6}$$

The frequency stability of the slave laser is governed by those of the master laser and the beat signal. However, since the frequencies of the master laser and the beat signal are stabilized by using mutually independent feedback loops, their residual frequency fluctuations are mutually uncorrelated. This means that the Allan variance of the frequency fluctuations in the slave laser $\sigma^2_{y\,\mathrm{s}}$ is obtained simply by summing those of the master laser and the beat signal, that is,

$$\sigma^2_{y\,\mathrm{s}}(\tau) = \sigma^2_{y\,\mathrm{m}}(\tau) + \sigma^2_{y\,\mathrm{b}}(\tau)\,; \tag{4.7}$$

$\sigma^2_{y\,\mathrm{m}}(\tau)$ is the Allan variance of the residual frequency fluctuations in the master laser given by curves $\mathbf{A}_2$, $\mathbf{B}_2$, and $\mathbf{C}_2$ in fig. 14. Comparison between these

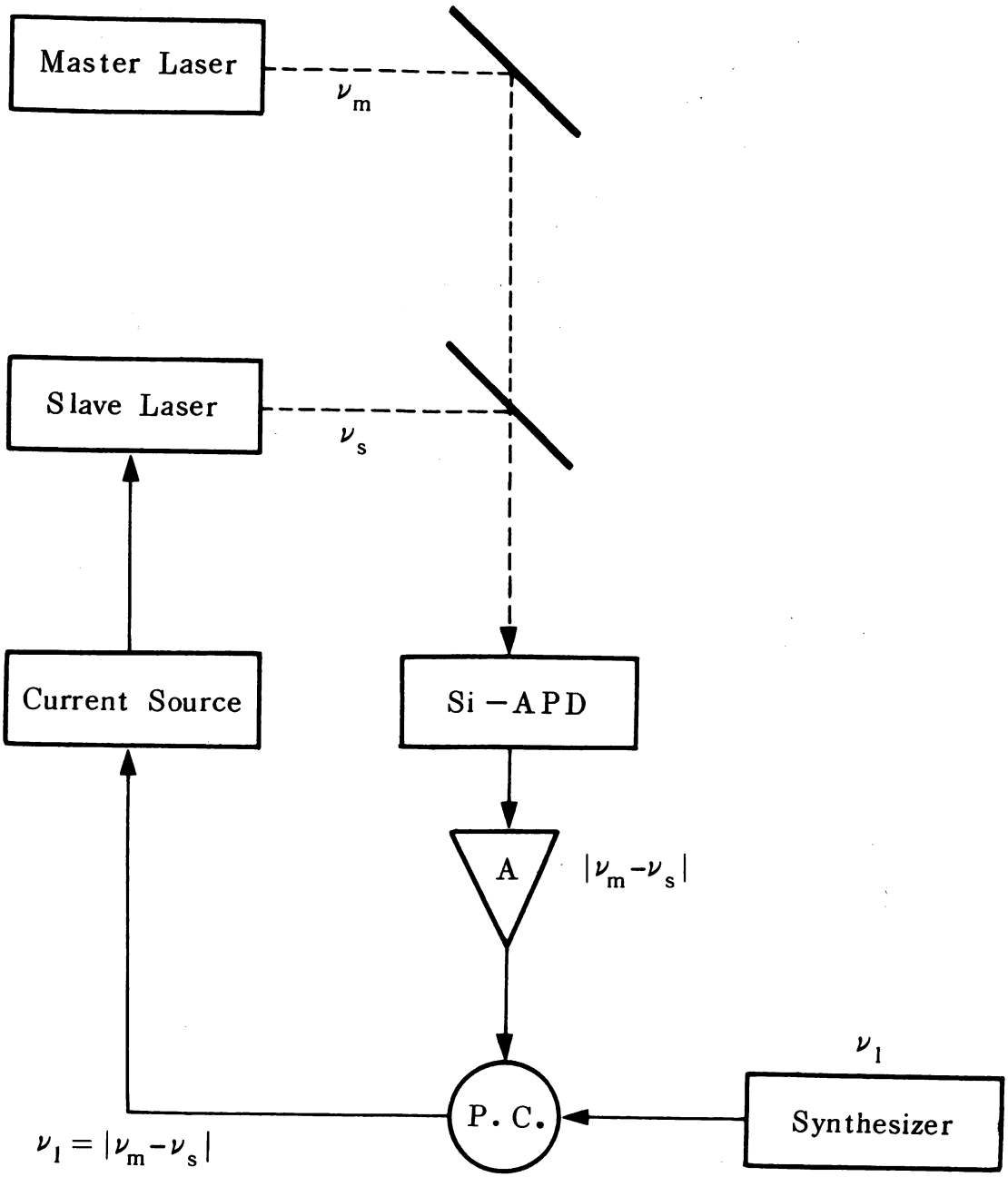

Fig. 18. Block diagram of frequency offset locking. P.C. stands for phase comparator. (After KUBOKI and OHTSU [1987].)

curves and curve **B** of fig. 19 shows that $\sigma_{y\,m}^2(\tau) \gg \sigma_{y\,b}^2(\tau)$, which means that $\sigma_{y\,s}^2(\tau) \approx \sigma_{y\,m}^2(\tau)$; that is, the frequency stability of the slave laser is almost equal to that of the master laser. It can be concluded from these results that the high coherence of the master laser could be transferred to the slave laser by frequency offset locking. The locking range of the beat frequency was 1.92 GHz, which will be described in more detail in § 4.3.5. Since the capture range of the beat frequency is 1.92 GHz wide, the free-running beat frequency can be captured and fixed at the microwave frequency if the beat frequency stays within this range.

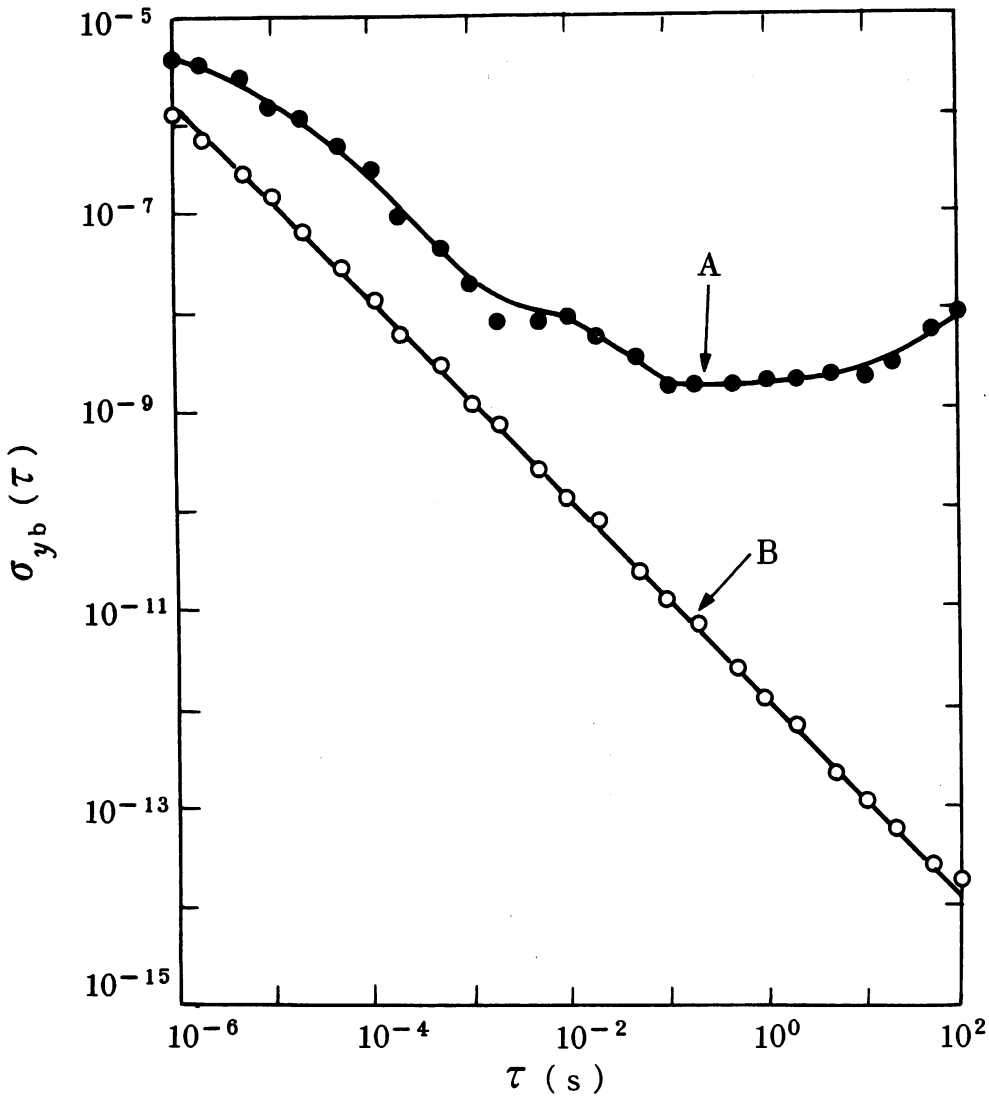

Fig. 19. Square roots of the Allan variances of (A) frequency noise in the master laser and (B) the beat signal between the master and slave lasers. (After KUBOKI and OHTSU [1987].)

This technique is simpler and more stable than the injection-locking technique because no nonlinear optical phenomena are used. Stability and accuracy for frequency tracking are important to reduce the fluctuations of IF frequency in heterodyne optical measurements and heterodyne/coherent optical communications. In the latter case, especially, preliminary frequency tracking experiments have been carried out for FSK heterodyne communications (FAVRE and LE GUEN [1983b], EMURA, SHIKADA, FUJITA, MITO, HONMOU and MINEMURA [1984]). Similar experiments have also been carried out for homodyne communications (WENKE and SAITO [1985]).

4.3.5. *Stable and wideband frequency sweep*

External cavity configurations have been employed for a wideband frequency sweep by installing an external diffraction grating, which was described in

§ 4.2.1. In this configuration a longitudinal oscillation mode was selected by rotating a diffraction grating (FLEMING and MOORADIAN [1981]), and the wavelength of a 1.5 μm InGaAsP laser was swept over 0.5 nm (frequency range of 67 GHz) (CAMERON, MATTHEWS, HODGKINSON and DEVLIN [1985]). This is a popular and convenient technique that has been frequently employed for infrared gas lasers and visible dye lasers. However, it is difficult to make a continuous frequency sweep by this technique because of the hopping between the longitudinal modes of the three-mirror cavity formed by the external grating and the laser facets. Furthermore, it presents several problems, such as chaotic instabilities dependent on the phase of the lightwave reflected from the grating, stochastic instabilities induced by random fluctuations of this phase, increases in cavity volume, and decreases in direct frequency modulation index.

KUBOKI and OHTSU [1987] have proposed recently that frequency offset locking can be used as an effective technique to overcome these difficulties. Thus, if the microwave frequency is slowly swept under frequency offset locking, the slave laser frequency can be swept while maintaining a frequency stability as high as that of the master laser. Experiments confirmed that the locking range of the beat frequency (i.e., the frequency range in which the beat frequency was swept) was as wide as 1.92 GHz for 0.8 μm AlGaAs lasers (KUBOKI, KATO and OHTSU [1986]), and the frequency stability of the beat signal within this locking range was as high as that shown in fig. 19 (KUBOKI and OHTSU [1987]). These results mean that the slave laser frequency was swept in a very stable manner within a frequency range of 3.84 GHz with respect to the master laser frequency. The value of this locking range was limited by the response bandwidth of the detector used for observing the beat signal.

There are two promising ways of further extending the range of stable frequency sweep of the slave laser that are schematically explained by fig. 20.

(1) The technique in fig. 20a demonstrates a discrete tuning of the master laser frequency by successively locking to one of the frequency reference grids $\nu_{r,i}$ ($i = 1, \ldots, N$), which are nearly equidistantly distributed along the frequency axis. For each locked frequency of the master laser, frequency offset locking is applied to the slave laser. This control scheme enables an extension of the range of stable and accurate sweep of the slave laser frequency. Absorption lines of combination tones or higher harmonics of vibration–rotation transitions in organic molecules are potential candidates for this frequency reference grid because a great number of lines are distributed within intervals of several gigahertz or several tens of gigahertz in the near infrared wavelength region, and

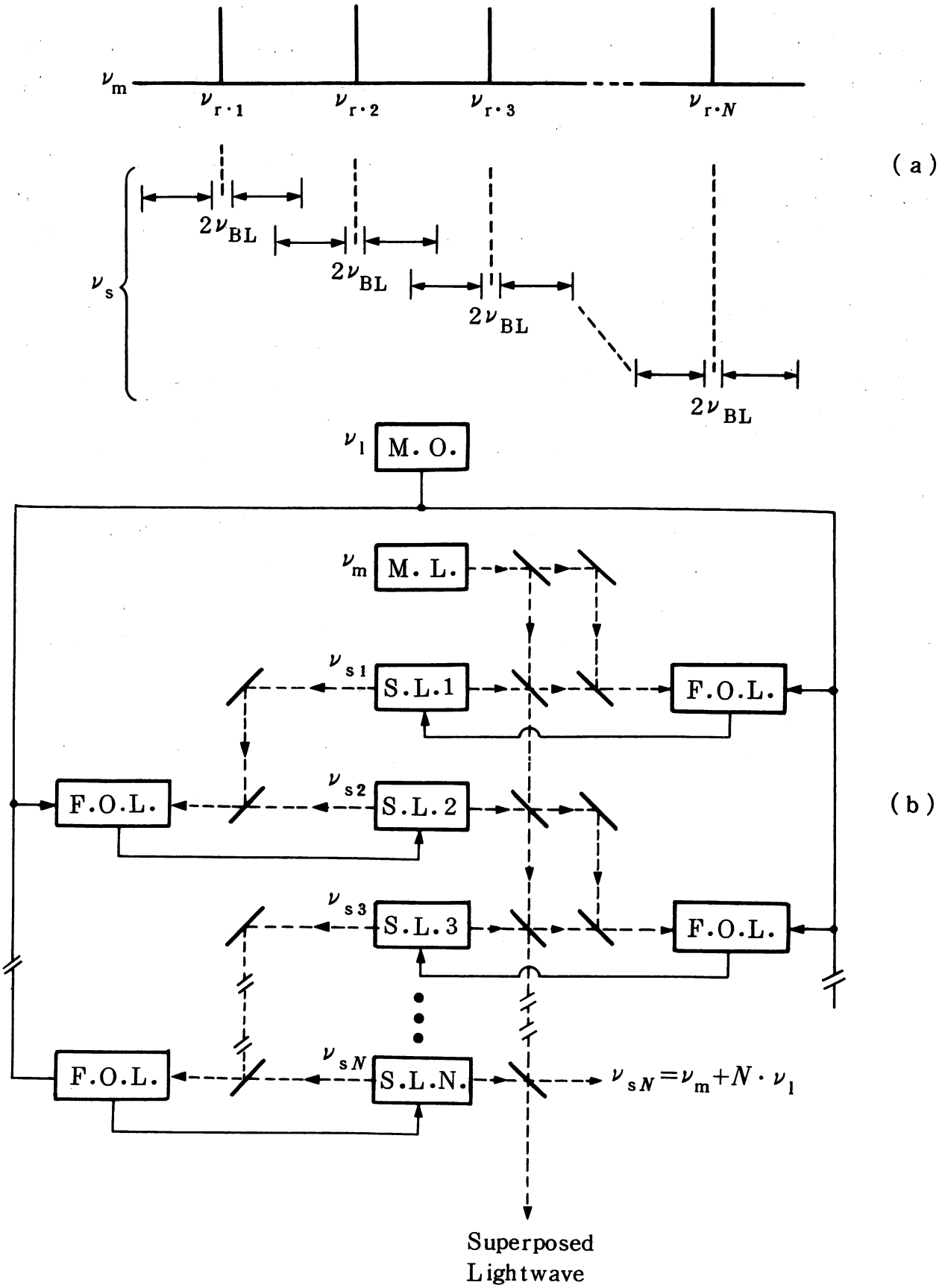

Fig. 20. Schematic explanations of two ways of extending the locking range in frequency offset locking. (a) Discrete tuning of the master laser frequency by successively locking to each of the frequency reference grids $\nu_{r,i}$, which are nearly equidistantly distributed along the frequency axis; ν_{BL} is the locking range of the beat frequency between the master and slave lasers. (b) use of a number of slave lasers; M.O.: microwave oscillator; M.L.: master laser; S.L.*i*: the *i*th slave laser (i = 1–N); F.O.L.: servocontroller for frequency offset locking.

some of their absolute frequencies have already been calibrated with 1×10^{-6}–7×10^{-8} accuracy (OHTSU, KOTANI and TAGAWA [1983] and FUKUOKA, OHTSU and TAKO [1984]). Equidistantly distributed resonance frequencies of a Fabry–Perot interferometer can be used as a simpler frequency reference grid, and experiments with it showed that it was possible to lock the master laser frequency to its successive fifteen resonance frequencies. For each locked frequency of the master laser, frequency offset locking was applied to the slave laser, thus extending the range of stable frequency sweep of the slave laser to 57.6 GHz (KUBOKI, KATO and OHTSU [1986]).

The number of lines of the frequency reference grid to which the master laser frequency can be locked was limited by mode-hopping in the master laser. It would be effective to use a laser without mode-hopping to extend this range. A recently developed 1.5 μm InGaAsP distributed feedback (DFB) laser is desirable for this purpose because its wavelength can be continuously varied within a range of 15 nm without mode-hopping by varying the ambient temperature under free-running conditions, which corresponds to a frequency range 2 THz wide (TOHMORI [1986]). A stable and wideband frequency sweep for more than 1 THz can be expected if this kind of laser is employed for frequency offset locking.

(2) The second technique, schematically explained in fig. 20b, is to prepare a number of slave lasers and to apply frequency offset locking between the adjacent lasers by using a common microwave oscillator. Since the frequency of the Nth slave laser can be fixed to $\nu_m + N\nu_l$ (with ν_m the master laser frequency, and ν_l the frequency of the local microwave oscillator), the range of stable frequency sweep for this laser becomes N times wider than that of the first slave laser. Such a frequency offset locked laser array is also interesting from the standpoint of ultrashort light pulse generation, because the lightwave superposed by all the laser beams from the array is mode-locked. This is because the frequency difference between each pair of slave lasers is fixed at ν_l, and all the slave lasers commonly possess the high coherence of the master laser.

The possibility of a stable and wideband frequency sweep has been demonstrated here. This technique is made possible because the gain spectra of semiconductor lasers have broad linewidth, and fast modulation and control of the frequency are enabled by controlling the injection current. From these findings can be concluded that semiconductor lasers provide promise for realizing such a stable and wideband frequency sweep.

The techniques for carrying out the five approaches to realize high coherence were separately described in the preceding five subsections. These techniques

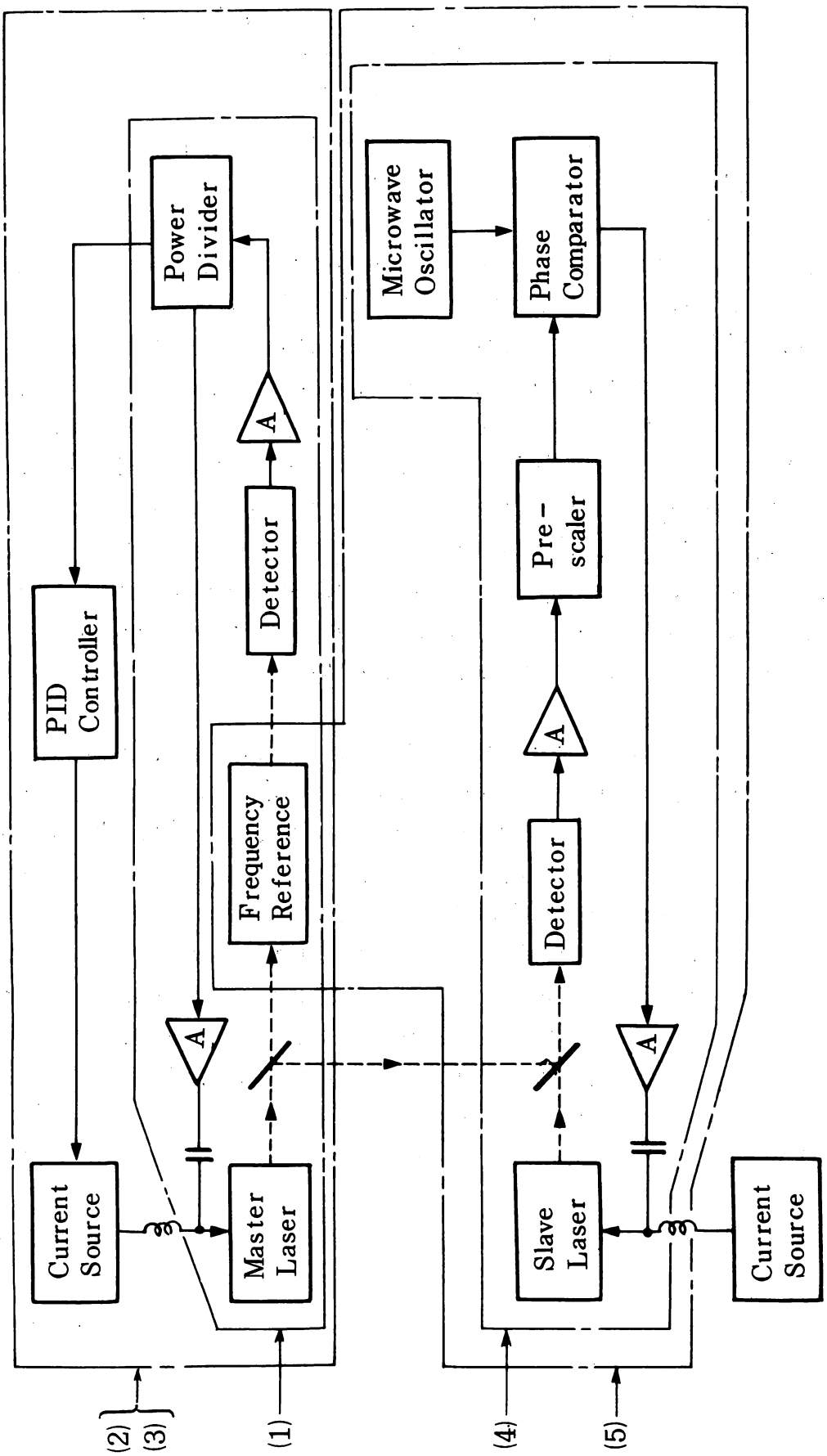

Fig. 21. An example of a synthesized system of electrical feedback for carrying out simultaneously the five subjects described in § 4.3.

can be synthesized as shown by fig. 21 in order to carry out the five approaches simultaneously, since all the techniques commonly employ electrical feedback. Thus, electrical feedback is a promising technique for realizing high temporal coherence in semiconductor lasers.

4.4 DESIGN OF NOVEL SEMICONDUCTOR LASERS TO IMPROVE COHERENCE

The previous section described the effectiveness of controlling the injection current in such a way that it improves the coherence. However, the structures of the semiconductor lasers available so far have not necessarily been appropriately designed for this purpose because they are designed primarily for optical communication or readout of optical memories, by modulating their power by means of an injection current. An appropriate laser structure needs to be designed to improve coherence by negative electrical feedback. Recent designs of such a novel structure are presented in this section.

Figure 22 shows a distributed Bragg reflector (DBR) InGaAsP laser at 1.55 μm with a segmented electrode (TOHMORI, SUEMATSU, TSUSHIMA and ARAI [1983]). One part of the cavity was used as the active region for laser oscillation, and the other part was used for a phase modulator for wavelength tuning. The mole fraction of the guided layer of the modulator was adjusted so that its band-gap energy was larger than that of the guided layer of the active region, which made the loss of the modulator negligibly low. Phase modulation was carried out by modulating the current injected into this region through variation of the refractive index by the plasma effect. Theoretical estimation showed that the wavelength can be tuned at a rate of -0.1 nm/mA without varying the value of the threshold current for laser oscillation, which experiments confirmed.

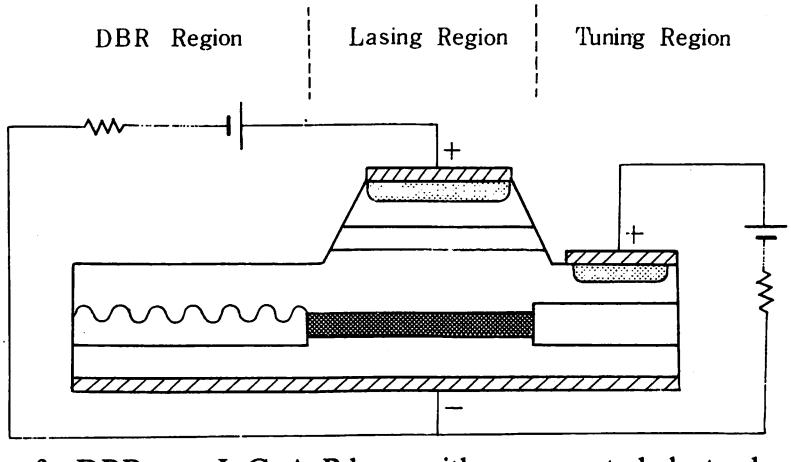

Fig. 22. Structure of a DBR-type InGaAsP laser with a segmented electrode. (After TOHMORI, SUEMATSU, TSUSHIMA and ARAI [1983].)

Use of this type of laser is advisable because frequency fluctuations can be reduced by controlling the injection current of the modulator while power fluctuations are kept at a sufficiently low level by controlling the injection current of the active region.

A 1.3 μm DFB InGaAsP laser with segmented electrode has recently been fabricated by YAMAGUCHI, KITAMURA, MURATA, MITO and KOBAYASHI [1985]. In contrast to fig. 22, the same materials were used for the active region and the phase modulator, which means that wavelength tuning was carried out by using both the plasma effect and anomalous dispersion of the refractive index. By using this laser, flat response characteristics of direct frequency modulation up to 300 MHz were realized by compensating for the thermal effect by controlling the injection current of the phase modulator (YAMAZAKI, EMURA, SHIKADA, YAMAGUCHI and MITO [1985]). It was confirmed by this control that distortions in demodulated waveforms were reduced in FSK coherent/heterodyne optical communication.

A 1.5 μm hybrid DFB/DBR InGaAsP laser with segmented electrode has also been fabricated (WESTBROOK, NELSON, FIDDYMENT and COLLINS [1984]). The same materials were used also for both of the regions. Wideband wavelength tuning of 5 nm was obtained by sweeping the injection current of the phase modulator.

Simultaneous and independent control of frequency and power can be accomplished by using these segmented electrode in the laser cavity, which leads to an improved frequency control with higher accuracy and wider bandwidth. It is also helpful to integrate opto-electronic components of the feedback loop together with the laser device for this purpose; this technique of an opto-electronic integrated circuit (OEIC) has important uses in the future.

§ 5. Deterioration of Coherence Caused by Specific Noise in Semiconductor Lasers

Several specific kinds of noise can often be generated in semiconductor lasers because of their low cavity Q and the wideband response characteristics of carrier density variations. Since these kinds of noise interfere with attempts to improve coherence, their origins should be investigated and a technique for suppressing them found. Reflected lightwave noise and mode-hopping noise are typically troublesome, and their characteristics are reviewed here.

5.1. OSCILLATION INSTABILITIES INDUCED BY REFLECTED LIGHTWAVE AND CHAOS

It was observed that laser oscillation became highly unstable when the emitted light was injected into the laser cavity after it was reflected from a mirror surface, fiber edge, optical disk surface, or other reflective items (see fig. 23). Changes in oscillation characteristics have been observed, such as changes in the threshold current, wavelength shift (LANG and KOBAYASHI [1980]), and linewidth broadening (MILES, DANDRIDGE, TVETEN, TAYLOR and GIALLORENZI [1980]), increases in intensity noise (BROOM, MOHN, RISCH and SALATHE [1970]), and changes in relaxation oscillation characteristics (KOBAYASHI [1976]). These instabilities are frequently induced, since reflected waves can be easily injected into the cavity because of its low facet reflectivities.

HIROTA and SUEMATSU [1982] have discussed this phenomenon by utilizing a model of injection locking at the initial theoretical stage of their study. According to their theory, the intracavity laser light can be injection locked by the reflected wave under specific conditions. The possibility of injection locking depends in a complicated manner on operating parameters, for example, magnitudes of frequency fluctuations, intensity fluctuations, random mechanical vibrations of the reflecting surface, and random fluctuations in refractive index of the optical path. Thus, this was interpreted to mean that the instabilities were induced by random fluctuations in the values of the operating parameters by means of injection locking.

Following this study it was found that this instability can be induced even in the absence of such random fluctuations, so that it is not a stochastic but a deterministic instability. In other words, instability can be induced by the injection of a reflected wave into a nonlinear self-sustained oscillator, with the phase delay given by the round-trip time to the external mirror, even if no operating parameters have random fluctuations. This fact supports the suggestion of optical chaos made by IKEDA [1979]. Chaotic behavior of semicon-

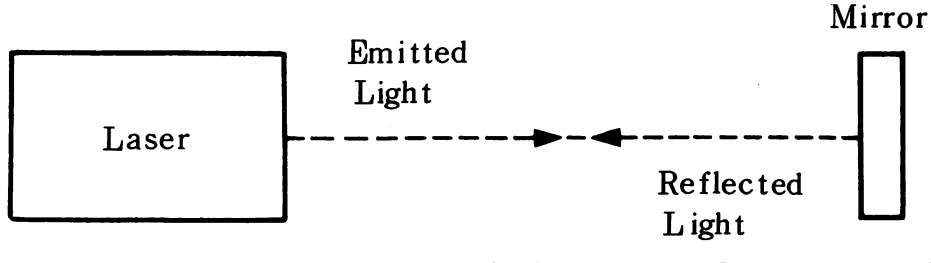

Fig. 23. Schematic explanation of the injection of reflected waves from an external reflector.

ductor lasers has been experimentally confirmed by injection of the reflected wave (KAWAGUCHI and OTSUKA [1984]).

Computer simulations have also been made by employing a three-mirror model. However, the accuracy of this model can be reduced if the round-trip time is taken too long in comparison with the rise time of laser oscillations. The longest time limit for the round trip for this model is about 0.1 ns, which corresponds to a separation between the laser facet and the external mirror of about 1.5 cm. If the separation is larger than 1.5 cm, a more accurate model should be employed, for which a Van der Pol's equation is used by adding a term representing the electric field of the reflected wave with a phase delay (TERAMACHI and OHTSU [1984], OHTSU [1985b]). In the case of single-mode oscillation the electric field of the lightwave is expressed as

$$\tilde{E}_i(t) = E_i(t) \exp(i\omega_0 t) . \tag{5.1}$$

The Van der Pol equation for $\tilde{E}_i(t)$ can be derived from $E_i(t)^2$ of eq. (2.3), and is given by

$$\frac{d^2\tilde{E}_i(t)}{dt^2} = \frac{c}{2n}\frac{d}{dt}\{(\tilde{\alpha}_i^{(1)} - \alpha_{th})\tilde{E}_i - \tfrac{4}{3}\tilde{\alpha}_i^{(3)}\tilde{E}_i^3\}$$

$$- \Omega^2(N_c)\tilde{E}_i + \kappa\frac{d}{dt}\tilde{E}_i(t - T) , \tag{5.2}$$

where $\Omega(N_c)$ is the resonance angular frequency of the cavity mode, κ is the coupling coefficient of the reflected wave into the laser cavity, and T is the round-trip time between the laser facet and the external mirror (i.e., the delay time). The angular frequency Ω depends on the carrier density N_c, and is expressed as

$$\Omega^2(N_c) = \Omega_0^2\left\{1 - \frac{2A}{n}(N_c - N_{cth})\right\} , \tag{5.3}$$

where A is the coefficient shown in eq. (4.1), representing the proportionality between the change in refractive index and that of the carrier density. Ω_0 and N_{cth} are the resonance angular frequency of the cavity mode and the carrier density at the threshold. Computer simulations can be carried out to analyze temporal variations of $\tilde{E}_i(t)$ by using eqs. (2.4), (5.2) and (5.3).

Equation (5.2) is a nonlinear difference–differential equation that depends on the carrier density variations of eq. (2.4). This equation shows that the electric field exhibits an irregular behavior because it suffers the effect of

feedback with a delay time T. Figure 24 shows variations of the laser output power P_0 simulated by using eqs. (2.4), (5.2), and (5.3). It can be seen that the magnitude of fluctuations increases with increasing κ, that is, increasing injected power.

Occurrence of instability can be noticed in this figure when the injection rate is as low as 0.003%, which means that an accurate optical isolator should be

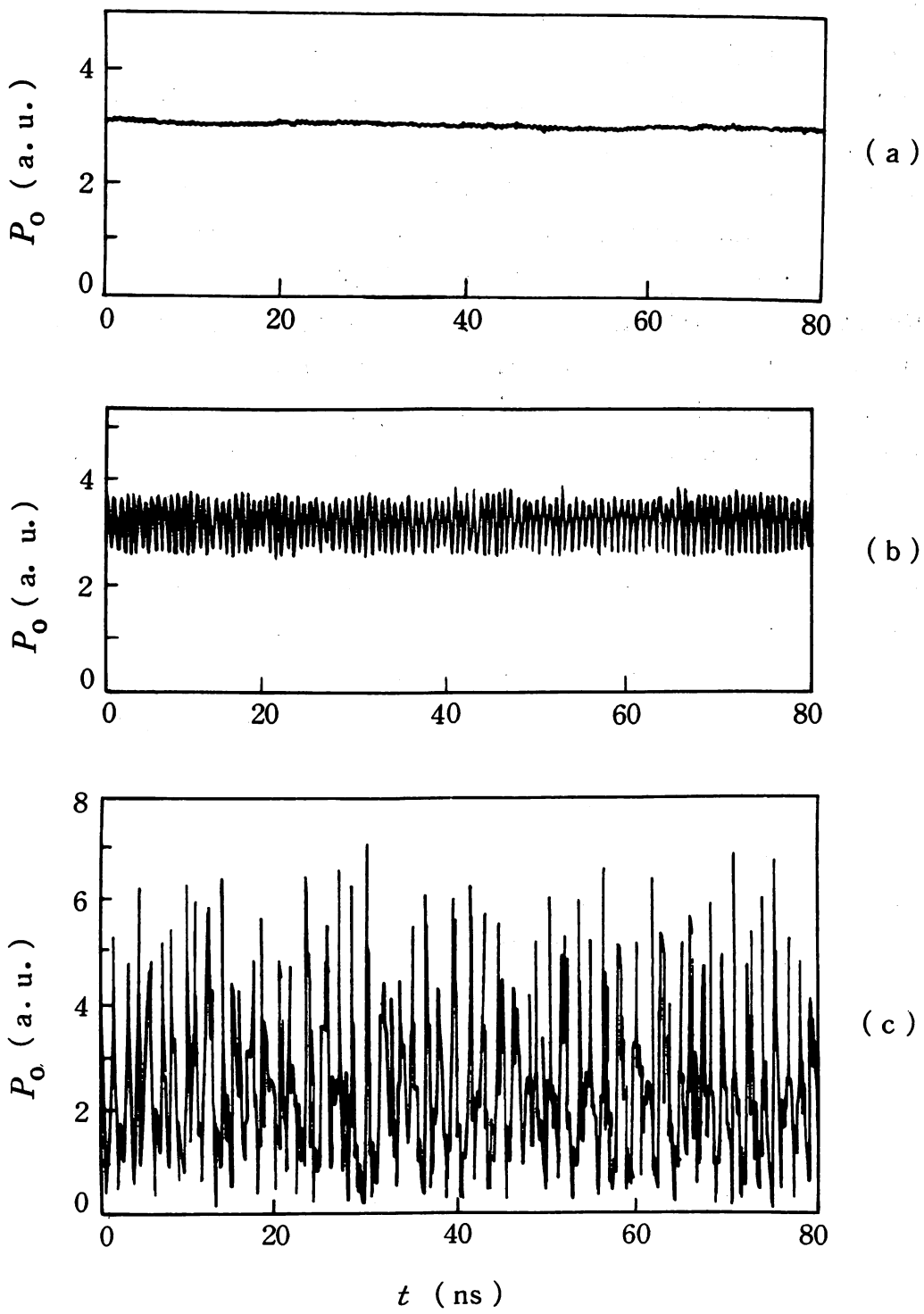

Fig. 24. Calculated results of power fluctuations induced by the injection of reflected waves. (After OHTSU [1985b].) Injection rates are (a) 0%, (b) 0.003% and (c) 5%.

used. However, industrial application of optical isolators made of ferromagnetic Faraday rotators is inadvisable because of their high cost. To overcome this difficulty, several attempts have been made to use special lasers that are insensitive to the effects of a reflected wave, such as a laser with low temporal coherence. Although it is not the main purpose of this review to describe low-coherence lasers, we introduce them briefly for reference here.

Reproducible low temporal coherence has been realized by utilizing a multilongitudinal oscillation of refractive index-guided lasers, which would oscillate with a single mode under stationary conditions driven by a dc current. Although the magnitude of the intensity noise of multimode lasers is larger than that of single-mode lasers because of mode-hopping noise, multimode lasers are insensitive to the effects of the reflected wave because of the low temporal coherence in the superposed lightwaves, which can suppress the increase of intensity noise under injection of reflected light.

Multimode oscillation can be realized, for example, by superposing a radio-frequency injection current of several 100 MHz to the dc current (ARIMOTO, OJIMA, CHINONE and OISHI [1984]) or by inducing a sustained oscillation by increasing the difference in refractive index between the active and cladding layers (HAYASHI, MATSUI, TANETANI, YAMAMOTO, YANO and HIJIKATA [1984]). Lasers prepared by these techniques oscillate with about ten longitudinal modes, which reduces the temporal coherence in the superposed lightwave. Therefore they are insensitive to the effects of a reflected wave, and intensity noise is not increased even if a reflected wave is injected. This is shown by fig. 25, which represents experimentally obtained relations between the magnitudes of relative intensity noise (RIN) and the power ratio of the reflected wave and the emitted wave, P_r/P_0 (CHINONE, OJIMA and NAKAMURA [1983]).

The artificially prepared low-coherence lasers just described can be replaced in the future by improved single-mode lasers that are free from the effect of reflected waves. Development of such a high-performance single-mode laser and more practical optical isolators is essential if the temporal coherence of the semiconductor lasers is ultimately to be improved.

5.2. MODE-HOPPING NOISE

Refractive index-guided semiconductor lasers usually show single longitudinal mode oscillation, as was described in § 2.1. However, because there is no longitudinal mode control, the longitudinal oscillation can "hop" from one mode to another if the ambient temperature or injection current is varied. This switching phenomenon, which is shown in fig. 26 (ARIMOTO, OJIMA and

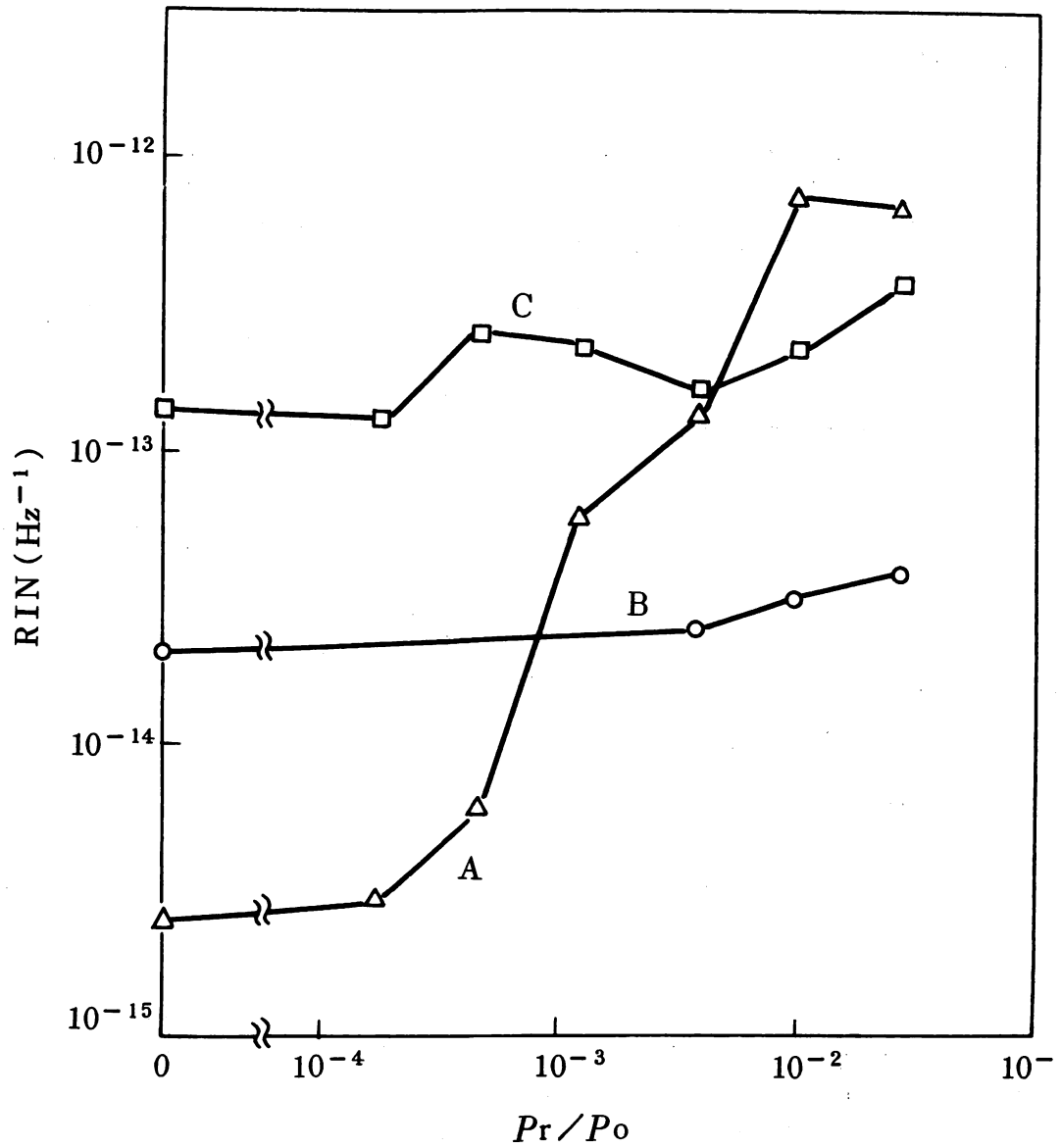

Fig. 25. Relations between the relative intensity noise (RIN) and the power ratio of the reflected and the emitted wave P_r/P_o. (A) Single-mode, index-guided laser. (B) Multimode laser obtained by superposing a radiofrequency injection current on the single-mode, index-guided laser. (C) Multimode, gain-guided laser. (After CHINONE, OJIMA and NAKAMURA [1983].)

TATSUNO [1982]), is called mode hopping, and it interferes with improvements in coherence because of discontinuous jumps of oscillation frequency. Furthermore, fig. 26 shows that the total laser power fluctuates randomly, a characteristic which is called mode-hopping noise.

Mode hopping can be suppressed if longitudinal mode-controlled lasers (e.g., DFB lasers or DBR lasers) are used. However, it is difficult to implement longitudinal mode control for visible AlGaAs lasers because of oxidation of the crystal surface and inaccuracies in the fabrication of diffraction gratings resulting from the short pitch of the grooves. This makes mode hopping a specific noise source for these lasers. The mode hopping of these visible lasers

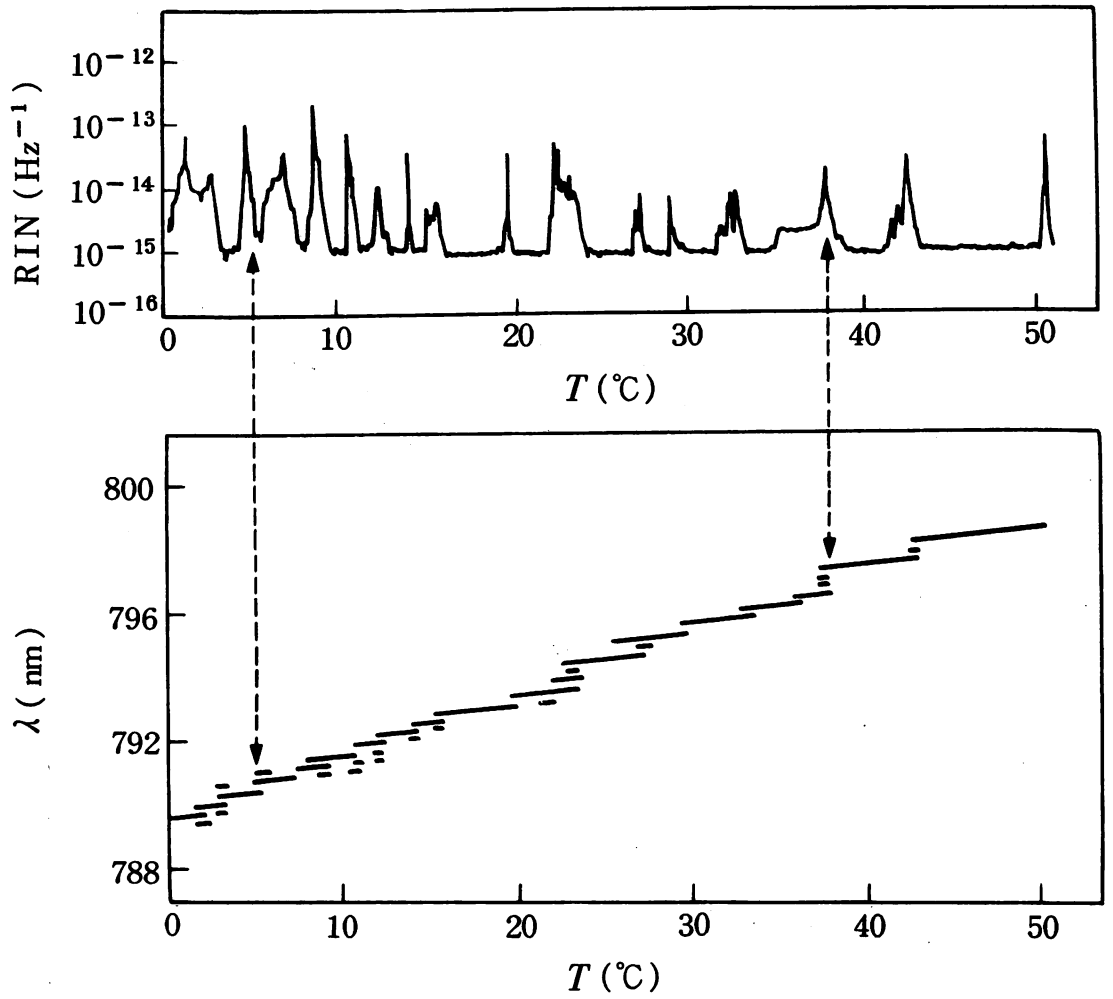

Fig. 26. Dependence of the wavelength of a CSP-type AlGaAs laser on the ambient temperature, exhibiting mode hopping (lower part of figure). Increases in the magnitude of the relative intensity noise induced by this hopping are simultaneously shown in the upper part of this figure. (After ARIMOTO, OJIMA and TATSUNO [1982].)

should be suppressed to maintain the magnitude of the intensity noise at a level sufficiently low to apply them to optical measurements.

To provide a theoretical background for improving coherence, mechanisms of mode hopping and its suppression are reviewed here by describing the work done by OHTSU, OTSUKA and TERAMACHI [1985] and OHTSU, TERAMACHI, OTSUKA and OSAKI [1986]. Hopping between two longitudinal modes is discussed for the sake of simplicity. The time-averaged powers of these modes can be measured by using a grating monochromator followed by photodetectors and dc amplifiers, as is shown in fig. 27a. However, their instantaneous powers do not have constant values but have rectangular waveforms, as shown in fig. 27b, in which mode-hopping can be seen clearly. Since the heights of the two rectangular waveforms in fig. 27b are not usually equal, the total power also can vary, which can be interpreted as mode-hopping noise.

Figure 28a shows the power spectral densities of the intensity fluctuations

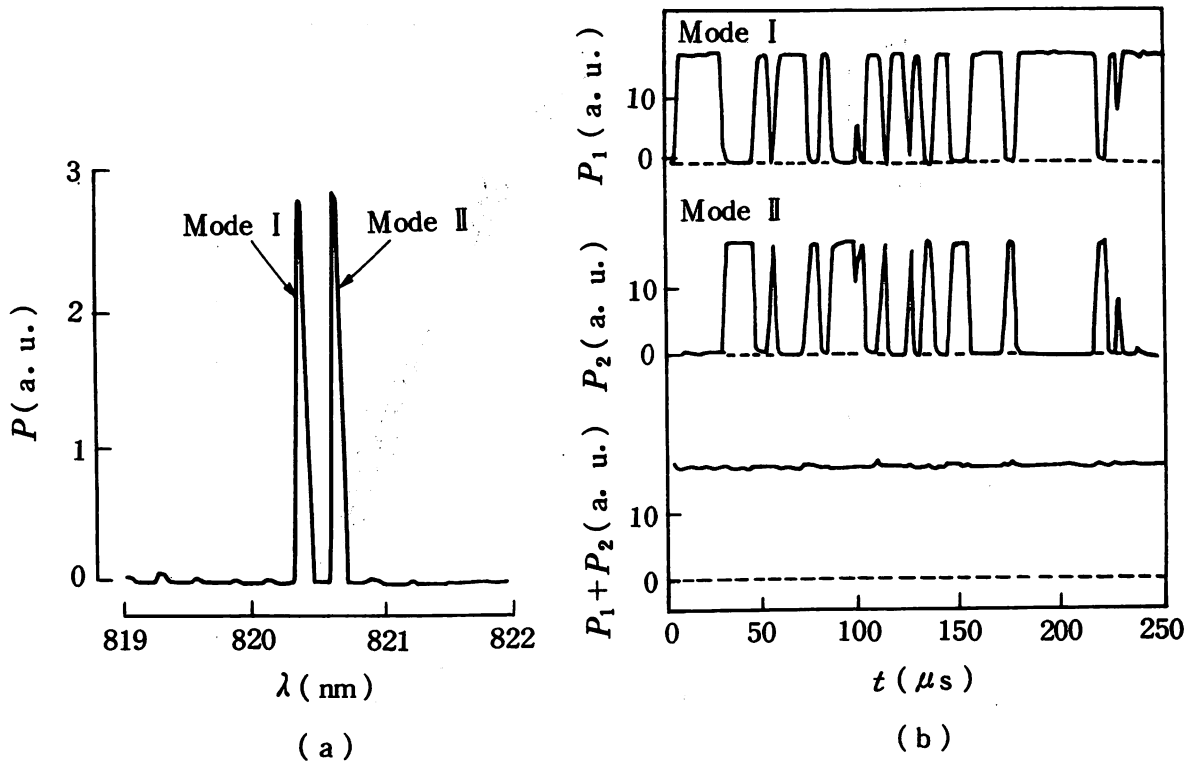

Fig. 27. (a) An example of the mode spectrum of the CSP-type AlGaAs laser measured by a grating monochromator and dc amplifiers. (b) Temporal intensity variations of the modes shown in (a) and of their sum. (After OHTSU, TERAMACHI, OTSUKA and OSAKI [1986].)

in fig. 27b. These curves are typical Lorentzian, with a cutoff frequency f_c, which means that the mode hopping follows the stochastics of a Poisson process, that is, mode hopping occurs completely randomly in time. Since the average duration of the rectangular waveforms of fig. 27b corresponds to $1/\pi f_c$, f_c represents the average frequency of mode hopping. Figure 29 shows the experimentally obtained relation between f_c and the injection current I normalized to its threshold value I_{th}. It is found from this figure that f_c decreases exponentially with increasing I/I_{th}, which means that operation at higher bias is effective in reducing mode hopping.

It can be deduced that this Poisson process is caused by randomly fluctuating driving forces. Since the fluctuations of spontaneous emission can be considered as the principal driving force, computer simulations are carried out by adding Langevin terms representing the spontaneous emission to eq. (2.3), where eq. (2.4) was also used for simulations. The simulated results also showed a rectangular waveform and Lorentzian power spectral densities (see fig. 28b) that were similar to those in figs. 27b and 28a. This agreement between the experimental and theoretical results confirmed that the mode hopping is induced by fluctuations of spontaneous emission.

Further calculations are carried out in the case where the light intensities of the two modes of fig. 27a equal each other, that is, the heights of the rectangular

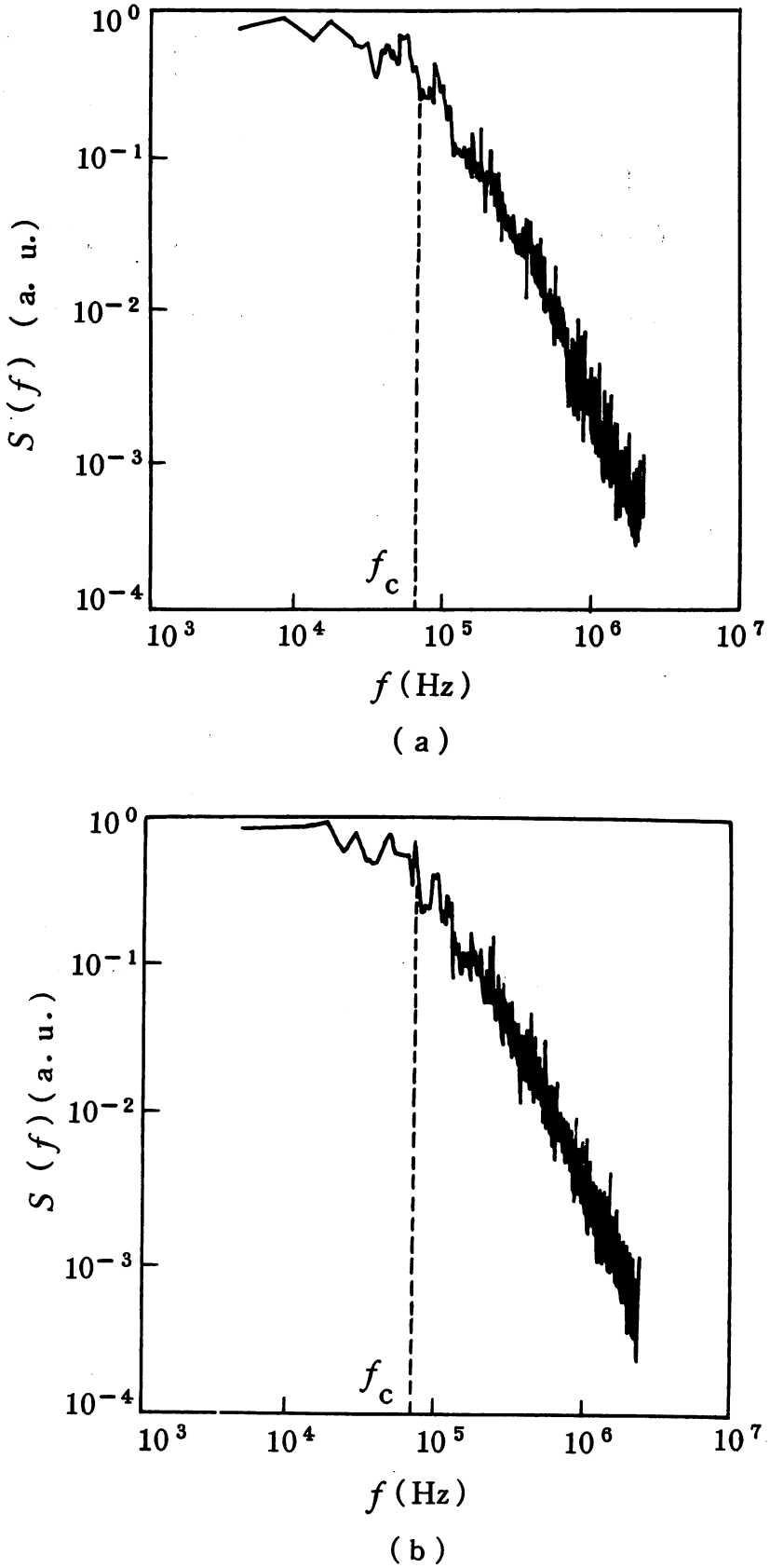

Fig. 28. (a) Power spectral density of intensity fluctuations of one of the modes of fig. 27. (b) Result of computer simulation of power spectral density by using a two-mode semiclassical Langevin equation of motion. f_c is the 3 dB cutoff frequency. (After OHTSU, TERAMACHI, OTSUKA and OSAKI [1986].)

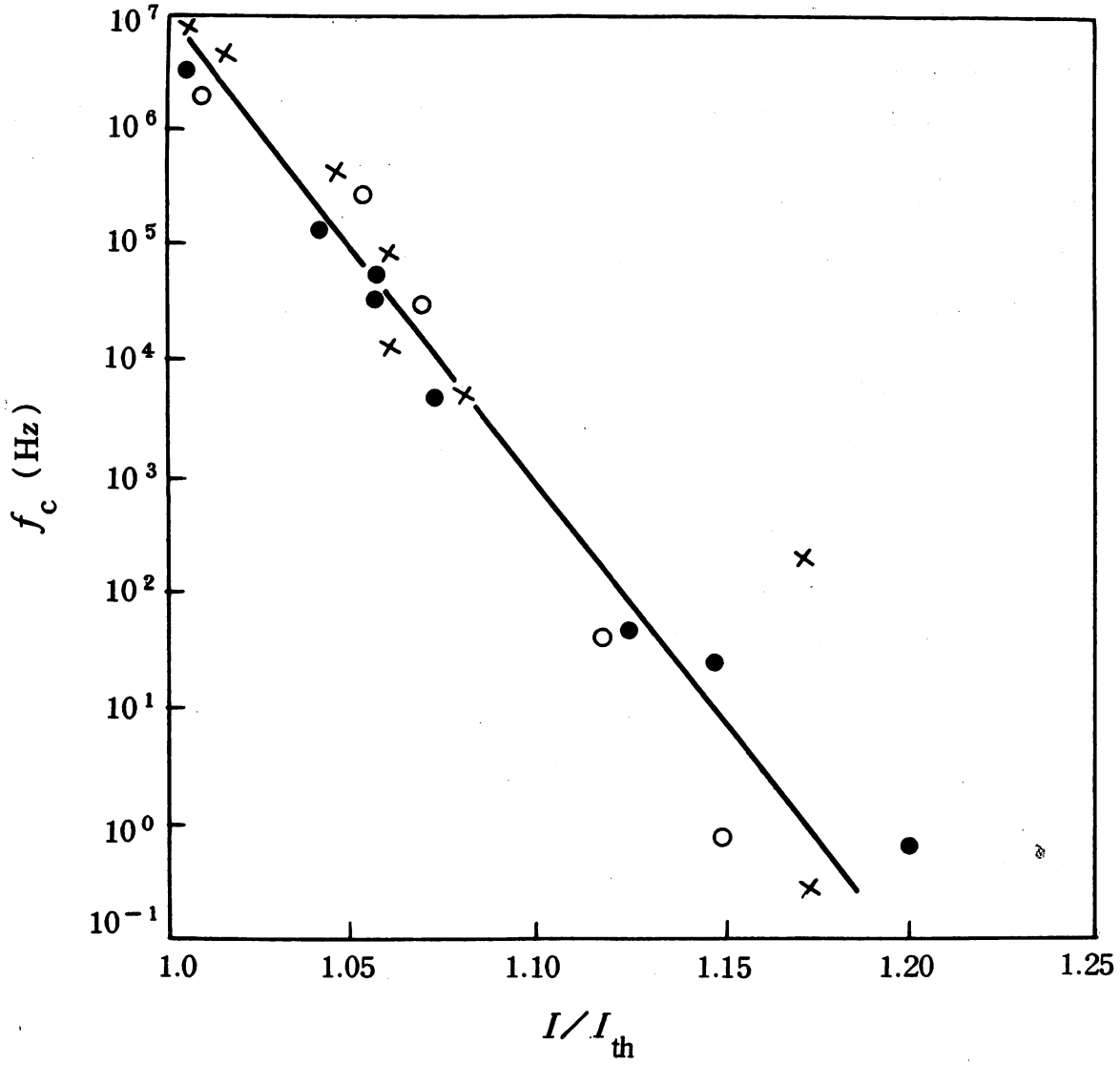

Fig. 29. Relation between the injection current normalized to its threshold value I/I_{th} and the cutoff frequency f_c. The solid line is a least-squares fit to the experimental values. (After OHTSU, TERAMACHI, OTSUKA and OSAKI [1986].)

waveforms of fig. 27b are equal. In this case the stimulated emission rate of the first term of the right-hand side of eq. (2.4) is constant in time, even though mode hopping occurs, because the total power is kept constant, and this also maintains the carrier density at a constant value. This means that the gain coefficients of eq. (2.3), $\tilde{\alpha}_i^{(1)}$, $\tilde{\alpha}_i^{(3)}$, and $\tilde{\alpha}_{i(j)}^{(3)}$, are kept constant and that the equation we have to solve in order to describe mode hopping is eq. (2.3) only. Equation (2.4) does not have to be taken into account. From this estimation it can be concluded that the formulations used for gas or dye lasers can also be applied for semiconductor lasers as long as the intensities of the two modes are equal.

Mode hopping phenomena in ring dye lasers (HIOE and SINGH [1981]) and the analogy between mode hopping and first-order phase transitions (LETT,

CHRISTIAN, SINGH and MANDEL [1981]) have been discussed in the literature; this will now be applied to eq. (2.3).

Langevin equations of motion can be derived for the two-mode oscillation by adding Langevin forces of spontaneous emission to eq. (2.3). Furthermore, a Fokker–Planck equation for the probability $p(E_1^2, E_2^2, t)$ is derived from these equations. The average frequency of mode hopping f_c is derived from the time-dependent solution of the Fokker–Planck equation given by

$$f_c = \frac{1}{\pi\zeta_t} a^2 \frac{\sqrt{1+\xi}-1}{\sqrt{\pi(1+\xi)}} \exp\left[-\frac{a^2\cdot(\sqrt{1+\xi}-1)^2}{1+\xi}\right], \tag{5.4}$$

where ζ_t is a constant used to normalize the Langevin equations of motion with respect to time. The quantities a and ξ are the pump parameter and a coupling constant between the two modes, which are defined as

$$a = (E_i)_s^2/E_{N\,i}^2, \qquad \xi = \tilde{\alpha}_{i(j)}^{(3)}/\tilde{\alpha}_i^{(3)} \qquad (i, j = 1,2; i \neq j), \tag{5.5}$$

where $(E_i)_s^2$ is the squared amplitude of the stationary electric field of the ith mode and $E_{N\,i}^2$ is the mean square value of the fluctuations of spontaneous emission that drive the ith mode. Substitution of numerical values for AlGaAs lasers given by YAMADA and SUEMATSU [1981] into eq. (5.5) gives $\xi = \frac{4}{3}(>1)$. This means that the interaction between the longitudinal modes in semiconductor lasers corresponds to "strong coupling" if the classification based on Lamb's theory (LAMB [1964]) is applied. Therefore the two modes do not oscillate simultaneously but exhibit mode hopping as shown by fig. 27b. Figure 30 shows the relation between f_c and a. Since a is proportional to I/I_{th}, fig. 30 agrees well with fig. 29. The value of f_c decreases exponentially with increasing a, since the laser oscillation is less sensitive to the effects of fluctuations of spontaneous emission when the laser is operated at a higher bias. It can be confirmed again from this figure that operation at higher bias is effective in suppressing mode hopping.

The time-independent solution of the Fokker–Planck equation gives the following stationary-state probability density for the normalized laser power I_1 and I_2 of the two modes:

$$p_s(I_1, I_2) = B^{-1} \exp[-U(I_1, I_2)], \tag{5.6}$$

where B is the normalization constant and U is the potential. The calculated result for the potential U is given by fig. 31, which has two minima separated by a saddle point. Both of these minima correspond to highly probable states for which one mode intensity is zero and the other is nonzero. Fluctuations of

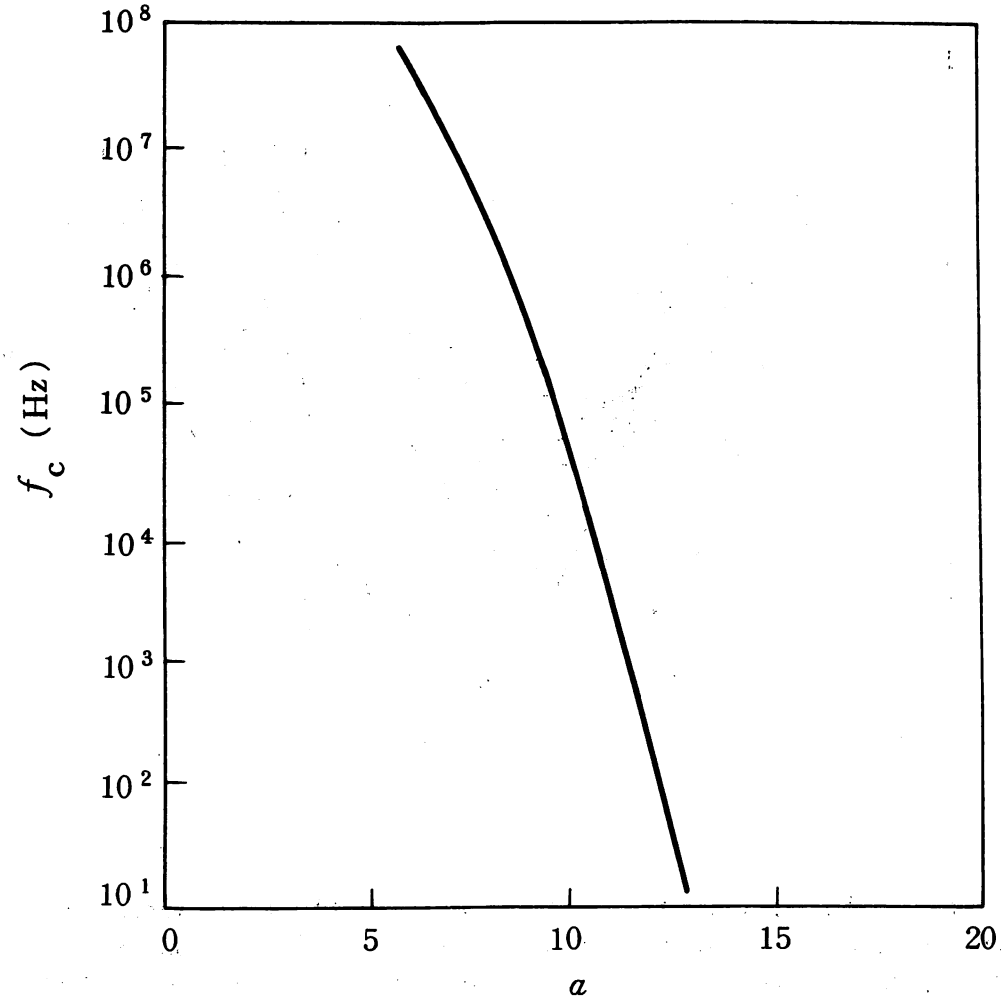

Fig. 30. Relation between f_c and a given by eq. (5.4). (After OHTSU, TERAMACHI, OTSUKA and OSAKI [1986].)

spontaneous emission drive the representative point in phase space from one minimum to the other at random times. The intensity of each mode therefore tends to jump randomly between zero and nonzero values, which corresponds to mode-hopping.

The difference of U between the minimum and the saddle point can be expressed as

$$\Delta U = -\frac{a^2}{2(1+\xi)} + \frac{a^2}{4}. \tag{5.7}$$

As ΔU increases with increasing a, the frequency of mode hopping decreases with increasing a.

Furthermore, since eq. (5.7) shows that ΔU increases with increasing ξ, one more effective way to reduce the mode hopping is to increase the coupling constant ξ. CHINONE, KURODA, OHTOSHI, TAKAHASHI and KAJIMURA [1985] have doped tellurium (Te) atoms into the cladding layer of the laser. It has been pointed out by MERZ, VAN DER ZIEL and LOGAN [1979] that these impurity atoms form DX centers and work as saturable absorbers. Since

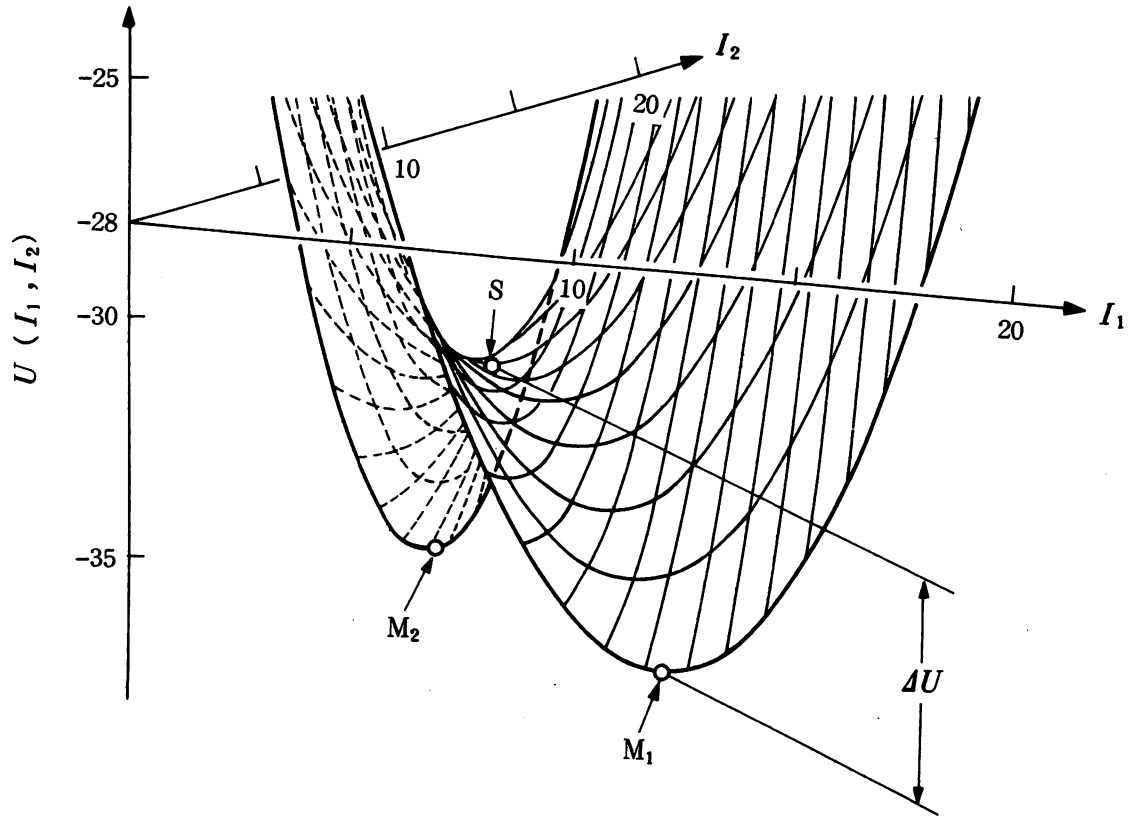

Fig. 31. The form of the potential $U(I_1, I_2)$, where $a = 12.09$. M_1 and M_2 represent the minima, and S is the saddle point of the potential. ΔU represents the depth of the minima measured from the saddle point. (After OHTSU, TERAMACHI, OTSUKA and OSAKI [1986].)

saturable absorbers in the cladding layer increase the coupling constant ξ, mode hopping can be reduced. As shown in fig. 32, it has been estimated by OHTSU, TERAMACHI and MIYAZAKI [1987] that the average mode hopping frequency f_c is drastically decreased above a certain value of the Te density N_T, which also depends on the laser power confinement ratio $\xi^{(1)}$ in the active region. This drastic decrease agrees well with the experimental results of CHINONE, KURODA, OHTOSHI, TAKAHASHI and KAJIMURA [1985].

Formulations based on the quantum theory of lasers are required to increase the accuracy of discussion of mode hopping by using eq. (2.9)–(2.11). MARCUSE [1985] discusses intensity fluctuations of the main longitudinal mode under coupling between the weakly oscillating submodes by using the quantum theory. A similar procedure can be used to analyze mode hopping more accurately for finding new experimental methods to suppress mode hopping and the associated intensity noise.

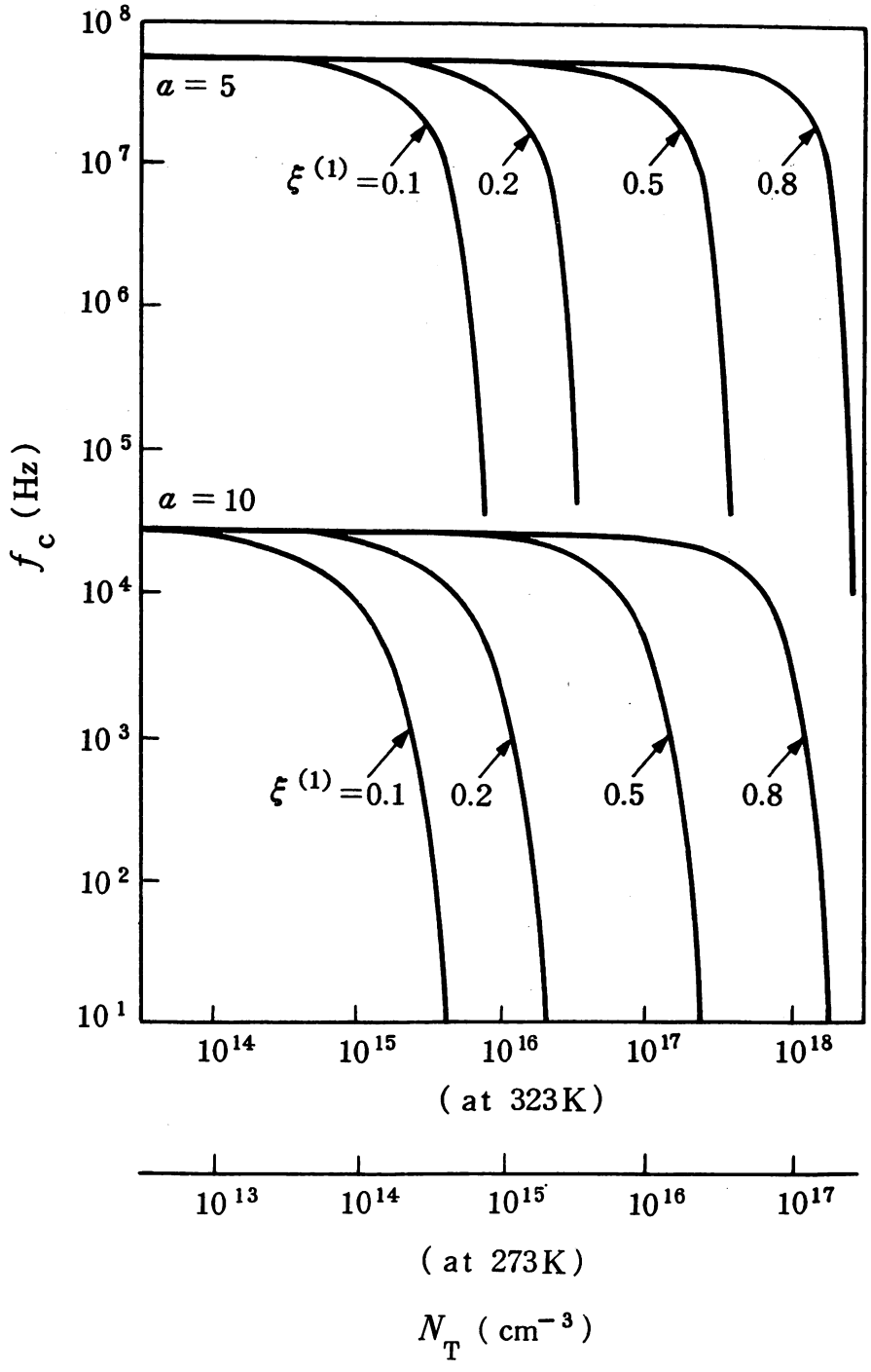

Fig. 32. Relation between f_c and tellurium density N_T doped into the cladding layer of an AlGaAs laser. a, pump parameter; $\xi^{(1)}$, laser power confinement ratio in the active region of the laser cavity. (After OHTSU, TERAMACHI and MIYAZAKI [1987].)

§ 6. Applications of Highly Coherent Semiconductor Lasers

Semiconductor lasers have been widely used for several optical measurements because of their small size and low power consumption. This section reviews the new areas of application that can be found if the coherence of these lasers is improved.

6.1. OPTICAL MEASUREMENTS AND OPTICAL FIBER SENSORS

There are several practical applications of optical measurements in which highly coherent light sources are required. One example is the Doppler velocimeter, which utilizes the Doppler effect for remote measurement of the velocity of moving particles or of vibrating surfaces (DURNST, MELLING and WHITELAW [1976]). In this apparatus, optical fibers have been used for light transmission and signal detection (TANAKA and BENEDEK [1975] and UEHA, SHIBATA and TSUJIUCHI [1977]), in order to reduce the effect of air turbulence on the laser transmission and to improve the stability of the system. Reduction of system volume and power consumption can be expected if conventional gas lasers are replaced with semiconductor lasers. In this case, techniques given in § 4.3 are required because the long coherence length (i.e., narrow linewidth of the semiconductor lasers) is indispensable to improve the resolution of heterodyned signal frequency measurements. Apparatus using a highly coherent semiconductor laser and an optical fiber are now being developed, and further improvements can be expected in the future.

Fiber gyroscopes are another example that has been investigated. Although mechanical gyroscopes have been employed as a conventional rotation sensor in inertial navigation systems so far, several attempts are being carried out to construct this sensor by optical technology. The Sagnac effect has been utilized for this purpose (SAGNAC [1913], POST [1967]). This is a relativistic effect in which the optical path length is varied in proportion to rotational speed. A gyroscope employing a ring gas laser has been proposed by ROSENTHAL [1962] and has had practical applications. This device can be called an active gyroscope because an active medium for laser oscillation itself is used as the optical path for the detection of rotation. However, this type of optical gyroscope has presented several problems, such as drift of the output signal caused by flow of laser gases and difficulties in detecting very low rotational speeds because of frequency-locking between the two oppositely propagating running waves in the laser cavity (ARNOWITZ and COLLINS [1970]).

To overcome these problems, a new gyroscope has been developed recently by using an optical fiber as a transmission line. The progress of this development has been summarized by EZEKIEL and ARDITTY [1982].

The fiber gyroscope that has received most study so far has an inteferometer (e.g., Mach–Zehnder type) composed of an optical fiber. This device can be called a passive nonresonant gyroscope. Low temporal coherence semiconductor lasers or superluminescent diodes have been employed as a light source for this gyroscope to reduce the chaotic instabilities induced by a reflected wave

from the edges of fibers and to reduce the Rayleigh backscattering in the fiber.

However, a higher sensitivity gyroscope can be expected if a high temporal coherence laser, which is independent of the externally induced noise sources, can be developed. An example of this gyroscope is the passive-ring resonator-type fiber gyroscope, which has been proposed by SANDERS, PRENTISS and EZEKIEL [1981]. In this type a ring Fabry–Perot interferometer is used as an optical transmission line. The advantage of this gyroscope compared with the nonresonant type is that a higher sensitivity can be obtained with a shorter fiber, which makes it possible to have a small-sized, practical apparatus for a rotation sensor. Experimental work has been carried out using a gas laser as a coherent light source, and an uncertainty of rotation detection as low as 0.5 deg/h has been obtained by MAYER, EZEKIEL, STOWE and TEKIPPE [1983].

Further reductions in volume of the system can be expected if the gas laser is replaced with a semiconductor laser. Although experimental results from using semiconductor lasers have not been fully documented because their coherence has not yet been high enough for this system, one example has been developed by OHTSU and OTSUKA [1983] and OHTSU and ARAKI [1987], which is schematically explained by fig. 33. A ring Fabry–Perot interferometer, composed of a fiber and two fiber couplers, uses the fiber couplers as input and output mirrors of the interferometer. The light beam from the laser is divided into two parts, which propagate through the fiber in mutually opposite directions. Since a difference will be induced between the resonance frequencies of the ring Fabry–Perot interferometer for the clockwise and counterclockwise beams (ν_{cw} and ν_{ccw}) by the Sagnac effect when the interferometer rotates, its rotational speed Ω can be detected by measuring the frequency differences $\nu_{cw} - \nu_{ccw}$. This is expressed as

$$\nu_{cw} - \nu_{ccw} = \frac{1}{\lambda}\sqrt{\frac{4A}{\pi}}\,\Omega, \tag{6.1}$$

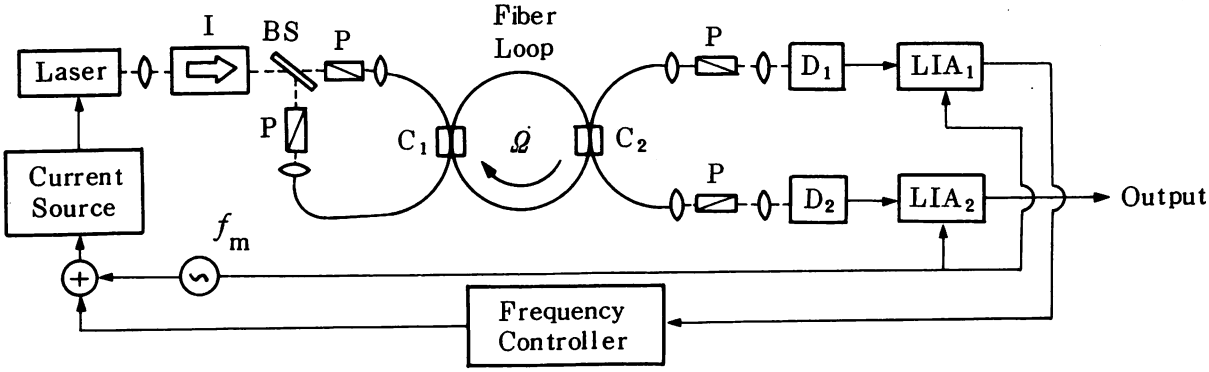

Fig. 33. Block diagram of a passive ring cavity type fiber gyroscope with an InGaAsP laser. C_1, C_2, fiber directional couplers; I, optical isolator. (After OHTSU and OTSUKA [1983] and OHTSU and ARAKI [1987].)

where λ is the wavelength of the light and A is the area surrounded by the fiber loop. For this measurement the laser frequency is controlled so that it is locked to the resonant frequency ν_{ccw}. The laser frequency is modulated for this locking scheme in fig. 33. At the same time this modulation is utilized to detect the intensity variation of the transmitted light from the clockwise beam, from which the rotational speed Ω can be measured by using eq. (6.1). The sensitivity limit of the detection of rotation, which is governed by the detector shot noise, is estimated as

$$\Omega_s = \frac{\sqrt{2} \times 0.01\lambda c}{nNA} \sqrt{\frac{h\nu}{\eta\tau}} \frac{1}{\sqrt{P_0}} \frac{1}{\sqrt{\alpha_t R}} \frac{(1-\alpha_t R)^2}{1-R} \left(\frac{\Gamma + \Delta\nu}{\Gamma}\right)^{\frac{3}{2}}, \qquad (6.2)$$

where λ and c are the wavelength and the speed of the light in vacuum, n is the refractive index of the fiber, N is the number of turns of the fiber loop, h is Planck's constant, η is the quantum efficiency of the detectors, τ is the integration time of the measurement, P_0 is the laser power incident to the ring Fabry–Perot interferometer, R is the reflectance of the fiber coupler, α_t is the round-trip loss of the fiber loop in which losses due to the reflectance R of the fiber couplers are not counted, Γ is the full width at a half maximum of the resonant spectrum of the interferometer, and $\Delta\nu$ is the linewidth of the laser oscillation.

The value of Ω_s has a minimum at a specific value of the reflectance R_m. The relation between R_m and α_t is given by fig. 34a for several values of $\Delta\nu$. The minimum of Ω_s under this condition is shown in fig. 34b for $\alpha_t = 0.1$ dB and several values of $\Delta\nu$. It is seen from this figure that the sensitivity is sufficiently high to measure the rotational and revolutional speed of the earth. However, it is essential to use a narrow-linewidth semiconductor laser in order to obtain such high sensitivity. As shown in fig. 34b, it is estimated that a linewidth of 100 kHz is sufficiently narrow, and this can be obtained by using the technique described in § 4.3.

The experimental setup of fig. 33 has already been developed by using a 1.5 μm InGaAsP laser and a single-mode fiber. Preliminary experiments have demonstrated an uncertainty of rotation detection as low as 1.5 deg/h at an integration time of 100 s (OHTSU and ARAKI [1987]). This uncertainty can be further decreased by improving the optical and electronic components of the system. Contributions from the Kerr effect (BERGH, CULSHAW, CUTLER, LEFEVRE and SHAW [1982]) and RAYLEIGH backscattering (CUTLER, NEWTON and SHAW [1980]) in the fiber should also be taken into account to achieve further improvements in performance for this type of gyroscope.

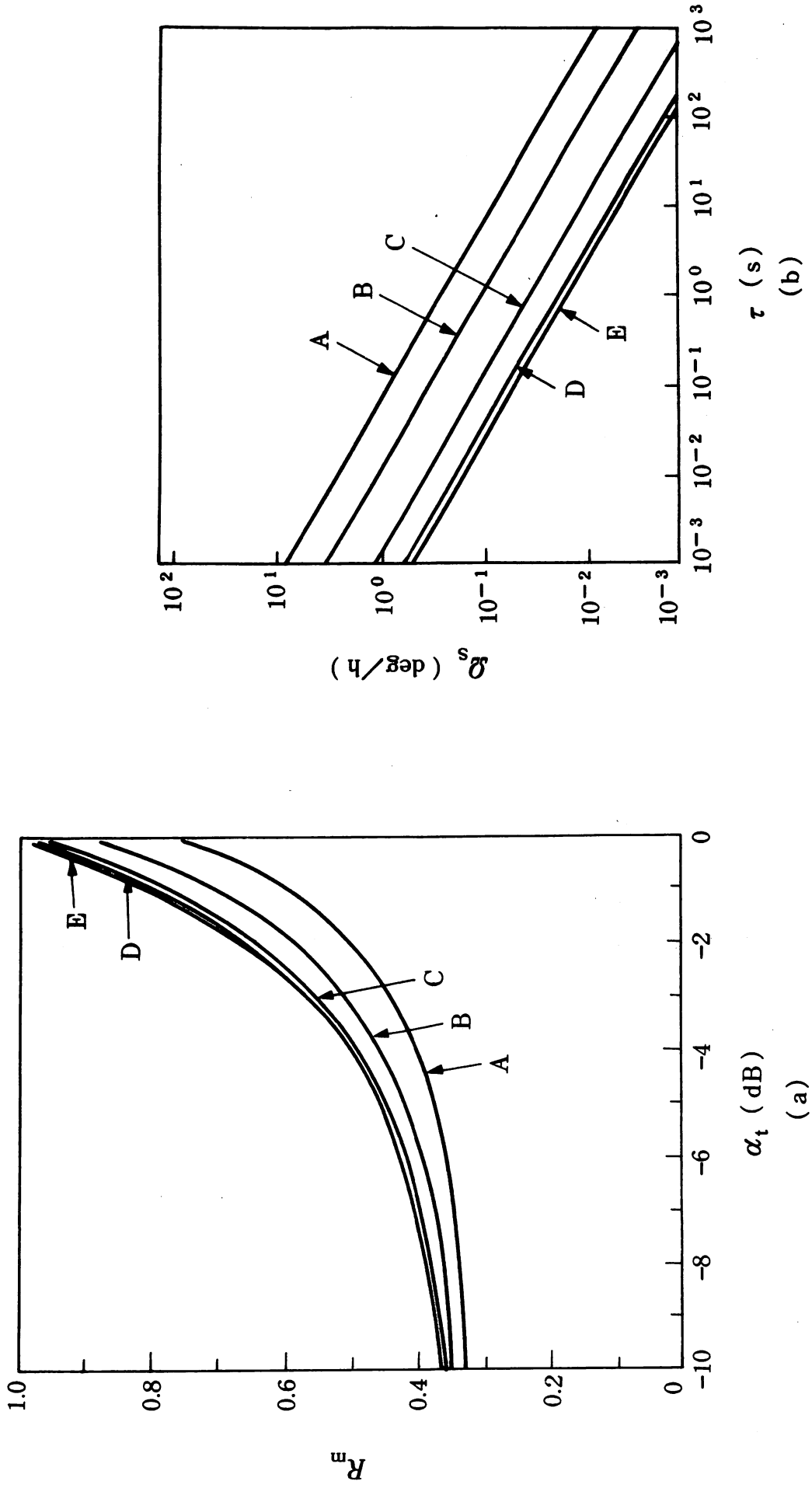

Fig. 34. (a) Relation between R_m and α_t. (b) Values of the minimum of Ω_s for which the value of R is fixed at R_m of (a), where $\alpha_t = 0.1$ dB. The laser linewidths $\Delta\nu$ are (curve A) 13 MHz, (B) 5 MHz, (C) 1 MHz, (D) 100 kHz and (E) 0. (After OHTSU and OTSUKA [1983] and OHTSU and ARAKI [1987].)

If such a high sensitivity can be realized by using this compact gyroscope, it can be applied not only to inertial navigation systems but also to the fields of astronomy, geophysics, space science, and others. For example, applications to earthquake detection and prediction will be possible by measuring the anomalous Chandler wobble of the earth excited by earthquakes (KANAMORI [1977]) or slight fluctuations of the rotational speed of the earth (OKAZAKI and SAKAI [1981]).

The accuracy of these measurements has been improved by using very long baseline interferometry (VLBI), for example; however, more practical and compact apparatus can be obtained if sensitive fiber gyroscopes are utilized. Furthermore, since these gyroscopes can be borne by satellites, it is possible to investigate the structure of the inner shells of other planets.

6.2. COHERENT OPTICAL COMMUNICATION

Intensity modulation and direct detection of semiconductor laser light have been employed in the conventional optical communication systems developed so far because the systems can be made simpler, less expensive, and more reliable. However, properties of temporal coherence in semiconductor lasers have not yet been utilized in these systems. Compared with these conventional systems, receiver sensitivities can be increased if the amplitude, frequency, or phase of the lightwave is coherently modulated and is demodulated by employing heterodyne or homodyne techniques.

This communication system has been called coherent optical communication, which is schematically explained in fig. 35. Although theoretical (GORDON

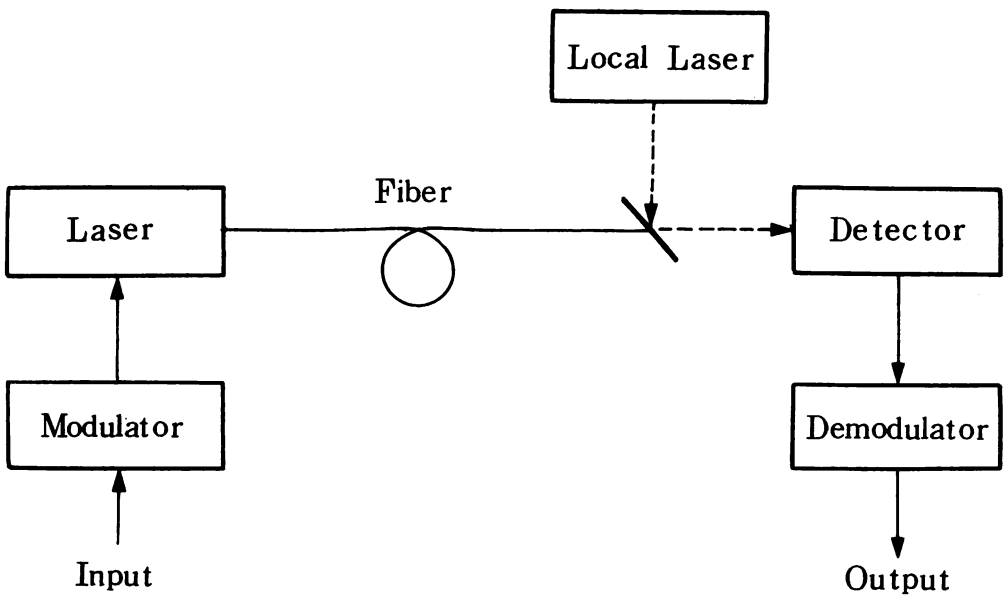

Fig. 35. Schematic explanation of the principle of coherent optical communication.

[1962]) and experimental (GOODWIN [1967]) studies were carried out in the 1960s, practical systems were not developed at that time because of several problems with the coherence and lifetime of practical lasers. However, on the basis of recent progress in the performance of semiconductor lasers, more practical systems of coherent optical communication have been proposed recently (YAMAMOTO [1980], OKOSHI and KIKUCHI [1981]) by employing semiconductor lasers and optical fibers. Intensive studies for developing practical coherent optical communication systems have been carried out in many countries by using these techniques.

Significant improvement in receiver sensitivity can be obtained in this system at a wavelength of 1.5–1.6 μm, in which optical fibers exhibit the lowest loss (0.2 dB/km), since heterodyne or homodyne detection and several modulation schemes can be employed.

To demonstrate this improvement, heterodyne detection is described here. Equations (6.3)–(6.5) are taken from a review article by OKOSHI [1982]. As a result of heterodyning between the modulated light transmitted through the optical fiber and the high-power local oscillator laser, the output current from the photodetector is given by

$$i = 2\sqrt{P_{LO}P_S}\left(\frac{\eta e}{h\nu}\right), \tag{6.3}$$

where P_{LO} is the laser power of the local oscillator, P_S is the signal power, η is the quantum efficiency of the photodetector, e is the electron charge, h is Planck's constant, and ν is the optical frequency. If $P_{LO} \gg P_S$, the standard deviations σ_M and σ_S of the noise power in the mark and space states are equal, and they are expressed as

$$\sigma_M = \sigma_S = \sqrt{2e\left(\frac{\eta e}{h\nu}\right)P_{LO}\cdot\Delta f + \frac{4kTF}{R}\cdot\Delta f}\sqrt{R}, \tag{6.4}$$

where Δf is the receiver bandwidth, T is the temperature, k is Boltzmann's constant, F is the noise figure of the front-end amplifier, and R is the load resistance of the photodetector. The first and second terms represent shot noise and thermal noise, respectively. The signal-to-noise ratio of the detection is derived from eqs. (6.3) and (6.4) and is approximated as follows if $P_{LO} \to \infty$ and the magnitude of the shot noise is sufficiently larger than that of the thermal noise

$$S/N = \frac{i^2R}{[(\sigma_M + \sigma_S)/2]^2} \approx \frac{\eta P_S}{h\nu\Delta f}. \tag{6.5}$$

This means that the signal-to-noise ratio approaches the quantum-noise limited value. As will be demonstrated later, experimental results obtained so far have already reached values less than 1 dB from this limit.

In contrast, the signal-to-noise ratio obtained by direct detection of a conventional optical communication system is still more than 10 dB lower than the quantum-noise limited value because of the excess noise factor and dark current of the avalanche photodiodes. These estimations confirm that a considerably higher sensitivity can be obtained by means of heterodyne detection.

Furthermore, the quantum-noise limited value of eq. (6.5) depends on the kind of modulation scheme because it is inversely proportional to the receiver bandwidth Δf. The dependence of the value of eq. (6.5) on modulation scheme has been derived OKOSHI, EMURA, KIKUCHI and KERSTEN [1981]; it is shown in fig. 36. The results from homodyne detection are also given in fig. 36. This figure shows that improvements in detection sensitivity can be expected by an appropriate choice of detection scheme and that the highest sensitivity can be expected from the use of phase shift keying (PSK) modulation and homodyne detection.

OKOSHI, EMURA, KIKUCHI and KERSTEN [1981] have derived the relationship between the detected light power level and the bit rate of the signal transmission required to maintain the bit error rate (BER) at a level as low as 10^{-9}. The result for a wavelength of 1.5 μm is shown in fig. 37, indicating that heterodyne detection can improve the detection sensitivity by as much as 10–30 dB when compared with direct detection.

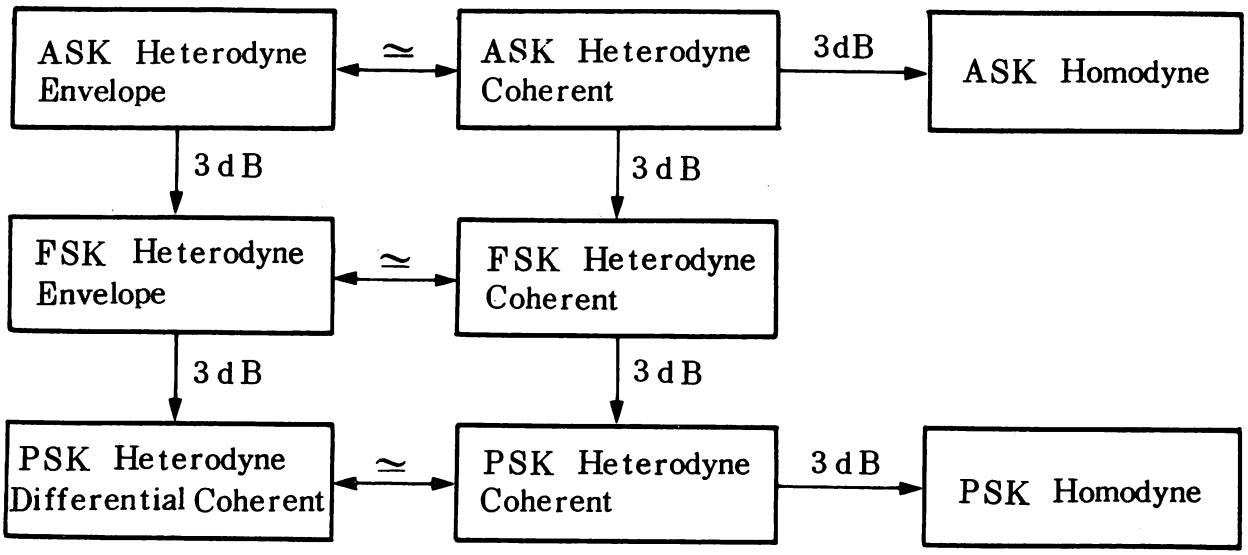

Fig. 36. Dependence of the signal-to-noise ratio on each modulation–demodulation scheme. (After OKOSHI, EMURA, KIKUCHI and KERSTEN [1981].)

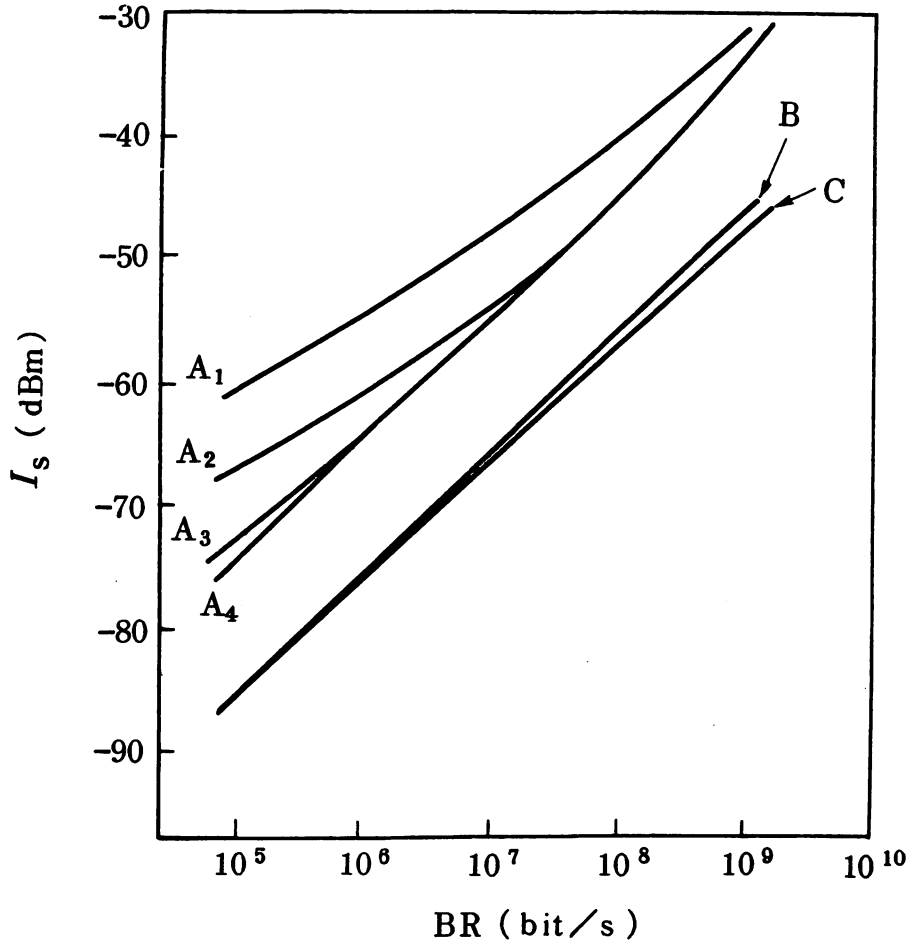

Fig. 37. Relations between the detected light power level I_s and the bit rate of signal transmission BR to maintain the bit error rate (BER) as low as 10^{-9}. Curves $A_1 \sim A_4$, Direct detection with the dark current of the detector 100 nA, 1 nA, 10 pA, and 0, respectively; Curve B, non-synchronous heterodyne detection; Curve C, synchronous heterodyne detection. (After OKOSHI, EMURA, KIKUCHI and KERSTEN [1981].)

Furthermore, the coherent optical communication system presents the following advantages:

(1) Extension of the transmitted fiber length and faster signal transmission speed (bit rate) can be expected as a result of improvements in the detection sensitivity.

(2) There is a possibility of frequency multiplexing.

(3) Stimulated Brillouin scattering and self-phase modulation effect in the optical fiber can be reduced because of the random phase modulation in the PSK system. This will increase the upper limit of the allowable input laser power to the single-mode fiber, which will induce further improvements in detection sensitivity.

(4) An external phase modulator can be employed in the PSK system, thus making the modulation speed faster than that of the conventional direct modulation, that is, the one limited by the relaxation oscillation of the laser.

(5) The effect of dispersion in the optical fiber can be neglected because a single-wavelength lightwave is transmitted, which can eliminate the requirements on the bandwidth of the optical fiber.

However, high temporal coherence in semiconductor lasers is necessary to obtain these ingenious systems. This can be achieved by means of the following requirements:

(i) Frequency fluctuations should be reduced to a value lower than 1×10^{-6}, because the IF frequency of the heterodyne detection is fixed at 0.2–2.0 GHz, that is, 1×10^{-6}–1×10^{-5} times that of the optical carrier frequency.

(ii) The linewidth should be narrower than 1×10^{-4}–1×10^{-3} times the bit rate of the signal transmission, which is required to maintain the BER at a sufficiently low level by reducing the phase fluctuations of the IF signal. KAZOVSKY [1985] summarized the values of the laser linewidth required for each modulation and detection scheme; they are given in table 3. As an approximate value, a linewidth several tens of kilohertz wide is required.

(iii) A wideband ASK, FSK, and PSK should be carried out.

Some of these requirements have already been fulfilled using the techniques described in § 4.3. Practical coherent optical communication systems can be expected if higher coherence of the semiconductor lasers can be achieved in the future.

TABLE 3
Maximum permissible linewidth of the laser, $\Delta\nu_m$, for use in coherent optical communication systems. (After KAZOVSKY [1985].)

Modulation format	Receiver type	$\Delta\nu_m/BR$ (%)[a]	
ASK	Coherent postdetection	4.54	
	Envelope postdetection	9.0	
FSK	Predetection Frequency discriminator	$12.4\,(f_d/BR)^2$ 9.0	if $f_d/BR < 0.85$, if $f_d/BR > 0.85$
	Postdetection Frequency discriminator	$7.69\,(f_d/BR)^2$ $9.0 + 6.0\,(f_d/BR)$	if $f_d/BR < 1.54$, if $f_d/BR > 1.54$
	Postdetection Dual filter	$10.75\,(f_d/BR)^2$ 9.0	if $f_d/BR < 0.84$, if $f_d/BR > 0.84$
DPSK	Autocorrelation	2.45	

[a] BR stands for the bit rate (bits/s).
f_d is the frequency deviation of FSK systems (= half the frequency separation between the "mark" and "space" frequencies).

Several intensive studies have been done to develop these systems in laboratories throughout the world. Gas lasers have sometimes been employed in this research because the coherence in semiconductor lasers is not always high enough. Current trends in this research have been reviewed by MATSUMOTO and SHIMADA [1986] and are summarized in fig. 38.

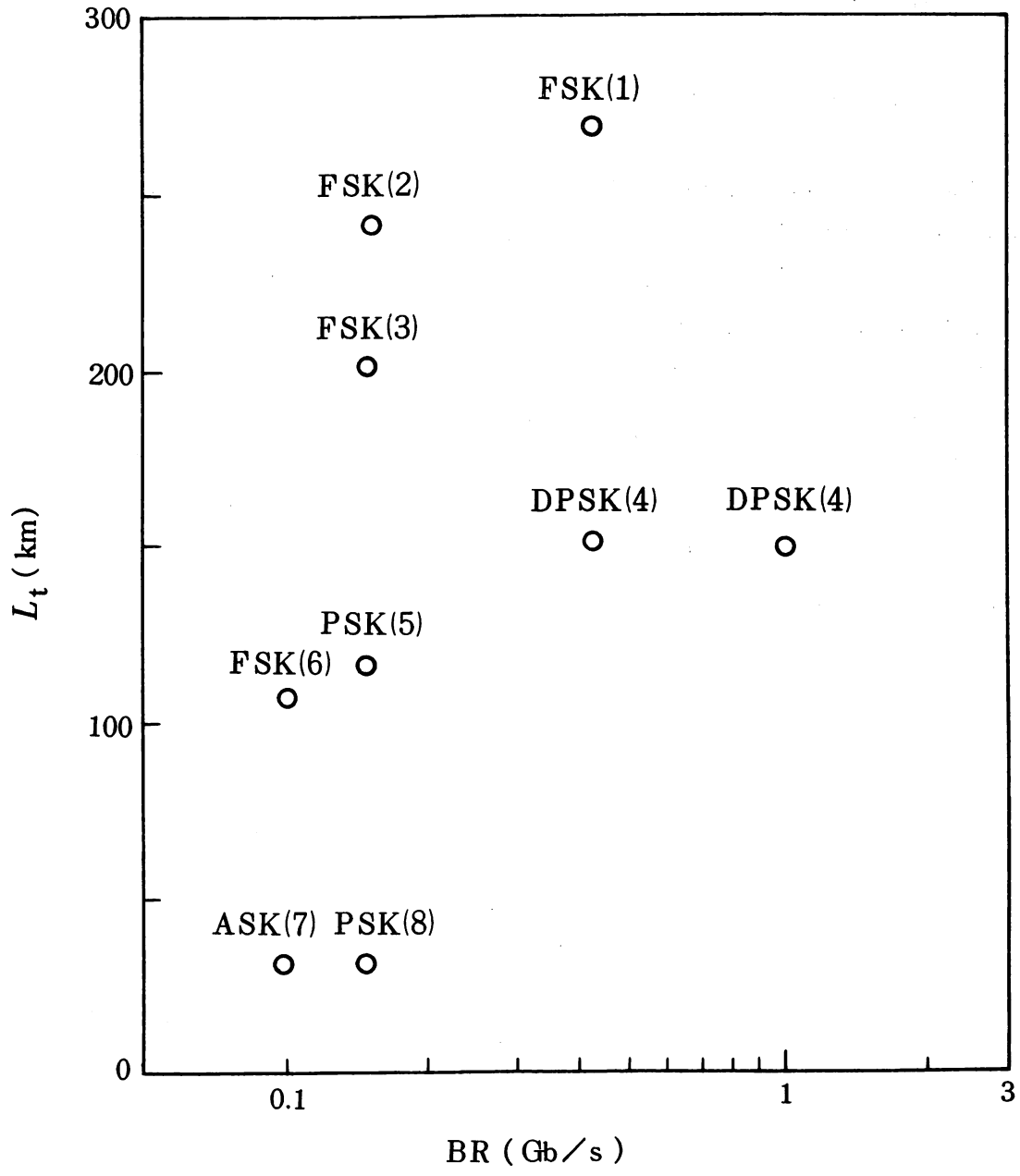

Fig. 38. Summary of recent works on coherent optical transmission. L_t, fiber length; BR, bit rate. (Point 1) IWASHITA, IMAI, MATSUMOTO and MOTOSUGI [1986]; (2) YAMAZAKI, EMURA, SHIKADA, YAMAGUCHI, MITO and MINEMURA [1985], DFB lasers; (3) WYATT, SMITH, HODGKINSON, HARMON and DEVLIN [1984], DCPBH lasers; (4) LINKE, KASPER, OLSSON, ALFERNESS, BUHL and MCCORMIK [1985], BH lasers; (5) WYATT, HODGKINSON and SMITH [1983], He–Ne lasers; (6) EMURA, SHIKADA, FUJITA, MITO, HONMOU and MINEMURA [1984], DFB lasers; (7) SHIKADA, EMURA, FUJITA, KITAMURA, ARAI, KONDO and MINEMURA [1984], DFB lasers; (8) MALYON [1984], He–Ne lasers. (After MATSUMOTO and SHIMADA [1986].)

As shown in fig. 36, higher sensitivity can be expected by using the PSK scheme compared with other modulation schemes; however, phase control of the lightwave has not yet been developed effectively. Although the frequency offset locking technique described in § 4.3.4 is promising for this purpose, more studies are still required. If the PSK scheme is developed effectively, further increases in detection sensitivity can be expected by means of the homodyne detection scheme.

6.3. ATOMIC AND MOLECULAR SPECTROSCOPY

Characteristics and recent progress in infrared lead-chalcogenide lasers have been reviewed by PRIER [1979]. These lasers have been employed for the spectroscopy of fundamental tones of vibration–rotation transitions in gaseous organic molecules (HINKLEY [1970]). Developments in molecular spectroscopy have been reviewed by ENG, BUTLER and LINDEN [1980]. Furthermore, highly sensitive detection of pollutant gases in the atmosphere has been carried out as an application of this spectroscopy. For example, REID, EL-SHERBINY, GARSIDE and BALLIK [1980] have detected nitric oxide molecules of 100 ppt (10^{-10}) concentration in the atmosphere by using a multipath cell. However, further study is required to improve the characteristics of these lasers because of their low operation temperature, low direct modulation speed, and other factors.

In contrast to these lasers, the performances of 0.8 μm AlGaAs lasers and 1.3–1.6 μm InGaAsP lasers, discussed at length in this review, are more advanced in development, and spectroscopy of vibration–rotation transition lines of organic molecules can also be carried out by these lasers.

Spectroscopy studies in the near infrared wavelength region have not yet been completed because of the lack of highly coherent light sources, the low intensities of absorption lines of higher harmonics or combination tones of vibration–rotation transitions, and difficulties in the assignment of many of these absorption lines. However, this spectroscopy has shown considerable progress recently with the help of improvements in the coherence of these semiconductor lasers.

The number of gaseous organic molecules that can be studied by the use of these lasers is large, for example, H_2O, NH_3, CO_2, C_2HD, CH_4, C_4H_2, HCN, D_2, C_2H_2, and others. An example of the experimental results for this spectroscopy is shown in table 4, which lists the wavelengths of absorption lines of H_2O measured by a 0.8 μm AlGaAs laser (FUKUOKA, OHTSU and TAKO [1984]). In this table the center wavelengths of vibration–rotation transition

TABLE 4
Vacuum wavelength of H_2O absorption line in (2, 1, 1) vibration band[a]. (After FUKUOKA, OHTSU and TAKO [1984].)

Assignments $(J_i - J_k)$	λ (pm)	$\bar{\lambda}_x$ (pm)	σ_{n-1} (pm)	n	σ_{n-1}/λ_x
$2_1 - 2_2$	822876.0	822875.517	0.087	15	1.1×10^{-7}
$4_2 - 4_1$	822975.3	822974.79	0.14	10	1.7×10^{-7}
$3_0 - 3_1$	823390.7	823393.47	0.10	7	1.2×10^{-7}
$1_1 - 2_0$	826344.5	826346.408	0.057	12	6.9×10^{-8}
$3_{-3} - 3_0$	827870.8	827870.814	0.046	6	5.5×10^{-8}
$2_0 - 3_{-1}$	828202.7	828202.70	0.10	3	1.2×10^{-7}

[a] Symbols:
J_i, J_k: Rotational quantum numbers of upper and lower levels of the transition, respectively.
λ: Wavelength values reported by Baumann and Mecke [1933].
$\bar{\lambda}_x$: Average wavelength of present measurements.
σ_{n-1}: Standard deviation.
n: Number of data points.

spectral lines of $(v_1, v_2, v_3) = (2, 1, 1)$ vibration band were measured with an inaccuracy of 2×10^{-7}. These results show that accuracy has improved to more than ten times that shown in conventional results, for which grating monochromators were employed in the studies on atmospheric absorption lines of the solar spectrum (BAUMANN and MECKE [1933]).

It was advantageous to try measuring the absorption lines of table 4, since they show larger absorption coefficients when compared with other higher harmonics or combination tones in H_2O. As pointed out by DARLING and DENNISON [1940], these large absorption coefficients result from the resonant interactions of the (2, 1, 1) level with the (0, 1, 3) level. Although the absorption coefficients of other higher harmonics or combination tones are lower, sensitive measurements of these unidentified absorption lines can be carried out by using highly coherent and high-power semiconductor lasers.

In the wavelength region of 1.5 μm, spectroscopy for NH_3 (vibration transition of $2v_1$ or $2v_3$), H_2O (vibration transition of $2v_2 + v_3$), and other gaseous organic molecules have been already carried out, and their wavelengths have been measured with an inaccuracy of 1×10^{-6} (OHTSU, KOTANI and TAGAWA [1983]).

As an application of this spectroscopy, a detection system for the density of these gaseous organic molecules has been developed that uses 1.5 μm InGaAsP lasers and low-loss optical fibers, and a sensitivity of NH_3 detection as high as 3 ppm · m has been obtained (OHTSU, KOTANI and TAGAWA [1983]).

TAKEUCHI, BABA, SAKURAI and UENO [1986] have developed a random modulation continuous-wave (RM–CW) lidar by using a 0.8 μm AlGaAs laser, which is more practical than conventional lidar systems because of its smaller size and the lower consumption of the light source. They have succeeded in carrying out accurate remote sensing of clouds, smoke, snowfall, and spatial aerosol profiles at nighttime.

The 0.8 μm AlGaAs lasers are also tunable to absorption lines in electronic transitions of alkali vapors such as cesium and rubidium. For example, absorption spectroscopy of cesium and rubidium has been carried out by YABUZAKI, IBARAKI, HORI, KITANO and OGAWA [1981] and by OHTSU, HASHIMOTO and OZAWA [1985], respectively. In this technique, measurements can be performed by using a low-pressure vapor because of the large absorption coefficients, which means that Doppler-free saturated absorption lines can also be measured. Figure 39 shows saturated absorption lineshapes

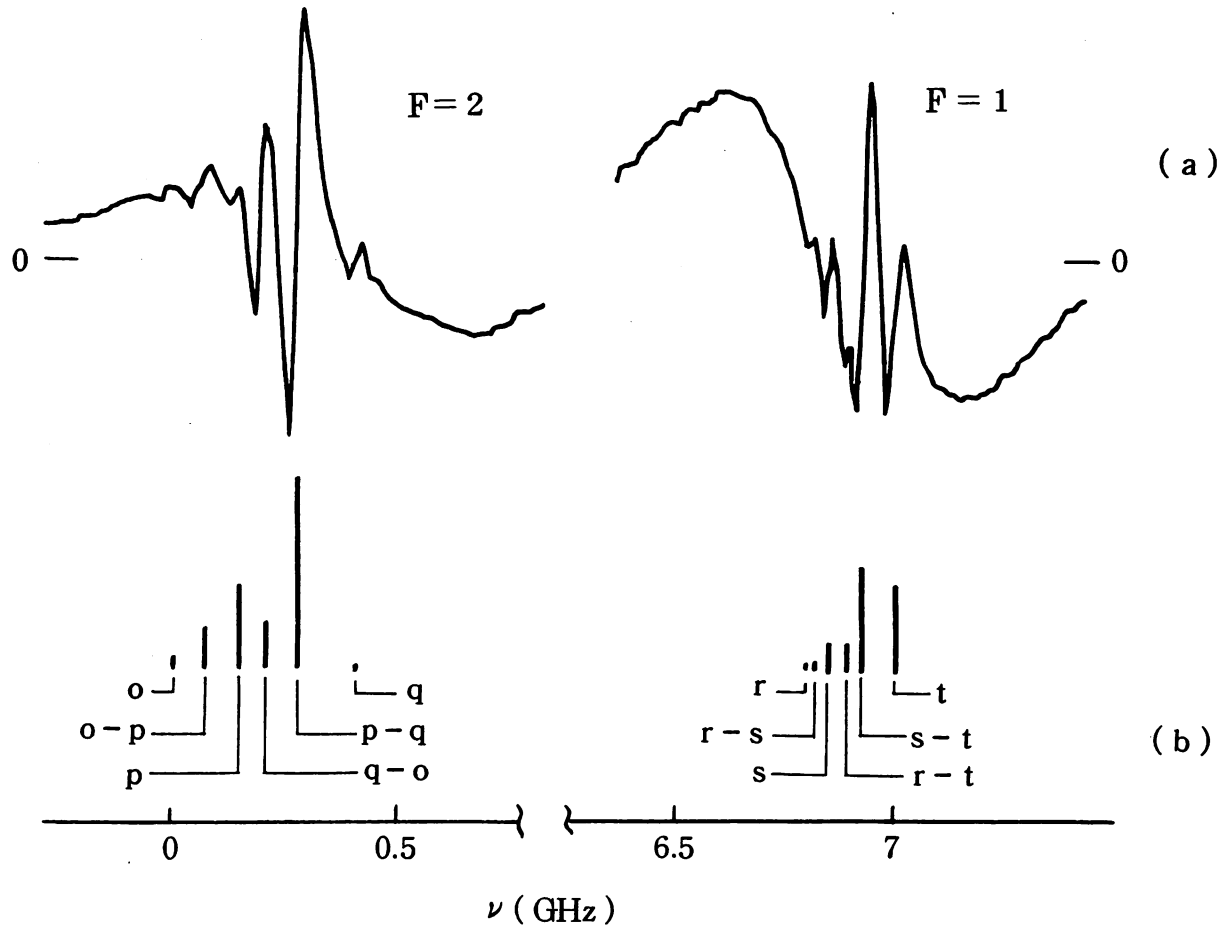

Fig. 39. Derivative of saturated absorption lineshapes in $^{87}Rb–D_2$; ν is the frequency of the laser. (a) Experimental results. (b) Assigned spectral lines. The height of each bar is proportional to the spectral intensity. Relevant energy levels are illustrated in fig. 45. For the transition from the $F = 1$ level of the ground state, two saturated absorption lines (s and t) and three cross-resonance lines (r–s, r–t, and s–t) are observed. For the transition from the $F = 2$ level, three saturated absorption lines (o, p and q) and three cross-resonance lines (o–p, q–o, and p–q) are observed. (After OHTSU, HASHIMOTO and OZAWA [1985].)

in $^{87}Rb-D_2$ (OHTSU, HASHIMOTO and OZAWA [1985]), in which eleven narrow spectral lines, including cross-resonance lines, appear. They have linewidths as narrow as 40 MHz, proving that the linewidth of the semiconductor laser was narrower than these values and its frequency stability was sufficiently high.

These spectral lines can be used as frequency references for frequency stabilization of the semiconductor lasers discussed in 4.3.2. Furthermore, the results from cesium and rubidium can be applied to atomic clocks, which are described in the next subsection.

As a new application of semiconductor lasers to alkali vapor spectroscopy, they can be used to produce Rydberg states of alkali vapor by stepwise excitation, which is shown in fig. 40 for cesium and rubidium. Information about highly excited states can be obtained through the use of this spectroscopy (RINNENBERG [1986]).

In another application coherent semiconductor lasers can be used for laser cooling of alkali atoms. WATTS and WIEMAN [1986] have succeeded in this experiment for a cesium atomic beam, for which a frequency chirp technique was employed with a semiconductor laser so that the decelerated atoms remained in the resonance condition. Since frequency chirp in semiconductor lasers can easily be obtained by modulating their injection current, this technique uses an experimental setup that is simpler than the conventional setup for laser cooling. The atoms were cooled to a temperature of 1 K (limited by the laser linewidth) and had a density of $10^6/cm^3$ (limited by the laser power). Further reduction in temperature and increase in density can be obtained by using narrower linewidths and higher power lasers. This laser cooling technique can be used as a highly stable frequency standard (WINELAND, BERGQUIST, DRULLINGER, HEMMATI, ITANO and WALLS [1981]), for measurements of parity nonconservation (WIEMAN [1986]), and in other advanced experiments on fundamental atomic physics.

6.4. OPTICAL PUMPING IN CESIUM AND RUBIDIUM ATOMIC CLOCKS

An important application of laser spectroscopy of alkali vapors described in the previous subsection, is the optical pumping in cesium and rubidium atomic clocks. Principles of these atomic clocks were briefly described in § 4.1. They utilize the transition frequency between hyperfine structures in the ground state of cesium or rubidium (9.2 GHz and 6.8 GHz, respectively) in order to stabilize the frequency of voltage-controlled crystal oscillators for supplying stable microwave frequency signals. The cesium atomic clock has been used as a primary standard of time. Since the rubidium clock is small in size, it

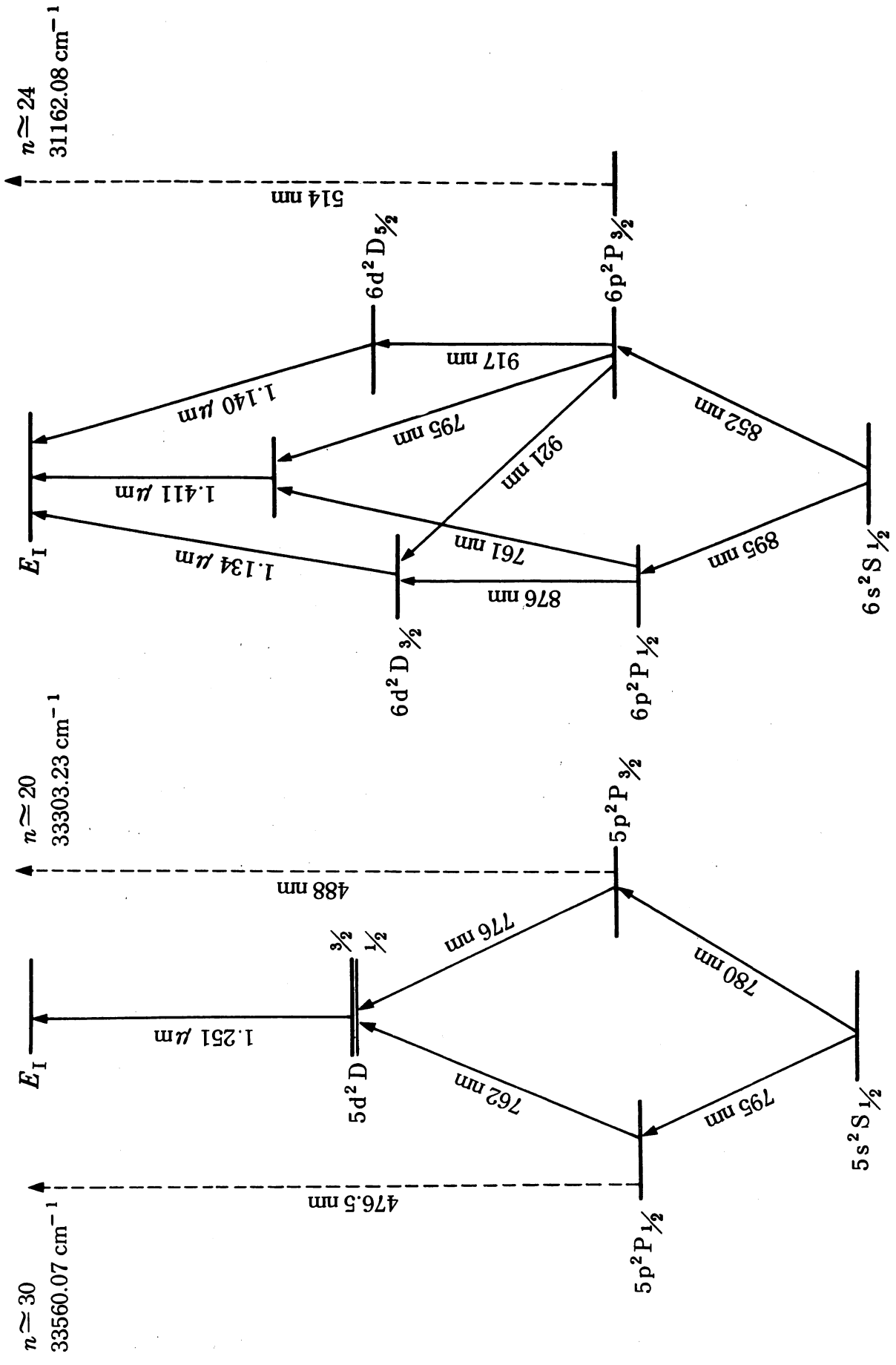

Fig. 40. Stepwise excitations of rubidium (a) and cesium (b) atoms by semiconductor lasers and argon-ion lasers to obtain Rydberg states. E_I is the ionization level.

has been used as a practical stable microwave clock in a wide field of applications such as communication, remote sensing, astronomy and ranging.

Recent recognition that the performance of these clocks can be improved if they are driven by highly coherent semiconductor lasers has stimulated their study in many countries.

6.4.1. *Cesium atomic clocks*

An atomic beam of cesium has been conventionally employed to observe the microwave spectral profile of the transition between hyperfine structures of the cesium ground level. This principle has been thoroughly reviewed by RAMSEY [1956]. The atoms first pass through the state-selection magnet where atoms of two hyperfine levels ($6S_{1/2}$, $F = 4, 3$, $m_F = 0$) are selected by magnetic field deflection, and then are passed through two spatially separated microwave cavity resonators. These microwave perturbations induce transitions between the hyperfine levels, and a narrow-linewidth Ramsey spectral profile can be observed, which is used as the frequency reference for this atomic clock.

However, the efficiency of this state selection is rather low because only one eighth of the total number of atoms are selected. Furthermore, it has been difficult to compensate for the effect of the phase difference between the microwaves in the two cavities, the second-order Doppler effect caused by a slight deflection of cesium beam trajectory due to magnetic field deflection, and other problems. For these reasons it has been estimated that the frequency accuracy of cesium atomic clocks is lower than 1×10^{-13}, and experimental results have approached this theoretical value (LEWIS, WALLS and GLAZE [1981]). Although this value demonstrates a high frequency accuracy, further progress is necessary to improve the performance this of primary standard of time.

It has been pointed out optical pumping is effective for state selection and transition detection in improving performance (KASTLER [1950]), and a proposal has been made to use 852 nm AlGaAs lasers (PICQUE [1977]). In addition, experimental studies have been started by ARDITI [1982].

Figure 41 shows an experimental setup proposed by LEWIS, HOWE, STEIN, MANNEY, MOHLER, BERGQUIST, WINELAND and WALLS [1980] and discussed by BRILLET [1981]. Two semiconductor laser beams are irradiated to the cesium atomic beam in order to pump these atoms optically, that is, to induce the transition of $F = 3 \rightarrow F' = 4$ and $F = 4 \rightarrow F' = 4$ as shown in fig. 42. The transition between $F = 4, m_F = 0 \rightarrow F' = 4, m'_F = 0$ is forbidden if the two laser beams are linearly polarized and the direction of polarization is parallel to that

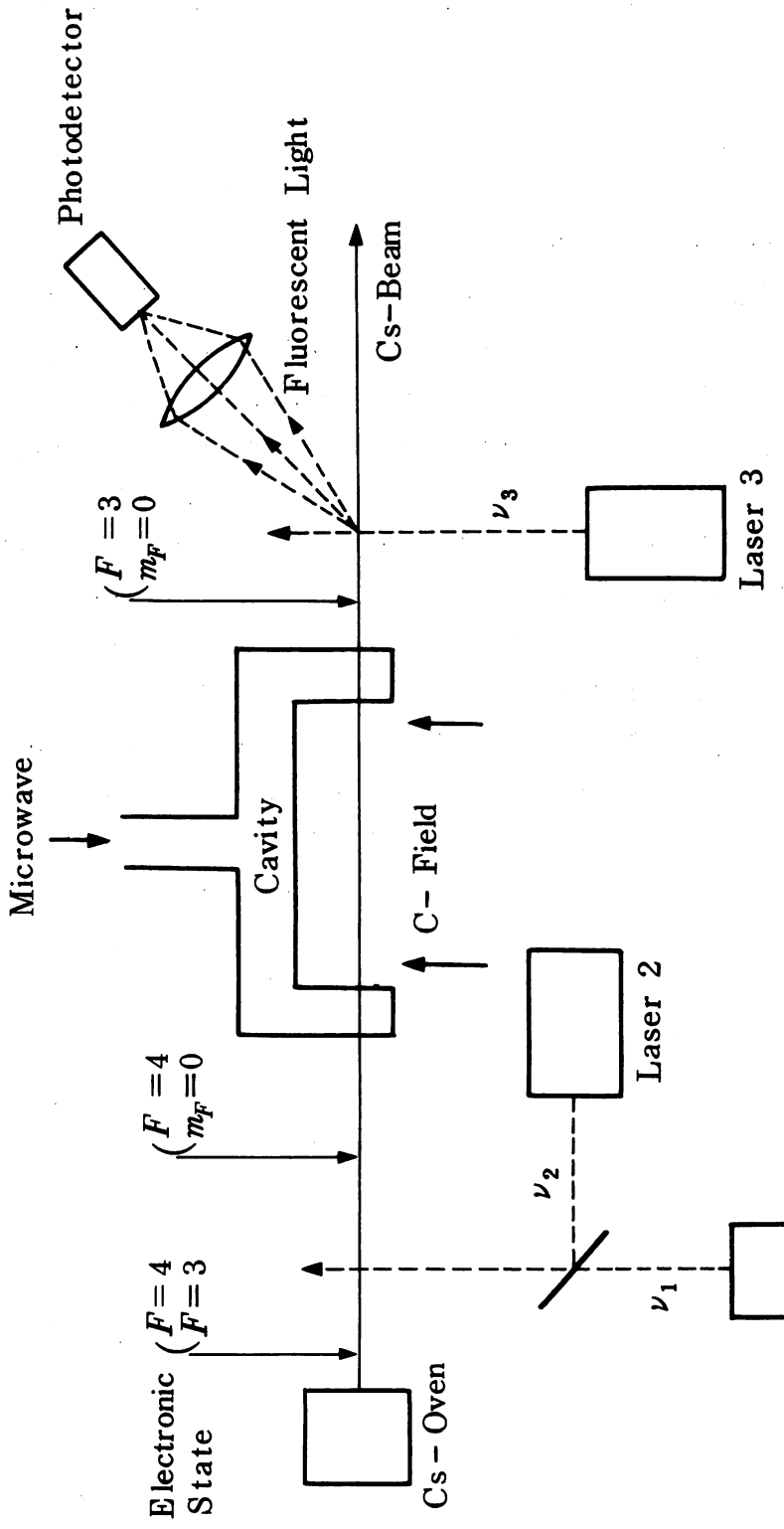

Fig. 41. Experimental setup for optical pumping of a cesium atomic clock. (After LEWIS, HOWE, STEIN, MANNEY, MOHLER, BERGQUIST, WINELAND and WALLS [1980].)

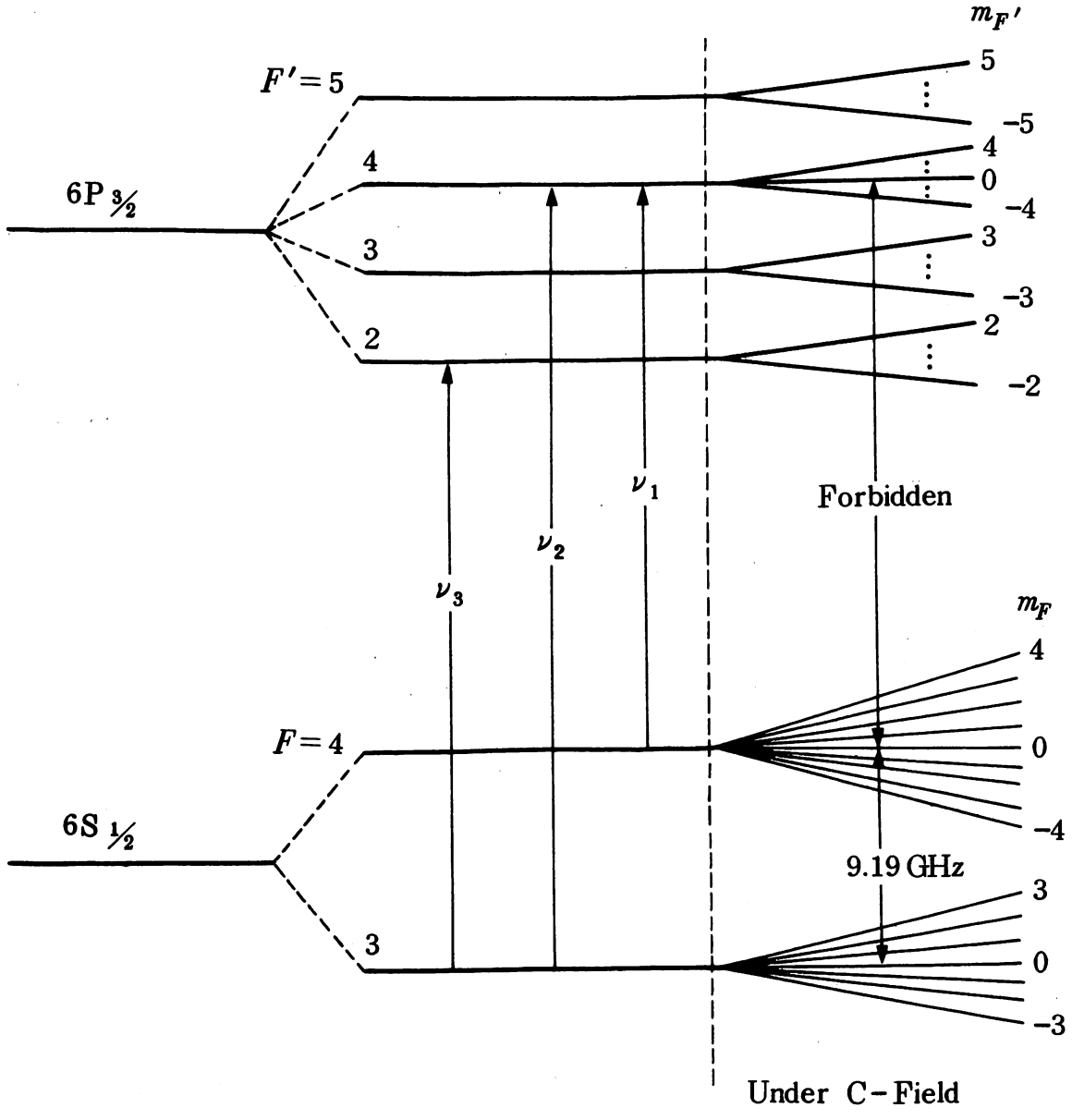

Fig. 42. Energy levels of cesium atoms.

of the C-magnetic field of fig. 41. By utilizing this phenomenon, all the atoms come into the $F = 4$, $m_F = 0$ level by cyclic transition between the ground and excited states due to optical pumping and relaxation. Therefore, all the atoms participate in Ramsey transition, which increases the Ramsey spectral intensity to 8 times larger than that of the conventional state selection by using a magnetic field deflection.

A third semiconductor laser is employed for detecting the Ramsey spectral shape. That is, the atoms of the $F = 3$, $m_F = 0$ level are irradiated by the third laser and are excited to the $F' = 2$ level. The Ramsey spectral shape can be detected by observing the resultant fluorescence from the $F' = 2$ level. Figure 43 shows an example of Ramsey spectral shape measured by this technique

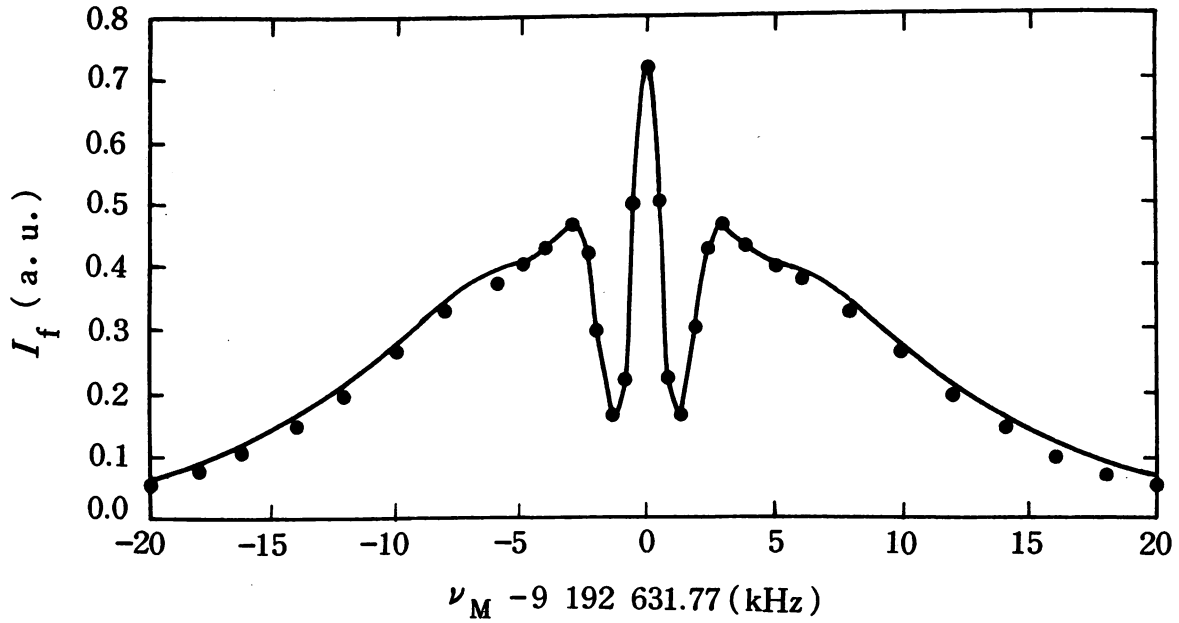

Fig. 43. An example of Ramsey spectral shape in cesium obtained by optical pumping. I_f is the fluorescence intensity, ν_M the microwave frequency. (After DERBYSHIRE, DRULLINGER, FELDMAN, GLAZE, HILLIARD, HOWE, LEWIS, SHIRLEY, PASCARU and STANCIULESCU [1985].)

(DERBYSHIRE, DRULLINGER, FELDMAN, GLAZE, HILLIARD, HOWE, LEWIS, SHIRLEY, PASCARU and STANCIULESCU [1985]).

As just described, state selection and detection by lasers have the following advantages when compared with conventional techniques:

(1) Detection sensitivity is increased because all the atoms are used.

(2) Cesium atomic beam apparatus (fig. 41) can be designed in a bilateral symmetrical shape, which enables beam direction to be reversed easily. By means of this beam reversal the effect of phase difference between the two microwave cavities can be compensated.

(3) The beam reversal can increase the lifetime of the beam source, resulting in an apparatus that is economical to operate.

These properties improve the frequency accuracy of stabilized microwaves of the optically pumped cesium atomic clock in comparison with conventional cesium atomic clocks. The effect of light shift by the pumping light which BRILLET [1981] discussed makes it possible to obtain a frequency accuracy as high as 10^{-14}.

Many countries have begun to develop this promising apparatus for which highly coherent semiconductor lasers are essential. Since a high reliability is required for a practical primary standard of time, high frequency stability and reproducibility are requirements for improving temporal coherence (see § 4).

6.4.2. *Rubidium atomic clocks*

Optical pumping has been employed for rubidium atomic clocks from the initial stage of their development. Incoherent light from a radio-frequency-excited ^{87}Rb lamp and microwaves are irradiated to the ^{87}Rb vapor in order to obtain an optical–microwave double resonance signal, and the center frequency of its spectral line is used as a frequency reference to stabilize the microwave frequency of 6.8 GHz. The progress of these developments has been reviewed by VANIER, KUNSKI, BRISSON and PAULIN [1981].

However, in this technique of microwave frequency stabilization, it has been difficult to evaluate quantitatively the light shift of the microwave frequency and to compensate for this shift because of the broad linewidth of the incoherent pumping light, which has reduced the microwave frequency accuracy to less than 1×10^{-10}. It has also been difficult to improve the short-term stability of the microwave to a level higher than 1×10^{-12} because of the low light intensity from the lamp. Furthermore, the lamp of a satellite-borne rubidium atomic clock is sometimes impaired by bombardment from cosmic rays.

These problems can be overcome if the lamp is replaced with a semiconductor laser. Preliminary experiments that employed a semiconductor laser have been carried out by LEWIS and FELDMAN [1981]. Figure 44 shows the

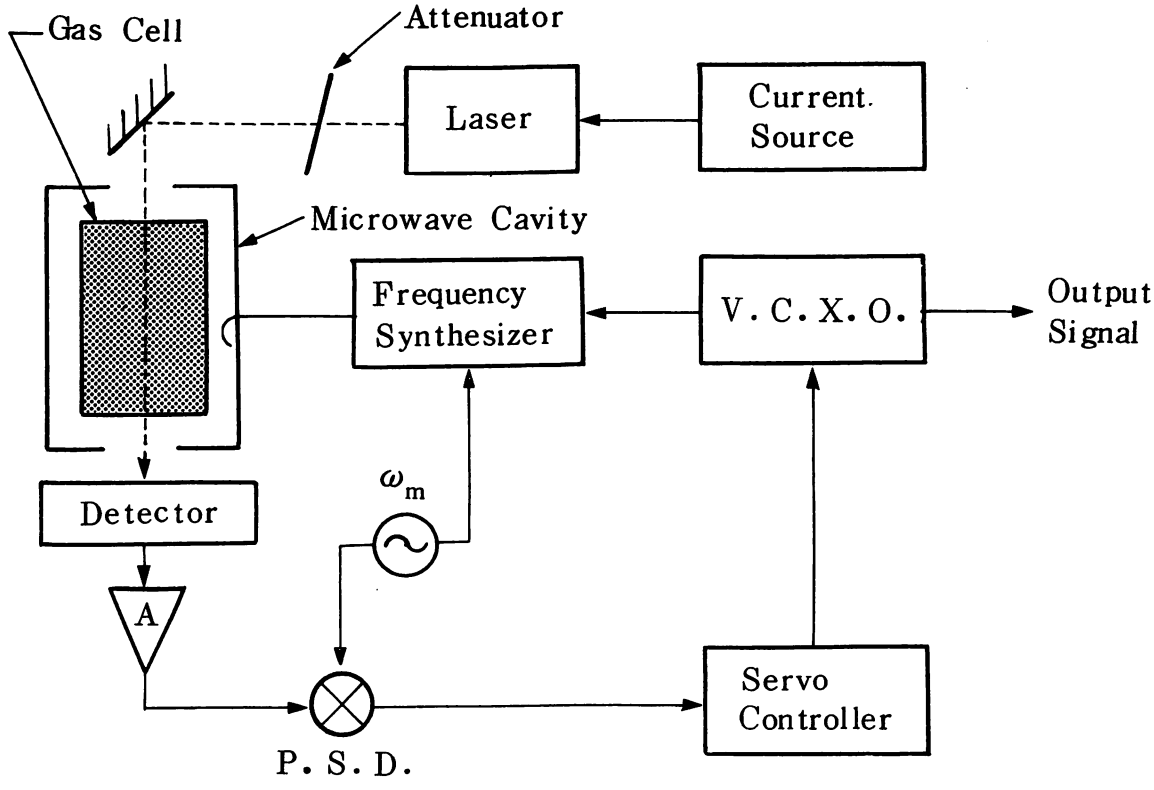

Fig. 44. Experimental setup of a semiconductor laser-pumped rubidium atomic clock. VCXO, voltage-controlled crystal oscillator; PSD, phase-sensitive detector.

experimental setup, and fig. 45 represents the relevant energy levels of rubidium for double resonance. A 780 nm AlGaAs laser is used for optical pumping from the ground state $5S_{1/2}$ to the excited state $5P_{3/2}$ of the ^{87}Rb–D_2 line. Optical–microwave double resonance is induced if a microwave frequency of 6.8 GHz is simultaneously applied. Figure 46 shows the derivative of the double-resonance spectral shape measured by HASHIMOTO and OHTSU [1987]. The signal-to-noise ratio of the double-resonance signal detection was larger than 60 dB, and further improvements of the short-term frequency stability can be expected by using this double-resonance signal as a frequency reference.

Furthermore, the narrow-linewidth lightwave from the semiconductor laser allows quantitative evaluation of the light shift, that is, the shift of the center frequency of the double-resonance spectral shape induced by variations of frequency and power of the semiconductor laser. Figure 47 shows the magni-

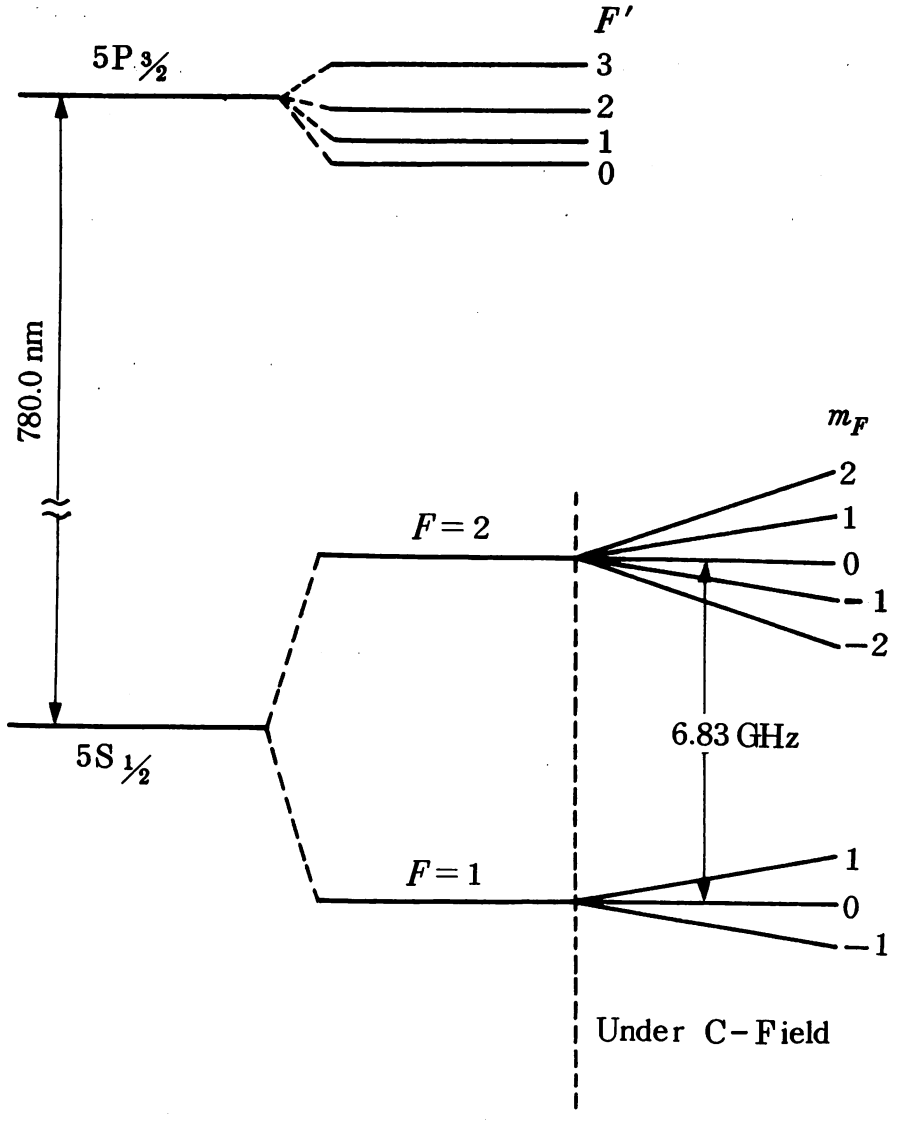

Fig. 45. Energy levels of rubidium atoms.

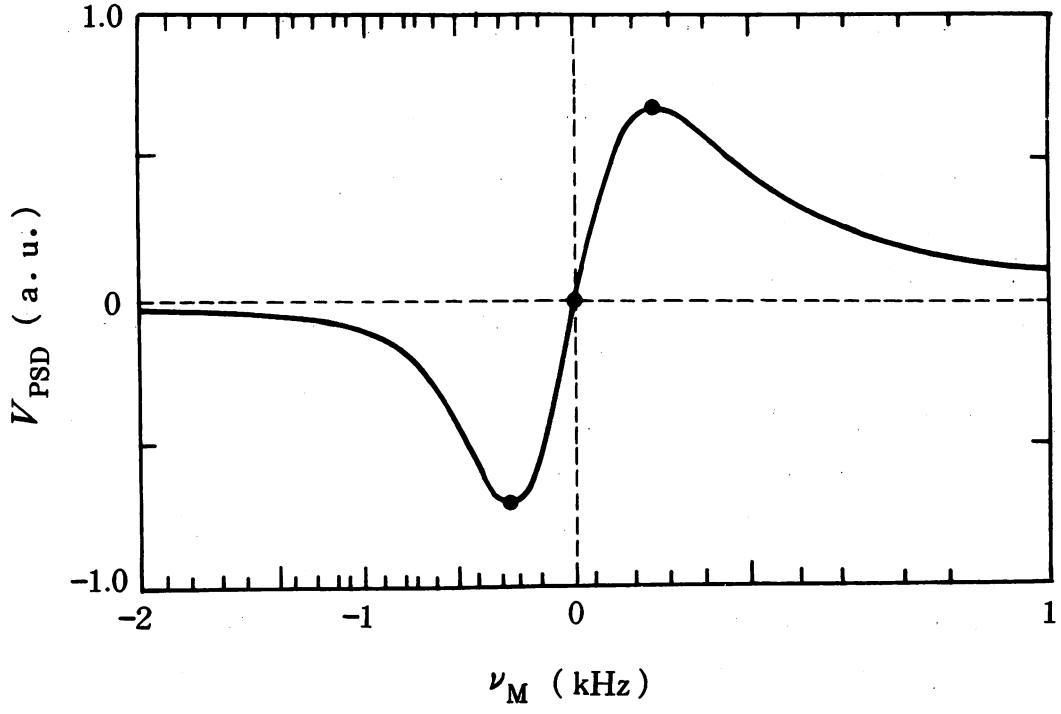

Fig. 46. An example of the derivative of the double-resonance spectral shape obtained by using an AlGaAs laser as a pumping source. V_{PSD} is the output voltage from the phase-sensitive detector (PSD) of fig. 44, ν_M the microwave frequency. (After HASHIMOTO and OHTSU [1987].)

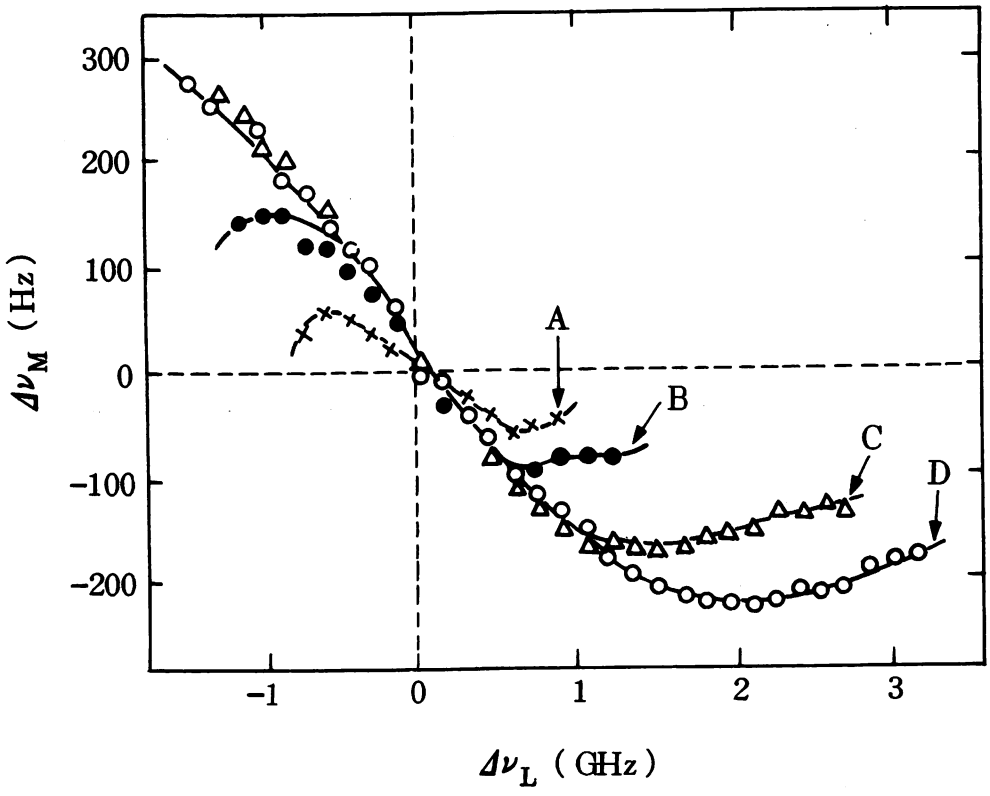

Fig. 47. Magnitude of the light shift of the microwave frequency $\Delta\nu_M$ as a function of laser frequency detuning $\Delta\nu_L$; laser power densities: (curve A) 43 μW/cm², (B) 79.2, (C) 288, (D) 562. (After HASHIMOTO and OHTSU [1987].)

tude of the light shift measured by HASHIMOTO and OHTSU [1987]. Each curve in this figure exhibits a typical dispersive shape, which is consistent with the theoretical prediction given by VANIER, KUNSKI, BRISSON and PAULIN [1981]. These results can be used as basic data to compensate for the effect of light shift induced by variations of frequency and power of the semiconductor laser and present the possibility of using the rubidium atomic clock not only as a practical secondary standard of time but also as a primary standard of time.

Since recently available semiconductor lasers have a lifetime as long as 1×10^7 hours (100 years) (IMAI, HORI, TAKUSAGAWA and WAKITA [1981]) and are little impaired by bombardment from cosmic rays, higher reliability can be expected than when a conventional ^{87}Rb lamp is used. Therefore, compact and highly reliable rubidium atomic clocks are possible that can be used as a highly stable microwave oscillator for communication, a global positioning system (GPS), precise measurements, and for other applications.

It should be pointed out that such a reliable rubidium atomic clock can be obtained by utilizing high frequency stability and reproducibility in semiconductor lasers, as was the case for cesium atomic clocks.

At the end of this subsection a new detection scheme for a double-resonance signals is demonstrated, which is obtained by means of the high temporal coherence of the pumping light source. Figure 48a shows an example of the derivative of a double-resonance spectral shape measured by the new detection scheme of HASHIMOTO and OHTSU [1987]. A spectral shape with a very

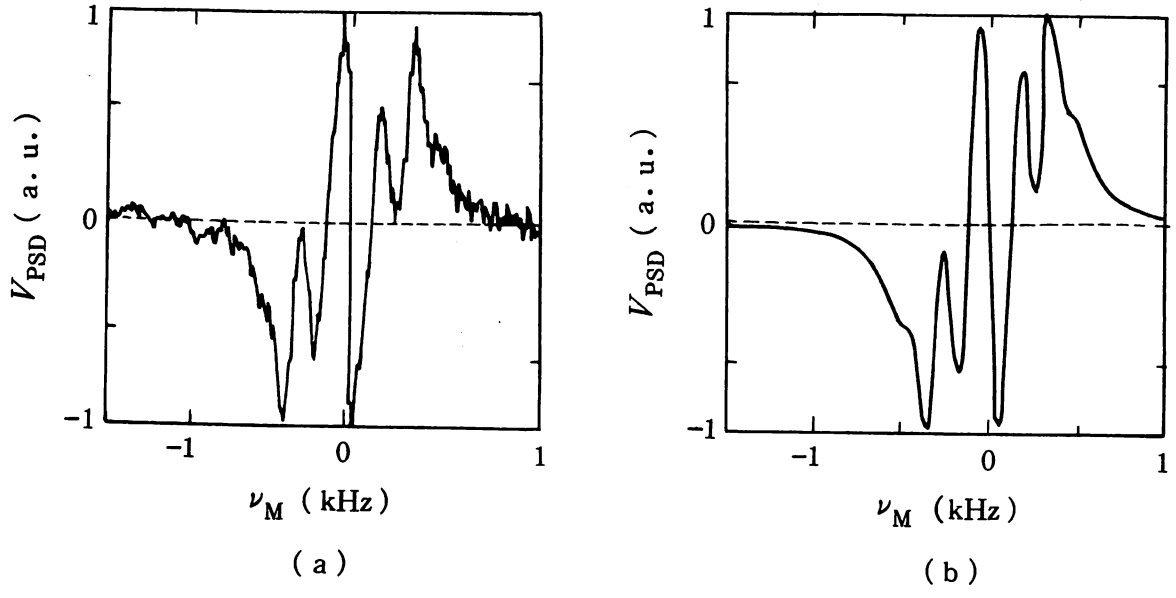

Fig. 48. Derivative of double-resonance spectral shape measured by a new detection scheme of utilizing frequency-modulated sidebands of the laser: (a) experimental result; (b) calculated result. (After HASHIMOTO and OHTSU [1987].)

narrow linewidth is observed at the center of the spectral shape. It was measured by appropriate adjustment of the phase angle of the phase-sensitive detector used to amplify the output signal from the photodetector of fig. 44. The sensitivity of microwave frequency discrimination will increase if the large slope of the center of this narrow spectral shape is used as a frequency discriminator, which will significantly improve the short-term stability of the microwave frequency.

This narrow-linewidth spectral shape was obtained by utilizing the high temporal coherence of the pumping light source. The principle of this detection is somewhat similar to that of the frequency-modulated laser spectroscopy proposed by BJORKLUND [1980], and can be explained as follows: the microwave frequency is modulated with a low modulation frequency in order to enable phase-sensitive detection. This frequency modulation induces a modulation of the complex susceptibility of three-level ^{87}Rb atoms to the electric field of the light. Through this induced modulation, the phase and amplitude of the electric field of the light will be simultaneously modulated when it is transmitted through the ^{87}Rb vapor. As a result, upper and lower sidebands are generated in the field spectrum of the laser. These sidebands, as well as the optical carrier component, have high temporal coherence and work as a multifrequency light source for optical pumping of ^{87}Rb atoms. The double-resonance spectral shape is observed under these optical pumping conditions by sweeping the microwave frequency and by employing phase-sensitive detection. The output signal from the phase-sensitive detector therefore comprises the amplitudes of the heterodyned signal between the adjacent sidebands and optical carrier component, which is expressed as

$$V_{\mathrm{PSD}} = V_{\mathrm{o}}(\tfrac{1}{2}B\cos\theta + \tfrac{1}{2}C\sin\theta)\,, \tag{6.6}$$

where V_{o} is a constant proportional to the laser power incident on the ^{87}Rb vapor and θ is the phase angle for phase-sensitive detection, that is, the phase difference between the microwave frequency modulation and the modulated output signal from the photodetector. As shown in fig. 49, the in-phase component B in this equation is proportional to the first derivative of the imaginary part of the complex susceptibility, that is, the amplitude attenuation of the electric field of the light due to the absorption by ^{87}Rb. The quadrature component C is proportional to the second derivative of its real part, namely, that of the phase shift of the electric field of light. Appropriate adjustment of the phase angle θ will give the lineshape that corresponds to fig. 48a. Since the signs of the slope of the curves B and C in fig. 49 are opposite each other, their sum in eq. (6.6) will exhibit a large slope and narrow linewidth.

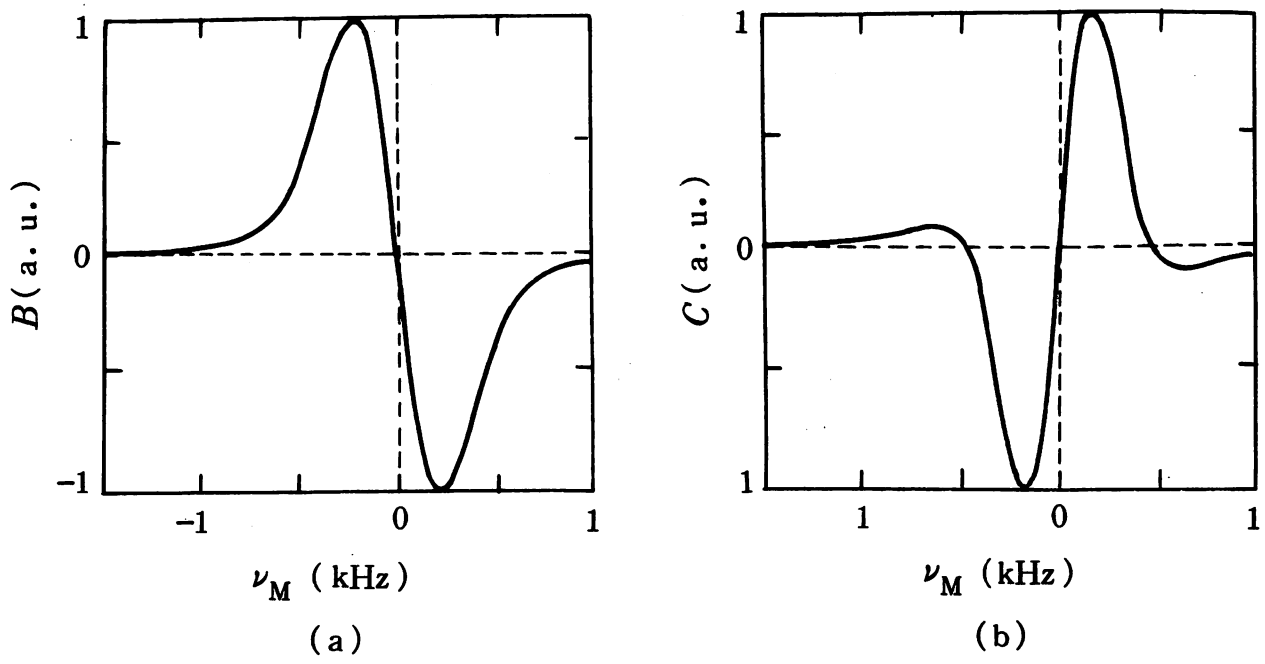

Fig. 49. Calculated result of the lineshape of components (a) B and (b) C in eq. (6.6). (After HASHIMOTO and OHTSU [1987].)

The curves in fig. 49 are the result of a detailed calculation based on the density matrix formulation of the three-level atoms (HASHIMOTO and OHTSU [1987]). Figure 48b shows the result of the calculation obtained by using the results of fig. 49 and eq. (6.6). The two curves in fig. 48a and b agree with each other, thus proving the validity of the present discussion. As noted earlier, this detection scheme utilized the modulation transfer from the microwave to the lightwave by means of nonlinear complex susceptibility of the three-level atoms. This transfer has not been observed in conventional ^{87}Rb atomic clocks because coherent light has not been used so far. In conventional ^{87}Rb atomic clocks the lineshape is proportional only to the derivative of laser power absorption, irrespective of the phase angle of the phase-sensitive detection, as shown in fig. 46.

In fig. 48a the minimum linewidth of the center part of the spectral shape was 20 Hz, which is $\frac{1}{25}$ times that of the curve in fig. 46. Reasonably high stability can be expected if such a narrow linewidth, or in other words, large slope, is used as a frequency discriminator.

Inert gases have been employed as buffer gases to reduce the linewidth in conventional ^{87}Rb atomic clocks. Recent developments that employ buffer gases have been reviewed by VANIER, KUNSKI, BRISSON and PAULIN [1981], and the minimum linewidth obtained by this narrowing scheme is several hundred hertz. No significant progress has been made for 30 years in attempts to reduce this linewidth. However, a fairly narrow linewidth, as shown in fig. 48a was obtained recently by using a semiconductor laser. This is the first

successful example of the application of a highly coherent semiconductor laser, and it will have a considerable impact on the design of highly stable microwave oscillators.

§ 7. Summary

Theoretical backgrounds and experimental results on temporal coherence in semiconductor lasers have been described in this chapter. Techniques to improve coherence and applications to the field of optics have also been reviewed. It should be pointed out that the presently available semiconductor lasers still have a primitive structure for obtaining high temporal coherence. Improvements in coherence will require the fabrication of more sophisticated lasers, which are to be connected with external electronic and optical components. Furthermore, reproducibility and reliability of semiconductor lasers also need improvement at the stage of laser fabrication.

Close cooperation between device fabrication and system design is essential in order to obtain extremely high temporal coherence. In addition, developments of external optical components, such as high-performance optical isolators, optical fibers, fiber couplers, and opto-electronic integrated circuits (OEIC), are required to support efforts to improve coherence. Ultrahigh coherence in semiconductor lasers will be achieved under these conditions, thus giving new applications and impact to optics.

Appendix

The definitions in the present review of frequency stability, reproducibility, and accuracy of quantum oscillators follow those given by BEEHLER, MOCKLER and RICHARDSON [1965] and BEEHLER and GLASE [1966]:

Stability: A sequence of N readings of a particular oscillator frequency in a particular adjustment, against a reference oscillator assumed temporally constant, will show fluctuations. The standard deviation of these observations is called the stability.

Reproducibility: A sequence of comparisons for independent adjustments of a particular oscillator frequency, against a reference oscillator frequency available and temporally constant, will yield a standard deviation. The standard deviation of such observations is called the reproducibility. In this sense, reproducibility indicates the degree of resettability of the frequency.

Accuracy: Accuracy means the fractional uncertainty in determining an atomic transition frequency of the free atom and is expressed by 3σ limits for statistically determined frequencies.

References

ABE, Y., K. KISHINO, Y. SUEMATSU and S. ARAI, 1981, Electron. Lett. **17**, 945.
AIKI, K., M. NAKAMURA, J. UMEDA, A. YARIV, A. KATZIR and H.W. YEN, 1975, Appl. Phys. Lett. **27**, 145.
ALFEROV, ZH.I., V.M. ANDREEV, E.L. PORTNOI and M.K. TRUKHAN, 1969, Fiz. Tekh. Poluprovodn. **3**, 1328 [1970, Sov. Phys.-Semicond. **3**, 1107].
ALLAN, D., 1966, Proc. IEEE **54**, 221.
ARDITI, M., 1982, Metrologia **18**, 59.
ARIMOTO, A., M. OJIMA and K. TATSUNO, 1982, J. Opt. **11**, 629 (in Japanese).
ARIMOTO, A., M. OJIMA, N. CHINONE and A. OISHI, 1984, Technical Digest of Conference on Lasers and Electro-Optics TUD2 (Anaheim, CA, USA).
ARNOWITZ, F., and F.J. COLLINS, 1970, J. Appl. Phys. **41**, 130.
BARNES, J.A., A.R. CHI, L.S. CUTLER, D.J. HEALELY, D.B. LEESON, T.E. MCGUNIGAL, J.A. MULLEN JR, W.L. SMITH, R.L. SYDNOR, R.F.C. VESSOT and G.M.R. WINKLER, 1971, IEEE Trans. Instrum. & Meas. **IM-20**, 105.
BAUMANN, W., and R. MECKE, 1933, Z. Phys. **81**, 445.
BEEHLER, R.E., and D.J. GLAZE, 1966, IEEE Trans. Instrum. & Meas. **IM-15**, 1966.
BEEHLER, R.E., R.C. MOCKLER and J.M. RICHARDSON, 1965, Metrologia **1**, 114.
BERGH, R.A., B. CULSHAW, C.C. CUTLER, H.C. LEFEVRE and H.J. SHAW, 1982, Opt. Lett. **7**, 563.
BJORKLUND, G.C., 1980, Opt. Lett. **5**, 15.
BLAQUIERE, A., 1962, Compt. Rend. **26**, 2929.
BRILLET, A., 1981, Metrologia **17**, 147.
BRILLET, A., and P. CEREZ, 1981, J. Phys. (France) **42**, C8-73.
BROOM, R.F., E. MOHN, C. RISCH and R. SALATHE, 1970, IEEE J. Quantum Electron. **QE-6**, 328.
CAMERON, K.H., M.R. MATTHEWS, T.G. HODGKINSON and W.J. DEVLIN, 1985, Technical Digest of Conference on Lasers and Electro-Optics, TUC5 (Baltimore, MD, USA).
CHINONE, N., M. OJIMA and M. NAKAMURA, 1983, Nikkei Electronics (October 10) p. 173 (in Japanese).
CHINONE, N., T. KURODA, T. OHTOSHI, T. TAKAHASHI and T. KAJIMURA, 1985, IEEE J. Quantum Electron. **QE-21**, 1264.
COPELAND, J.A., 1980, IEEE J. Quantum Electron. **QE-16**, 721.
CUTLER, C.C., S.A. NEWTON and H.J. SHAW, 1980, Opt. Lett. **5**, 488.
DARLING, B.T., and D.M. DENNISON, 1940, Phys. Rev. **45**, 128.
DERBYSHIRE, A., R.E. DRULLINGER, M. FELDMAN, D.J. GLAZE, D. HILLIARD, D.A. HOWE, L.L. LEWIS, J.H. SHIRLEY, I. PASCARU and D. STANCIULESCU, 1985, Proc. 39th Annual Symposium on Frequency Control (Philadelphia, PA, USA) p. 18.
DOI, A., N. CHINONE, K. AIKI and R. ITO, 1979, Appl. Phys. Lett. **34**, 393.
DURNST, F., A. MELLING and J.H. WHITSLAW, 1976, Principles and Practice of Laser–Doppler Anemometry (Academic Press, New York).
ELSÄSSER, W., E.O. GÖBEL and J. KUHL, 1983, IEEE J. Quantum Electron. **QE-19**, 981.
EMURA, K., M. SHIKADA, S. FUJITA, I. MITO, H. HONMOU and K. MINEMURA, 1984, Electron. Lett. **20**, 1022.
ENG, R.S., J.F. BUTLER and K.J. LINDEN, 1980, Opt. Eng. **19**, 945.
EZEKIEL, S., and H.J. ARDITTY, 1982, Fiber-Optic Rotation Sensor and Related Technologies (Springer, Berlin).
FAVRE, F., and D. LE GUEN, 1983a, Electron. Lett. **19**, 663.
FAVRE, F., and D. LE GUEN, 1983b, Proc. Int. Conf. on Lasers (San Francisco, CA, USA, 1983) p. 79.

FAVRE, F., D. LE GUEN and J.C. SIMON, 1982, IEEE J. Quantum Electron. **QE-18**, 1712.
FLEMING, M.F., and A. MOORADIAN, 1981, IEEE J. Quantum Electron. **QE-17**, 44.
FREED, C., W. BIELINSKI, W. LO and D.L. PARTIN, 1984, 13th Int. Quantum Electronics Conf., ThEE3, p. 130.
FUJITA, T., J. OHYA, K. MATSUDA, M. ISHINO, H. SATO and H. SERIZAWA, 1985, Electron. Lett. **21**, 374.
FUKUOKA, K., M. OHTSU and T. TAKO, 1984, Jpn. J. Appl. Phys. **23**, L117.
GOODWIN, F.E., 1967, IEEE J. Quantum Electron. **QE-16**, 1251.
GORDON, J.P., 1962, Proc. IRE **50**, 1898.
HALL, J.L., and C.J. BORDE, 1973, Phys. Rev. Lett. **30**, 1101.
HALL, J.L., C. SALAMON and D. HILS, 1986, Proc. 14th Int. Quantum Electronics Conf., TuII1 (San Francisco, CA, USA).
HALL, R.N., G.H. FENNER, J.D. KINGSLEY, T.J. SOLTYS and R.D. CARLSON, 1962, Phys. Rev. Lett. **9**, 366.
HASHIMOTO, M., and M. OHTSU, 1987, IEEE J. Quantum Electron. **QE-23**, 446.
HAUG, H., 1969, Phys. Rev. **184**, 338.
HAUG, H., and H. HAKEN, 1967, Z. Phys. **204**, 262.
HAYASHI, I., M.B. PANISH, P.W. FOY and A. SUMSKI, 1970, Appl. Phys. Lett. **17**, 109.
HAYASHI, I., K. MATSUI, M. TANETANI, S. YAMAMOTO, M. YANO and T. HIJIKATA, 1984, National Convention Records, Jpn. Soc. Appl. Phys. 29pM4 (in Japanese).
HENRY, C.H., 1982, IEEE J. Quantum Electron. **QE-18**, 259.
HINKLEY, E.D., 1970, Appl. Phys. Lett. **16**, 351.
HIOE, F.T., and S. SINGH, 1981, Phys. Rev. A **24**, 2050.
HIROTA, O., and Y. SUEMATSU, 1982, IEEE J. Quantum Electron. **QE-15**, 142.
HOLONYAK JR, N., and S.F. BEVANCQUA, 1962, Appl. Phys. Lett. **1**, 82.
HOLONYAK JR, N., R.M. KOLBAS, R.D. DUPIUS and P.D. DAPKUS, 1980, IEEE J. Quantum Electron. **QE-16**, 170.
IKEDA, K., 1979, Opt. Commun. **30**, 257.
IKEGAMI, T., and Y. SUEMATSU, 1967, Proc. IEEE **55**, 122.
IMAI, H., K. HORI, M. TAKUSAGAWA and K. WAKITA, 1981, J. Appl. Phys. **52**, 3167.
IWASHITA, K., T. IMAI, T. MATSUMOTO and G. MOTOSUGI, 1986, Electron. Lett., to be published.
JACOBSEN, G., H. OLESEN and F. BIRKEDAHL, 1982, Electron. Lett. **18**, 874.
KANAMORI, H., 1977, J. Geophys. Res. **82**, 2981.
KARTASCHOFF, P., 1978, Frequency and Time (Academic Press, London).
KASTLER, A., 1950, J. Phys. Radium **11**, 255.
KAWAGUCHI, H., and K. OTSUKA, 1984, Appl. Phys. Lett. **45**, 934.
KAWANISHI, H., Y. SUEMATSU, K. UTAKA, Y. ITAYA and S. ARAI, 1979, IEEE J. Quantum Electron. **QE-15**, 701.
KAZOVSKY, L.G., 1985, Proc. Conf. on Lasers and Electro-Optics, TUC4 (Baltimore, MD, USA).
KIKUCHI, K., and T. OKOSHI, 1985, IEEE J. Quantum Electron. **QE-21**, 669.
KOBAYASHI, K., 1976, Trans. IECE Jpn. E **59**, 8.
KOBAYASHI, K., I. HINO and T. SUZUKI, 1984, 15th Conf. on Solid State Devices and Materials, LD-6-1 (Kobe, Japan).
KOBAYASHI, S., and T. KIMURA, 1981, IEEE J. Quantum Electron. **QE-17**, 1515.
KOBAYASHI, S., and T. KIMURA, 1982, IEEE J. Quantum Electron. **QE-18**, 575.
KOBAYASHI, S., Y. YAMAMOTO, M. ITO and T. KIMURA, 1982, IEEE J. Quantum Electron. **QE-18**, 582.
KOGELNIK, H., and C.V. SHANK, 1971, Appl. Phys. Lett. **18**, 152.
KUBOKI, K., and M. OHTSU, 1987, IEEE J. Quantum Electron. **QE-23**, 388.
KUBOKI, K., T. KATO and M. OHTSU, 1986, Extended Abstracts, 47th Autumn Meeting, Jpn. Soc. Appl. Phys. (in Japanese).

LAMB JR, W.E., 1964, Phys. Rev. **134**, A1429.
LANG, R., 1982, IEEE J. Quantum Electron. **QE-18**, 976.
LANG, R., and K. KOBAYASHI, 1980, IEEE J. Quantum Electron. **QE-16**, 347.
LETT, P., W. CHRISTIAN, S. SINGH and L. MANDEL, 1981, Phys. Rev. Lett. **47**, 1982.
LEWIS, L.L., and M. FELDMAN, 1981, Proc. 35th Annual Symposium on Frequency Control (Ft. Monmouth, NJ, USA) p. 612.
LEWIS, L.L., D.A. HOWE, S.R. STEIN, C. MANNEY, M. MOHLER, J.C. BERGQUIST, D.J. WINELAND and D.F. WALLS, 1980, Abstracts Conf. on Precision Electromagnetic Measurements (CPEM1980) (IEEE, Catalognumber 80CH1497-71M) p. 129.
LEWIS, L.L., F.L. WALLS and D.J. GLAZE, 1981, J. Phys. Colloque **C-8**, Suppl. au no. 12, C8-241.
LINKE, R.A., B.L. KASPER, N.A. OLSSON, R.C. ALFERNESS, L.L. BUHL and A.R. MCCORMIK, 1985, Technical Digest, 5th Int. Conf. on Integrated Optics and Optical Communication/11th European Conf. on Optical Communication, Vol. III (Venice, Italy) p. 35.
MALYON, D.J., 1984, Electron. Lett. **20**, 281.
MARCUSE, D., 1985, IEEE J. Quantum Electron. **QE-20**, 1139.
MATSUMOTO, T., and S. SHIMADA, 1986, Proc. Conf. on Lasers and Electro-Optics, THJ2 (San Francisco, CA, USA).
MATSUOKA, T., H. NAGAI, Y. ITAYA, Y. NOGUCHI, U. SUZUKI and T. IKEGAMI, 1982, Electron. Lett. **18**, 27.
MAYER, R.E., S. EZEKIEL, D.W. STOWE and V.J. TEKIPPE, 1983, Opt. Lett. **8**, 644.
MERZ, J.L., J. VAN DER ZIEL and R.A. LOGAN, 1979, Phys. Rev. B **20**, 654.
MILES, R.O., A. DANDRIDGE, A.B. TVETEN, H.F. TAYLOR and T.G. GIALLORENZI, 1980, Appl. Phys. Lett. **37**, 990.
MIYA, T., Y. TERUMURA, T. HOSAKA and T. MIYASHITA, 1979, Electron. Lett. **15**, 4.
NAKAMURA, M., K. AIKI, N. CHINONE, R. ITO and J. UMEDA, 1978, J. Appl. Phys. **49**, 4644.
NAMIZAKI, H., H. KAN, M. ISHII and O. ITO, 1974, J. Appl. Phys. **45**, 2785.
NATHAN, M.I., W.P. DUMKE, G. BURNS, F.H. DILL and G. LASHER, 1962, Appl. Phys. Lett. **1**, 62.
OHTSU, M., 1985a, Proc. Technical Group Meeting, IECE Japan, QOE85-123 (in Japanese).
OHTSU, M., 1985b, Physics **6**, 297 (in Japanese).
OHTSU, M., and S. ARAKI, 1987, Appl. Opt. **26**, 464.
OHTSU, M., and S. KOTAJIMA, 1984, Jpn. J. Appl. Phys. **23**, 760.
OHTSU, M., and S. KOTAJIMA, 1985a, IEEE J. Quantum Electron. **QE-21**, 1905.
OHTSU, M., and S. KOTAJIMA, 1985b, Jpn. J. Appl. Phys. **24**, L256.
OHTSU, M., and Y. OTSUKA, 1983, Proc. Technical Group Meeting, IECE Japan, OQE83-61 (in Japanese).
OHTSU, M., S. KATSURAGI and T. TAKO, 1981, IEEE J. Quantum Electron. **QE-17**, 1100.
OHTSU, M., H. KOTANI and H. TAGAWA, 1983, Jpn. J. Appl. Phys. **22**, 1553.
OHTSU, M., H. FUKADA, T. TAKO and H. TSUCHIDA, 1983, Jpn. J. Appl. Phys. **22**, 1157.
OHTSU, M., Y. OTSUKA and Y. TERAMACHI, 1985, Appl. Phys. Lett. **46**, 108.
OHTSU, M., M. HASHIMOTO and H. OZAWA, 1985, Proc. 39th Annual Symposium on Frequency Control (Philadelphia, PA, USA) p. 43.
OHTSU, M., Y. TERAMACHI, Y. OTSUKA and A. OSAKI, 1986, IEEE J. Quantum Electron. **QE-22**, 535.
OHTSU, M., Y. TERAMACHI and T. MIYAZAKI, 1987, Opt. Commun. **61**, 203.
OKAZAKI, H., M. OHTSU and T. TAKO, 1984, Trans. IECE Japan, J67-C, 651 (in Japanese).
OKAZAKI, S., and T. SAKAI, 1981, Publ. Astron. Soc. Jpn. **33**, 197.
OKOSHI, T., 1982, J. IECE Jpn **65**, 1099.
OKOSHI, T., and K. KIKUCHI, 1981, J. Opt. Commun. **2**, 82.
OKOSHI, T., K. EMURA, K. KIKUCHI and R.TH. KERSTEN, 1981, J. Opt. Commun. **2**, 89.
PICQUE, J.L., 1977, Metrologia **13**, 115.

POST, E.J., 1967, Rev. Mod. Phys. **39**, 475.
PRIER, H., 1979, Appl. Phys. **20**, 189.
QUIST, M., R.H. REDIKER, R.J. KEYES, W.E. KRAG, B. LAX, A.L. MCWHORTER and H.J. ZEIGER, 1962, Appl. Phys. Lett. **1**, 91.
RAMSEY, N.F., 1956, Molecular Beams (Oxford University Press).
REID, J., M. EL-SEBINY, B.K. GARSIDE and E.A. BALLIK, 1980, Appl. Opt. **19**, 3349.
REINHART, F.K., R.A. LOGAN and C.V. SHANK, 1975, Appl. Phys. Lett. **27**, 45.
RINNENBERG, H., 1986, Technical Digest 14th Int. Conf. on Quantum Electronics, THKK1 (San Francisco, CA, USA).
ROSENTHAL, A., 1962, J. Opt. Soc. Am. **52**, 1143.
SAGNAC, G., 1913, Compt. Rend. **157**, 708.
SAITO, S., O. NILSSON and Y. YAMAMOTO, 1985, Appl. Phys. Lett. **46**, 3.
SANDERS, G.A., M.G. PRENTISS and S. EZEKIEL, 1981, Opt. Lett. **6**, 569.
SARGENT III, M., M.O. SCULLY and W.E. LAMB JR, 1974, Laser Physics (Addison-Wesley, Reading, MA) ch. XIX.
SHIKADA, M., K. EMURA, S. FUJITA, M. KITAMURA, M. ARAI, M. KONDO and M. MINEMURA, 1984, Electron. Lett. **20**, 164.
STATZ, H., C.L. TANG and J.M. LAVINE, 1964, J. Appl. Phys. **35**, 2581.
STOKES, L.F., M. CHODOROW and H.J. SHAW, 1982, Opt. Lett. **7**, 288.
SUEMATSU, Y., and K. FURUYA, 1977, Trans. IECE Japan E **60**, 467.
SUEMATSU, Y., S. AKIBA and T. HONG, 1977, IEEE J. Quantum Electron. **QE-13**, 596.
TABUCHI, N., T. OUCHI and M. OHTSU, 1986, Proc. Technical Group Meeting, IECE Japan, OQE86-29 (in Japanese).
TAKEUCHI, N., H. BABA, K. SAKURAI and T. UENO, 1986, Appl. Opt. **25**, 63.
TANAKA, T., and G.B. BENEDEK, 1975, Appl. Opt. **14**, 189.
TERAMACHI, Y., and M. OHTSU, 1984, Proc. US–Japan Seminar on Coherence, Incoherence, and Chaos in Quantum Electronics (Nara, Japan) p. 63.
TOHMORI, Y., 1986, Ph. D. Thesis (Tokyo Institute of Technology).
TOHMORI, Y., Y. SUEMATSU, H. TSUSHIMA and S. ARAI, 1983, Electron. Lett. **19**, 656.
TSANG, W.T., and S. WANG, 1976, Appl. Phys. Lett. **28**, 596.
TSANG, W.T., U.A. OLSSON and R.A. LOGAN, 1983, Appl. Phys. Lett. **42**, 650.
TSUCHIDA, H., M. OHTSU and T. TAKO, 1981, Jpn. J. Appl. Phys. **20**, L403.
TSUCHIDA, H., M. OHTSU, T. TAKO, N. KURAMOCHI and M. OURA, 1982, Jpn. J. Appl. Phys. **21**, L561.
TSUKADA, T., 1974, Appl. Phys. Lett. **45**, 4899.
UEHA, S., N. SHIBATA and J. TSUJIUCHI, 1977, Opt. Commun. **23**, 407.
UTAKA, K., K. KOBAYASHI, K. KISHINO and Y. SUEMATSU, 1980, Electron. Lett. **16**, 455.
UTAKA, K., S. AKIBA, K. SAKAI and Y. MATSUSHIMA, 1981, Electron. Lett. **17**, 961.
VAHALA, K., and A. YARIV, 1983, Appl. Phys. Lett. **43**, 140.
VAN DER POL, B., 1927, Philos. Mag. S **7.3**, 13.
VANIER, J., R. KUNSKI, A. BRISSON and P. PAULIN, 1981, J. Phys. Colloque **C-8**, Suppl. au no. 12, C8-139.
WATTS, R.N., and C.E. WIEMAN, 1986, Opt. Lett. **11**, 291.
WELFORD, D., and A. MOORADIAN, 1982a, Appl. Phys. Lett. **40**, 865.
WELFORD, D., and A. MOORADIAN, 1982b, Appl. Phys. Lett. **40**, 560.
WENKE, G., and S. SAITO, 1985, Jpn. J. Appl. Phys. **24**, L908.
WESTBROOK, L.D., A.W. NELSON, P.J. FIDDYMENT and J.V. COLLINS, 1984, Electron. Lett. **20**, 957.
WIEMAN, C.E., 1986, Technical Digest, 14th Int. Conf. on Quantum Electronics, THCC1 (San Francisco, CA, USA).

WINELAND, D.J., J.C. BERGQUIST, R.E. DRULLINGER, H. HEMMATI, W.M. ITANO and F.L. WALLS, 1981, J. Phys. Colloque **C-8**, Suppl. au no. 12, C8-307.
WYATT, R., and W.J. DEVLIN, 1983, Electron. Lett. **19**, 110.
WYATT, R., T.G. HODGKINSON and D.W. SMITH, 1983, Electron. Lett. **19**, 550.
WYATT, R., D.W. SMITH, T.G. HODGKINSON, R.A. HARMON and W.J. DEVLIN, 1984, Electron. Lett. **20**, 913.
YABUZAKI, T., T. IBARAGI, T. HORI, M. KITANO and T. OGAWA, 1981, Jpn. J. Appl. Phys. **20**, L451.
YAMADA, M., and Y. SUEMATSU, 1981, J. Appl. Phys. **52**, 2653.
YAMAGUCHI, M., M. KITAMURA, S. MURATA, I. MITO and K. KOBAYASHI, 1985, Electron. Lett. **21**, 63.
YAMAMOTO, Y., 1980, IEEE J. Quantum Electron. **QE-16**, 1251.
YAMAMOTO, Y., 1983, IEEE J. Quantum Electron. **QE-19**, 34.
YAMAMOTO, Y., S. SAITO and M. MUKAI, 1983, IEEE J. Quantum Electron. **QE-19**, 47.
YAMAMOTO, Y., O. NILSSON and S. SAITO, 1985, IEEE J. Quantum Electron. **QE-21**, 1919.
YAMAZAKI, S., K. EMURA, M. SHIKADA, M. YAMAGUCHI, I. MITO and K. MINEMURA, 1985, Technical Digest 5th Int. Conf. on Integrated Optics and Optical Fibre Communication/11th European Conf. on Optical Communication, Vol. III (Venice, Italy) p. 39.
YAMAZAKI, S., K. EMURA, M. SHIKADA, M. YAMAGUCHI and I. MITO, 1985, Electron. Lett. **21**, 283.

半導体レーザ周波数の精密制御

大津元一
東京工業大学　総合理工学研究科

1. まえがき

レーザを光源とする干渉測長などの分野において，測定精度の向上に伴いレーザを単に一定波長の光源としてではなく安定な周波数源とみなす必要が高まっている。ところで，従来よりレーザから出てくる光は周波数または位相のそろったきれいな波であるといわれているので，このような目的には適している。レーザの周波数変動の大きさを表す標準偏差値σの値は図1に示すようにレーザ発明当時(1960年)は約10^{-7}(すなわち，レーザ周波数100 THzに対して10 MHzの揺らぎ)であったが，その後この揺らぎを小さくするための努力が継続してなされ，昨年7月の時点でのトップデータとしてはすでに10^{-16}が実現している。[1] つまり揺らぎはわずか0.01 Hzにまで抑えられている。これは計測などで頻繁に使われている気体レーザの値であるが，この図によるとσの値は10年間ごとに約5桁ずつ減少しており，現在もその減少のようすに頭打ちが見られない。もちろんこのよう

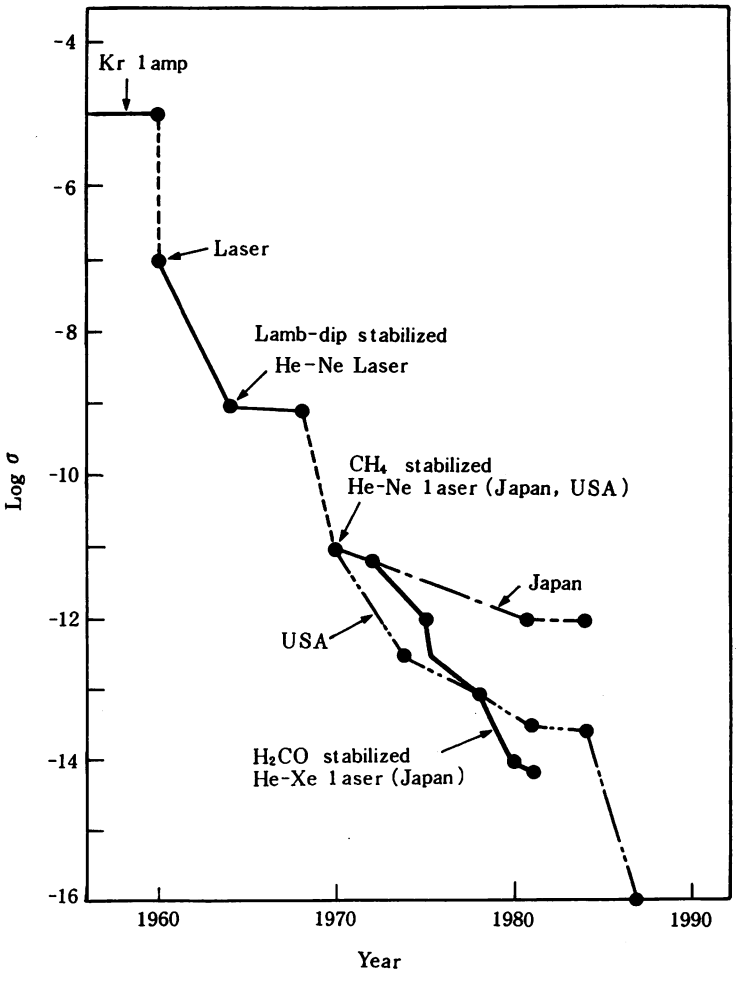

図1　He-Neレーザの周波数変動の大きさを表す標準偏差値σの値の進歩

な高度の安定度を得るにはレーザ物理，分光，制御技術などの進歩に負うところが大きいが，約30年にわたってこのように順調に進歩した技術の例は少ないのでなかろうか。この図をもとにした技術予測によると特に大きな壁にぶつかることなく21世紀初頭には10^{-18}～10^{-21}が達成しうるといわれている。[1)]

このような順調な進歩はつぎのような考察によって理解できる。即ち，レーザに限らず，一般の非線形自励発振器が外部の制御装置によって周波数制御を施されているとき，時刻tにおける周波数変動$\delta\nu(t)$は

$$\delta\nu(t)=\kappa\cdot\Gamma_0-\int_0^\infty h_f(\tau)\cdot\{\delta\nu(t-\tau)+\Gamma_n(\tau)\}d\tau \qquad (1)$$

と表される。[2)]ここでκはレーザ共振器の損失，Γ_0は量子効果（自然放出光揺らぎ）に起因する非制御時のレーザ周波数揺らぎを引き起こす雑音源，$\delta\nu(t-\tau)$は制御装置内の周波数揺らぎ検出系により検出された周波数揺らぎ，Γ_nは制御装置内で発生する雑音，h_fは制御装置のインパルス応答，を表す。この式をフーリエ変換して整理すると

$$F(f)=\frac{1}{1+H(f)}\cdot\kappa\cdot\Pi_0(f)-\frac{H(f)}{1+H(f)}\cdot\Pi_n(f) \qquad (2)$$

を得る。ここでF，Π_0，Π_n，Hは各々(1)式中の$\delta\nu$，Γ_0，Γ_n，h_fのフーリエ変換である。ここで制御利得Hを大きくすると（$|H|\to\infty$）この式右辺第1項は0に漸近する。一方第2項は$|\Pi_n|$に漸近する。このことは高利得の制御装置を用いて制御を施せば，量子効果に起因する非制御時の周波数揺らぎの値以下の値が実現でき，それは究極的には制御系の雑音によって制限される値をとることを意味する。

さて，この原理は工業的な応用上重要な半導体レーザにも当然当てはまる。半導体レーザの周波数揺らぎは非制御時には非常に大きいが，制御を施すことによりこれを抑圧でき，きれいな光波を得ることが可能である。これが実現すれば高性能の光周波数シンセサイザ，光トラッキングジェネレータとして光学分野で威力を発揮する。

半導体レーザは低消費電力，長寿命であるので操作が容易である。さらに小形軽量であるので光源そのものを機械的に動かすこともでき，光線操作系が不要となる，などの利点を有すると言われている。しかしながら，良質の周波数安定，単色光源として用いようとすると依然として多くの問題点を含んでいる。そこで以下の節では半導体レーザの周波数制御方法とその特性，および問題点を順次列挙したい。ただし，2節では単一縦モード発振する半導体レーザについて議論する。この単一モード性に関する問題点は3節で取り挙げる。尚，半導体レーザの周波数特性の基礎については文献3)～5）を，理論と実験の詳細については文献6)，7）を参照されたい。

2. 半導体レーザの周波数制御の実際

半導体レーザを使う場合，その周波数が一定値を取ること，その値が正確にわかっていること，すなわち，安定性と再現性が高いことが望まれる。さらに，これらとは一見相反するように感じられるが，周波数が広範囲にわたって掃引しうること，が挙げられる。これらの周波数制御性を実現するためには，従来マイクロ波発振器に対し確立している周波数制御技術[8)]との類推により，以下の各小節で述べるような各項目を実行すればよい。

2－1 発振スペクトル中心周波数の安定化

周囲温度変化，自己発熱などによりレーザ発振スペクトルの中心周波数が少なくとも10^{-7}程度ドリフトするのでこれを抑える必要がある。使用目的にもよるが，約1MHzの帯域の低周波制御装置が必要になる。レーザのヒートシンクの温度を制御してもよいが，高精度制御のためには注入電流制御の方がよい。周波数固定のための周波数基準として，簡便なものでは小形ファブリ・ペロー共振器が使われるが，周囲温度変化などによるこの共振周波数自身のドリフトがあるので，達成しうる安定度は10^{-9}が限界である。[9)]より高度の安定度

を得るには現在のところ原子，分子気体の吸収スペクトルが使われている。たとえば波長0.8μm～1.6μmの領域にはH_2O，NH_3，CO_2を始めとする多数の有機分子の振動回転遷移の高調波，結合調の吸収スペクトル線が約10GHz間隔で分布している。これらは多数分布しているので各半導体レーザ素子は少なくとも1本の吸収線に同調，安定化でき，都合がよい。これにより波長0.8μmのAlGaAsレーザ，1.5μmのInGaAsPレーザともに10^{-11}の周波数安定度が得られている。[10,11] この場合の問題点として，吸収強度が小さいので制御利得がやや小さいこと，吸収線の同定がまだ不十分なので周波数再現性がよくないこと，などが挙げられる。

波長0.8μm付近にはRb，Csなどのアルカリ金属の共鳴スペクトルがあり，この吸収強度は大きく，また同定も行われているので周波数基準としては有利である。これを用い10^{-12}の周波数安定度が得られている。[12] この場合の問題点はスペクトルの数が少ない為に同調しうるレーザ素子が限られることである。原理的には(2)式のΠ_nで決まる値，すなわち10^{-15}の安定度が可能であると推定されている。[13] ただし，この限界に達するにはさらに制御利得を増加させる必要があり，そのためにはFM分光法のような高感度な吸収スペクトル線検出法を採用する必要があろう。[14]

以上のような原子分子を周波数基準に用いた場合の共通の問題点としては，吸収スペクトル周波数が気体圧力によりシフトすることである。[15] これらは10^{-12}より良い長期周波数安定度，10^{-11}より良い周波数再現性を得ようとするとき問題になる。外部環境の変化に対してより安定な原子分子の探索が今後必要となろう。さらに，安定化された周波数の測定精度は現在のところ約10^{-7}である。[16] 干渉測長への応用の際，この値は長さ絶対値の確度を制限するので十分でない。10^{-10}程度の精度の波長測定装置の開発が必要である。

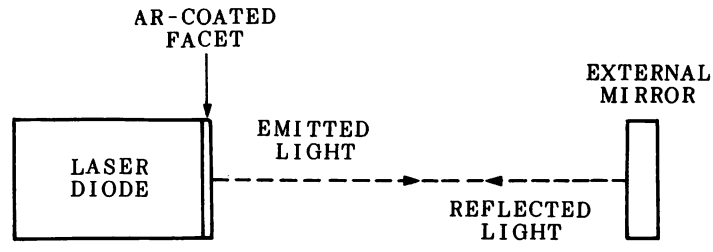

図2　外部反射体を用いた光帰還法により線幅を狭窄化する方法の原理

2－2　発振スペクトル線幅の狭窄化

より高速の周波数揺らぎの成分はレーザ発振スペクトル線の幅をひろげる。非制御時の線幅は数MHz～100MHzである。ヘテロダイン形干渉測長，コヒーレント・ライダーなどの広帯域光計測用光源としてはこのような線幅を狭窄化する必要がある。2.1節のような電流負帰還制御を施す場合，広帯域制御回路の設計は必ずしも容易ではないので10年以上前から現在まで，別の簡便な方法が採られてきた。これは(2)式において，$H=0$（負帰還制御はしない）とするがその代わりにκを小さくする（レーザ共振器損失を小さくする）ものである。こうするとレーザ共振器の帯域全範囲で周波数揺らぎが小さくなり，スペクトル線幅も狭くなる。これを実行するには図2のようにレーザの一方の端面に反射防止膜を塗り，その代わりにレーザ長以上離れたところに反射鏡または回折格子を置く。こうしてレーザ単体のときにくらべ格段に長い共振器を構成し，これによりκを小さくする。この方法により数10kHzの線幅が実現している。[17] 鏡を置く代わりにレーザ端面にファイバを接続した例[18]や，外部導波路をレーザと一緒に集積化した例もある。[19] この場合の問題点は系の安定性である。すなわち，負帰還制御を施していないので外部鏡，ファイバなどの機械的振動，熱膨張などの影響により線幅が時間的に変化する。これを抑えるためにレーザ端面の反射防止を強化し，レーザへ戻り光量を増す方法が採られるが，[20] それでもその安定性は実用的な光計測への応用には不十分である。その他の問題として，注入電流を変調してもレーザ周波数が変調されなくなること，縦モ

ード周波数間隔が狭くなるので単一モード発振が保証されなくなること，などが挙げられる。

これらの欠点のうち，とくに系の不安定性をおさえるには２－１節と同様，負帰還制御を施すのがよい。この場合は制御帯域は少なくとも非制御時の発振スペクトル線幅の値と同程度必要である。しかし最近のレーザの線幅は10 MHz 以下のもが多くなってきているので，あまり広い制御帯域は必要にならず，負帰還制御が容易になった。その制御装置の代表例を図３に示す。周波数揺らぎの検出には２－１節でも述べた簡単な小形ファブリ・ペロー共振器の透過光を用いる。0.8μmのAlGaAsレーザの場合，制御により線幅は100kHz まで狭くなった。これには非制御時の 1／50 である。また，この図ではファブリ・ペロー共振器の反射光を用いたもう一つの負帰還制御回路により同時に発振スペクトル中心周波数も安定化している。このような負帰還制御により線幅は安定に狭窄化された。

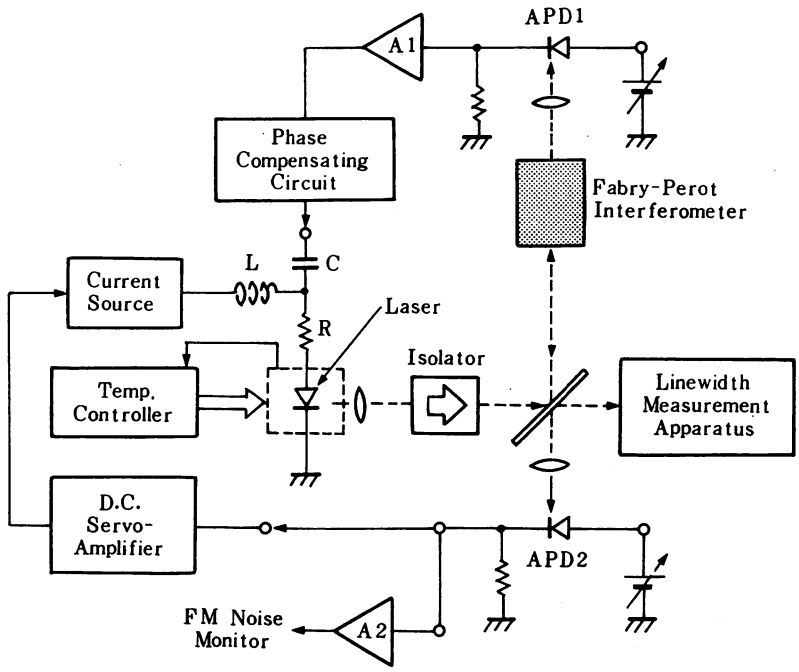

図３　電気的負帰還制御法の実験装置

図３の制御装置では(2)式のΠ_nの値によって決まる線幅狭窄化の限界は約1kHz であるが，現在のところ，この値に達していない。それは制御装置の制御帯域が約 20MHz であり，これは十分広くないので制御利得もまだ不十分であることによる。レーザの周波数応答特性も含めた回路解析によると，制御系の遅延時間が 0.6ns 以内になれば十分な制御帯域が確保でき，従って制御利得もより増加できて上記限界に達する。この遅延時間を実現するにはたとえばGaAs などの高速ＩＣを用いて制御増幅器を作り（この場合遅延時間は約 0.2ns）さらに制御ループの光路長，電気長を 12cm 以内（遅延時間は 0.4ns）にすればよい。こうすれば光集積回路などを用いた制御系の集積化などに頼る事なく，現在入手しうる光学，電気要素の組合せで図２の方法よりも狭い線幅が実現しうる。さらに図３のファブリ・ペロー共振器の周波数弁別感度の最適化により(2)式のΠ_nによって決まる線幅狭窄化の限界は約1Hz という小さな値になる。[21] 制御帯域を広げるためにはレーザそのものの周波数応答特性も重要で，特にその位相遅れが均一である方が有利である。最近はそれを実現するためにレーザの電極を２つに分割し，各々に流す直流電流値を調節することにより位相遅れ特性を改良する試みがなされている。[22]

この電気的な負帰還制御の問題点はやはり制御帯域が有限なことである。従って，制御帯域外，すなわちレーザ発振スペクトルの裾を構成する周波数揺らぎは抑圧されない。そこで図２の光帰還の方法と図３の電気的負帰還の方法との利点を生かした複合法を採用するのがよい。その例として図４に示すように外部ファブリ・ペロー共振器からわずかな量の戻り光をレーザに再注入して(2)式のκの値を減少させ，同時にレーザとファブリ・ペロー共振器との距離を電気的に負帰還制御して系の安定性を保つ方法が提案された。[23] これによ

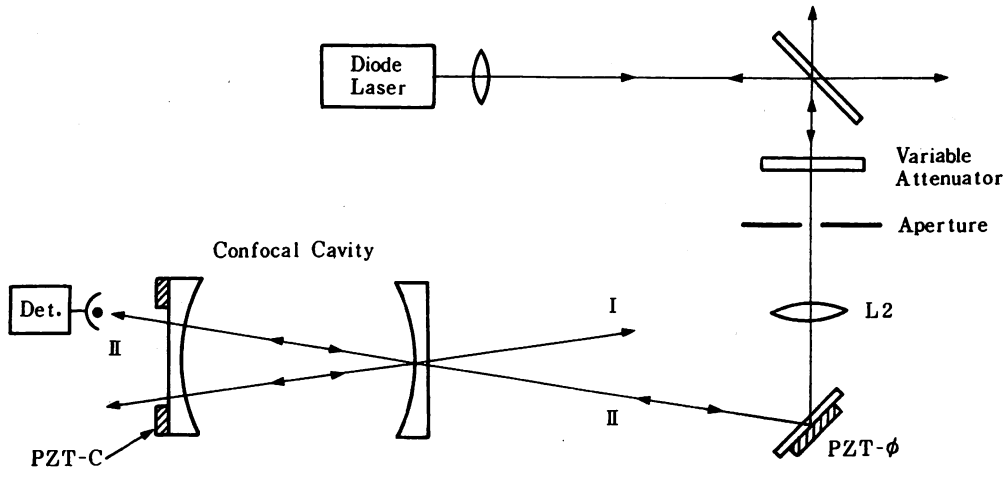

図4　外部共焦点ファブリ・ペロー共振器からの光帰還による線幅狭窄化の実験装置[23)]

り比較的安定に線幅20kHzが実現した。また，戻り光量が少ないので縦モード周波数間隔はレーザ単体のままに保たれており，単一モード性は失われない。さらにレーザの電流をファブリ・ペロー共振器の自由スペクトル域の値の有理数倍の値の周波数で変調するとレーザ周波数は変調される，[24)]などの利点を有する。

2－3　周波数の精密な追随

ヘテロダイン形の光計測では周波数の安定な主レーザに従レーザの周波数を高精度で追随させることが必要である。従来このためには注入同期現象が利用されていた。[25)]これは非線形光学効果にもとづく現象なので物理的には興味深いが安定性などの点で実用上問題がある。図5はそれに代わるもので，マイクロ波におけるヘテロダイン形位相同期ループに対応するものである。すなわち，主，従レーザのヘテロダイン信号の位相が局部発振器であるマイクロ波シンセサイザの位相に同期するよう従レーザの注入電流を制御するものである。[26)]ここで主レーザとしては2－1節および2－2節で示したように周波数安定度を向上させたレーザを用いればよい。この位相同期法のキャプチャ・レンジは約1.2GHzであった。また，ヘテロダイン信号周波数の安定度として1×10^{-14}が得られている。この安定度は2－1節で示した主レーザの発振スペクトル中心周波数の安定度よりよい。このことは従レーザの周波数は主レーザのそれに忠実に追随していること，言い

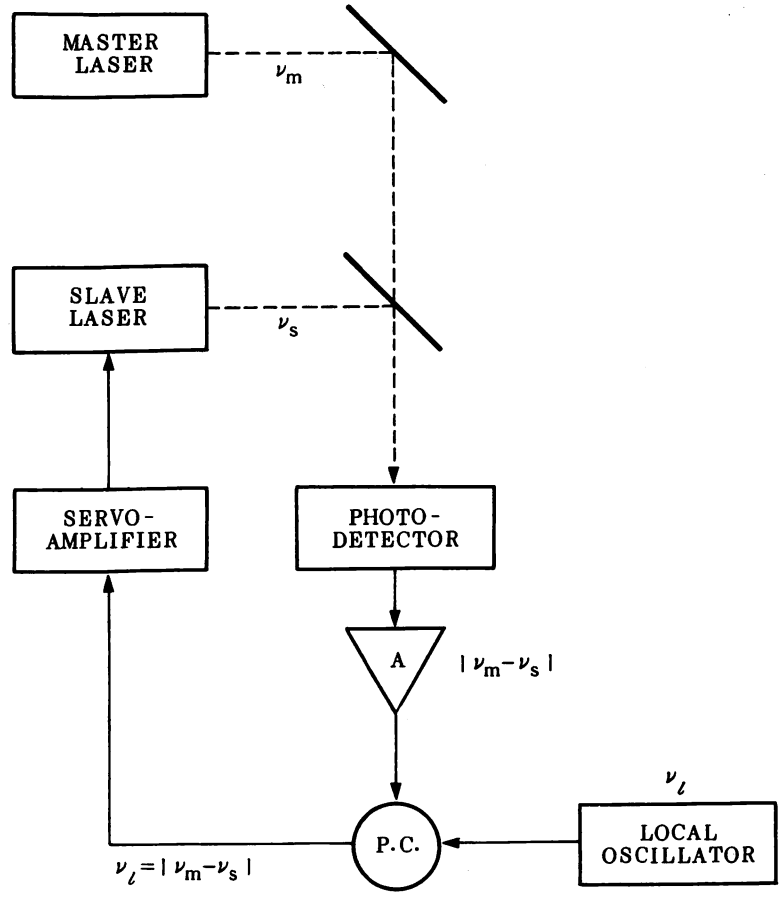

図5　周波数追随の原理[26)]　P.C.：位相比較器。ν_m，ν_s，ν_lは各々主レーザ，従レーザ，マイクロ波レンセサイザの周波数

替えれば主レーザの高安定性が従レーザに移乗していることを意味する。このことから良質の光トラッキング・ジェネレータが実現していることが確認される。周波数追随の制御帯域を広げ，利得を増加させることによりヘテロダイン信号の位相揺らぎを1ラジアン以下にするような位相同期ループを構成することが原理的に可能である。さらにこのように位相同期の成立するレーザを多数用意し，それら全てのレーザ光を重ね合わせると，これはモード同期レーザからの光と同じ特性を示す。すなわち，非線形光学効果を使わずにフェムト秒程度の超短光パルス発生が可能である。

2－4　安定な周波数掃引

周波数を安定に，かつ広帯域に掃引することは分光計測などには必須である。たとえば図2で示した光帰還法において，外部反射鏡のかわりに回折格子を使い，その面を回転させると周波数掃引が可能になる。波長1.5μmのInGaAsPレーザではこの方法により67GHz，波長に換算すると0.5 nm)にわたり周波数掃引された例がある。[27] しかしこの場合には周波数の安定度として2.1節で示した値は得られておらず，きわめて荒っぽい掃引である。従って，掃引中の周波数の校正もされていない。周波数掃引をより高精度に行うには2.4節の光位相同期の系を用い，局部発振器としてのマイクロ波シンセサイザ周波数を掃引すればよい。これにより2－3節で示した安定度を保ったまま53 GHzの範囲にわたって連続掃引された。[26] この場合，掃引可能範囲はレーザのモードホッピング特性により制限されている。従って，モードホッピングのない単一モードレーザを使えば，[28] 原理的には1THzの範囲にわたって周波数連続掃引可能である。

3.　半導体レーザの周波数制御のための問題点

光計測システムへの応用のために2節で述べたような周波数制御をする際，半導体レーザデバイスに関連した問題点を挙げるとつぎのようになろう。

(1)　縦モードの単一性

今まで半導体レーザが単一縦モード発振するという仮定のもとに議論を進めてきた。しかし，DFB形のように注意深く作られた単一モードレーザでも自然放出光揺らぎの混入により従モードが過渡的に発振し，このモードとの非線形モード結合により主モードパワーが過渡的に減少するパワー・ドロップアウトが見られる。[29,30] ドロップアウトの深さは10～60%，持続時間は数μs～数nsであり，これらはバイアス電流に依存する。従ってこのような時間範囲内では主モードの単一モード性は保証されない。使用する光計測システムの特性にもよるが，このドロップアウトを抑えるには主モード，従モードのパワーの時間平均値の比が20dB以上必要である。[29,30] デバイス試作段階ではこのような高パワー比をもったレーザは得られるが，このようなデバイスは実用的な光計測システムにはまだ十分安定に供給されていない。このようなドロップアウトが起こる一要因として，レーザの発振利得スペクトル幅にくらべ縦モード間隔が狭すぎ，隣合う縦モード間の利得差が少ないことが挙げられる。例えば波長0.8μmのAlGaAsレーザの場合，発振利得スペクトル幅，縦モード間隔は波長単位で表すと各々500Å，3Åである。一方長さ15cmの単一モードHe-Neレーザではそれらは各々，1GHz，1GHzである。縦モード間隔はレーザの長さに反比例するので，短いレーザのほうが単一縦モード性に優れているが，両レーザのこれらの数値を比較し，半導体レーザをそれと等価なHe-Neレーザに置き換えてみると，その長さはなんと25mにもなる。さらに，より詳しい議論をするとHe-Neレーザの縦モード間の結合は弱く，2つ以上の縦モードは同時に安定なパワーで発振しうるが，半導体レーザではその結合は強く縦モード間でパワー・スイッチング現象を示す。[31] これを考慮すると半導体レーザは長さ約100mのHe-Neレーザに対応する。だれもこのような巨大なレーザは使いたくないので，今後単一モード性を改善するには縦モード間隔を大きくするか，発振利得

スペクトルを狭くすべきである。縦モード間隔を大きくするにはレーザ長を短くすればよいが，パワー低下，周波数揺らぎ増加を引き起こすので不利である。むしろ量子井戸など[32]の新構造，さらには新材料を用いて発振利得スペクトルを狭くすべきである。

(2) 周波数の長期シスト

半導体レーザの周囲温度揺らぎを10^{-5}℃以内，さらに注入電流揺らぎを0.6 nA/√Hz 以内に抑圧した超高安定環境下で約6カ月の長期にわたり周波数のドリフトを測定すると，約20MHz/hのブルーシフトが見られる。[32]これはInボンディング層の酸化による熱抵抗の変化，レーザ端面付近でのキャリヤの非放射再結合による熱効果などによると言われている。[34]光計測では発振周波数，波長の絶対値の再現性に対する要求が今後一層強くなると考えられるので，このような再現性，すなわちスペクトル寿命を向上させるためにデバイス設計製作の段階での熱抵抗の低減，スクリーニングなどの配慮が必要である。

(3) 半導体レーザ装置の寸法

(1)では縦モードの単一性の面から半導体レーザ素子の等価的寸法がまだ非常に大きいことを指摘した。さらに指摘すべきことは，半導体レーザ素子の実際の寸法が小さい（長さ数100μm）での(2)式のκの値が大きく，従って周波数揺らぎが大きいために，その揺らぎを抑えるには図2,3のような外付け光電回路が必要となり，結果的には半導体レーザ装置全体の寸法はHe-Neレーザ装置程度の大型になってしまうということである。装置全体を小形化するには外付け回路の集積化のみでなく，広帯域の位相変調器の開発，さらにより重要な課題として周波数制御利得の高い半導体レーザを実現することが必要である。すなわち，2-2節でも述べたように電極を分割するなどして周波数変調効果が高く，その位相遅れ特性の均一なレーザの開発が望まれる。

4. あとがき

本稿ではまず半導体レーザは原理的にきわめて周波数安定度の高い光源となりうる可能性を理論的に示し，さらに4項目に関しその実験結果を示した。これらの実験結果により現在のところ簡易形の気体レーザなみの性能が得られていることがわかる。一方，半導体レーザデバイスそのものに注目すると，いくつかの問題があり，周波数安定性の点ではまだ不十分な段階である。これらの問題を克服し，より信頼性の高い周波数安定半導体レーザを実現するためには新デバイス設計，周辺デバイスの高性能・集積化，制御法の改良，などを有機的に行う必要があろう。

参考文献

1) J.L.Hall：US-Japan Seminar, Quantum Mechanical Aspects of Quantum Electronics, July 1987, Monterey, CA, Paper Ⅲ-4

2) M.Ohtsu, K.Kuboki, N.Tabuchi：Sixth International Conference on Integrated Optics and Optical Fiber Communication, January 1987, Reno, Nevada, TUC5

3) 大津元一：「レーザと原子時計」，1986年，オーム社，第6章

4) 大越孝敬編：「光ファイバセンサ」，1986年，オーム社，第3章

5) 応用物理学会編：「半導体レーザの基礎」，1987年，オーム社，第2章

6) M.Ohtsu：IEEE J.Lightwave Technology, LT-6, January 1988, in press

7) M.Ohtsu and T.Tako：Progress in Optics, 25, 1988, in press

8) P.Kartaschoff：Frequency and Time, Academic Press, London, 1978

9) K.Kuboki, M.Ohtsu, N.Tabuchi and T.Ouchi：Proceedings of SPIE (The International Society for Optical Engineering)

Vol.723, Progress in Semiconductor Laser Diodes, September 1986, Cambridge, MA, 73

10) H.Tsuchida, M.Ohtsu, and T.Tako：Jpn. J.Appl. Phys., 21(1982) L1

11) M.Ohtsu, H.Kotani, and H.Tagawa：Jpn. J.Appl. Phys., 22(1983) 1533

12) H.Tsuchida, M.Ohtsu, T.Tako, N.Kuramochi, and N.Oura：Jpn.J.Appl. Phys., 21 (1982) 1561

13) M.Ohtsu, H.Fukada, T.Tako, and H.Tsuchida：Jpn.J. Appl. Phys., 22(1983)1157

14) G.C.Bjorklund：Opt. Lett., 5(1980)15

15) 古田浩之，橋本実，大津元一：第48回応物学会学術講演会予稿，1987年10月，17a-ZC-2

16) K.Fukuoka, M.Ohtsu, and T.Tako：Jpn. J.Appl. Phys., 23(1984)L117

17) R.Wyatt and W.J. Devlin：Electron. Lett., 19(1983)110

18) F.Favre, D.Le Guen, and J.C.Simon：IEEE J.Quantum Electron., QE-18 (1982)1712

19) T.Fujita, J.Ohya, K.Matsuda, M.Ishino, H.Sato, and H.Serizawa：Electron, Lett., 21(1985)374

20) N.A.Olsson and J.P. van der Ziel：IEEE J. Lightwave Technol., LT-5(1987)509

21) M.Ohtsu：Technical Digest of Conference on Lasers and Electro-Optics, June 1986, San Francisco, CA, WB4

22) H.Yasaka, Y.Yoshikuni, Y.Nakano, and K. Oe：Electron, Lett., 23(1987)1161

23) B.Dahmani, L.Hollberg, and R.Drullinger：Opt. Lett., 12(1987)876

24) 大津元一：電子情報通信学会光量子エレクトロニクス研究会技術報告，1982年12月，OQE87-135

25) S.Kobayashi and T.Kimura：IEEE J. Quantum Electron., QE-18(1982)575

26) K.Kuboki and M.Ohtsu：IEEE J.Quantum Electron., QE-23(1987)388

27) K.H.Cameron, M.R.Matthews, T.G.Hodgkinson, and W.J.Devlin：Technical Digest of Conference on Lasers and Electro-Optics, Baltimore, MA, 1985, TUC5

28) Y.Tohmori：Ph.D. Thesis, Tokyo Institute of Technology, Tokyo, Japan, March 1986

29) R.Linke, B.L.Kasper, C.A.Burrus, I.P. Kaminov, J.S.Ko, and T.P. Lee：IEEE J.Lightwave Technol., LT-3(1985)711

30) 大津元一：電子情報通信学会光量子エレクトロニクス研究会技術報告，1987年12月，OQE87-136

31) M.Ohtsu, Y.Teramachi, Y.Otsuka, and A.Osaki：IEEE J. Quantum Electron., QE-22(1986)535

32) R.Chin, N.Holonyak, Jr. and B.A.Vojak：Appl. Phys. Lett., 36(1980)19

33) M.Ohtsu, M.Hashimoto, and H.Ozawa：Proceedings of the 39th Annual Frequency Control Symposium, May 1985, Philadelphia, PA, p.43

34) F.Favre and D.Le Guen：Electron, Lett. 19(1983)663

*　　*　　*

解　説

半導体レーザーの周波数制御

大　津　元　一

東京工業大学総合理工学研究科　〒227 横浜市緑区長津田 4259

（1988年1月26日受理）

Frequency Control of Semiconductor Lasers

Motoichi OHTSU

Graduate School at Nagatsuta, Tokyo Institute of Technology,
4259, Nagatsuta, Midori-ku, Yokohama 227

1. まえがき

光学では光源が不可欠であり，光学の多くの理論ではその光源は単色性が十分優れているものと仮定して議論を展開している．このような単色性の優れた光を実際に得るにはレーザーを使えばよいが，精密測長などには通常のレーザーの単色性では不十分なことが多い．レーザーには多数の種類があるが，そのなかでも半導体レーザーは実用上，有用である．ただし，半導体レーザーの周波数揺らぎは他種レーザーにくらべて大きく，単色性に関して劣るがこれは負帰還制御を施すことにより原理的には他種レーザーと同等以上に改良しうる（2. 章参照）．

電磁波としての光の特性量は振幅，偏波，周波数であるが，光周波数は 100 THz 程度の大きな値なので周波数のもつ情報容量は振幅，偏波に比べ非常に大きい．さらに，周波数計測は高精度である．したがって上記のように周波数揺らぎを抑圧し，単色性を向上させた光の周波数を利用してヘテロダイン方式の測長などの光学計測を行なえば，その測定精度が向上する．このように，レーザーを安定な周波数源として取り扱うと多くの利点がある．本稿では半導体レーザーを安定な周波数源にするための制御の方法，現状と問題点について筆者の研究内容などをもとに紹介する．

2. 周波数制御の原理

周波数制御の装置を**図1**（a）に示す．これは周波数基準部，周波数揺らぎ検出部，周波数変調部からなる．半導体レーザー共振器のQ値は小さいので，量子効果による周波数揺らぎは大きい．したがって原子分子分光法，干渉法，ヘテロダイン法など通常の光電計測技術を用いれば**図1**の周波数揺らぎ検出部においてこの揺らぎを検出することができる．とくに干渉法ではファブリ・ペロー干渉計が簡便な周波数基準および周波数揺らぎ検出器として使える．周波数揺らぎのパワースペクトル密度はフーリエ周波数約 10 kHz 以下ではキャリヤ移動度の揺らぎに起因する $1/f$ 揺らぎ，それ以上では量子揺らぎからなる[1]．

一方，半導体レーザーの周波数は注入電流によって広帯域変調されるので揺らぎ検出部出力を注入電流に負帰還すれば揺らぎを抑圧できる．電流による変調は数 kHz ～数 MHz 以下では活性層の屈折率の温度変化により，またそれ以上ではキャリア密度変調により引き起こされる．変調特性の測定例を**図2**に示す[1]．同図（a）は周波数偏移，（b）は位相遅れの特性である．上記の温度効果，キャリヤ効果の支配する変調周波数領域とも位相は遅れるので負帰還制御には位相進み補償用電子回路を付加する必要がある．

負帰還制御系の帯域が十分広いと仮定すると制御時の周波数揺らぎ $\delta\nu(t)$ は半導体レーザーの動作を記述するランジュバン方程式にもとづき次式で与えられる[2]．

$$\delta\nu(t)=\kappa\cdot\{\Gamma_s(t)+\Gamma_c(t)\}-\int_0^\infty h(\tau)\cdot\{\delta\nu(t-\tau)+\Gamma_n(\tau)\}\,d\tau \quad (1)$$

ここで κ はレーザー共振器損失，Γ_s および Γ_c は半導体レーザー固有の量子揺らぎを表わしそれぞれ自然放出光揺らぎおよびそれに誘起されるキャリヤ密度揺らぎに

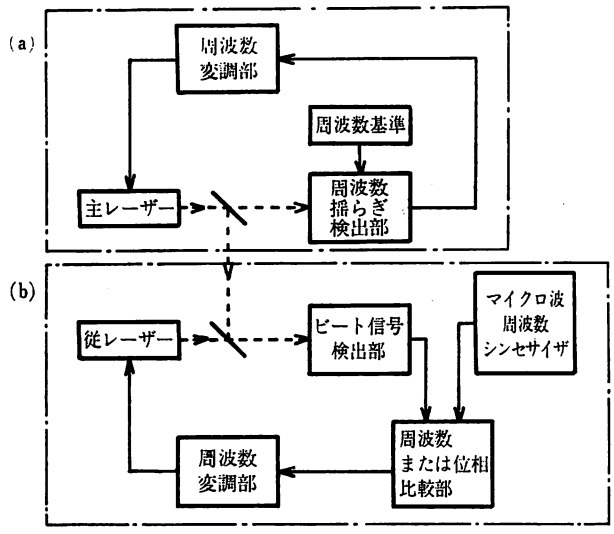

図 1　実験装置の概念図
（a）発振スペクトル中心周波数の安定化（3.1項参照），線幅狭窄化（3.2項参照）のための装置．（b）周波数同期（3.3項参照），周波数掃引（3.4項参照）のための装置

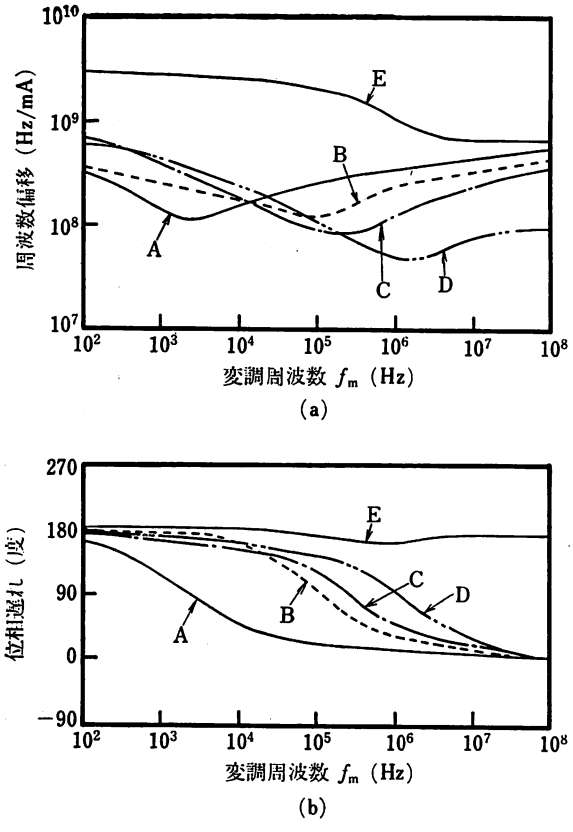

図 2　注入電流変調による半導体レーザーの周波数変調特性の測定例
（a）周波数偏移，（b）位相遅れ．曲線 A～D は波長 1.5 μm の InGaAsP レーザー，曲線 E は波長 0.8 μm の AlGaAs レーザーの例

対応する．h は制御系のインパルス応答関数，$\delta\nu(t-\tau)$ は制御系の周波数揺らぎ検出部で測定された周波数揺らぎの値，Γ_n は制御系内で発生する雑音の値である．右辺最終項の積分が負帰還制御の効果を表わす．この式をフーリエ変換すると

$$F(f)=\frac{\kappa}{1+H(f)}\cdot\{\Pi_s(f)+\Pi_c(f)\}-\frac{H(f)}{1+H(f)}\cdot\Pi_n(f) \qquad (2)$$

と表わせる．ここで F, Π_s, Π_c, H, Π_n はおのおの $\delta\nu$, Γ_s, Γ_c, h, Γ_n のフーリエ変換である．ここで制御利得が高くなると（$|H|\to\infty$）右辺第 1，2 項の値は 0 に，第 3 項は $|\Pi_n|$ にそれぞれ漸近する．すなわち量子揺らぎの効果は制御により抑圧でき，周波数揺らぎは制御系の雑音の大きさによって決まる値まで小さくすることができる．言い換えると高利得，低雑音制御系を使えば非制御時の量子揺らぎよりも小さい揺らぎの値を実現でき，単色性の優れた光が人工的に作り出せる．**図 2**（a）にも示したが半導体レーザーの周波数変調効率は他種レーザーに比べ大きいので制御利得を高くすることができ，（1），（2）式の原理に従う負帰還制御に適している．

周波数制御の効果を検討するには周波数揺らぎのパワースペクトル密度の値を知ればよいが，レーザーの応用上は揺らぎの低周波成分，すなわちゆっくりしたドリフト，に対応する発振スペクトルの中心周波数安定度（1），さらに，より高周波成分に対応する発振スペクトル線幅の値（2）を尺度とすることが多い．実用上さらに，他の高安定半導体レーザーへの周波数同期（3），周波数の広帯域掃引（4），の性能に注目することが多い．次章ではこれらの 4 項目の実験結果について記す．

3.　周波数制御の実際

3.1　中心周波数の安定化

温度効果による周波数ドリフトを抑えるには制御系内の周波数基準部も高安定なものが必要となる．そのような基準として気体原子分子のスペクトル線が適している．波長 0.7～1.6 μm の範囲には NH_3, H_2O, CO_2 など有機分子の振動回転遷移の結合調，高調波成分が約 10 GHz の周波数間隔で多数分布するのでこれらの吸収スペクトルが使用できる[3,4]．これらの吸収強度は小さく，またスペクトル基準周波数が温度シフトを示すこと（H_2O では 3 MHz/K[5]）が問題であるがこれに対し波長 0.8 μm 付近における Cs[6]，Rb[7] などのアルカリ金属蒸気の電子遷移スペクトルは吸収強度が大きく，また温度シフトも小さい（Rb では 0.5 MHz/K 以下[8]）．

Rb の飽和吸収スペクトルを周波数基準に用い，Al-

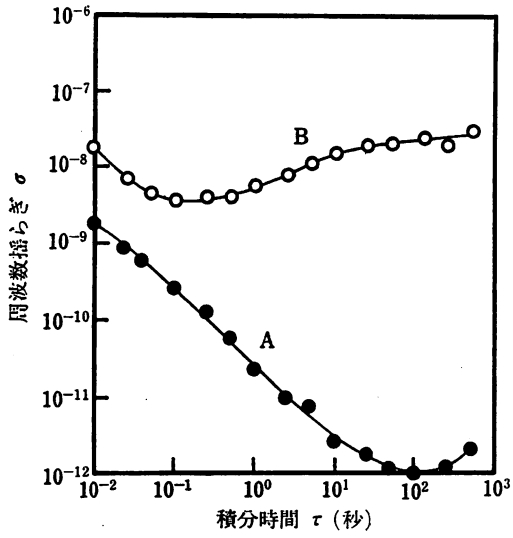

図 3　AlGaAs レーザーの周波数揺らぎの大きさを表わす分散 σ^2 の平方根とその測定の積分時間 τ との関係
曲線 A：制御時，曲線 B：非制御時

GaAs レーザーの周波数ドリフトを抑圧した結果，残留周波数揺らぎの大きさを表わす分散値 σ^2 の平方根を積分時間範囲 $10^{-2}\,\mathrm{s} \leqq \tau \leqq 10^{3}\,\mathrm{s}$ において**図 3** の曲線 A に示す[9]．この値は非制御時（曲線 B）に比べ σ の値の著しい減少が見られ，とくに $\tau=10^{2}\,\mathrm{s}$ において $\sigma=1.0\times10^{-12}$，すなわち揺らぎの振幅は約 400 Hz まで抑圧されている．これは(2)式の $|\Pi_s|$ の値とほぼ同等，すなわち自然放出光揺らぎによる量子揺らぎレベルに相当すると推定されている[10]．さらに制御利得を上げることにより(2)式の $|\Pi_n|$ で与えられる理論限界 $\sigma=1.7\times10^{-14}\tau^{-1/2}$ に近づく可能性があり[10]，現在最も高安定な原子発振器である水素メーザーと同等の高性能になる．

3.2　スペクトル線幅の狭窄化

レーザーの発振スペクトル線幅はレーザー光の単色性の度合を判断する尺度の一つである．この線幅の値を決定する主要因はフーリエ周波数 f が数十 MHz 以下の揺らぎ成分である．これを抑圧し，線幅を狭窄化するには 3.1 項よりも広帯域制御が必要である．

共振曲線の半値全幅 $\Delta\nu_{FP}=400$ MHz のファブリ・ペロー干渉計を周波数揺らぎ検出に使い，0.8 μm AlGaAs レーザーに帯域約 20 MHz の制御を施したときの線幅の値を**図 4** の曲線 A に示す[11]．図中 I，I_{th} はおのおのレーザーの注入電流とその閾値を表わす．$(I/I_{th}-1)^{-1}=1$ において線幅 100 kHz が得られており，これは非制御時（曲線 B）の 1/50 である．これは非制御時の自然放出光揺らぎによる量子揺らぎの値（(2)式の $|\Pi_s|$）以下になっていることが確認されている[11]．

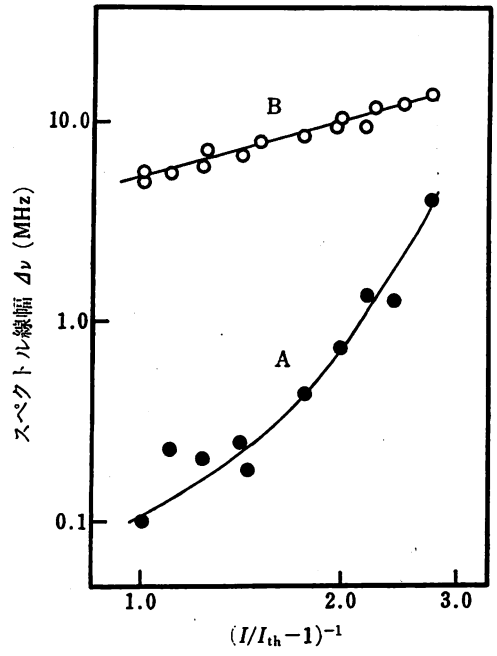

図 4　AlGaAs レーザーのスペクトル線幅 $\Delta\nu$ とバイアスレベル $(I/I_{th}-1)$ の逆数との関係
I，I_{th} はそれぞれ注入電流とその閾値．曲線 A：制御時，曲線 B：非制御時

現在，この線幅の狭窄度は制御系の帯域により制限されているが，群遅延時間 0.2 ns の GaAs 系高速制御用増幅器を使えば，制御ループを集積化する必要なく現在の制御系を用いて 1/630 の狭窄度が得られると推定されている[1]．最近はフィネス 10^{4} 以上の高性能ファブリ・ペロー干渉計が実現しており[12]，これを周波数揺らぎ検出に用いると制御利得がさらに増加し，より高い狭窄度が期待される．ファブリ・ペロー干渉計は制御系において低域通過フィルタとして働くがフィネスの増加（$\Delta\nu_{FP}$ の減少）とともに遮断周波数が減少し，これが制御系の帯域を狭める．したがってレーザーの線幅を最小にする $\Delta\nu_{FP}$ の最適値があり，その値は 820 kHz～6.8 MHz と推定されている．このときレーザーの線幅は非制御時の 6×10^{-9}～3×10^{-7} 倍，すなわち 58 mHz～2.9 Hz というきわめて小さい値をとる[1]．このように制御により超高性能気体レーザー[13]と同等の優れた単色性が期待できる．

帯域制限があるとレーザー発振スペクトルの形はローレンツ形からずれるのでスペクトル線幅の値は必ずしも単色性を表わすよい尺度ではなくなる．その代わりに周波数揺らぎのパワースペクトル密度を尺度としたほうが適切で，これによると $\Delta\nu_{FP}=1$ MHz の高フィネス・ファブリ・ペロー干渉計を使うと市販の半導体レーザーや制御用増幅器を用いて**図 5** のようにパワースペクトル密度が非制御時の −57 dB 減少することが推定されてい

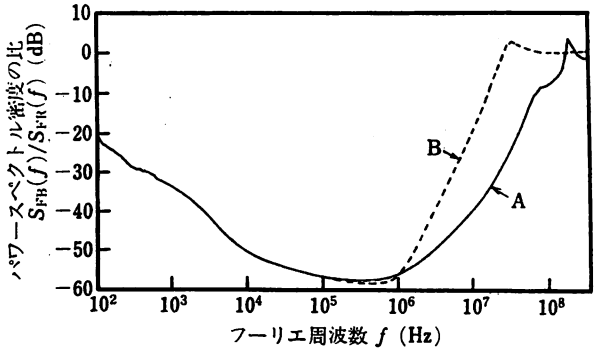

図 5　高フィネス・ファブリ・ペロー干渉計を用いた制御時の周波数揺らぎのパワースペクトル密度 $S_{FB}(f)$ を非制御時の値 $S_{FR}(f)$ で規格化したもの
曲線 A, B はそれぞれ干渉計の反射光，透過光を用いて周波数揺らぎ検出を行なった場合のシミュレーションの結果

る[14]．さらに，同図に示すように干渉計の反射光を使って周波数揺らぎを検出すると透過光を使うよりも制御帯域が広がることが指摘されている[14]．これは反射光を使った揺らぎの検出感度にはファブリ・ペロー干渉計の遮断周波数以上のフーリエ周波数において微分要素が付加されるからである．

このほか，負帰還制御を施すかわりに（(1)式で $h=0$），レーザー外部に反射鏡を置き，それからの反射光をレーザーに帰還して共振器損失を小さくする光帰還法（(1)式の κ の値を小さくする）がある[15]．これは周波数揺らぎを広帯域で抑圧できるが系が不安定になるという問題点がある．そこで負帰還制御法の安定性と，この光帰還法の広帯域性の両利点を活かすために，外部ファブリ・ペロー共振器にレーザーを弱く光結合させ，同時に全体の系を電気的に負帰還制御する方法が提案されている[16,17]．

3.3　他の高安定半導体レーザーへの周波数同期

3.1, 3.2 項で述べた方法で実現した単色性の優れた高安定レーザーを主レーザーとして用い，この周波数にもう一つのレーザー（従レーザー）周波数を同期，追随させることはヘテロダイン方式の光計測などのための光源技術として重要である．高精度の同期法の一つは**図 1**(b)に示すようにマイクロ波周波数シンセサイザを局部発振器とし，この周波数に二つのレーザー間のビート周波数を同期させる，周波数オフセット・ロック法である[18]．これによりビート周波数揺らぎは**図 6** の曲線Aに示すように非制御時（曲線B）にくらべ著しく抑圧される[19]．これは 0.8 μm AlGaAs レーザーに対する測定結果である．とくに $\tau=10^2$ s において $\sigma=1\times10^{-14}$，すなわち残留周波数揺らぎは約 4 Hz である．この揺らぎは**図 3** の曲線Aで示される主レーザーの揺らぎの値より小さい．このことは従レーザーの周波数揺らぎは主レーザーのそれと同等になっていること，言い換えれば主レーザーの高い安定性が従レーザーに移乗したことを意味する．

さらにこの方法の性能を向上させると両レーザー間の位相誤差を 1 rad 以下，すなわちヘテロダイン形光位相同期ループを実現することも可能である．このためにたとえば，あらかじめ主，従レーザー間のビート信号のスペクトル線幅を 1 MHz 以下にしておき制御利得 40〜50 dB，制御帯域 2〜3 MHz の同期用ループフィルタを使えばよいことが試算されている[20]．

一つの主レーザーを基準に複数個の従レーザーを周波数同期させ周波数同期網をつくると，これらすべてのレーザーからの合成光は互いに位相同期がかかっているので，ちょうどモード同期レーザー光と同等の状態になっている．すなわち，従来の非線形光学効果を使わずに超短光パルスを発生させることが可能である．

3.4　周波数の広帯域掃引

周波数掃引に重要なことはその範囲が広いことと同時に掃引中の周波数校正精度が高いこと，すなわち 3.1, 3.2 項に示した性能を保ちうることである．これを満たす掃引方法の一つが 3.3 項の周波数オフセット・ロック法である．すなわち，この方法で主，従レーザー間のビート周波数をマイクロ波周波数シンセサイザ周波数に同期させた状態でシンセサイザ周波数を掃引する．これによりビート周波数はシンセサイザ周波数に同期して掃引され，このとき**図 6** の曲線Aと同等の安定度が保たれる．したがって従レーザーも主レーザーと同等の安定度を保ったまま掃引される．

ビート周波数の掃引範囲すなわち周波数同期ループのロック・レンジはビート信号検出用光検出器の帯域によりきまり，アバランシェ・フォトダイオード (APD) を使うと 2 GHz[19] が得られている．3.1 項の方法で主レーザーをファブリ・ペロー干渉計の各共振周波数や有機分子の振動回転遷移のスペクトル線に次々と離散的に安定化し，そのたびに従レーザーに周波数オフセット・ロックを施すと上記のビート周波数のロック・レンジのもとで従レーザーの周波数掃引範囲を拡大できる．現在 AlGaAs レーザーに対し 60 GHz の掃引範囲が得られている[19]．この範囲は使用した AlGaAs レーザーのモード・ホッピング特性により制限されているが，今後動的単一モード・レーザーの使用により 1 THz まで拡大

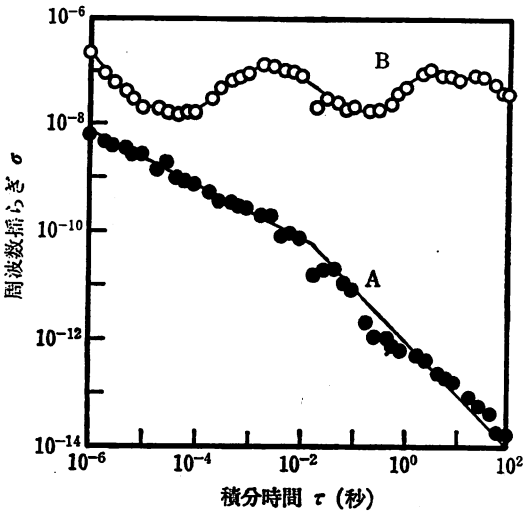

図 6　主，従レーザー間のビート周波数揺らぎの大きさを表わす分散 σ^2 の平方根とその測定の積分時間 τ との関係
曲線 A：制御時，曲線 B：非制御時

されると試算されている[2]．

4. 周波数制御のための問題点

半導体レーザーの周波数制御の性能を今後いっそう向上させるためには素子構造に関連するいくつかの問題を解決しなければならない．その第1は縦モードの単一性である．前章までの議論ではレーザーは一つの縦モードで発振すると仮定してきた．しかし，通常のファブリ・ペロー共振器形レーザー，さらに単一縦モード性のすぐれた分布帰還形 (DFB) レーザーでも実用上必ずしも単一モード発振が実現しているとは限らない．たとえば，静的測定によって一つの縦モード（主モード）に対し他の縦モード（副モード）のパワーが小さいことが確認されたとしても動的な実時間測定によると**図7**のように両モード間の競合により主モードパワーは瞬時的に減少する．このパワー・ドロップアウトのパルス幅およびその発生確率はバイアスレベルに逆比例して指数関数的に変化し，とくにパルス幅は 1 μs～1 ns の値をとる[21]．これは両モードに混入する自然放出光揺らぎ，およびキャリヤの伝導帯内緩和による相互利得飽和，レーザー発振の利得スペクトル幅にくらべ縦モード波長間隔が狭いこと，に起因する現象である[22]．

この現象を回避するには(1)高バイアスレベルで動作させること，(2)両モードの静的パワー比を常に 1000：1 以上にすること，が必要である．(1)を満足するには熱的に高安定，高信頼性の素子をつくることが必要である．(2)のためには両モードの共振器損失に差をつけること（DFB レーザーがこれにあてはまる）が行なわれている．素子試作段階では高いパワー比が得られるが，実用的なレーザー応用システムにはまだこのような高パワー比のレーザーは十分安定に供給されていない．(2)のためのより進んだ方法としては両モードの発振利得の差を大きくすることが考えられる．これにはレーザー長を短くして両モードの波長間隔を広げるのが一方法であるが，この場合(1)式の κ の増加に伴うパワー低下，および周波数揺らぎ増加をひきおこすので，むしろ量子井戸[23]などの新構造，さらには新材料を用いて利得スペクトルの幅を狭くすべきである．

第2の問題点は長期にわたる周波数ドリフトである．AlGaAs レーザーの周囲温度揺らぎを 10^{-5}℃ 以内，注

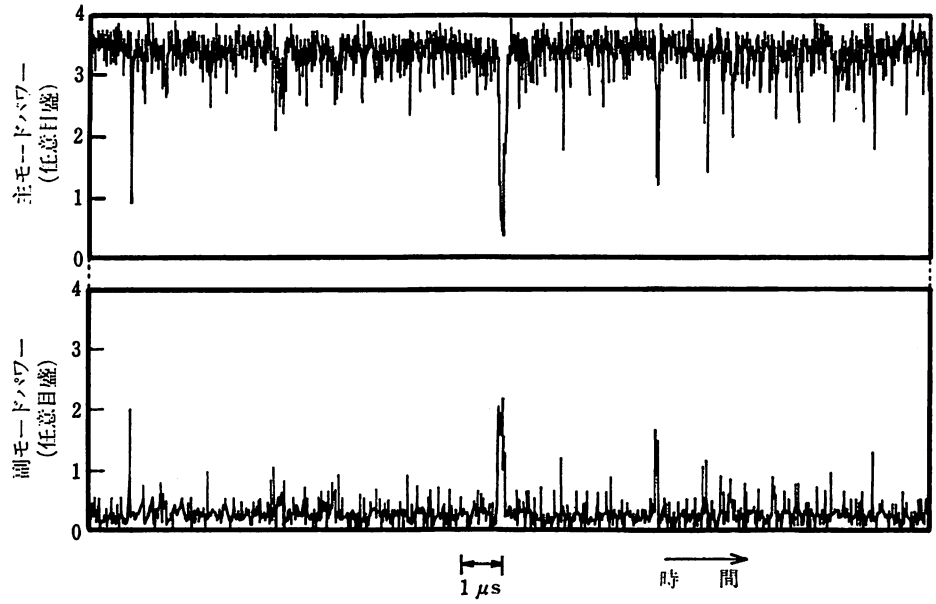

図 7　ほぼ単一縦モードで発振している AlGaAs レーザーの主モードと副モードのパワーの時間変化

入電流揺らぎを 0.6 nA/$\sqrt{\text{Hz}}$ 以内に抑圧した超高安定環境下で約6カ月にわたり周波数のドリフトを測定すると約 20 MHz/h のブルーシフトが見られる[9]．これと同時にモードホッピング特性の経時変化も観測される．これらは In ボンディング層の酸化による熱抵抗の変化，レーザー端面付近でのキャリヤの非放射再結合による熱効果などによると推定されている[24]．干渉測長などの光学計測では発振周波数の絶対値の再現性に対する要求が今後いっそう強くなると考えられるので，このような再現性，すなわちスペクトル寿命を向上させるために素子設計製作の段階での熱抵抗の低減とその経時変化の抑圧などの配慮が必要である．

第3の問題は周波数確度，再現性であるがこれらについてはまだ十分な実験的検討がなされていない．3.1 項で記した基準周波数の温度シフト，さらに上記の長期ブルーシフトが確度，再現性を制限する．また，安定化された周波数を高精度測定する手法も必要である．現在のところ測定精度は 10^{-7} であるが[3,4]，高精度干渉測長などへの応用にはさらに測定精度向上が必要となる．

5. 高安定半導体レーザーの光学的応用

半導体レーザーは小型，低消費電力，長寿命であるため光学分野での応用は多数あるが，代表的な例を列挙すると次のようなものが考えられる．光ファイバ応用測定およびセンサー，ドップラー流速計による血流速度測定や振動面の振動速度測定[25]，ホログラフィ，1 m～1 km の範囲の距離測定用の測距儀，半導体材料を加工する際の露光用マスクの位置決め，慣性航法用ファイバジャイロ[26]，地震予知・地球の極運動測定・惑星探査用高感度ファイバジャイロ[27]，大気中の汚染気体濃度測定およびレーザーレーダー[28]，マイクロ波領域の高精度セシウム，ルビジウム原子発振器の光励起[29]，計測用波長標準，長さ標準．

6. あ と が き

本稿ではまず半導体レーザーは原理的にはきわめて周波数安定度の高い光源となる可能性を指摘し，さらに4項目に関しその実験結果を示した．一方，半導体レーザー素子そのものに注目するとまだいくつかの問題点があり，周波数安定性の点ではまだ不十分な段階である．これらの問題を克服し，より信頼性の高い周波数安定化半導体レーザーを実現するためには新素子設計，周辺素子の高性能・集積化，制御法の改良，などを有機的に行なう必要があろう．

文　献

1) M. Ohtsu and N. Tabuchi: "Electrical feedback and its network analysis for linewidth reduction of a semiconductor laser," J. Lightwave Technol., **LT-6** (1988) 357-369.
2) M. Ohtsu: "Realization of ultrahigh coherence in semiconductor lasers by negative electrical feedback," J. Lightwave Technol., **LT-6** (1988) 245-256.
3) K. Fukuoka, M. Ohtsu and T. Tako: "Accurate wavelength measurements of the absorption lines in H_2O vapor by a 0.8 μm AlGaAs laser," Jpn. J. Appl. Phys., **23** (1984) L 117-L 120.
4) M. Ohtsu, H. Kotani and H. Tagawa: "Spectral measurements of NH_3 and H_2O for pollutant gas monitoring by 1.5 μm InGaAsP/InP lasers," Jpn. J. Appl. Phys., **22** (1983) 1553-1557.
5) V. Pevtschin and S. Ezekiel: "Investigation of absolute stability of water-vapor-stabilized semiconductor laser," Opt. Lett., **12** (1987) 172-174.
6) T. Yabuzaki, A. Ibaragi, H. Hori, M. Kitano and T. Ogawa: "Frequency locking of a GaAlAs laser to a Doppler-free spectrum of the Cs-D_2 line," Jpn. J. Appl. Phys., **20** (1981) L 451-L 454.
7) H. Tsuchida, M. Ohtsu, T. Tako, N. Kuramochi and N. Oura: "Frequency stabilization of AlGaAs semiconductor laser based on the ^{85}Rb-D_2 line," Jpn. J. Appl. Phys., **21** (1982) L 561-L 563.
8) 古田浩之，橋本　実，大津元一："半導体レーザーの周波数絶対安定度評価"，「レーザー・原子発振器の周波数制御と応用」第2回シンポジウム予稿集（応用物理学会量子エレクトロニクス研究会，1987) pp. 71-77.
9) M. Ohtsu, M. Hashimoto and H. Ozawa: "A highly stabilized semiconductor laser and its application to optically pumped Rb atomic clock," *The 39th Annual Symposium of Frequency Control* (IEEE Sonics and Ultrasonic Group, 1985) pp. 43-53.
10) M. Ohtsu, H. Fukada, T. Tako and H. Tsuchida: "Estimation of the ultimate frequency stability of semiconductor lasers," Jpn. J. Appl. Phys., **22** (1983) 1157-1166.
11) 加藤　徹，久保木勝彦，大津元一："周波数オフセットロックシステムの性能評価"，「レーザー・原子発振器の周波数制御と応用」第2回シンポジウム予稿集（応用物理学会量子エレクトロニクス研究会，1987) pp. 69-70.
12) たとえば，The Newport Catalog with Applications, No. 100 (1987) H 2-H 3.
13) D. Hills and J. L. Hall: "Progress toward phase-stable lasers," *Technical Digest of the 15th International Quantum Electronics Conference*, Baltimore, MA, WDD 3 (1987) pp. 102-103.
14) 村田守啓，大津元一："高フィネス・ファブリ・ペロー共振器の反射モードによる半導体レーザの FM 雑音抑圧，" 第35回応用物理学関係連合講演会，29 p ZP 9 (1988).
15) R. Wyatt and W. J. Devlin: "10 kHz linewidth 1.5 μm InGaAsP external cavity laser with 55 nm tuning range," Electron. Lett., **19** (1983) 110-112.
16) B. Dahmani, L. Hollberg and R. Drullinger: "Frequency stabilization of semiconductor lasers by resonant optical feedbaack," Opt. Lett., **12** (1987) 876-878.
17) 大津元一："周波数変調可能な狭スペクトル線幅半導体レーザ"，電子情報通信学会技術研究報告，12 月 (1987)

OQE 87-135.
18) K. Kuboki and M. Ohtsu: "Frequency offset locking of AlGaAs semiconductor lasers," IEEE J. Quantum Electron., **QE-23** 1987) 388-394.
19) 久保木勝彦，加藤　徹，申哲　浩，大津元一："半導体レーザの周波数オフセット・ロック"，「レーザー・原子発振器の周波数制御と応用」第2回シンポジウム予稿集（応用物理学会量子エレクトロニクス研究会，1987) pp. 67-68.
20) 申　哲浩，久保木勝彦，加藤　徹，大津元一："半導体レーザによるヘテロダイン型光位相同期ループの実現のためのシミュレーション"，第35回応用物理学関係連合講演会，29 p ZP 14 (1988).
21) 中原敏夫，寺町康昌，大津元一："擬単一モード半導体レーザのモード分配雑音の評価"，第35回応用物理学関係連合講演会，29 p ZP 6 (1988).
22) 宮崎哲弥，中村康治，大津元一，寺町康昌："半導体レーザの縦モード安定性の実験と解析"，電子情報通信学会技術研究報告，3月 (1987) OQE 86-189.
23) R. Chin, N. Holonyak, Jr. and B. A. Vojak: "Temperature dependence of threshold current for quantum-well $Al_xGa_{1-x}As$ heterostructure laser diodes," Appl. Phys. Lett., **36** (1980) 19-21.
24) F. Favre and D. Le Guen: "Emission frequency stability in single-mode-fibre optical feedback controlled semiconductor lasers," Electron. Lett., **19** (1983) 663-665.
25) F. Durnst, A. Melling and J. H. Whitelaw: *Principle and Practice of Laser-Doppler Anemometry* (Academic Press, New York, 1976).
26) T. G, Giallorenzi, J. A. Bucaro, A. Dandridge, G. H. Sigel, Jr., J. H. Cole, S. C. Rashleigh and R. C. Priest: "Optical fiber sensor technology," IEEE J. Quantum Electron., **QE-18** (1982) 626-665.
27) M. Ohtsu and S. Araki: "Using a 1.5 μm DFB InGaAsP laser in a passive ring cavity-type fiber gyroscope," Appl. Opt., **26** (1987) 464-470.
28) N. Takeuchi, H. Baba, K. Sakurai and T. Ueno: "Diode-laser random-modulation cw lidar," Appl. Opt., **25** (1986) 63-67.
29) M. Hashimoto and M. Ohtsu: "Experiments on a semiconductor laser pumped rubidium atomic clock," IEEE J. Quantum Electron., **QE-23** (1987) 446-451.

"PERFORMANCE AND ITS EVALUATION OF OPTICAL TRACKING GENERATOR/ OPTICAL FREQUENCY SYNTHESIZER BY SEMICONDUCTOR LASERS"

K. Kuboki, C. H. Shin, T. Kato and M. Ohtsu
Graduate School at Nagatsuta, Tokyo Institute of Technology
4259, Nagatsuta, Midori-ku, Yokohama
Kanagawa 227, Japan

Abstract

Optical tracking generator/ Optical frequency synthesizer by semiconductor lasers was developed. Residual frequency fluctuations of the heterodyne signal were 3.7(Hz) at τ = 100s. Frequency of the heterodyne signal could be swept for 0.02 GHz $\leq \nu_B \leq$ 2.03 GHz, and overall frequency tunable range of the slave laser was 64.3 GHz.

Introduction

Heterodyne type optical frequency locked loop and wideband optical frequency tunable system are indispensable for coherent optical communications, coherent optical measurements, and so on. For this purpose, frequency control of semiconductor lasers by negative electrical feedback was proposed to realize optical tracking generator/ optical frequency synthesizer [1], and the results of the preliminary experiment had been reported [2]. In the present study, further improvements of the performance of this system are reported.

Experimental Setup

Fig.1 shows an experimental setup. Two 0.8μ m AlGaAs lasers were employed as the master and the slave laser, respectively. The center frequency of the master laser was stabilized, and its spectral linewidth was also reduced by using a Fabry-Perot resonator as a frequency reference. The injection current of the slave laser was controlled in order that the frequency of the heterodyne signal between the two lasers could be locked to the stable radio frequency synthesizer. In other words, high coherence of the master laser was transferred to the slave laser by this control. Two feedback loops were employed as shown in Fig.1. One was a narrowband feedback loop to reduce a long-term frequency drift of the heterodyne signal. In this loop, the scaling factor of the prescaler for the heterodyne frequency was decreased to 50 to realize further reduction of the drift than that by the previous system [2]. The other was a wideband feedback loop to improve a short-term frequency stability, which has not been used in the previous system [2]. Frequencies of the heterodyne signal and slave laser could be swept in a stable manner by sweeping the synthesizer frequency under the condition of frequency locking. To realize a wider range of stable frequency sweep, a double balanced mixer and a synthesizer #3 was added in the loop (see Fig.1) for frequency down-conversion. The Allan variance $\sigma^2_{yB}(\tau)$ of residual frequency fluctuations of the heterodyne signal was used to evaluate this system quantitatively. The Allan variance real-time processing system (ARPS), which has been developed by the authors [3], was improved in order that the shortest measurable integration time could be extended to 1 μ s. To measure the Allan variance, the frequency of the signal is counted by TTL counters in the improved ARPS. Then the counted data are stored in RAM's at every integration time τ with no deadtime of measurement. When the number of the data is reached to a preset sample number N (= 100), these are transferred to the computer. The Allan variance is calculated with these data by the computer, and then the results are plotted on the X-Y plotter. By this improvement, the measurement time of the Allan variance was reduced to 1/6 and the Allan variance could be measured more precisely than that by the previous system for 1μ s $\leq \tau \leq$ 100 s.

Experimental Results

Residual frequency fluctuations of the master laser were reduced to $\sigma_{yM} = 6.4 \times 10^{-11} \cdot \tau^{-0.8}$ for 1μ s $\leq \tau <$ 100 ms, and 3.9×10^{-10} for 100 ms $\leq \tau \leq$ 100 s. The spectral linewidth of the master laser was reduced to 100kHz. Fig.2 shows the square root of the Allan variance $\sigma_{yB}(\tau)$ of the heterodyne signal. The value of curve B in Fig.2 is approximated as $\sigma_{yB}(\tau) = 8.1 \times 10^{-12} \cdot \tau^{-1/2}$ (1μ s $\leq \tau <$ 20 ms), $1.0 \times 10^{-12} \cdot \tau^{-1}$ (20 ms $\leq \tau \leq$ 100 s). In particular, the high stability of $\sigma_{yB} = 1.0 \times 10^{-14}$ was obtained at τ= 100 s, i.e., frequency fluctuations were only 3.7 Hz. (Previous result was 11 Hz [2].) Since frequencies of the master laser and the heterodyne signal were controlled by using different and independent feedback loops, their residual fluctuations can be considered as being mutually uncorrelated. Therefore, the Allan variance for frequency fluctuations of the slave laser $\sigma^2_{yS}(\tau)$ can be expressed as $\sigma^2_{yS}(\tau) = \sigma^2_{yM}(\tau) + \sigma^2_{yB}(\tau)$. It can be estimated from the experimental results that $\sigma^2_{yB}(\tau) \ll \sigma^2_{yM}(\tau)$, from which the relation of $\sigma^2_{yS}(\tau) \cong \sigma^2_{yM}(\tau)$ was derived, i.e., the residual frequency fluctuations of the slave laser were reduced as low as those of the master laser. It can be confirmed from these results that accurate frequency tracking to the master laser was realized, in other words, high coherence of the master laser was transferred to the slave laser. Fig.3 shows a result of stepwise sweep of the heterodyne frequency ν_B by sweeping of the synthesizer frequency at the 5 MHz interval. A stable sweep could be carried out in the range of 0.02 GHz $\leq \nu_B \leq$ 2.03 GHz. (Previous result was 0.08 GHz $\leq \nu_B \leq$ 1.3 GHz [2].) Fig.4 shows the transmission spectral lineshape of the Fabry-Perot resonator which were used as the frequency reference for the frequency locking of the master laser. As the master laser frequency could be locked to the slopes of its successive sixteen resonance spectral lines, the frequency sweep of the slave laser was extended to 64.3 GHz. (Previous result was 37 GHz [2].)

Summary

Optical tracking generator/ Optical frequency synthesizer by semiconductor lasers was developed. The square root of the Allan variance $\sigma_{yB}(\tau)$ of residual frequency fluctuations of the heterodyne signal was $\sigma_{yB}(\tau) = 8.1 \times 10^{-12} \cdot \tau^{-1/2}$ (1μs $\leq \tau <$ 20 ms) and $1.0 \times 10^{-12} \cdot \tau^{-1}$ (20 ms $\leq \tau \leq$ 100 s). In particular, frequency fluctuations were reduced to only 3.7 Hz at τ = 100 s. Frequency sweep of the heterodyne signal was carried out for 0.02 GHz $\leq \nu_B \leq$ 2.03 GHz, and the frequency tunable range of the slave laser was extended to 64.3 GHz. From these results, it was confirmed that the performance of the present system was considerably improved as compared with that of the previous system [2] by several improvements on the loop and the measuring system.

References

[1] M.Ohtsu, "Realization of Ultrahigh Coherence in Semiconductor Lasers by Negative Feedback," IEEE J. Lightwave Technol., to be published in January 1988.

[2] K.Kuboki and M.Ohtsu, "Frequency Offset Locking of AlGaAs Semiconductor Lasers," IEEE J. Quantum Electron., vol. QE-23, pp. 388-394, April 1987.

[3] I.Siio, M.Ohtsu, and T.Tako, "Development of the Allan variance real-time processor" (in Japanese), Trans. IECE Japan, vol. J64-C, pp. 204-208, 1981.

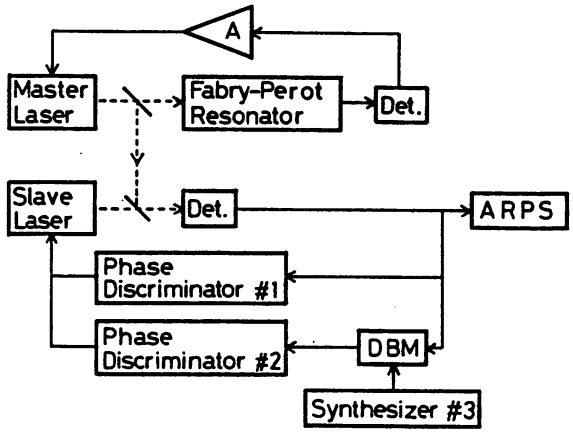

Fig.1 Experimental setup. Phase Discriminator #1 (wideband) was composed of an analogue wideband phase comparator and a frequency synthesizer #1. Phase Discriminator #2 (narrowband) was composed of a digital wide-dynamic-range phase comparator and a frequency synthesizer #2. A double balanced mixer (DBM) and a synthesizer #3 are for frequency down-conversion to expand the range of stable frequency sweep.

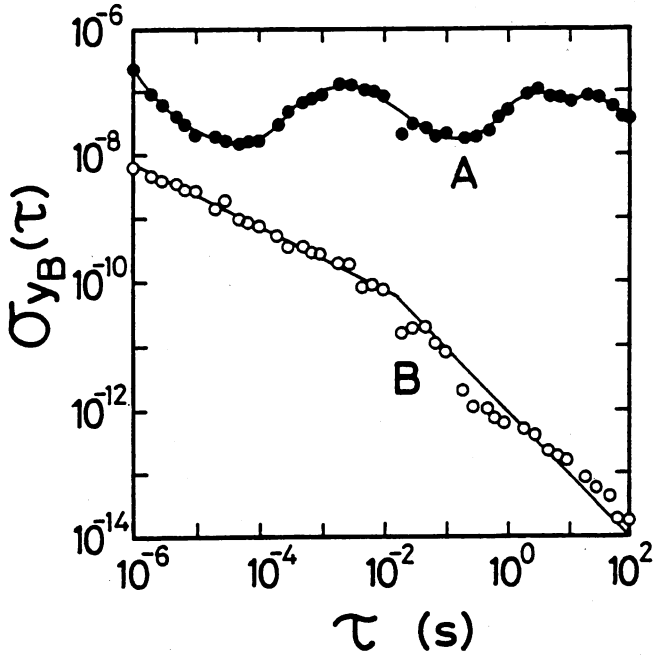

Fig.2 The square root of the Allan variance $\sigma_{yB}(\tau)$ of residual frequency fluctuations of the heterodyne signal.
A : Results of a free-running condition. B : Results under a frequency locking.

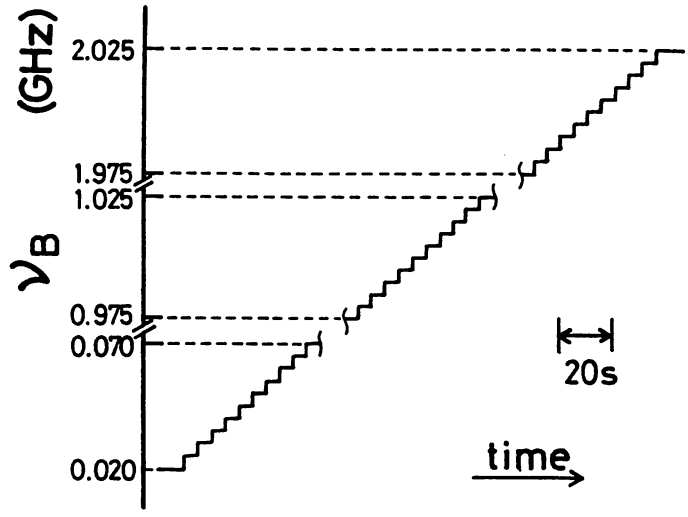

Fig.3 The heterodyne frequency ν_B which was varied by a stepwise sweep of the synthesizer frequency at 5 MHz interval.

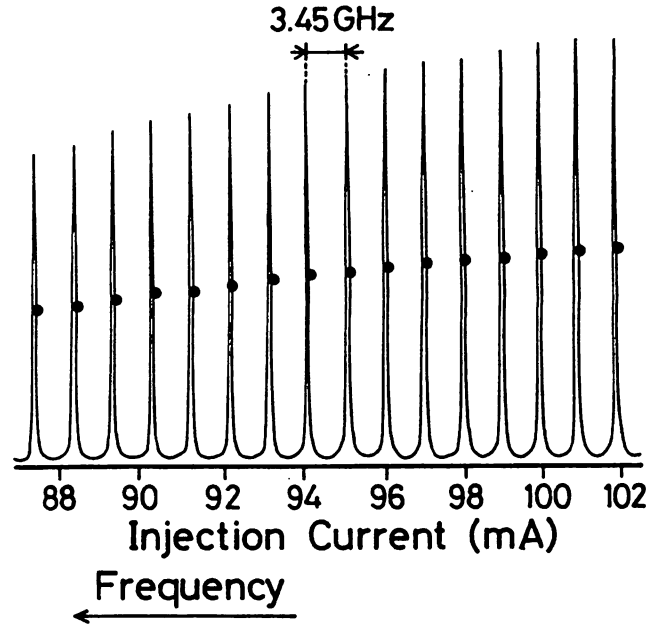

Fig.4 Transmission spectral lineshape of the Fabry-Perot resonator which was used as the frequency reference grid for the master laser. The circles are the points at which the master laser frequency was locked.

INTERFEROMETRIC METHOD FOR PREVENTING MODE-HOPPING IN TUNABLE EXTERNAL-CAVITY SEMICONDUCTOR LASERS

Indexing terms: Semiconductor lasers, Mode-hopping

A problem in frequency-tuning of external-cavity lasers is mode-hopping between neighbouring external-cavity modes. We demonstrate a new interferometric method for monitoring mode-hoping and an automatic control circuit for a 1·3 μm grating external-cavity laser that maintains single-mode operation when the lasing frequency is tuned.

The grating external-cavity laser[1,2] has been used as a narrow-linewidth tunable local oscillator in several experimental coherent optical-fibre communication systems. A problem in frequency-tuning of this laser, however, is mode-hopping between neighbouring external-cavity modes. Mode-hopping also occurs in the monolithic integrated tunable distributed Bragg reflector (DBR) laser.[3] We demonstrate in this letter an interferometric method for monitoring mode-hopping in a grating external-cavity laser and an automatic control circuit that maintains single-mode operation in the laser while the lasing frequency is tuned. The same method can be used to control a monolithic integrated external-cavity DBR laser.

The linewidth of an external-cavity laser decreases with the length of the external cavity. For an air external-cavity length of a few centimetres, which is required to reduce the linewidth to about 100 kHz, the longitudinal mode spacings are several gigahertz. These closely spaced modes cannot be resolved by a grating monochromator. Although a Fabry–Perot interferometer has sufficient resolution, the instrument is bulky and the

alignment may drift with time. We found, however, that the heterodyned signal between two closely spaced cavity modes can be detected using a wideband photodiode and can be used for mode-hopping monitoring.

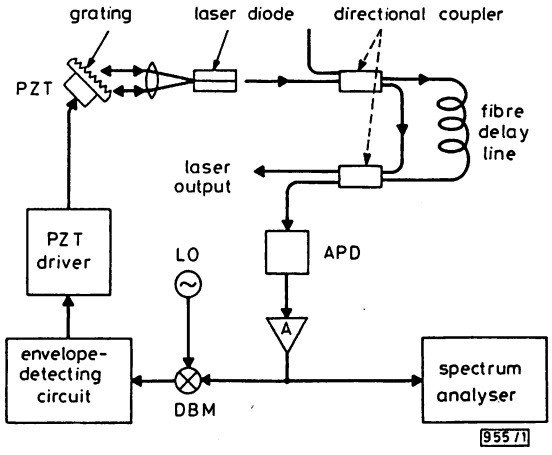

Fig. 1 *Experimental apparatus*

LO is a microwave local oscillator, DBM is a double balanced mixer and APD is an avalanche photodiode

The experimental set-up is shown in Fig. 1. A fibre Mach-Zehnder interferometer and an avalanche photodiode were used for heterodyning the optical fields of the two hopping modes. A tunable external-cavity laser was constructed by optically coupling a 1·3 μm semiconductor laser chip to a diffraction grating mounted on a piezoelectric transducer (PZT), as shown in Fig. 1. The semiconductor laser facet on the grating side was antireflection-coated and was coupled to the grating by an objective lens of 0·85 numerical aperture. The grating can be rotated for wideband frequency-tuning and the PZT voltage can be adjusted for fine tuning. However, a large change in the PZT voltage or grating angle introduces hopping to successive longitudinal modes. The length of the external-cavity laser used in the experiment was 7·5 cm, which gave a longitudinal mode spacing of about 2 GHz. Fig. 1 also shows the other components used in the automatic control circuits, which will be discussed later.

During mode-hopping between two neighbouring external-cavity modes, the electric field of the total laser light can be expressed as

$$E(t) = \alpha_1(t)E_1(t) + \alpha_2(t)E_2(t) \quad (1)$$

where E_1 and E_2 are the electric fields of the two hopping modes, and α_1, α_2 are random variables with $\alpha_1(t) + \alpha_2(t) = 1$. The photocurrent of the avalanche photodiode (APD) located after the Mach–Zehnder interferometer gives a heterodyned signal between the two modes, which is expressed as

$$i \propto \alpha_1(t)\alpha_2(t-\tau_d)E_1(t)E_2(t-\tau_d) + \alpha_1(t-\tau_d)\alpha_2(t)E_1(t-\tau_d)E_2(t) \quad (2)$$

where τ_d is the delay time due to the fibre delay line of the interferometer.

Since the 2 GHz separation between the two neighbouring external-cavity modes is smaller than the inverse of the intra-band relaxation time, the two modes are strongly coupled and are expected to exhibit complete power switching during mode-hopping,[4] i.e. $\alpha_1(t)$ and $\alpha_2(t)$ take a value of either 0 or 1. Since $\alpha_1(t) + \alpha_2(t) = 1$, we have $\alpha_1(t)\alpha_2(t) = 0$. From eqn. 2 the photocurrent i is not equal to zero only when a delay line is used, so that $\tau_d > 1/f_c$, where f_c is the average mode-hopping frequency. Because of finite mode-hopping transit times, however, mode-hopping can still be detected without a delay line, but the signal level is smaller than that detected with a delay line.

When the grating angle or the PZT voltage was controlled to generate mode-hopping in the laser, the spectrum analyser displays in Fig. 2 show the heterodyned mode-hopping signals A, detected with a 2·8 km fibre delay line, and B, detected without the delay line. The peak height of B is about 28 dB lower than A. The 2·8 km fibre in this experiment provides effectively an infinitely long delay line, which removes the $\alpha_1\alpha_2 = 0$ anticorrelation relationship. On the other hand, the signal level B is related to the mode-hopping transit times and the average mode-hopping frequency in the external-cavity laser. The averaged mode-hopping frequency f_c was estimated to be in the range 0·5 MHz to 2·5 MHz for the external-cavity laser with 7·5 cm length. Therefore a delay line of several hundred metres will be long enough to satisfy the $\tau_d > 1/f_c$ relationship to achieve a stable, high-sensitivity mode-hopping signal.

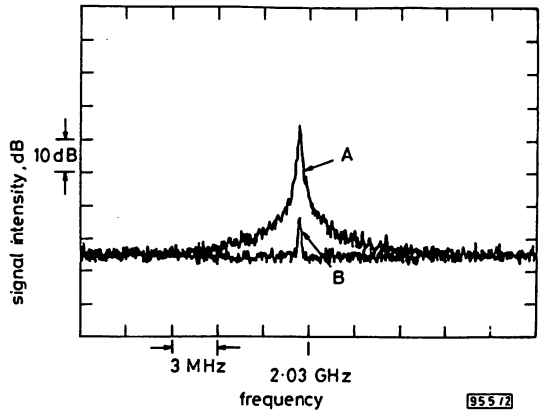

Fig. 2 *Spectrum analyser displays of mode-hopping signal near 2 GHz*

A is signal obtained with a 2·8 km fibre delay line and B without using delay line

Mode-hopping prevention in the grating external-cavity laser was demonstrated using the circuit shown in Fig. 1. The separation between successive external-cavity modes is about 2 GHz. The mode-hopping monitoring signal, at the 2 GHz beat frequency between the two neighbouring modes, was heterodyned with a microwave local oscillator (LO) using a double balanced mixer to down-shift the signal frequency. After envelope detection, the signal was negatively fed back to a PZT control circuit, which adjusts the cavity length automatically to maintain single-mode operation. In the experiment, the grating angle was fixed and the PZT voltage was swept, which generated mode-hopping events. When the control loop was open, the two-mode spectrum during mode-hopping is shown clearly in the scanning Fabry–Perot interferometer output recorded in Fig. 3*a*. The spectrum analyser display in Fig. 3*b* shows the corresponding mode-hopping signal at about 2 GHz frequency: the peak on the right-hand side of the microwave LO peak. On the contrary, when the control loop was closed and the PZT voltage was swept, the laser always remained single-mode as shown in Fig. 3*c*, and

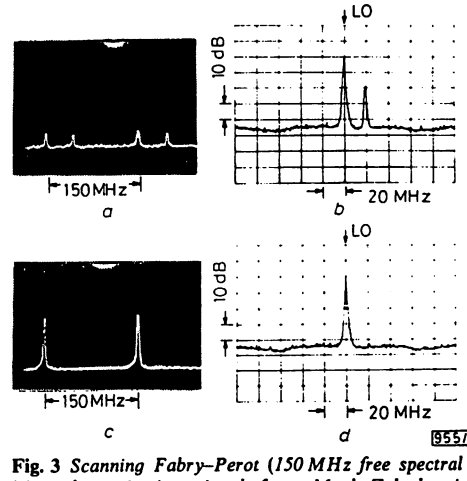

Fig. 3 *Scanning Fabry–Perot (150 MHz free spectral range) spectrum (a) and monitoring signal from Mach–Zehnder interferometer (b) showing two-mode-hopping when control loop was open*

c, *d* show single-mode operation when feedback loop was closed. LO peak is from microwave local oscillator, and peak next to LO peak in (*b*) indicates mode-hopping

the mode-hopping signal peak disappeared in Fig. 3*d*. Wide-range frequency-tuning by grating rotation is still accomplished by mode-hopping, but the automatic feedback loop controls the PZT voltage to fine-tune the frequency of the selected external-cavity mode and maintains single-mode operation.

In summary, we have demonstrated a new mode-hopping detection method for a grating external-cavity laser and an automatic mode-hopping prevention circuit. This method can be used for a laser with a long cavity length for which the heterodyned signal between adjacent cavity modes can be detected with a photodiode. It can be applied, for example, to a monolithic integrated tunable laser in the future if the integrated passive cavity length of the laser is longer than about 0·5 cm.

M. OHTSU*
K.-Y. LIOU
E. C. BURROWS
C. A. BURRUS
G. EISENSTEIN

AT&T Bell Laboratories
Crawford Hill Laboratory
Holmdel, NJ 07733, USA

* On leave from Tokyo Institute of Technology

24th August 1987

References

1 WYATT, R., and DEVLIN, W. J.: '10 kHz-linewidth 1·5 μm InGaAsP external cavity laser with 55 nm tuning range', *Electron. Lett.*, 1983, **19**, pp. 110–112

2 OLSSON, N. A., and VAN DER ZIEL, J. P.: 'Performance characteristics of 1·5 μm external cavity semiconductor lasers for coherent optical communication', *J. Lightwave Technol.*, 1987, **LT-5**, pp. 501–515

3 MURATA, S., MITO, I., and KOBAYASHI, K.: 'Over 720 GHz (5·8 nm) frequency tuning by a 1·5 μm DBR laser with phase and Bragg wavelength control regions', *Electron. Lett.*, 1987, **23**, pp. 403–405

4 OHTSU, M., TERAMACHI, Y., OTSUKA, Y., and OSAKI, A.: 'Analyses of mode-hopping phenomena in an AlGaAs laser', *IEEE J. Quantum Electron.*, 1986, **QE-22**, pp. 535–543

Mode Stability of a Two-Wavelength Fabry–Perot/ Distributed-Feedback Laser

MOTOICHI OHTSU AND KANG-YIH LIOU

Abstract—**A theory based on a Fokker–Planck equation has been developed to analyze the observed two-mode operation of a Fabry–Perot/ distributed-feedback (FP/DFB) laser. Simultaneous oscillation of the DFB mode and the FP mode near the gain peak with negligible mode power fluctuation can be achieved if the DFB mode is detuned sufficiently from the gain peak. We present calculated results for the design of stable two-wavelength lasers.**

I. Introduction

BY PROPERLY detuning the Bragg wavelength of a distributed-feedback (DFB) semiconductor laser away from the peak wavelength of the gain spectrum, simultaneous oscillation of the DFB mode near the Bragg wavelength and the Fabry–Perot (FP) mode near the gain peak can be achieved. Such a two-wavelength laser can be used for measurement of fiber dispersion or for interferometric sensing. The dispersion of fiber can be determined directly from the spreading of a light pulse consisting of two wavelengths propagating in the fiber. For precise distance measurements, a two-wavelength method has been used for correcting the error caused by the fluctuation of the index of refraction [1]–[3]. In the case of temperature measurements, a two-wavelength technique has been developed to increase the sensing range for an interferometric fiber temperature sensor [4]. A stable two-wavelength semiconductor laser designed using the FP/DFB scheme can be an attractive light source for these applications.

We present in this paper calculations of the longitudinal mode stability for the design of a stable two-wavelength semiconductor laser and the observed stable two-wavelength operation of FP/DFB laser. The emission wavelength of the FP/DFB laser in the experiment was 1.3 μm. The theory, however, is general for all wavelengths. Using a stochastic approach, the stability of the two lasing modes is calculated as a function of a coupling parameter or the wavelength separation between the two modes. The results show that FP/DFB lasers can be designed to oscillate with two stable wavelengths.

Manuscript received April 10, 1986; revised May 18, 1987.

M. Ohtsu is with AT&T Bell Laboratories, Crawford Hill Laboratory, Holmdel, NJ 07733, on leave from Tokyo Institute of Technology, Tokyo, Japan.

K.-Y. Liou is with AT&T Bell Laboratories, Crawford Hill Laboratory, Holmdel, NJ 07733.

IEEE Log Number 8717511.

II. Experimental Observations

In general, DFB lasers are designed to oscillate near the Bragg wavelength, which is usually set well within 100 Å of the gain peak to achieve stable single-mode operation. In our experiment, we used DFB lasers with the Bragg wavelength detuned from the gain peak to demonstrate the feasibility of stable two-wavelength operation. The DFB lasers were of the double-channel planar-buried-heterostructure (DC-PBH) type and had second-order gratings [5]. The emitting wavelengths were near 1.3 μm. Fig. 1 shows the longitudinal mode spectrum of a DFB laser with the DFB mode detuned to about 110 Å shorter than the gain peak. The laser was operated CW (continuous wave) at 25°C. The two-wavelength spectrum with nearly equal DFB and FP mode intensities shown in the figure is due to similar threshold conditions for the DFB and FP modes. Here the decrease in gain for the DFB mode detuned from the gain peak is compensated for by the smaller loss for the DFB mode than for the FP mode due to the distributed reflection near the Bragg wavelength.

Fig. 1 is a time averaged spectrum recorded using a grating spectrometer. Temporal mode power stability was examined when only one mode was passed by the spectrometer and was detected with a high-speed InGaAs p-i-n photodiode. The result indicated stable two-wavelength operation with a 110-Å separation for the laser shown in Fig. 1. The detected light power for each of the two modes stayed constant in time and the total output power of the two modes was also stable. In another case, when the wavelength spacing between two lasing modes with equal average intensities was about 10 Å, instantaneous power switching between the two modes was observed. The detected total output power, however, still remained constant in time.

The observed two-mode competition behavior for the FP/DFB laser is qualitatively similar to that previously reported for AlGaAs FP lasers emitting near 0.8-μm wavelength [6]. The dependence of the two-mode stability on the wavelength separation is due to the fact that the coupling between the two modes decreases with increasing wavelength separation. The laser operates with two stable modes without mode switching when the coupling between them becomes negligible.

Mode switching phenomena in semiconductor lasers

0733-8724/88/0100-0047$01.00 © 1988 IEEE

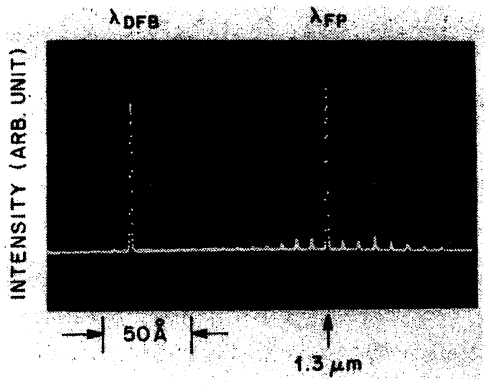

Fig. 1. Longitudinal mode spectrum of a Bragg wavelength detuned DFB laser showing simultaneous oscillation of the DFB mode and the FP mode. The laser was CW operated at 25°C with 3-mW/facet output power.

due to optical feedback effects or temperature fluctuations have been reported previously [7]–[9]. Optical isolators were used in our experiment to suppress the optical feedback effect and the temperature of the laser was stabilized to observe mode switching and mode power fluctuations caused mainly by the spontaneous emission noise.

The experimental results indicate that stable two-wavelength operation with similar light powers can be achieved for a FP/DFB laser if 1) the FP mode and the DFB mode have similar threshold gains and 2) the wavelength separation between them is sufficiently large. Condition 1) can be satisfied by controlling the amount of detuning of the Bragg wavelength from the gain peak and the coupling coefficient of the grating, such that the decrease in mode gain for the detuned DFB mode equals the decrease in the effective end loss due to the distributed reflection. Condition 2), however, is more complicated, and we will see later that the temporal stability is also related to the CW pumping level of the laser. In the following theoretical discussions, we will then analyze the two-mode stability under the condition that the two lasing modes have nearly equal time-averaged light powers.

III. Theory

In the theory, a stochastic approach is used to calculate the stability for the two-mode condition. We start with the two-mode rate equations for the square of the optical electric field $\tilde{E}_i$ and for the carrier density $n^{(0)}$ which are written in the density matrix formalism [10]

$$\frac{d\tilde{E}_i^2}{dt} = \frac{1}{n\sqrt{\epsilon_0\mu_0}}\left[\tilde{\alpha}_i^{(1)} - \alpha_{thi} - \tilde{\alpha}_i^{(3)}\tilde{E}_i^2 - \tilde{\alpha}_{ij}^{(3)}\tilde{E}_j^2\right]\tilde{E}_i^2 \qquad (i, j = 1, 2;\ i \neq j) \qquad (1)$$

$$\frac{dn^{(0)}}{dt} = -n\sqrt{\frac{\epsilon_0}{\mu_0}}\left(\frac{2}{\hbar\omega_1}\tilde{\alpha}_1^{(1)}\tilde{E}_1^2 + \frac{2}{\hbar\omega_2}\tilde{\alpha}_2^{(1)}\tilde{E}_2^2\right) - \frac{n^{(0)}}{\tau_s} + \frac{I}{Ve} \qquad (2)$$

where the subscripts $i = 1$ and 2 represent the DFB mode and the FP mode, respectively; n is the refractive index, ϵ_0 and μ_0 are the dielectric constant and the permeability in vacuum, $\hbar\omega$ is the photon energy, V is the volume of the laser cavity, I is the injection current, and e is the electronic charge. The quantity α_{thi} in (1) is the loss of the laser cavity. For the FP mode, α_{thi} is the sum of the internal loss and the mirror loss at the facets. For the DFB mode, α_{thi} includes an additional loss factor owing to the distributed grating reflection, which is dependent on the grating coupling coefficient [11]. The quantities $\tilde{\alpha}_i^{(1)}$, $\tilde{\alpha}_i^{(3)}$, and $\tilde{\alpha}_{ij}^{(3)}$ are, respectively, a linear gain, the self-saturation coefficient, and the cross-saturation coefficient, which are all dependent on the carrier density $n^{(0)}$ given by (2).

To a first-order approximation, the gain saturation due to interband relaxation of the carriers with time constant τ_s is expressed by a decrease in $\tilde{\alpha}_i$ in (1) via (2). Equation (2), however, does not include the intraband relaxation, with relaxation time τ_{in} [10]. To consider gain saturation due to intraband relaxation, we include in (1) the third-order terms with the coefficients $\tilde{\alpha}_i^{(3)}$ and $\tilde{\alpha}_{ij}^{(3)}$. It is important to note that the gain saturation expressed by $\tilde{\alpha}_i^{(1)}$ via (2) and that expressed by $\tilde{\alpha}_i^{(3)}$ and $\tilde{\alpha}_{ij}^{(3)}$ are of different origins.

From our experimental measurements, discussed in the previous section for the case of two lasing modes with equal time-averaged powers, the total output power remains nearly constant in time even though the power of each mode can fluctuate. This is because the total power is partitioned into the two modes which fluctuate in an anticorrelated fashion due to mode competition. Under this condition, the carrier density in (2) can be approximated as being constant in time. The validity of this approximation, even in the case of mode hopping among two longitudinal modes, has been verified by computer simulations and experiments for AlGaAs lasers [6], [12]. The ratio of carrier fluctuation to the threshold carrier density $\delta n^{(0)}/n_{th}^{(0)}$ estimated by computer simulation, is of the order of 10^{-4}–10^{-3} [12]. The result of computer modeling of mode hopping in AlGaAs lasers using the constant-carrier-density approximation agrees well with experimental observations [6].

For a constant $n^{(0)}$, the coefficients $\tilde{\alpha}_i^{(1)}$, $\tilde{\alpha}_i^{(3)}$, and $\tilde{\alpha}_{ij}^{(3)}$ in (1) can also be approximated as time independent constants. To calculate the magnitudes of the power fluctuations for the two modes, we now need only to solve (1), from which we can derive the Langevin equations for the normalized electric field E_i

$$\frac{dE_i}{d\tau} = (a_i - |E_i|^2 - \xi|E_j|^2)E_i + q_i(\tau) \qquad (i, j = 1, 2;\ i \neq j) \qquad (3)$$

where τ is a normalized time, and $q_i(\tau)$ is a Langevin noise term which is assumed to be a delta-correlated Gaussian random process with a zero mean. The quantity a_i is a pump parameter which is proportional to the steady-

state mode power $(\tilde{\alpha}_i^{(1)} - \alpha_{thi})/\tilde{\alpha}_i^{(3)}$. It can be approximated by the expression

$$a_i = C_1(I/I_{th}) - C_2. \tag{4}$$

Although the constants C_1 and C_2 can vary from device to device, $C_1 \simeq 45$ and $C_2 \simeq 40$ have been measured for both 0.8 and 1.55-μm lasers at $I > 1.01\ I_{th}$ [6]. Power fluctuations of the DFB and FP modes arise from the coupling between them, which is described by the coupling constant ξ in (3), given by

$$\xi = \tilde{\alpha}_{ij}^{(3)}/\tilde{\alpha}_i^{(3)} = \tfrac{4}{3}/[1 + (2\pi c\tau_{in}\Delta\lambda/\lambda^2)^2] \tag{5}$$

where c and λ are the light velocity and wavelength in vacuum and $\Delta\lambda$ is the wavelength difference between the DFB and FP modes.

If we express the amplitude of the normalized complex field E_n as $E_n = x_n + iy_n$ with $n = 1, 2$ for the two modes, the state of the laser can be represented by the vector $\vec{x} = (x_1, x_2, y_1, y_2)$. The components of $\vec{x}$ obey a set of coupled Langevin equations of motion given by (3). Defining $p(\vec{x}, \tau)$ as the probability of finding the fields being characterized by $\vec{x}$ at time τ, one can then replace the coupled nonlinear equations of (3) with the linear multidimensional Fokker–Planck equation

$$\frac{\partial}{\partial\tau}p(\vec{x}, \tau) = \sum_{i=1}^{2}\left[-\frac{\partial}{\partial x_i}A_i^{(x)}p - \frac{\partial}{\partial y_i}A_i^{(y)}p + \left(\frac{\partial^2}{\partial x_i^2} + \frac{\partial^2}{\partial y_i^2}\right)p\right] \tag{6}$$

where

$$A_i^{(\eta)} = [a_i - (x_i^2 + y_i^2) - \xi(x_j^2 + y_j^2)]\eta_i \qquad (i, j = 1, 2;\ i \neq j, \quad \eta = x, y). \tag{7}$$

The time-dependent solution of (6) can be expressed as

$$p(\vec{x}, \tau) = p_s(\vec{x}) \cdot e^{-\gamma\tau} \cdot V(\vec{x}) \tag{8}$$

where $V(\vec{x})$ is the eigenfunction of the Fokker–Planck operator belonging to the eigenvalue γ. The function $p_s(\vec{x})$ is the steady-state solution, given by

$$p_s(\vec{x}) = B^{-1}\exp[-U(\vec{x})] \tag{9}$$

where B is a normalization constant and

$$U(\vec{x}) = \tfrac{1}{4}(I_1^2 + I_2^2 + 2\xi I_1 I_2) - \tfrac{1}{2}(a_1 I_1 + a_2 I_2) \tag{10}$$

with $I_1 = x_1^2 + y_1^2$, $I_2 = x_2^2 + y_2^2$.

To analyze the stability of the two-mode operation, we can use $p_s(\vec{x})$ to calculate the normalized variance of the intensity fluctuation

$$\sigma_i^2 \equiv \frac{\langle \delta I_i^2 \rangle}{\langle I_i \rangle^2} = \frac{\langle I_i^2 \rangle - \langle I_i \rangle^2}{\langle I_i \rangle^2} \tag{11}$$

where $\langle I_i^n \rangle$ is the nth moment of the mode intensity, given by

$$\langle I_i^n \rangle = \int_0^\infty\int I_i^n \cdot p_s(\vec{x})\, dI_1\, dI_2. \tag{12}$$

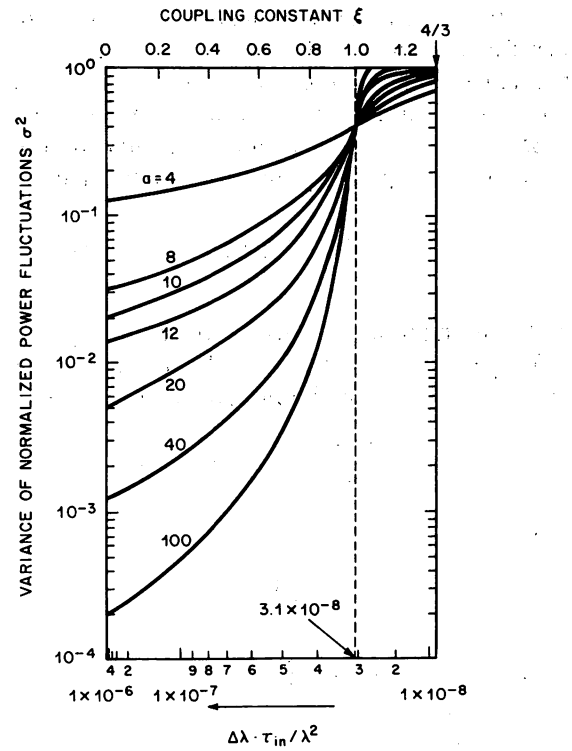

Fig. 2. Calculated variance σ^2 of normalized intensity fluctuations versus the coupling constant ξ between the DFB and the FP modes for different pumping levels a.

Fig. 2 shows the calculated variance of the intensity fluctuation at different pump parameters for the DFB mode as a function of the coupling constant ξ between the DFB and FP modes. Since ξ is related to $\Delta\lambda \cdot \tau_{in}$ given by (5), Fig. 2 is also plotted as a function of $\Delta\lambda \cdot \tau_{in}$. Fig. 2 is calculated with $a_1 = a_2 = a$ for the case that the DFB and FP modes have nearly the same intensity. A common critical point at $\xi = 1$ is found for all values of a. Discrete mode hops between the DFB mode and the FP mode due to a strong coupling occur for $\xi > 1$. In the weak coupling regime, where $\xi < 1$, DFB and FP modes oscillate simultaneously. We note that σ^2 decreases drastically with decreasing ξ and that stable two-wavelength operation with negligible mode power fluctuations can be achieved for a sufficiently large pumping level.

When Fig. 2 is used for designing a stable two-wavelength FP/DFB laser, one should note that the pump parameter a for the DFB mode is dependent on the coupling coefficient κ of the DFB grating. The wavelength difference $\Delta\lambda$ is determined by the detuning of the Bragg wavelength from the gain peak. The DFB to FP mode coupling ξ, however, is dependent on both $\Delta\lambda$ and the intraband relaxation time τ_{in}. Since ξ is dependent on the intraband relaxation time τ_{in} this phenomenon provides a way to determine τ_{in} accurately. One can measure σ^2 as a function of $\Delta\lambda/\lambda^2$ for a laser at different values of a. The intraband relaxation time τ_{in} is then determined by plotting σ^2 as a function of $\Delta\lambda/\lambda^2$ for different a values and then finding the critical point similar to that in Fig. 2 where the curves intersect.

The temporal intensity fluctuation $\delta I_i = I_i - \langle I_i \rangle$ can

be derived from the time dependent solution of the Fokker–Planck equation. If $(|\delta I_i|/\langle I_i \rangle) \leq \epsilon$ is required for the temporal mode stability when the laser is used for certain applications, the escape probability P_e that $(|\delta I_i|/\langle I_i \rangle)$ exceeds ϵ can be calculated. First we calculate the occupation probability, defined as

$$P(\tau) = \iint_D p(\vec{x}, \tau)\, dI_1\, dI_2 \tag{13}$$

with the integration carried over the space D where $(|\delta I_i|/\langle I_i \rangle) \leq \epsilon$, with $i = 1$ and 2. From (8) we find that $P(\tau)$ obeys the simple rate equation [13]

$$\frac{dP(\tau)}{d\tau} = -\gamma(P(\tau) - P_s) \tag{14}$$

where

$$P_s \equiv \iint_D p_s(\vec{x})\, dI_1\, dI_2. \tag{15}$$

Equation (14) can be rearranged and expressed in the following form

$$\frac{dP(\tau)}{d\tau} = -\frac{1}{T_{\text{in}}} P(\tau) + \frac{1}{T_{\text{out}}}(1 - P(\tau)). \tag{16}$$

The state of the laser $\vec{x} = (x_1, x_2, y_1, y_2)$ is either inside region D in phase space or outside of D; T_{in} and T_{out} in (16) represent the periods of time that the laser spends inside or outside of D, respectively. The escape probability is then given by

$$P_e = \frac{T_{\text{out}}}{T_{\text{in}} + T_{\text{out}}}. \tag{17}$$

Comparing (14) and (16) one finds

$$\frac{1}{T_{\text{in}}} + \frac{1}{T_{\text{out}}} = \gamma \tag{18}$$

$$\frac{1}{T_{\text{out}}} = \gamma P_s \tag{19}$$

and therefore

$$P_e = 1 - P_s. \tag{20}$$

Fig. 3 shows calculated P_e for different ξ and a values. The calculations were done with $\epsilon_1 = \epsilon_2 = \epsilon$ and again $a_1 = a_2 = a$ was used for the case that the DFB and FP modes have nearly the same intensity. For P_e and ϵ values specified for a system in which a two-wavelength laser is used as the light source, Fig. 3 gives the coupling constant ξ (or $\Delta\lambda$) and pump parameter a that should be designed into the laser to achieve satisfactory system performance. One can also plot P_e as a function of ξ and a for a specified ϵ. The escape probability P_e is equivalent to the bit error rate in the case of an optical fiber communication system, in which ϵ is often specified to be 0.5. As an example of using these calculations for designing a stable two-wavelength laser, we plot P_e as a function of

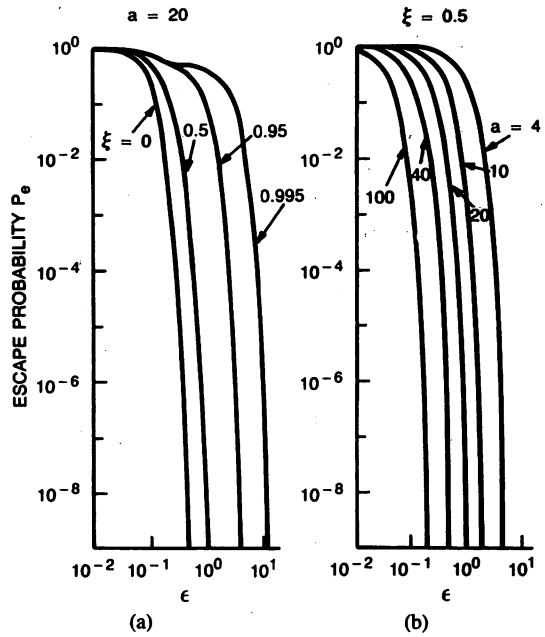

Fig. 3. Calculated probability P_e that the amplitude of the intensity fluctuation of the DFB mode exceeds a normalized intensity range ϵ. (a) is calculated for $a = 20$ at different ξ values and (b) is calculated for $\xi = 0.5$ at different a values.

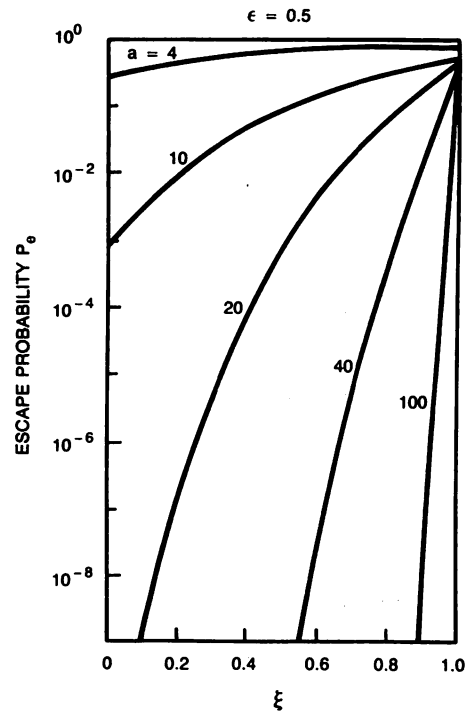

Fig. 4. Calculated P_e as a function of ξ for $\epsilon = 0.5$.

ξ at several pump levels a in Fig. 4 for the case of $\epsilon = 0.5$. From (4), $a = 40$ corresponds to $I \simeq 1.8\, I_{\text{th}}$. If $P_e \leq 1 \times 10^{-8}$ is required, the laser should be designed to operate with $\xi \leq 0.59$. This corresponds to $\Delta\lambda > 34$ Å for $\lambda = 1.3\ \mu$m, assuming $\tau_{\text{in}} = 0.3$ ps.

IV. Conclusions

In conclusion, we have developed a theory based on a Fokker–Planck equation to analyze the observed mode

behavior of a two-wavelength FP/DFB laser. With similar threshold currents for the detuned DFB mode and the FP mode near the gain peak, simultaneous operation of the DFB and FP modes, separated by 110 Å, was observed. In the theory, we have studied the mode power fluctuations as a function of a coupling coefficient ξ between the two lasing modes and the pumping levels of the laser.

It is shown in the theory that stable two-wavelength operation requires a sufficiently small ξ, which is dependent on the wavelength spacing between the two lasing modes and on the intraband relaxation time τ_{in}. A method of estimating τ_{in} directly from measurements of the mode power fluctuations caused by coupling between the two modes is proposed. Stability of two wavelength operation was also shown in the theory to improve with increasing pump level. The results of the parametric calculations provide the mode stability criteria for the design of stable two-wavelength lasers.

References

[1] P. L. Bender and J. C. Ownes, "Correction of optical distance measurements for the fluctuating atmospheric index of refraction," *J. Geophysical Res.*, vol. 70, pp. 2461-2462, 1965.

[2] L. E. Slater and G. R. Huggett, "A multiwavelength distance measuring instrument for geophysical experiments," *J. Geophysical Res.*, vol. 81, pp. 6299-6306, 1976.

[3] H. Matsumoto and K. Tsukahara, "Effects of the atmospheric phase fluctuation on long-distance measurement," *Appl. Opt.*, vol. 23, pp. 3388-3394, 1984.

[4] A. D. Kersey and A. Dandridge, "Two-wavelength interferometric fiber temperature sensor," presented at OFC'87, Reno, NV, Jan. 1987, pap. TuI2.

[5] N. K. Dutta, S. G. Napholtz, T. Cella, T. Wessel, R. L. Brown, and P. J. Anthony, "1.3-μm InGaAsP distributed feedback laser," *J. Appl. Phys.*, vol. 59, pp. 1811-1814, 1986.

[6] M. Ohtsu, Y. Teramuchi, Y. Otsuka, and A. Osaki, "Analysis of mode-hopping phenomena in an AlGaAs laser," *IEEE J. Quantum Electron.*, vol. QE-22, pp. 535-543, 1986.

[7] N. Ogasawara, R. Ito, M. Kato, and Y. Takahashi, "Mode switching in injection lasers induced by temperature variation and optical feedback," *Japan J. Appl. Phys.*, vol. 22, pp. 1684-1690, 1983.

[8] N. Chinone, T. Kuroda, T. Ohtoshi, T. Takahashi, and T. Kajimura, "Mode-hopping noise in index-guided semiconductor lasers and its reduction by saturable absorbers," *IEEE J. Quantum Electron.*, vol. QE-21, pp. 1264-1270, 1985.

[9] N. Ogasawara and R. Ito, "Output power change associated with longitudinal mode jumping in semiconductor injection lasers," *Japan J. Appl. Phys.*, vol. 25, pp. L617-L619, 1986.

[10] M. Yamada and Y. Suematsu, "Analysis of gain suppression in undoped injection lasers," *J. Appl. Phys.*, vol. 52, pp. 2653-2664, 1981.

[11] Y. Itaya, T. Matsuoka, K. Kuroiwa, and T. Ikegami, "Longitudinal mode behavior of 1.5-μm range GaInAsP/InP distributed feedback lasers," *IEEE J. Quantum Electron.*, vol. QE-20, pp. 230-235, 1984.

[12] M. Ohtsu, Y. Teramachi, and T. Miyazaki, "Analyses of suppression of mode hopping in an AlGaAs laser by saturable absorber," *Opt. Commun.*, vol. 61, pp. 203-207, 1987.

[13] R. Bonifacio, L. Lugiato, J. D. Farina, and L. M. Narducci, "Long time evolution for a one-dimensional Fokker-Plank process: Application to absorptive optical bistability," *IEEE J. Quantum Electron.*, vol. QE-17, pp. 357-365, 1981.

*

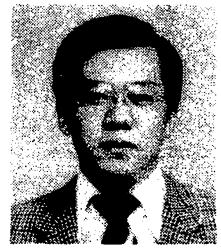

Motoichi Ohtsu was born in Kanagawa, Japan, on October 5, 1950. He received the B.S., M.S., and Ph.D. degree in electronics engineering from the Tokyo Institute of Technology, Tokyo, Japan, in 1973, 1975, and 1978, respectively.

He is an Associate Professor in the Graduate School at Nagatsuta, Tokyo Institute of Technology. He is currently working at AT&T Bell Laboratories for photonic device research (from September 1986 to 1987). He is interested in frequency control of lasers and its applications to coherent optical measurements and optical communications. He has written over 60 papers and received 2 patents. He is the author or coauthor of 8 books.

Dr. Ohtsu is a member of the Institute of Electronics and Communication Engineers of Japan, the Institute of Electrical Engineers of Japan, the Japan Society of Applied Physics, and the Optical Society of America. He was awarded a prize from the Japan Society of Applied Physics in 1982. He was also awarded the Issac Koga Gold Medal from the International Union of Radio Science in 1984.

*

Kang-Yih Liou received the B.S. degree in physics from National Taiwan University, Taipei, Taiwan, in 1970, the M.S. degree in physics from Temple University, Philadelphia, PA, in 1974, and the Ph.D. degree in materials science from the University of Wisconsin at Madison in 1978.

From 1979 to 1980, he was a Research Scientist at Argonne National Laboratory at Argonne, IL, where he contributed to theories and experiments of radiation modified thermodynamics of solids, ion implantation, and defects in crystals. He joined AT&T Bell Laboratories at Allentown, PA, in 1980 where he did work on semiconductor lasers and transmitters, and single-frequency coupled cavity lasers. Since December 1984 he has been with the Crawford Hill Laboratory of AT&T Bell Laboratories at Holmdel, NJ. His current research interests include semiconductor lasers and related optoelectronic devices for lightwave systems.

Papers

Mode Stability Analysis of Nearly Single-Longitudinal-Mode Semiconductor Lasers

MOTOICHI OHTSU, YASUAKI TERAMACHI, AND TETSUYA MIYAZAKI

Abstract—**Power fluctuations in a main mode of a nearly single-longitudinal-mode AlGaAs laser, caused by spontaneous emission fluctuations and coupling with a stationary nonoscillating side mode, are investigated. Average CW mode powers were measured to analyze the static characteristics of oscillation. For the dynamic characteristics, the escape probability was measured to evaluate the magnitude and the frequency of fluctuations. These experimental results were analyzed theoretically by a stochastic model which had already been developed by the authors to analyze the mode hopping phenomenon. Theoretical results agreed with experimental results. This theoretical model was also applied to the description of experimental results of rate of power dropout events reported by Linke *et al.* And then, it was confirmed that the theoretical results also agreed with their experimental results. By these agreements, it was proposed that this theoretical model can be used for the systematic description of the mode stability of semiconductor lasers, i.e., not only the experimental results obtained in the present work but also power dropout events in a nearly single-longitudinal-mode laser and mode hopping of two-mode lasers.**

I. Introduction

STABLE single-longitudinal-mode oscillation of semiconductor lasers has been required for applications to the coherent optical communication and optical measurements. To realize the single-longitudinal-mode oscillation, the dependence of the cavity loss on wavelengths has been utilized in distributed feedback lasers [1]. For Fabry–Perot cavity-type lasers, single-longitudinal mode oscillation has been realized by utilizing a spatial hole-burning effect due to the saturable absorber in the cladding layer [2]–[4] or by a spectral hole-burning effect [5]. Static measurements of average CW mode spectra have shown that these lasers oscillate with the single-longitudinal-mode. Even under such a static single-mode condition, Linke *et al.* [6] and Abbas and Lee [7] have found that the power of the main mode fluctuated due to coupling with a very low power side mode, which means that these lasers did not show the complete single-longitudinal-mode oscillation in their dynamic behaviors. From this, they have been called nearly single-longitudinal-mode lasers. A relation between bit error rates and mode power fluctuations in these lasers has been also discussed for application to optical communication [6]. Furthermore, several theoretical studies on mode power fluctuations have been reported [8]. However, direct comparisons have not yet been made between the experimental and the theoretical results. Even though theoretical analysis based on a quantum mechanical Langevin equation has been made [9], this theoretical approach lost the theoretical self-consistency because a gain saturation term was introduced heuristically. Furthermore, this theoretical analysis has not yet been fully applied to the evaluation of experimental results.

In the present work, precise measurements on power fluctuations in nearly single-longitudinal-mode lasers were made. These experimental results were theoretically analyzed by means of a stochastic model which has been developed by the authors to investigate the mode-hopping phenomenon in two longitudinal-mode lasers [10]. Furthermore, experimental results of power dropout events obtained by Linke *et al.* [6] were analyzed by using this theoretical model. From the comparisons between these experimental and theoretical results, it was demonstrated that this theoretical model was useful to describe systematically the mode stability of the semiconductor lasers including a phenomenon of mode hopping of the two-longitudinal-mode lasers and power dropout events in nearly single-longitudinal-mode lasers.

II. Precise Measurements of Mode Stability

The experimental setup is shown in Fig. 1. An AlGaAs laser (channeled-substrate-planar type) of 0.78 μm wavelength was employed for the experiments. The laser was installed in a small vacuum chamber, and the temperature of the heat sink made of a copper block for the laser was controlled by means of a Peltier element for which a thermister bridge was used as a temperature sensor. As a result of this control, temperature fluctuations of the heat sink were suppressed to 2×10^{-4} K. The laser was driven by a low-noise dc current source with the current noise (root-mean-square value) of 0.6 nA/$\sqrt{\text{Hz}}$ at the Fourier frequency of 1 kHz. Two kinds of measurements were carried out for the longitudinal-mode spectra. One was a static measurement by using a conventional grating monochromator, a photodiode, and a dc amplifier. The

Manuscript received October 12, 1987; revised January 8, 1988.

M. Ohtsu and T. Miyazaki are with the Graduate School at Nagatsuta, Tokyo Institute of Technology, Midoriku, Yokohama, Kanagawa 227, Japan.

Y. Teramachi is with Department of Information Engineering, the Institute of Vocational Training, Sagamihara, Kanagawa 229, Japan.

IEEE Log Number 8820115.

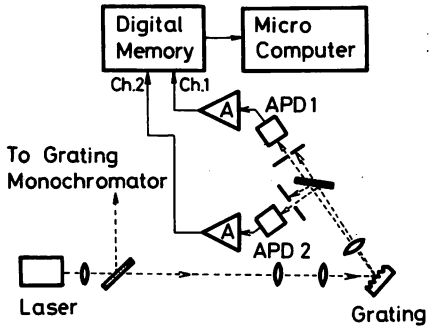

Fig. 1. Experimental setup.

results represented the longitudinal-mode-spectra averaged over a certain time interval, i.e., average CW mode spectra. The other was a dynamic measurement of power fluctuations in each longitudinal mode. In this measurement, power fluctuations of each mode were detected by using avalanche photodiodes (APD) and wideband amplifiers after each mode was separated spatially by using a diffraction grating. The output signal from the amplifiers were recorded by a two-channel digital memory. The bandwidth of the detection system was 50 MHz. Then, recorded signals were processed by using a microcomputer.

Open circles in Fig. 2(a) represent a temperature dependence of the threshold current I_{th}. Hatched areas given by the heat sink temperature T and the injection current I showed the regions of individual single-longitudinal-mode oscillation of the laser used. Here, we defined the single-longitudinal-mode oscillation as the oscillating state of which the amplitude of the mode power fluctuations caused by competition with the other mode was less than 1 percent of the average CW mode power, i.e., the value of the parameter ϵ defined in the last part of this section was less than 0.01. In this figure, for example, modes $M14$ and $M15$ were adjacent to each other, and their wavelength separation was 2.3 Å. On the other hand, four nonoscillating modes existed between the modes $M4$ and $M9$. Wavelength separation between these two modes was 12 Å.

Between the hatched areas for the modes $M9$ and $M14$, e.g., at point A in Fig. 2(a), both modes oscillated with almost equal average CW mode powers. However, these mode powers exhibited a switching phenomenon with each other, i.e., mode hopping. This phenomenon has been investigated by [10]. Fig. 2(b) shows an average CW mode spectral profile observed by fixing the temperature T and current I at point B in Fig. 2(a), which was inside the hatched area for the mode 14 and was close to its boundary. It is seen from this figure that the mode $M14$ showed nearly single-longitudinal-mode oscillation, however, a mode $M9$ can be seen as the next most significant mode which can be considered to be a side mode. Static and dynamic characteristics of mode power will be discussed in the following when the main mode is perturbed by only one side mode.

Fig. 3(a) shows the experimental results of average CW mode powers of each mode, which were obtained by varying the current I in the vicinity of point B in Fig. 2(a) while the temperature T was fixed. Similar results have

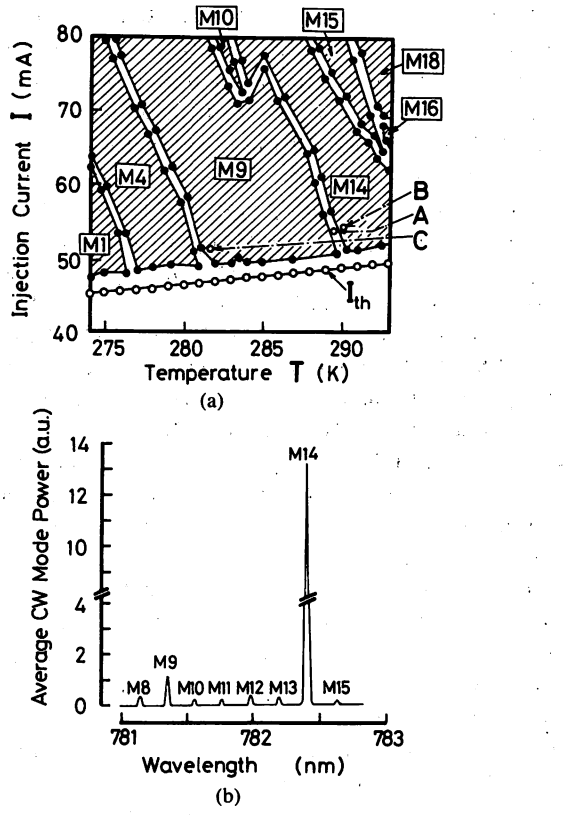

Fig. 2. (a) Regions of the heat sink temperature T and the injection current I where single-longitudinal-mode oscillation was observed (hatched areas). $M1$–$M18$ represent a series of longitudinal modes. Open circles represent the threshold current I_{th}. Measurements were carried out at points A, B, and C. (b) Average CW mode spectra observed at position B in (a).

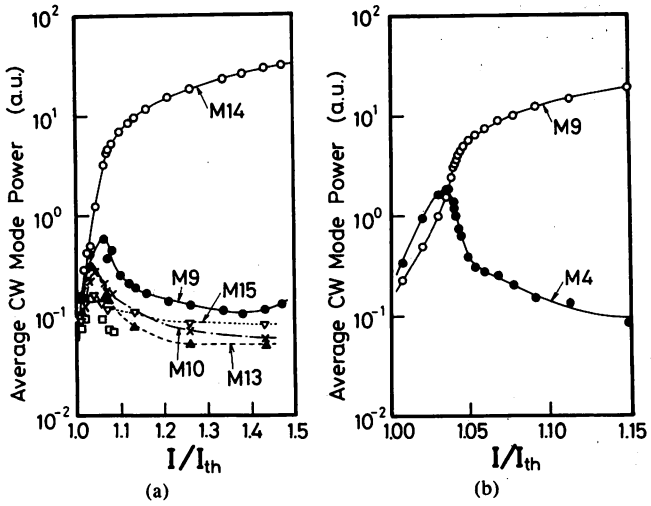

Fig. 3. (a), (b) Relation between the injection current I and average CW mode powers measured at around positions B and C in Fig. 2(a), respectively, while the heat sink temperature T was fixed. Main modes in (a) and (b) are modes $M14$ and $M9$, respectively. Among several side modes, only the most significant side mode ($M4$) is shown in (b).

been reported by Nakamura *et al.* [11]. This figure shows that the power of the main mode ($M14$) increased with the increase of I, while that of the most significant side mode ($M9$) decreased monotonously after a slight increase. In this figure, average CW mode powers of other side modes are also shown. Dependences of powers of these side modes on the current I are similar to that of the most significant side mode $M9$. Since powers of these side

modes were less than 50 percent that of the mode $M9$, these modes will be neglected in the theoretical analysis of Section III. Since this was a good approximation in the range of $I/I_{th} < 1.5$, all the measurements were carried out within this range of the bias level near the threshold.

Fig. 3(b) shows the experimental results of average CW mode powers obtained by varying the current I around the position C in Fig. 2(a) while temperature T was fixed. In Fig. 3(b), powers of only the most significant side mode ($M4$) are shown together with the main mode ($M9$) because powers of other side modes were significantly lower than that of the mode $M4$. A feature of this figure is that the power of the main mode $M9$ was, on the contrary, lower than that of the side mode $M4$ at $I/I_{th} < 1.04$, i.e., close to threshold. This phenomenon can be described by the present theoretical model as discussed in Section III.

Fig. 4 shows a result of dynamic measurements of power fluctuations in each mode, which were carried out at position B in Fig. 2(a). It is seen from Fig. 4 that the power of the main mode ($M14$) was almost constant with time, however, its waveform had several sharp dips. On the other hand, the power of the side mode ($M9$) was nearly zero, however, its waveform shows several pips. The total power was almost constant all the time and had neither dips or pips. Since these dips and pips were synchronized with each other, it can be considered that they originated from the interaction between the two modes. Similar dips have been observed also by Linke *et al.* [6] and Abbas and Lee [7], and have been called power dropout events. Open circles in Fig. 5 represent a relation between the current I and the measured values of probability of occurrences P_e of the dips of the main mode. This probability P_e, corresponding to the escape probability defined in Section III, was measured here based on the following formula:

$$P_e = \sum_i t_i / T_m \qquad (1)$$

where t_i is a time period in which a ratio between the magnitude of power fluctuations $|\delta I_M|$ and the average CW mode power $\langle I_M \rangle$ exceeded a certain value ϵ (i.e., $|\delta I_M|/\langle I_M \rangle \geqq \epsilon$). The value of ϵ was fixed at 0.05. T_m represents total time of a measurement. For this measurement, a sampling time period t_s for data acquisition by the digital memory was fixed at between 10 and 500 ns. Since the characteristic time of the waveform of power fluctuations were dependent on the bias level, the value of t_s was appropriately adjusted within this range in order for the resolution of the waveform recording to be maintained high enough. The number of successive data points N_d was 2048, and the number of the measurements (N) carried out repeatedly was 10. Therefore, T_m was between 0.2 and 10 ms. If stationarity of the system was assumed, the total sample number corresponded to $N_d \cdot N$. In this case, the resolution of measurements of P_e was $1/N_dN = 4.8 \times 10^{-5}$.

Fig. 5 shows also that the value of P_e decreased with increasing current I. This means that the laser is less sensitive to the agitation by spontaneous emission fluctuations and shows a more stable oscillation at a higher bias level.

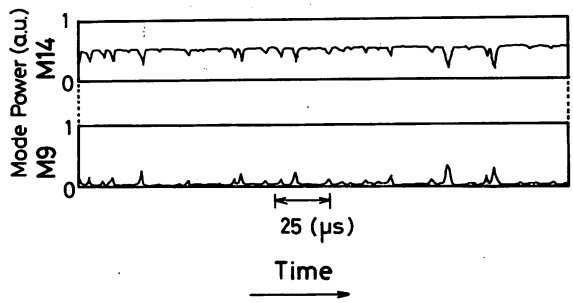

Fig. 4. Experimental results of temporal power fluctuations in the modes $M14$ (main mode) and $M9$ (side mode) measured at position B in Fig. 2(a).

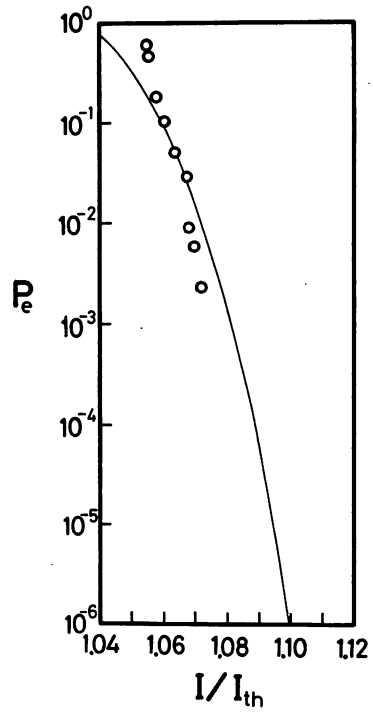

Fig. 5. Relation between the injection current I and escape probability P_e. Open circles represent experimental results measured by following (1) at around position B in Fig. 2(a) while the temperature T was fixed. Solid curve represents a theoretical results calculated by using (23) in Section III.

III. Theoretical Analysis

In this section, experimental results given by Figs. 3 and 5 are analyzed on the basis of a stochastic approach, where only one side mode is taken into account for simplicity. Van der Pol equations derived from density matrix formulation [5] and the equation of motion of carrier density are used as the key equations. If the amplitude of the electric field of the lightwave of the ith mode and the carrier density are expressed as $\tilde{E}_i$ and $\bar{n}^{(0)}$, respectively, these equations are given by

$$\frac{d\tilde{E}_i}{dt} = \frac{1}{2n_I\sqrt{\epsilon_0\mu_0}}\left[\tilde{\alpha}_i^{(1)} - \alpha_{th} - \tilde{\alpha}_i^{(3)}\tilde{E}_i^2 - \tilde{\alpha}_{i(j)}^{(3)}\tilde{E}_j^2\right]\tilde{E}_i,$$

$$(i, j = 1, 2;\ i \neq j) \qquad (2)$$

and

$$\frac{d\bar{n}^{(0)}}{dt} = -n_I\sqrt{\frac{\epsilon_0}{\mu_0}}\left(\frac{2}{\hbar\omega_1}\tilde{\alpha}_1^{(1)}\tilde{E}_1^2 + \frac{2}{\hbar\omega_2}\tilde{\alpha}_2^{(1)}\tilde{E}_2^2\right) - \frac{\bar{n}^{(0)}}{\tau_s} + \frac{I}{V_I e} \tag{3}$$

where $\tilde{\alpha}_i^{(1)}$ and α_{th} are the linear gain and the cavity loss, respectively, which are expressed as

$$\tilde{\alpha}_i^{(1)} = \xi^{(1)}g^{(1)}\left[\bar{n}^{(0)} - n_G^{(1)} - h'(\lambda_i - \lambda_0)^2\right], \quad (i = 1, 2) \tag{4}$$

and

$$\alpha_{th} = \xi^{(1)}g^{(1)}(\bar{n}_{th}^{(0)} - n_G^{(1)}). \tag{5}$$

In these equations, λ_i is the oscillation wavelength of the ith mode, λ_0 is a center wavelength of the gain spectrum, and $\bar{n}_{th}^{(0)}$ is the threshold carrier density. In (2), $\tilde{\alpha}_i^{(3)}$ and $\tilde{\alpha}_{i(j)}^{(3)}$ are the self-saturation coefficient and the cross-saturation coefficient, respectively.

It should be noted that two kinds of gain saturation mechanisms are expressed by (2) and (3). The gain saturation, due to the interband relaxation of carriers with time constant τ_s, is expressed by a decrease in $\tilde{\alpha}_i^{(1)}$ in (2) via (3). Equation (2), however, does not include the intraband relaxation, with relaxation time τ_{in}. To consider the gain saturation due to the intra-band relaxation, we include (2), the third-order terms with the coefficients $\tilde{\alpha}_i^{(3)}$ and $\tilde{\alpha}_{i(j)}^{(3)}$. Since these gain saturation terms are directly derived from density matrix formulation without the introduction of heuristic values [5], the present theory keeps its self-consistency theoretically. On the contrary, the use of heuristic gain saturation terms could not be avoided in the quantum mechanical Langevin equation [9]. It is important to note that the origin of the gain saturation expressed by $\tilde{\alpha}_i^{(1)}$ via (3) is different from that of $\tilde{\alpha}_i^{(3)}$ and $\tilde{\alpha}_{i(j)}^{(3)}$. Definitions and numerical values of other quantities in (2)–(5) have been given in [10]. The following approximation is valid because it was confirmed by several preliminary calculations that the fluctuations of $\tilde{\alpha}_i^{(3)}$ and $\tilde{\alpha}_{i(j)}^{(3)}$ with a change of $\bar{n}^{(0)}$ are much less than that of $\tilde{\alpha}_i^{(1)} - \alpha_{th}$ [10]: $\tilde{\alpha}_i^{(3)}(\bar{n}^{(0)}) \cong \tilde{\alpha}_i^{(3)}(\bar{n}_{th}^{(0)})$, $\tilde{\alpha}_{i(j)}^{(3)}(\bar{n}^{(0)}) \cong \tilde{\alpha}_{i(j)}^{(3)}(\bar{n}_{th}^{(0)})$.

An analog computer simulation was carried out by using (2)–(5). Two uncorrelated Gaussian white noises, generated from two noise generators, were applied to the analog computer as the spontaneous emission terms which should be added to (2) [10]. Fig. 6(a)–(d) shows the output waveforms of mode powers ($|E_1|^2$ and $|E_2|^2$), total power ($|E_1|^2 + |E_2|^2$), and carrier density fluctuations ($\delta\bar{n}^{(0)}/\bar{n}_{th}^{(0)}$), respectively. It is seen from Fig. 6(a), (b), and (c) that the main and side mode powers show dips and pips even though the total power is maintained almost constant with time. This is consistent with the experimental results shown in Fig. 4, from which it is confirmed that this theoretical model is accurate enough to describe the oscillation characteristics of semiconductor lasers.

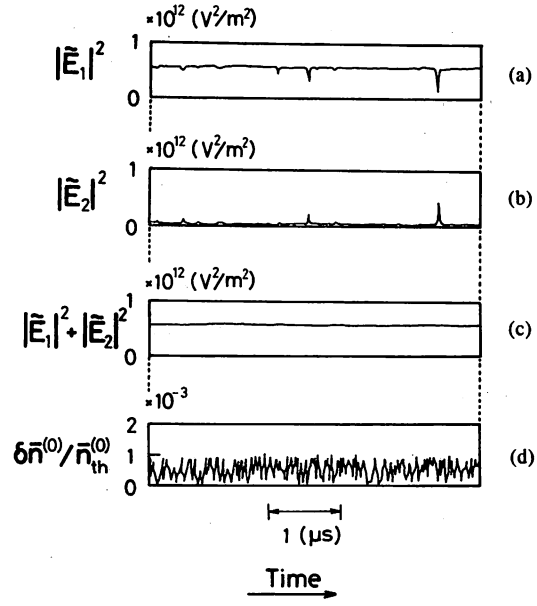

Fig. 6. Results of the analog computer simulation of temporal fluctuations of mode powers and carrier density. (a) Main mode power ($|E_1|^2$). (b) Side mode power ($|E_2|^2$). (c) Total power ($|E_1|^2 + |E_2|^2$). (d) Carrier density fluctuations normalized to the threshold value ($\delta\bar{n}^{(0)}/\bar{n}_{th}^{(0)}$).

Fig. 6(d) shows that the magnitude of carrier density fluctuations $\delta\bar{n}^{(0)}$ is less than 10^{-3} that of $\bar{n}_{th}^{(0)}$, and that the waveforms of $\delta\bar{n}^{(0)}$ are not correlated with those of Fig. 6(a) and (b). These phenomena are due to the fact that the total stimulated emission rate, proportional to the total power ($|E_1|^2 + |E_2|^2$) on the right-hand side of (3), was kept constant all the time even though the dips or pips appeared in each mode. This is concluded from the fact that the total power was kept constant with time.

Since it was found by the analog computer simulation that the carrier density $\bar{n}^{(0)}$ was almost constant with time, (3) is excluded in the following discussions. The equation we have to solve is (2), in which the values of gain coefficients $\tilde{\alpha}_i^{(1)}$, $\tilde{\alpha}_i^{(3)}$, and $\tilde{\alpha}_{i(j)}^{(3)}$ are constant with time. Therefore, the stochastic model, which had been developed by the authors to analyze the mode-hopping phenomenon [10], can be also used here. That is, the analysis is carried out by using the Langevin equation for the normalized electric field of laser which is derived from (2) and is expressed as

$$\frac{dE_i}{d\tau} = \left(a_i - |E_i|^2 - \xi|E_j|^2\right)E_i + q_i(\tau), \quad (i, j = 1, 2;\ i \neq j) \tag{6}$$

where E_i is the normalized amplitude of the electric field of the ith mode, τ is the normalized time, a_i is the pump parameter, and ξ is the coupling constant between two modes. The quantities $q_i(\tau)$ $(i = 1, 2)$ are Langevin noise terms which represent the fluctuations of spontaneous emission. They are supposed to be delta-correlated Gaussian random processes with the zero mean and

$$\langle q_i^*(\tau) \cdot q_j(\tau')\rangle = 4 \cdot \delta_{ij} \cdot \delta(\tau - \tau'), \quad (i, j = 1, 2) \tag{7}$$

where * means the complex conjugate, δ_{ij} is the Kronecker delta, and $\delta(\tau - \tau')$ is the delta function. The quantities a_i and ξ are derived from the coefficients in (2), and are expressed as

$$\left.\begin{aligned} a_i &= (\tilde{\alpha}_i^{(1)} - \alpha_{\text{th}})/\tilde{\alpha}_i^{(3)}\zeta_{Ei}^2 \\ \xi &= \tilde{\alpha}_{i(j)}^{(3)}/\tilde{\alpha}_i^{(3)} \end{aligned}\right\} \quad (i, j = 1, 2;\ i \neq j) \tag{8}$$

where ζ_{Ei} $(=\tilde{E}_i/E_i)$ is a normalized constant used for the derivation of (6) from (2). Equation (8) shows that a_i is proportional to the linear gain or, in other words, the bias level, and that the coupling constant ξ can be approximated to $4/3$ as long as the wavelength separation $\lambda_1 - \lambda_2$ between two modes is less than about 20 Å [10], which was the condition in the experiments of Section II.

Either modes in (6) can be the main mode or side mode by appropriately adjusting the values of parameters. For example, stability analysis of (6) [12] shows that only mode 1 shows a stable stationary oscillation if

$$a_1/a_2 > \xi \quad (=4/3). \tag{9}$$

Mode 2 oscillates only momentarily with no stationary oscillation in this case. That is, the average CW mode powers ($|E_1|^2$ and $|E_2|^2$) of modes 1 and 2 are a_1 and 0, respectively. This means that modes 1 and 2 correspond to the main and the side modes in Section II, respectively. On the other hand, mode 2 becomes the main mode if $a_1/a_2 < 1/\xi$. Furthermore, two mode powers tend to jump randomly between the two stable stationary states $(|E_1|^2, |E_2|^2) = (a_1, 0)$ and $(0, a_2)$ driven by fluctuations of spontaneous emission if $1/\xi < a_1/a_2 < \xi$. This phenomenon corresponds to the mode hopping which has been investigated in [10].

If we express the normalized complex field amplitude E_i in terms of real and imaginary parts

$$E_k = x_k + i \cdot y_k \quad (k = 1, 2) \tag{10}$$

the vector $\vec{x}$ $[=(x_1, x_2, y_1, y_2)]$ represents the state of the laser, and its components obey a set of coupled Langevin equations given by (6). This multidimensional nonlinear Langevin equation can be transformed to the linear Fokker–Planck equation describing the probability density $p(\vec{x}, \tau)$, which is expressed as

$$\frac{\partial}{\partial\tau}p(\vec{x}, \tau) = \sum_{i=1}^{2}\left[-\frac{\partial}{\partial x_i}A_i^{(x)}p - \frac{\partial}{\partial y_i}A_i^{(y)}p + \left(\frac{\partial^2}{\partial x_i^2} + \frac{\partial^2}{\partial y_i^2}\right)p\right] \tag{11}$$

where

$$A_i^{(\eta)} = \left[a_i - (x_i^2 + y_i^2) - \xi(x_j^2 + y_j^2)\right]\eta_i \quad (i, j = 1, 2;\ i \neq j,\ \eta = x, y). \tag{12}$$

The solution of (11) is given by [13]

$$p(\vec{x}, \tau) = p(\vec{x}, \infty) \cdot e^{-\gamma\tau} \cdot V(\vec{x}) \tag{13}$$

where $V(\vec{x})$ is the eigenfunction of the Fokker–Planck operator corresponding to the eigenvalue γ. The steady-state solution is expressed as $p(\vec{x}, \infty)$, which is given by

$$p(\vec{x}, \infty) = B^{-1}\exp\left[\tfrac{1}{2}(a_1I_1 + a_2I_2) - \tfrac{1}{4}(I_1^2 + I_2^2 + 2\xi I_1I_2)\right] \tag{14}$$

where I_i is the normalized mode power given by $x_i^2 + y_i^2 (= |E_i|^2)$ and B is the normalization constant. The average CW mode power, corresponding to the experimental results of Fig. 3, is given by

$$\langle I_i\rangle = \int_0^\infty\!\!\int p(\vec{x}, \infty) \cdot I_i \cdot dI_1\, dI_2. \tag{15}$$

To derive the probability P_e given by (1), the method proposed by Bonifacio *et al.* [13] is employed. First, we calculate the occupation probability $P(\tau)$, defined as

$$P(\tau) = \int_D\!\!\int p(\vec{x}, \tau)\, dI_1\, dI_2 \tag{16}$$

where the region D is bounded by

$$D: \begin{cases} a_1(1 - \epsilon) \leqq I_1 \leqq a_1(1 + \epsilon) \\ 0 \leqq I_2 \leqq \infty. \end{cases} \tag{17}$$

The quantity ϵ can be called the threshold setting to calculate $P(\tau)$, as was given in Section II. From (13), we find that $P(\tau)$ obeys the simple rate equation

$$\frac{dP(\tau)}{d\tau} = -\gamma(P(\tau) - P(\infty)) \tag{18}$$

where

$$P(\infty) = \int_D\!\!\int p(\vec{x}, \infty) \cdot dI_1\, dI_2. \tag{19}$$

Equation (18) can be rearranged and be expressed in the following form:

$$\frac{dP(\tau)}{d\tau} = -\frac{1}{T_{\text{in}}}P(\tau) + \frac{1}{T_{\text{out}}}(1 - P(\tau)). \tag{20}$$

The state of the laser $\vec{x}$ is either inside the region D of phase space or outside of D, and then T_{in} and T_{out} in (20) represent the periods of time that the state of the laser is inside and outside of D, respectively. The escape probability given by (1) is then defined as

$$P_e = T_{\text{out}}/(T_{\text{in}} + T_{\text{out}}). \tag{21}$$

Comparing (18) and (20), one finds

$$\left.\begin{aligned} T_{\text{in}} &= 1/\gamma(1 - P(\infty)) \\ T_{\text{out}} &= 1/\gamma P(\infty) \end{aligned}\right\}, \tag{22}$$

and thereby

$$P_e = 1 - P(\infty). \tag{23}$$

The probability calculated by (19) and (23) can be used to analyze the experimental results shown in Fig. 5.

The value of pump parameter a_i should be evaluated exactly to compare the calculated results of $\langle I_i \rangle$ and P_e from (15) and (23) with experimental results. Since the result of the analog computer simulation showed that the carrier density fluctuations can be neglected, the value of carrier density $\bar{n}^{(0)}$ can be approximated to its stationary value $\bar{n}_{st}^{(0)}$. The value of $\bar{n}_{st}^{(0)}$ is derived from (2) and (3), which is expressed as

$$\bar{n}_{st}^{(0)}/\bar{n}_{\text{th}}^{(0)} - 1 = \theta \cdot (I/I_{\text{th}} - 1). \tag{24}$$

By using numerical values of the parameters for AlGaAs lasers (see [10, eq. (11)]), the proportional constant θ is given by

$$\theta = 1.7 \times 10^{-2}. \tag{25}$$

The oscillation wavelength of the ith mode λ_i and the center wavelength of the gain spectrum λ_0 depend on the current I, which are expressed as

$$\left.\begin{aligned} \lambda_i &= \lambda_{i0} + \chi \cdot (I - I_0) \\ \lambda_0 &= \lambda_{00} + \chi_0 \cdot (I - I_0) \end{aligned}\right\} \tag{26}$$

where I_0 represents the current to satisfy $a_1 = a_2$. The oscillation wavelength of the ith mode λ_{i0} and the center wavelength of the gain spectrum λ_{00} at this current satisfy the relation $\lambda_{10} - \lambda_{00} = \lambda_{00} - \lambda_{20}$. Proportional constants χ and χ_0 in (26) represent the shift of λ_i and λ_0 due to the changes of the refractive index and the bandgap energy of the active layer, respectively, by a temperature change induced by a current change. Pump parameters a_1 and a_2, are then expressed by using (4), (5), (8), and (24)–(26) as

$$\left.\begin{aligned} a_1 &= a_{10} \frac{(I/I_{\text{th}} - 1) - (h'/\bar{n}_{\text{th}}^{(0)} \cdot \theta)\left((\lambda_{10} - \lambda_{00}) - (\chi_0 - \chi)(I - I_0)\right)^2}{(I_0/I_{\text{th}} - 1) - (h'/\bar{n}_{\text{th}}^{(0)} \cdot \theta)(\lambda_{10} - \lambda_{00})^2} \\ a_2 &= a_{10} \frac{(I/I_{\text{th}} - 1) - (h'/\bar{n}_{\text{th}}^{(0)} \cdot \theta)\left((\lambda_{00} - \lambda_{20}) + (\chi_0 - \chi)(I - I_0)\right)^2}{(I_0/I_{\text{th}} - 1) - (h'/\bar{n}_{\text{th}}^{(0)} \cdot \theta)(\lambda_{00} - \lambda_{20})^2} \end{aligned}\right\}, \tag{27}$$

where a_{10} is the value of a_1 at $I = I_0$. Since $d\lambda_0/dT = 4$ (Å/K) for AlGaAs lasers [14] and dT/dI is estimated as 0.22 (K/mA) from the slope of a border line of the hatched area in Fig. 2(a), the value of χ_0 is approximated as 0.88 (Å/mA). The value of χ, on the other hand, is estimated as 0.06 (Å/mA) by preliminary measurements of the wavelength shift of the laser used.

Fig. 7(a) and (b) shows calculated results of $\langle I_i \rangle$ from (15) and (27) using numerical values corresponding to the experimental conditions of Fig. 3(a) and (b), respectively. The value of a_{10} was used as the fitting parameter for these calculations. Typical numerical values used here were: $\bar{n}_{\text{th}}^{(0)} = 2.6 \times 10^{24}$ (m^{-3}), $h' = 3 \times 10^{39}$ (m^{-5}), $\lambda_{10} - \lambda_{00} = \lambda_{00} - \lambda_{20} = 6$ (Å), $1.08 \leqq I_0/I_{\text{th}} \leqq 1.35$, $22.5 \leqq a_{10} \leqq 40$. Calculated results were insensitive to the values of $\bar{n}_{\text{th}}^{(0)}$ and h'. However, as can be clearly shown in Fig. 7, they were varied by changing the values of wavelength differences $\lambda_{10} - \lambda_{00}$, $\lambda_{00} - \lambda_{20}$, and the bias level I/I_{th}. The profiles of the curves in these figures agree well with those experimental results of Fig. 3(a) and (b). A specific cross-over between the main and the side mode powers observed in Fig. 3(b) is also well reproduced in Fig. 7(b), which could not be done by the conventional theoretical model [15]. The reasons for this reproducibility are that the values of the parameters can determine which mode works as a main mode in the present model and that the present model is based on the stochastic approach.

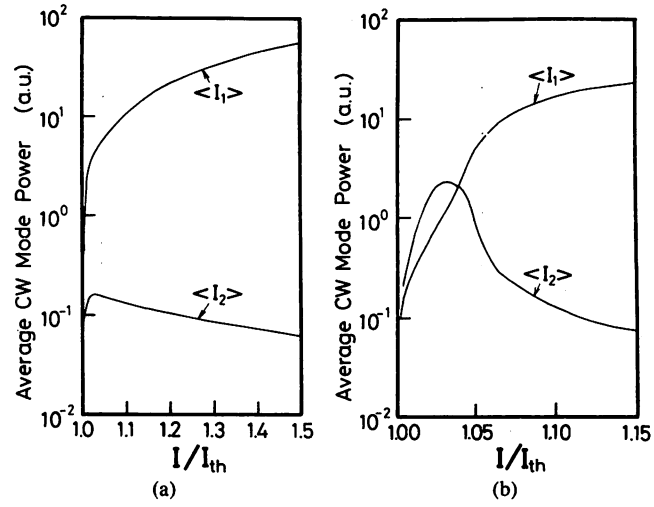

Fig. 7. Theoretical results of relations between the injection current I and average CW mode powers. $\langle I_1 \rangle$ and $\langle I_2 \rangle$ represent the average CW mode powers of main and side mode powers, respectively. (a) and (b) represent the results calculated by using numerical values corresponding to the experimental conditions of Fig. 3(a) and (b).

Fig. 8 shows calculated results of P_e from (23) and (27).

It is seen that P_e decreases with the increase of the bias level, such as the case of the experimental results. The calculated result of P_e for $\epsilon = 0.05$ is given by the solid curve in Fig. 5, which agrees with the experimental results of open circles. It can be concluded from this agreement that arbitrary small values of P_e can be estimated by the present theoretical model even though the value of P_e is lower than 2.8×10^{-4}, which could not be measured by the experiment.

The present theoretical approach to derive P_e can be also applied to evaluate the experimental results, reported by Linke *et al.* [6] and by Abbas and Lee [7]. Linke *et al.* have measured a rate of power fluctuations of the main

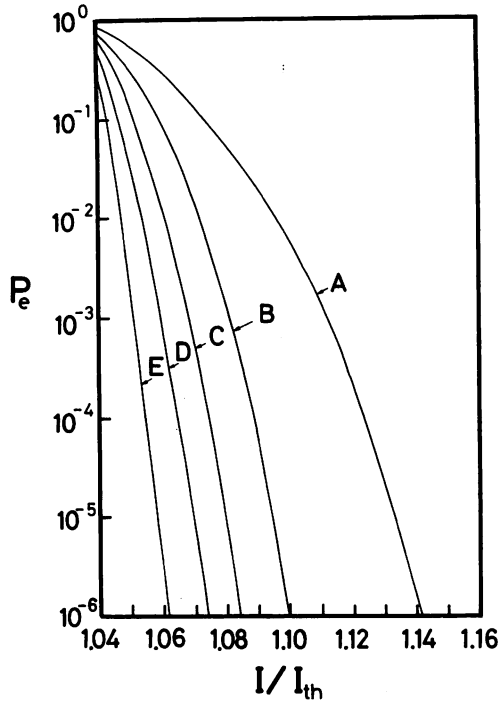

Fig. 8. Theoretical results of a relation between the injection current I and escape probability P_e. Numerical values used for calculation are the same as those of Fig. 7(a). Values of the threshold setting ϵ for the curves A, B, C, D, E are 0.03, 0.05, 0.07, 0.10, and 0.15, respectively.

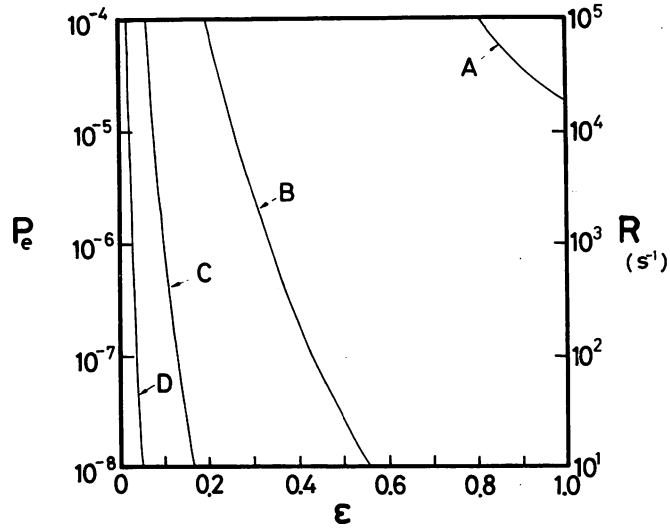

Fig. 9. Theoretical results of a relation between the threshold setting ϵ and the escape probability P_e for a 1.3 μm InGaAsP laser. Values of rate of power dropout events R are also given on the ordinate for comparison to the experimental results reported by Linke *et al.* [6]. For curves A, B, C, and D, values of the ratio of pump parameters a_1/a_2 were fixed to be 12, 27, 40, and 53, respectively. These values are equal to those of the main-to-side mode power ratio used by Linke *et al.* in their measurements (see [6, Fig. 2]).

mode of a nearly single-longitudinal-mode laser (a 1.3 μm wavelength short cavity BH laser) as a function of threshold setting ϵ of (17). These fluctuations have been called a rate of power dropout events with a duration time t_d of about 1 ns [6, Fig. 2]. In these measurements, the laser was fixed at higher bias level than that of the present work. Fig. 2 of [6] shows that values of the rate of dropout events R were between 10 (s^{-1}) and 1×10^5 (s^{-1}), which corresponds to $1 \times 10^{-8} \leqq P_e \leqq 1 \times 10^{-4}$. These values of P_e are smaller than those of the experimental results of Fig. 5. The dips appearing in Fig. 4 can be considered the same phenomena as the power dropout events observed by Linke *et al.*, but dips in Fig. 4 were able to be observed with much smaller bandwidth of the measurement than that by Linke *et al.* because of a kind of critical slowing down by carrying out the measurement at bias levels close to the threshold. If the power dropout events measured by Linke *et al.* are the same phenomena as the dips of the present measurements, these power dropout events should be able to be described by the present theoretical model. To confirm it, the value of P_e was calculated from (23) by using a ratio of pump parameters a_1/a_2 as a parameter, where numerical values for an InGaAsP laser given in [16] were employed. Fig. 9 shows the calculated result. The abscissa in this figure represents ϵ as in [6, Fig. 2]. The values of P_e and R are given on the ordinate, where duration time t_d of 1 ns is assumed to derive R from P_e. Values of the parameter a_1/a_2 in this figure are selected to be the same as those of main-to-side mode power ratio employed in Fig. 2 of [6]. Comparison between the profiles of the curves in Fig. 9 shows that the magnitude of the slope of the curve increases with the increase of a_1/a_2. This feature is consistent with that of the results shown in Fig. 2 of [6] which have been obtained with no relation to the present work. Slight differences between them are due to inaccuracies of measurements of ϵ in the experiments and of numerical values of parameters used for calculations. From this agreement between the experimental and theoretical results, it was concluded that the power dropout events measured by Linke *et al.* are the same phenomena as was given in Fig. 4. Furthermore, it can be confirmed that the present theoretical model can be used to describe systematically the mode stability of semiconductor lasers, i.e., the characteristics of the mode hopping phenomenon [10], average CW mode power, escape probability, and rate of power dropout events.

IV. Conclusion

Precise measurements on average CW mode powers and escape probability of a nearly single-longitudinal-mode AlGaAs laser were carried out. These results were analyzed by the stochastic model which has been developed to describe a phenomenon of mode hopping between the two modes. The results of analysis agreed well with the experimental results. Furthermore, rate of power dropout events calculated by this theoretical model agreed with those of experimental results reported by Linke *et al.* From these agreements, we propose here that this theoretical model can be used for systematic description of the characteristics of mode stability of semiconductor lasers.

Acknowledgment

The authors thank Y. Nakamura of the Tokyo Institute of Technology for his experimental support.

REFERENCES

[1] Y. Suematsu, S. Arai, and K. Kishino, "Dynamic single-mode semiconductor lasers with a distributed reflector," *J. Lightwave Technol.*, vol. LT-1, pp. 161–176, 1983.

[2] J. A. Copeland, "Single mode stabilization by traps in semiconductor lasers," *IEEE J. Quantum Electron.*, vol. QE-16, pp. 721–727, 1980.

[3] N. Chinone, T. Kuroda, T. Otoshi, Y. Takahashi, and T. Kajimura, "Mode-hopping noise in index-guided semiconductor lasers and its reduction by saturable absorbers," *IEEE J. Quantum Electron.*, vol. QE-21, pp. 1264–1270, 1985.

[4] M. Ohtsu, Y. Teramachi, and T. Miyazaki, "Analyses of suppression of mode hopping in an AlGaAs laser by saturable absorber," *Opt. Commun.*, vol. 61, pp. 203–207, 1987.

[5] M. Yamada and Y. Suematsu, "Analysis of gain suppression in undoped injection lasers," *J. Appl. Phys.*, vol. 52, pp. 2563–2664, 1981.

[6] R. A. Linke, B. L. Kasper, C. A. Burrus, Jr., I. P. Kaminov, J. S. Ko, and T. P. Lee, "Mode power partition events in nearly single-frequency lasers," *J. Lightwave Technol.*, vol. LT-3, pp. 706–712, 1985.

[7] G. L. Abbas and T. K. Lee, "Power dropout statistics of nearly-single-longitudinal-mode semiconductor lasers," *IEEE J. Quantum Electron.*, vol. QE-21, pp. 1303–1307, 1985.

[8] C. H. Henry, P. S. Henry, and M. Lax, "Partition fluctuations in nearly single-longitudinal-mode lasers," *J. Lightwave Technol.*, vol. LT-2, pp. 209–216, 1984.

[9] D. Marcuse, "Computer simulation of laser photon fluctuations: Theory of single-cavity laser," *IEEE J. Quantum Electron.*, vol. QE-20, pp. 1139–1147, 1984.

[10] M. Ohtsu, Y. Teramachi, Y. Otsuka, and A. Osaki, "Analyses of mode-hopping phenomena in an AlGaAs laser," *IEEE J. Quantum Electron.*, vol. QE-22, 1986.

[11] M. Nakamura, K. Aiki, N. Chinone, R. Ito, and J. Umeda, "Longitudinal-mode behaviors of mode-stabilized $Al_xGa_{1-x}As$ injection lasers," *J. Appl. Phys.*, vol. 49, pp. 4644–4648, 1978.

[12] M. Sargent III, M. O. Scully, and W. E. Lamb, Jr., *Laser Physics*. Reading, MA: Addison-Wesley, 1974, ch. 9.

[13] B. Bonifacio, L. Lugiato, J. D. Farina, and L. M. Narducci, "Long time evolution for a one-dimensional Fokker-Planck process: Absorptive optical bistability," *IEEE J. Quantum Electron.*, vol. QE-17, pp. 357–364, 1981.

[14] Y. Suematsu, *Semiconductor Lasers and Integrated Optics* (in Japanese). Tokyo: Ohm-sha, 1984, ch. 10.

[15] M. Yamada and Y. Suematsu, "Theory of single mode injection lasers taking account of electronic intra-band relaxation," in *Proc. 10th Conf. Solid State Devices*, Tokyo, Japan, 1978; also in *Japan J. Appl. Phys.*, vol. 18, supplement 18-1, pp. 347–354, 1979.

[16] M. Ohtsu, Y. Otsuka, A. Osaki, and Y. Teramachi, "Analysis of mode hopping phenomena in an In GaAsP laser," (in Japanese), *Rev. Laser Eng.*, vol. 13, pp. 416–425, 1985.

Motoichi Ohtsu was born in Kanagawa, Japan, on October 5, 1950. He received the B.S., M.S., and Ph.D. degrees in electronics engineering from the Tokyo Institute of Technology, Tokyo, Japan, in 1973, 1975, 1978, respectively.

In 1978, he was appointed a Research Associate, and in 1982, became an Associate Professor at the Tokyo Institute of Technology. From September 1986 to July 1987, while on leave of absence from the Tokyo Institute of Technology, he joined AT&T Bell Laboratories, Crawford Hill Laboratory, Holmdel, NJ. His main fields of interest are the frequency control of lasers, analysis of dynamic behavior of lasers, and its applications to coherent optical measurements, optical communications, and microwave atomic clocks. He has written seven books.

Dr. Ohtsu is a member of the Institute of Electronics, Information and Communication Engineers of Japan, the Institute of Electrical Engineers of Japan, the Japan Society of Applied Physics, and the Optical Society of America. In 1982, he was awarded a prize from the Japan Society of Applied Physics. He was also awarded the Issac Koga Gold Medal from the International Union of Radio Science (URSI) in 1984.

Yasuaki Teramachi was born in Japan in 1947. He received the Doctor's degree in electrical engineering from the Tokyo Institute of Technology, Tokyo, Japan, in 1975.

In 1976 he was appointed a Research Associate in the Department of Applied Electronics, Tokyo Institute of Technology. In 1986, he became an Associate Professor in the Department of Information Engineering, the Institute of Vocational Training. He has been involved in the research program on the body surface potential mapping system and on nonlinear instability of lasers.

Dr. Teramachi is a member of the Physical Society of Japan and the Japan Society of Medical Electronics and Biological Engineering.

Tetsuya Miyazaki was born in Chiba, Japan, in March 1962. He received the B.E. degree in physics from Tsukuba University, Tsukuba, Japan, in 1985, and the M.E. degree in information processing from the Tokyo Institute of Technology, Tokyo, Japan, in 1987. He is currently with KDD Corporation, Tokyo, Japan.

Mr. Miyazaki is a member of the Institute of Electronics, Information and Communication Engineers of Japan.

TUH3 Simple interferometric method for preventing mode hopping in tunable external-cavity semiconductor lasers

K.-Y. LIOU, M. OHTSU, E. C. BURROWS, C. A. BURRUS, G. EISENSTEIN, AT&T Bell Laboratories, Crawford Hill Laboratory, Holmdel, NJ 07733.

A problem in frequency tuning of narrow-linewidth external-cavity lasers is mode hopping between neighboring external-cavity modes. Mode hopping occurs in both the grating-tuned external-cavity laser[1,2] and the monolithic integrated tunable distributed Bragg reflector (DBR) laser.[3] We demonstrate an interferometric method for mode-hopping detection and an automatic control circuit that maintains single-mode operation while the frequency of a grating external-cavity laser is tuned. The same method can be used to control a monolithic integrated external-cavity DBR laser.

For an air external-cavity length of a few centimeters, which is required to reduce the linewidth to ~100 kHz, the longitudinal mode spacings are several gigahertz. These closely spaced modes cannot be detected effectively using previously known methods. We found, however, that the heterodyned beat signal between the closely spaced cavity modes can be detected using a wideband photodiode and can be used for mode-hopping monitoring.

The experimental setup is shown in Fig. 1. An external-cavity laser was constructed by coupling a 1.3-μm semiconductor laser with an antireflection coated facet to a diffraction grating mounted on a PZT element. The grating was rotated for wideband frequency tuning, and the PZT voltage was adjusted for fine tuning. However, a large change in the PZT voltage or grating angle introduces hopping to successive modes.

During mode hopping, the two randomly switched mode powers are anticorrelated in time. A long fiber delay line (2.8 km) was used in a fiber Mach-Zehnder interferometer, shown in Fig. 1, to remove the anticorrelation for optimizing the heterodyned signal between the two hopping modes. Without the delay line, however, mode hopping can still be detected, but the signal level is smaller. The spectrum analyzer displays in Fig. 2 show the mode-hopping signals *A* and *B* detected with and without the delay line, respectively.

Mode-hopping prevention was demonstrated using the circuit shown in Fig. 1. The mode spacing for a 7.5-cm external-cavity length used was ~2 GHz. The mode-hopping signal at the 2-GHz beat frequency between the two modes was heterodyned with a microwave local oscillator (LO) to downshift the frequency. After envelope detection, the signal was negatively fed back to a PZT control circuit, which adjusted the cavity length automatically to maintain single-mode operation. When the PZT voltage was swept with the control loop open, mode hopping occurred, which is shown by the two-mode spectrum in the scanning Fabry-Perot interferometer output in Fig. 3(a). Fig. 3(b) shows the detected mode-hopping signal: the peak near the microwave LO peak. When the control loop was closed, the laser always remained single mode as shown in Fig. 3(c), and the mode-hopping peak disappeared in Fig. 3(d).

The average frequency of mode hopping in the external-cavity laser was analyzed theoretically and estimated by fitting the mode-hopping signals to be in the 0.5–2.5-MHz range. Calculated results show that a ~300-m delay line is sufficient for monitoring mode hopping with high sensitivity and stability using the present method. **(12 min)**

1. R. Wyatt and W. J. Devlin, Electron. Lett. **19**, 110 (1983).
2. N. A. Olsson and J. P. van der Ziel, IEEE/OSA J. Lightwave Technol. **LT-5**, 510 (1987).
3. S. Murata, I. Mito, and K. Kobayashi, Electron. Lett. **23**, 403 (1987).

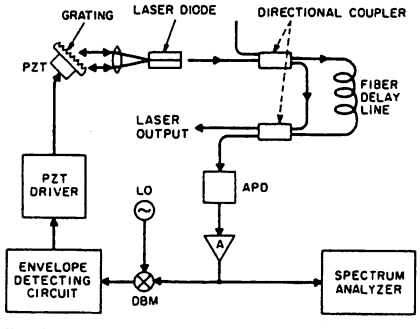

TUH3 Fig. 1. Experimental apparatus. LO, microwave local oscillator; DBM, double-balanced mixer; APD, avalanche photodiode.

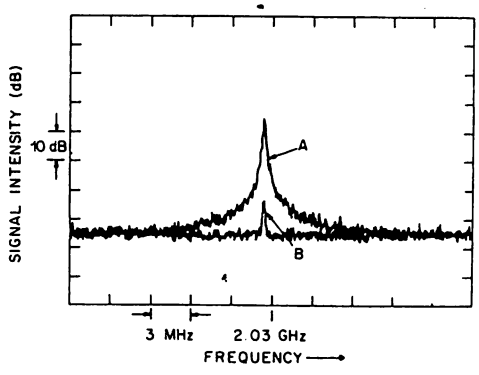

TUH3 Fig. 2. Spectrum analyzer displays of the mode-hopping signal near 2 GHz: *A*, signal obtained with a 2.8-km fiber delay line; *B*, without using the delay line.

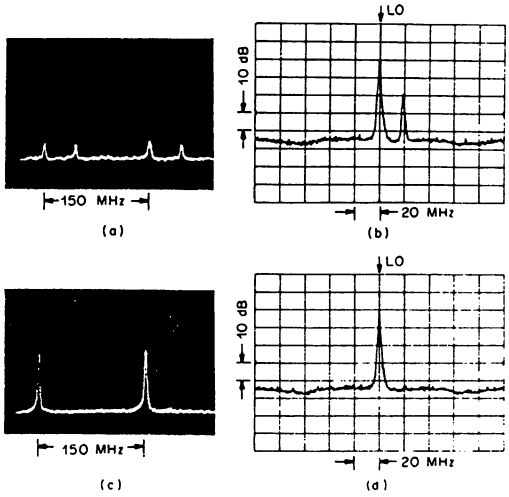

TUH3 Fig. 3. Scanning Fabry-Perot (150-MHz free spectral range) spectrum (a) and the monitoring signal from the Mach-Zehnder interferometer showing two-mode hopping when the control loop was open; (c) and (d) show single-mode operation when the feedback loop was closed. The LO peak is from the microwave local oscillator.

TUC5 Power partition fluctuations in two-mode-degenerate distributed-feedback injection lasers

K.-Y. LIOU, M. OHTSU, C. A. BURRUS, AT&T Bell Laboratories, Crawford Hill Laboratory, Holmdel, NJ 07733; U. KOREN, T. L. KOCH, AT&T Bell Laboratories, Holmdel, NJ 07733.

Power partition fluctuations in distributed-feedback (DFB) lasers, when two degenerate DFB modes[1] are the only significant longitudinal modes, have not been reported previously, although such information is important for designing reliable fiber-optic systems employing DFB lasers. We present measurements and theoretical analysis of the partition noise in a DFB laser operating cw with the two degenerate modes.

The experiment used a novel two-electrode DFB laser[2] in which the two-mode degeneracy can be electrically controlled. The laser, emitting near 1.3 μm, is of the semi-insulating planar-buried-heterostructure type with a first-order grating. The contact metallization on the p side is split into two sections along the laser cavity. Figure 1(a) shows the two-current control of the two degenerate modes, λ_{+1} and λ_{-1}, separated by a 20-Å stop band. The power ratio, P_{+1}/P_{-1}, of the two modes was varied from 1:1 to 2500:1 for the measurements, while all the other side modes were suppressed by more than a 4000:1 ratio.

Partition fluctuations were analyzed using a method similar to that used by Linke *et al.*[3] The two modes were separated by a diffraction grating and then detected with a PIN photodiode. Figure 1(b) shows the partition (dropout) events for the case of $P_{+1}/P_{-1} = 14$. The main-mode dropout is correlated to a side-mode power increase, similar to that observed for nearly single-mode Fabry-Perot lasers.[3] One difference, however, is the observation that the dropout depths in the DFB laser were <30% of the main-mode power even for $P_{+1}/P_{-1} = 1$, except when the laser was subjected to external optical feedback. The measured dropout rates vs depth for various P_{+1}/P_{-1} ratios are plotted in Fig. 2(a).

In addition to transient dropouts, the two mode powers were observed to oscillate at ~1.3-GHz frequency, while the total power remained constant. This anticorrelated two-mode relaxation oscillation may be caused by an oscillation of the local optical intensity in the DFB laser, which is different from the well-known relaxation oscillation due to photon–carrier interaction. The measured oscillation amplitudes in Fig. 3 show that the oscillation disappears when $P_{+1}/P_{-1} > 500$.

A theory we developed earlier to analyze a Fabry-Perot/DFB dual-wavelength laser[4] is modified here for the case of a two-mode-degenerate DFB laser. The theory is based on a Fokker-Planck equation derived from the rate equations for two-mode oscillation. The solution of the Fokker-Planck equation gives the probability distribution of the oscillation state of the laser, from which the transient dropout frequency is calculated. The calculated results in Fig. 2(b) are in good agreement with the experimental curves in Fig. 2(a), except for some differences in the slopes, which may be affected by the two-mode relaxation oscillation. Our results indicate that both the transient dropouts and the two-mode relaxation oscillation become insignificant when the power ratio of the two DFB modes is higher than 500:1. **(12 min)**

1. H. Kogelnik and C. V. Shank, J. Appl. Phys. **43**, 2327 (1972).
2. K.-Y. Liou, C. A. Burrus, U. Koren, and T. L. Koch, Appl. Phys. Lett. **51**, 634 (1987).
3. R. A. Linke, B. L. Kasper, C. A. Burrus, I. P. Kaminow, J.-S. Ko, and T. P. Lee, IEEE/OSA J. Lightwave Technol. **LT-3**, 706 (1985).
4. M. Ohtsu and K.-Y. Liou, in *Technical Digest, Conference on Lasers and Electro-Optics* (Optical Society of America, Washington, DC, 1987), paper THD3.

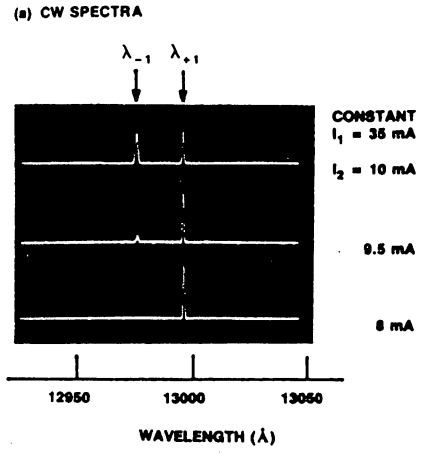

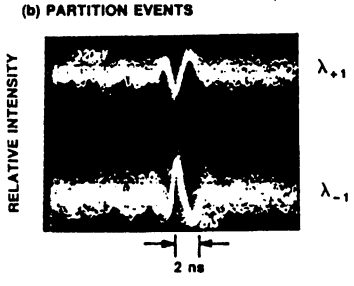

TUC5 Fig. 1. (a) Continuous wave spectra of a two-electrode DFB laser showing control of the two degenerate DFB modes, λ_{+1} and λ_{-1}, by adjusting the currents I_1 and I_2 applied to the two electrodes; (b) oscilloscope traces showing triggered partition (dropout) events for power ratio $P_{+1}/P_{-1} = 14$.

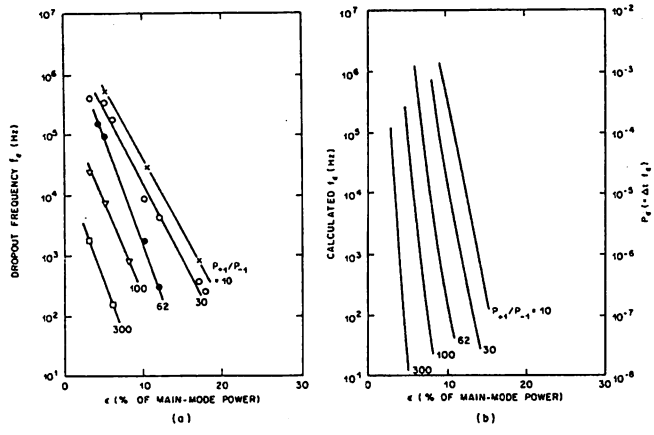

TUC5 Fig. 2. (a) Measured dropout rate f_ϵ with dropout depths deeper than a fraction ϵ of the main-mode power for various power ratio (P_{+1}/P_{-1}) at constant 2-mW total output power; (b) calculated f_ϵ vs ϵ by the Fokker-Planck analysis.

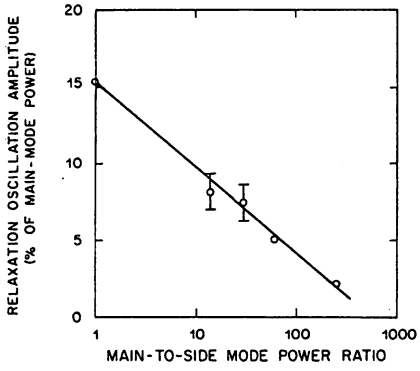

TUC5 Fig. 3. Measured amplitude (one-half of the maximum peak-to-peak range) of the two-mode relaxation oscillation vs the power ratio of the two degenerate DFB modes.

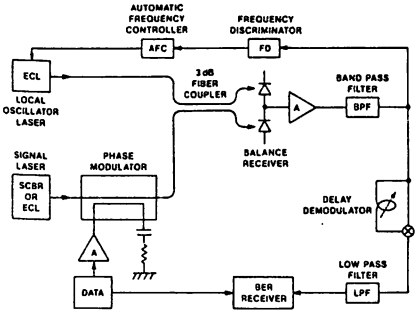

TUC6 Fig. 1. Schematic diagram for the 400-Mbit/s DPSK system.

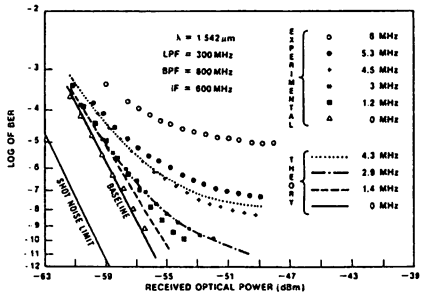

TUC6 Fig. 2. BER curves at −4.6-dBm LO power. Continuous curves at the experimental points are theoretical curves reproduced from Ref. 2.

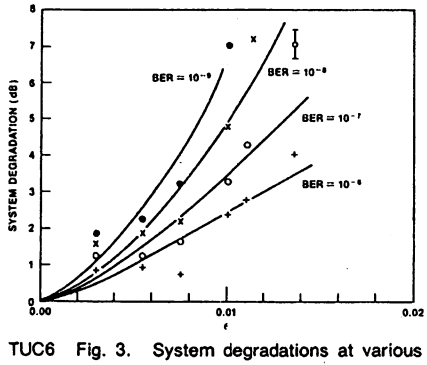

TUC6 Fig. 3. System degradations at various bit error rates as a function of linewidth-to-bit-rate ratio.

two points are measured, and interference fringe counts are recorded in a microcomputer to then be processed. A differential interference fringe counter was used for this. The displacement of interference fringes is converted to electrical signals with a corresponding accuracy of $\sim\Delta L/L = 1 \times 10^{-10}$.[2] A prediction error filter is adopted to detect the vibration of the ground while discounting voiding any anomalous artificial vibration.[3] Data are counted every second and recorded every 10 min. When abnormal vibrations occur, for example, ΔL exceeds 1 μm. Those measurements in particular are recorded every second. This measurement has been done in an environment with an ambient temperature of $T = 20°C$ (ΔT/day $\simeq$ 0.04°C) and a relative humidity of 40%. The interferometer is enclosed in a vacuum pipe to remove any fluctuation due to the refractive index of air. The absolute barometric pressure inside this pipe is $\sim 10^{-3}$ Torr. The interferometer and vacuum pipe are mounted on an optical bench, which is uncoupled from the floor.

We observed a vibration that lasted for a period of one day for a peak-to-peak amplitude of several micrometers ($\Delta L/L \simeq 3 \times 10^{-7}$). Figure 3 shows a record of slow changes of earth strain for 4 yr (Feb. 1983–1987). It is found that the strain has a periodicity of 1 yr, and this tends to increase (stretch) year by year. We measured precipitation to analyze the correlation and temperature to the variation, and it has a noticeable correlation.

The irregular ripples in the measured strain mainly came from the changes of temperature and precipitations. For example, a large dip near Aug. 1983 shows a shrinkage due to heavy rains of 250 mm. Most important, we detected a gradual change of strain, which is much larger than the system error, even if we adjust for the global effect of temperature and precipitation.

In summary: It is expected that this system can be effectively used to observe the long-term variation of earth strain including some abnormal vibration, such as earthquakes. Therefore, by installing this kind of system at multiple points to measure long-term vibration and abnormal strain, the prediction of earthquakes becomes possible.

(12 min)

1. K. Asakawa and T. Tako, Oyo Butsuri **49**, 1185 (1980).
2. K. Asakawa, T. Tako, and S. Hirata, Oyo Butsuri **48**, 519 (1979).
3. T. Tako and K. Asakawa, Kogaku **7**, 120 (1978).

NOTES

TUQ5 Long-term measurement of earth strains and vibrations by a 50-m laser interferometer

K. IGA, T. SAKAGUCHI, M. KUROIWA, T. TAKO, M. OHTSU, E. HATAKOSHI, Tokyo Institute of Technology, 4259 Nagatsuta, Midori-ku, Yokohama 227, Japan.

Minute vibrations and strains of the earth are being measured by a long-distance laser interferometer.[1] Since Feb. 1983, it has been installed in an underground optical tunnel (Fig. 1). The periodicity and correlation are analyzed by measuring the change of temperature and precipitation.

This system consists of a 50-m modified Michelson interferometer, which is prepared in a vacuum path as shown in Fig. 2. The employed light source is a frequency-stabilized 633-nm He–Ne laser (HP model 5500C). The cat's eye diaphragm acts as a reflective mirror, and the isolator is used to remove the effect of reflection from the interferometer.

Relative fluctuations of the distance between

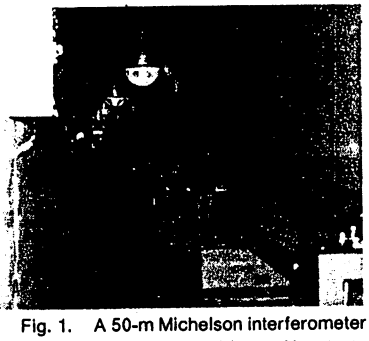

TUQ5 Fig. 1. A 50-m Michelson interferometer in an underground optical tunnel in the Nagatsuta campus of Tokyo Institute of Technology.

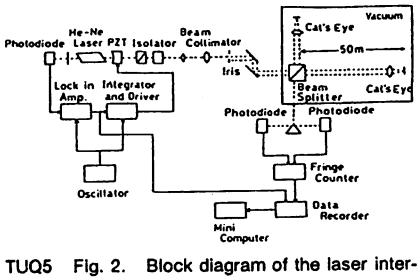

TUQ5 Fig. 2. Block diagram of the laser interferometer system.

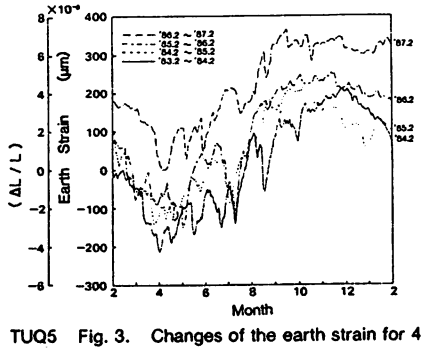

TUQ5 Fig. 3. Changes of the earth strain for 4 yr (Feb. 1983–1987).

IMPROVEMENT OF FREQUENCY ACCURACY In A SEMICONDUCTOR LASER PUMPED ^{87}Rb ATOMIC CLOCK

M. Hashimoto and M. Ohtsu
Department of Information Processing
Graduate School at Nagatsuta, Tokyo Institute of technology
4259 Nagatsuta, Midori-ku, Yokohama, Kanagawa 227, Japan

<ABSTRACT>

Light shift of rubidium atomic clock was accurately measured. By controlling the laser frequency detuning based on the results of the measurements, the microwave frequency inaccuracy of a rubidium atomic clock was reduced to $\pm 3.2 \times 10^{-11}$.

I. Introduction

Highly precision rubidium (^{87}Rb) atomic clocks have been required for various applications, e.g., the signal sources for GPS satellites. For the improvement of their performances, the ^{87}Rb atomic clock pumped by a semiconductor laser have been investigated[1][2].

In this paper, we proposed a new technique to improve frequency accuracy in the ^{87}Rb atomic clock pumped by a semiconductor laser.

II. Measurements of Light Shift

Figure 1 shows a block diagram of a ^{87}Rb atomic clock pumped by a semiconductor laser. The optical-microwave double resonance affects the electric field of laser light transmitted through the ^{87}Rb vapor. The amplitude transmissivity (T) can be defined as $T = e^{-\delta - i\phi}$, where δ and ϕ are the amplitude attenuation and phase shift, respectively. The phase of the transmitted laser light is modulated by means of modulation of microwave signal at angular frequency ω_m. Therefore, due to the nonlinear susceptibility of the three-level ^{87}Rb atoms, the several harmonic components ($n\omega_m$; n=1,2,3,...) would be induced in the light power ($I_T(t)$) detected by photodetector[3][4][5]. $I_T(t)$ can be written as

$$I_T(t) = I_0 \sum_{n=0}^{\infty} [C_n \cos(n\omega_m t) + S_n \sin(n\omega_m t)], \quad (1)$$

where C_n and S_n are the in-phase and the quadrature components, respectively. Such a component can be measured by using phase sensitive detection technique. The measured spectral profile of these components are shown in Fig.2. As the profiles of fundamental components (C_1 , S_1) and 3rd harmonic components (C_3, S_3) cross the abscissa at the transition frequency, they can be used as frequency discriminators. The microwave frequency should be stabilized at the zero-cross point of these frequency discriminators. However, the dynamic stark effect by the electric field of pumping light would induce the light shift,i.e., the shift in microwave transition frequency[6]. Since this frequency is used as a frequency reference for ^{87}Rb atomic clocks, the light shift would limit their frequency accuracy as well as frequency stability. Precise measurements of the light shift have been rather difficult in the conventional ^{87}Rb atomic clocks because of the complicated spectral profile of the ^{87}Rb lamp. However, it can be measured more precisely by using a highly coherent semiconductor lasers.

Figure 3 shows the relations between the microwave frequency shift $\Delta\nu_{HFS}$ of the center of the spectrum and the laser frequency detuning $\Delta\nu_L$ from the center frequency of the $5S_{1/2}$, F=1 -> $5P_{3/2}$ transition. In particular, it is first observed that the microwave frequency shift is also increased with increasing the laser power density at the laser frequency detuning $\Delta\nu_L$=0 as being shown in Fig.4. This phenomenon can be explained as the shift of energy level of the $5S_{1/2}$, F=2 when the laser frequency was tuned to the resonance frequency of the $5S_{1/2}$, F=1 -> $5P_{3/2}$ transition.

III. Self-Tuning System for Improving Frequency Accuracy

For the improvement of the microwave frequency accuracy, the laser frequency should be controlled based on the results of measurements of the light shift described in II. To this end, we proposed a novel technique to evaluate the microwave frequency shift by using a deformation of spectral shape. As shown by Fig.5, the spectral lineshape of S_1, used as a frequency discriminator, was deformed and lost its symmetry by detuning the laser frequency. We defined an asymmetrical factor ΔS as the area difference between S_+ and S_- in Fig.6(a). As shown in Fig.6(b), the value of this factor ΔS was directly calculated by a computer. From the results of Figs.3 and 6, difference between the exact transition frequency in ^{87}Rb and the microwave frequency of ^{87}Rb atomic clock, i.e., $\Delta\nu_{HFS}$ can be estimated by given value of ΔS. It is should be noted that this technique does not require a separate reference frequency source, therefore, this system can be referred as self-tuning system.

Drift of the controlled atomic clock frequency was compensated by the self-tuning system (see Fig.1) at every 10 minutes. Working time of self-tuning system was about 2 minutes. The microwave frequency inaccuracy as low as $\pm 3.2 \times 10^{-11}$ was obtained as shown in fig.7. This value is 1/10 times that of conventional ^{87}Rb atomic clocks[7].

IV. Summary

Light shift of rubidium atomic clock was accurately measured. The light shift induced by the laser power density was first observed even when the laser frequency detuning was exactly tuned to the transition frequency for zero power level of the laser. Self-tuning system, which did not require a separate reference frequency source, was constructed to compensate for the effect of light shift. The microwave frequency inaccuracy obtained by using this novel technique was as low as $\pm 3.2 \times 10^{-11}$, which is 1/10 times that of conventional ^{87}Rb atomic clocks.

REFERENCES

[1]L.Lewis and M.Feldman, "Preliminary Investigation of a New Optically Pumped Atomic Rubidium Standards", Proc.35th Ann.Freq.Control Symposium, Ft.Monmouth, NJ, May 1981, pp.612-624

[2]J.C.Camparo, R.P.Frueholz, and C.H.Volk, "Inhomogeneous light shift in alkali-metal atoms", Phys.Rev.,Vol.27, 1983,pp.1914-1925

[3]G.C.Bjorklund, "Frequency-modulation spectroscopy: a new method for measuring weak absorptions and dispersions", Optics Letters, Vol.5, 1980, pp.15-17

[4]M.Hashimoto and M.Ohtsu, "Experiments on a Semiconductor Laser Pumped Rubidium Atomic CLOCK", IEEE J.Quantum Electronics,Vol.QE-23,1987,pp.446-451

[5]M.Hashimoto, M.Ohtsu, and H.Furuta, "Ultra-Sensitive Frequency Discrimination in a Diode Laser Pumped ^{87}Rb Atomic Clock",Proc.41st Ann. Freq. Control Symposium, Philadelphia, PA, May 1987, pp.25-35

[6]B.S.Mathur, H.Tang, and W.Happer, "Light Shifts in the Alkali Atoms", Phys.Rev., Vol.171, 1968, pp.11-19

[7]H.hellurig, Proc.28th Ann.Freq. Control Symposium,

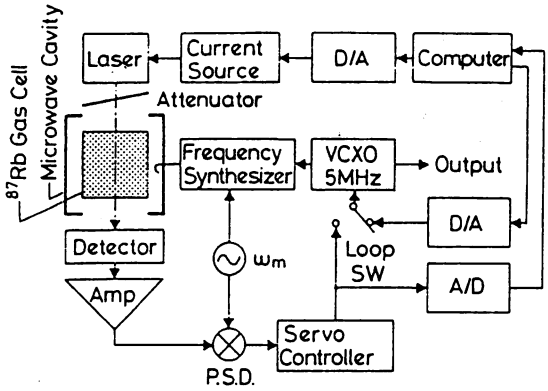

Fig.1 A block diagram of the ^{87}Rb atomic clock pumped by a semiconductor laser.
P.S.D. : Phase sensitive detector.
Amp : Post-detector Amplifier.
ω_m : Angular frequency of a low frequency for microwave frequency modulation.
D/A : Digital to analogue converter.
A/D : Analogue to digital converter.

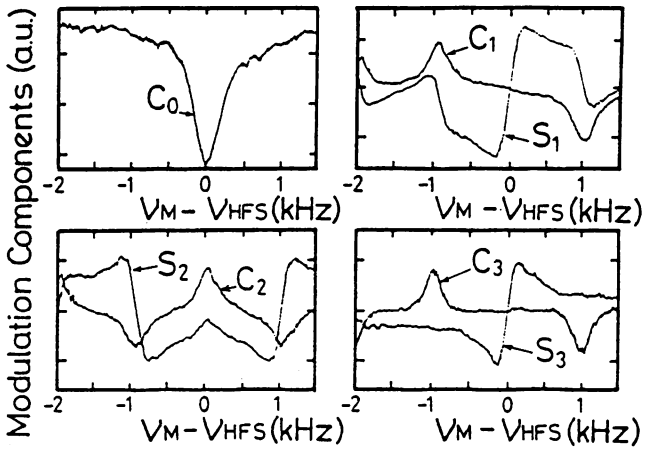

Fig.2 The spectral profiles of modulation components on the microwave frequency ν_M. The modulation frequency was fixed at $\omega_m/2\pi$ =1 kHz.
ν_M : The microwave frequency.
ν_{HFS} : The microwave transition frequency.

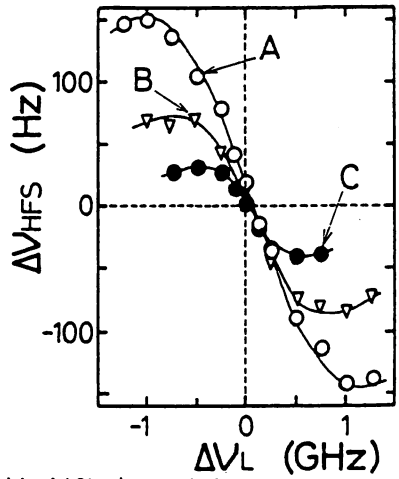

Fig.3 Light shift $\Delta\nu_{HFS}$ induced by laser frequency. The laser power density was fixed at 1520 $\mu W/cm^2$(A,○), 380 $\mu W/cm^2$(B,▽), and 152 $\mu W/cm^2$(C,●).
$\Delta\nu_L$: The laser frequency detuning.
$\Delta\nu_{HFS}$: The microwave resonance frequency shift.

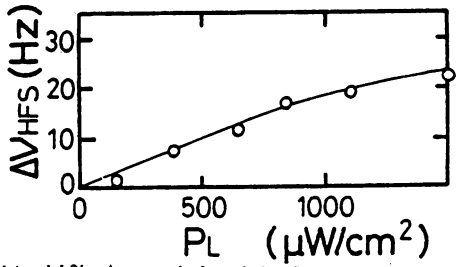

Fig.4 Light shift $\Delta\nu_{HFS}$ induced by laser power density. The laser frequency was tuned to the $5S_{1/2},F=1 \rightarrow 5P_{3/2}$ transition.
P_L : The laser power density.

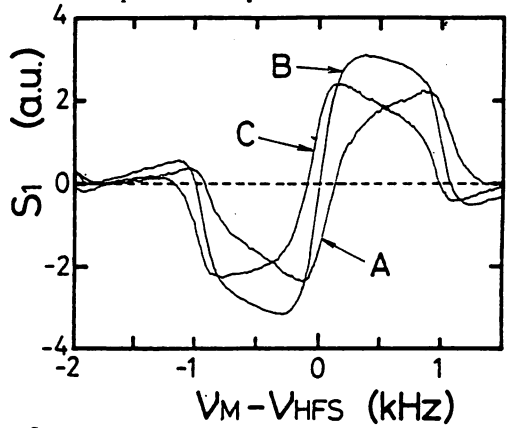

Fig.5 Spectral profile of S_1, which was used as a frequency discriminator for microwave frequency control. The laser frequency detuning was fixed at -750 MHz(A), 0 MHz (B), and 750 MHz(C).

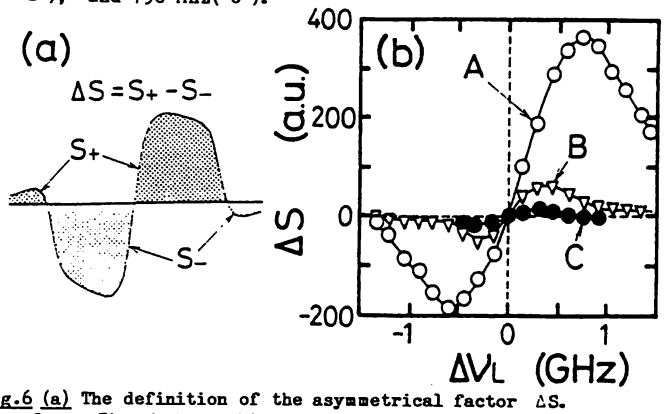

Fig.6 (a) The definition of the asymmetrical factor ΔS.
S_+ : The integration of the spectral profile with positive amplitude.
S_- : The integration of the spectral profile with negative amplitude.
(b) Relation between the asymmetrical factor ΔS (defined by Fig.6 (a)) and the laser frequency detuning $\Delta\nu_L$. The laser power density was fixed at 1520 $\mu W/cm^2$(A,○), 380 $\mu W/cm^2$(B,▽), and 152 $\mu W/cm^2$(C,●).
$\Delta\nu_L$: The laser frequency detuning.
ΔS : The asymmetrical factor.

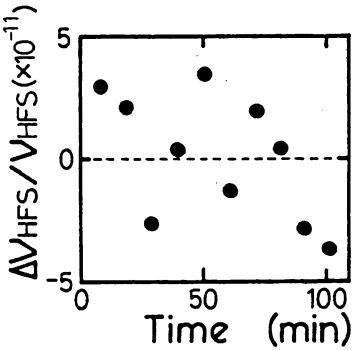

Fig.7 Normalized variation of difference between the exact transition frequency in ^{87}Rb and the microwave frequency of ^{87}Rb atomic clock.
$\Delta\nu_{HFS}/\nu_{HFS}$: The microwave frequency inaccuracy.